VIBRATION-TRANSLATION ENERGY TRANSFER IN VIBRATIONALLY EXCITED DIATOMIC MOLECULES

Robert Lawrence McKenzie

Ames Research Center
Moffett Field, Calif. 94035

NATIONAL AERONAUTICS AND SPACE ADMINISTRATION • WASHINGTON, D. C. • OCTOBER 1976

1. Report No.	2. Government Accession No.	3. Recipient's Catalog No.
NASA TR R-466		

4. Title and Subtitle	5. Report Date
VIBRATION-TRANSLATION ENERGY TRANSFER IN VIBRATIONALLY EXCITED DIATOMIC MOLECULES	October 1976
	6. Performing Organization Code

7. Author(s)	8. Performing Organization Report No.
Robert Lawrence McKenzie	A-6453
	10. Work Unit No.
9. Performing Organization Name and Address	506-25-61-01-00-21
Ames Research Center Moffett Field, Calif. 94035	11. Contract or Grant No.
	13. Type of Report and Period Covered
12. Sponsoring Agency Name and Address	Technical Report
National Aeronautics and Space Administration Washington, D. C. 20546	14. Sponsoring Agency Code

15. Supplementary Notes

Submitted to York University, Toronto, Ontario, as partial fulfillment of Ph.D., April 1976.

16. Abstract

A semiclassical collision model is applied to the study of energy transfer rates between a vibrationally excited diatomic molecule and a structureless atom. The molecule is modeled as an anharmonic oscillator with a multitude of dynamically coupled vibrational states. Three main aspects in the prediction of vibrational energy transfer rates are considered. The applicability of the semiclassical model to an anharmonic oscillator is first evaluated for collinear encounters. Second, the collinear semiclassical model is applied to obtain numerical predictions of the vibrational energy transfer rate dependence on the initial vibrational state quantum number. Thermally averaged vibration-translation rate coefficients are predicted and compared with CO-He experimental values for both ground and excited initial states. The numerical model is also used as a basis for evaluating several less complete but analytic models. Third, the role of rotational motion in the dynamics of vibrational energy transfer is examined. A three-dimensional semiclassical collision model is constructed with coupled rotational motion included. Energy transfer within the molecule is shown to be dominated by vibration-rotation transitions with small changes in angular momentum. The rates of vibrational energy transfer in molecules with rotational frequencies that are very small in comparison to their vibrational frequency are shown to be adequately treated by the preceding collinear models.

17. Key Words (Suggested by Author(s))	18. Distribution Statement
Diatomic molecules Vibrational relaxation rates Vibration-rotation energy transfer Semiclassical collision models	Unlimited STAR Category - 72

19. Security Classif. (of this report)	20. Security Classif. (of this page)	21. No. of Pages	22. Price*
Unclassified	Unclassified	242	$7.50

*For sale by the National Technical Information Service, Springfield, Virginia 22161

TABLE OF CONTENTS

APPENDIX

VIBRATION-TRANSLATION ENERGY TRANSFER IN VIBRATIONALLY EXCITED DIATOMIC MOLECULES

Robert Lawrence McKenzie

Ames Research Center

CHAPTER I

INTRODUCTION

1.1 New Aspects in Modern Vibrational Relaxation Processes

While the collisional excitation of vibrations in diatomic molecules has been a frequently studied topic for decades,[1-4] an increasing interest in processes that depend on the details of energy transfer to specific vibrational states has put new demands on the analysis of such collisions. The following comparison of the early class of relaxation processes with those introduced in the past decade demonstrates the new features required in a theoretical model of vibrational energy transfer.

Early studies of vibrational relaxation in gases were concerned mainly with the influence of vibrational energy transfer on the bulk thermodynamic properties during the relaxation process. Phenomena such as the absorption and dispersion of ultrasonic waves[5,6] or the vibrational excitation behind shock waves[7,8] were described analytically in terms of an effective "relaxation time," τ, that characterized the rate at which the collisional exchange of vibrational and translational energies brought the total energy in vibrations toward equilibrium. Only a single relaxation equation was then necessary, in the simple form:

---

*Submitted to York University as partial fulfillment of Ph.D., April 1976.

$$\frac{de_v}{dt} = \frac{e_v^* - e_v}{\tau} \tag{1.1}$$

where e_v is the total specific energy in vibrations and e_v^* is the corresponding value at thermodynamic equilibrium with the local state of the gas (see Appendix A for a list of symbols). The factors controlling these early processes are evident in the derivation leading to equation (1.1) (e.g., Vincenti and Kruger,[8] Ch. 7). The gas is considered to be an admixture of harmonic oscillators in a thermal heat bath of structureless inert atoms. The harmonic oscillator quantal properties allow only single-quantum transitions and lead to the Landau-Teller[4] relationship describing the quantum number dependence of rate coefficients:

$$k_{v,v-1} = vk_{1,0} \tag{1.2}$$

where $k_{v,v-1}$ denotes the rate coefficient for transitions from oscillator state v to $v-1$ induced by oscillator-atom collisions. A set of simplified rate equations describing the detailed kinetics can then be collected into a simple equation from which the parameter, τ, emerges in the form

$$\tau = [(1 - e^{-\hbar\omega/kT})k_{1,0}\rho/m]^{-1} \tag{1.3}$$

where ω is the fundamental oscillator frequency and T, ρ, and m are the kinetic temperature, density, and average molecular mass of the gas mixture, respectively. Equations (1.1) and (1.3) combine to illustrate the principal common feature of processes described this way; viz, the only collision parameter required is the rate of single-quantum transitions to the ground state. The description is independent of the population distributions among higher vibrational states and no assumptions regarding their definition is made. In a more detailed account of the kinetics that includes the exchange of vibrational energy between oscillators, Montroll and Shuler[9] show that a population

distribution of harmonic oscillator states rapidly recovers from an arbitrary distortion and achieves a Boltzmann distribution described by some nonequilibrium "vibrational temperature." The recovery occurs in a time period small compared to τ, causing the subsequent relaxation to proceed through a continuous sequence of Boltzmann distributions. This result further reduced any concern for the details of energy transfer to excited vibrational states beyond the description given by equation (1.2).

As experimental studies of vibrational relaxation became more detailed, the kinetic models based on harmonic oscillator properties appeared less capable of describing the observations. Motivated by some large discrepancies between theory and experiment in nonequilibrium supersonic expansions, Treanor, Rich, and Rehm[10] recently showed that the small anharmonicity of most diatomic molecules was sufficient to generate non-Boltzmann distributions among upper vibrational states during some relaxation processes. The importance of oscillator anharmonicity in the vibrational kinetics has since been amplified by the introduction of infrared gas lasers,[11-15] where the effects of anharmonicity are essential to produce the necessary population inversions among vibration-rotation states.[13] Some recent proposals using lasers to selectively excite specific vibrational states for photochemical or isotope separation experiments will also be strongly influenced by the effects of anharmonicity. These modern applications of vibrational nonequilibrium constitute a new class of relaxation processes that depend on the degree of distortion from a Boltzmann population distribution. Their analysis requires a detailed solution to the set of relaxation equations — one for each contributing vibrational state — that describes the change in number density, N_v, of each state v. A general form of the relaxation equations can be written as

$$\frac{dN_v}{dt} = \sum_i \sum_{v'} k_{v',v} N_i N_{v'} \qquad (1.4)$$

where N_i denotes the number density of all species or states i and $k_{v',v}$ is the rate coefficient for transitions from state v' to v. Equation (1.2) is not an accurate description of the quantum number dependence of $k_{v',v}$ when the oscillator is anharmonic, and the selection rule allowing only single-quantum transitions is also invalid. Thus the simplifications of equation (1.4) leading to equation (1.1) and the concept of an effective relaxation time given by equation (1.3) are no longer applicable. Rate coefficients for transitions from excited vibrational states are as essential to the analysis of such processes as $k_{1,0}$ is and vibrational anharmonicity will have a major influence on their values. Since this study is concerned mainly with the rate of energy transfer to excited states, oscillator anharmonicity is therefore a basic feature to be included.

1.2 Role of Vibration-Translation Energy Transfer

In most modern applications involving vibrational nonequilibrium and particularly in the analysis of infrared gas lasers, the collisional exchange of vibrational and translational energies must usually be considered as one of several paths for energy transfer to the molecular state in question. As equation (1.2) indicates, the rate of vibration-translation (V-T) energy transfer increases with quantum number even in the simplest model of the oscillator. Thus, the V-T process can dominate the flow of energy from upper vibrational levels even where it may be insignificant to the kinetics of lower levels. In some cases, it may provide the principal path for vibrational energy loss from the system. An essential feature of the V-T rates is therefore their dependence on the initial state quantum number, particularly in

deexcitation processes where excess vibrational energy has been produced. Unfortunately, very little quantitative information defining the quantum number dependence of V-T rates for even the simplest diatomic molecules is presently available from either experiment or theory.

Experimental ground-state excitation rates have been obtained from measurements behind shock waves[16] or in fluorescence experiments[17] for many years by determining the value of τ in equation (1.1) that best fits the observations. However, the difficulty of obtaining experimental V-T rates for molecules in well-defined excited vibrational states is indicated by the sparsity of attempts. Numerous experimenters have recently measured the rates of vibration-vibration (V-V) energy exchange between pairs of oscillators in excited states[18,19] because the fast V-V transfer can easily be made a dominant mechanism; but to date, only one comprehensive set of upper-level V-T rate measurements has been reported.[18] Even then, while the experiment was cleverly designed and carefully analyzed, the conditions were complex and the measurements required substantial correction to compensate for extraneous modes of energy transfer.

Theoretical studies addressed to the analysis of initially excited oscillators have been similarly sparse. Since the relaxation time, τ, is determined solely by the rate of single-quantum transitions to the ground state, $k_{1,0}$, the usual theoretical approach has centered on a harmonic oscillator model of the molecule initially in the ground state. The small-amplitude oscillations characteristic of the ground state then allow a linearized interaction potential between the oscillator and an incident particle to be used. By assuming further that the particle trajectory is collinear with the molecular axis and by adopting a semiclassical approximation, the linearized

interaction makes possible an exact and convenient analytical solution for the oscillator transition probabilities for any initial state. However, the inaccuracy of the harmonic oscillator model has been demonstrated by Mies[20-21] even for transitions originating from the ground state. Mies found that the use of an anharmonic oscillator potential introduces matrix elements associated with oscillator transitions that are no longer equal on the diagonal. (A harmonic oscillator with an interaction linear in the oscillator coordinate has constant diagonal matrix elements.) The nonzero differences in the diagonal matrix elements introduce additional phase differences between the time-dependent oscillator eigenfunctions during a collision and can lead to large corrections to the harmonic oscillator model. Because the origin of these corrections resides in the unperturbed oscillator eigenfunctions (from which the matrix elements are computed), their effects are not always reproduced by the popular practice of simply inserting oscillator eigenenergies, corrected for anharmonicity, into a harmonic oscillator theory. Nevertheless, in the absence of better analytic solutions, such theoretical models are frequently used to predict the quantum number dependence of V-T rates.[11-15] Thus, a need clearly exists for the development of a suitable analytic solution containing anharmonicity as a fundamental feature.

1.3 Purpose and Objectives of This Study

While the modern literature is abound with comprehensive and detailed studies of the collisional excitation of diatomic molecules in vibration and rotation (see almost any recent issue of the Journal of Chemical Physics), vibrational states higher than the second are rarely considered. The objectives are usually either to examine improved techniques for calculating the collision dynamics or to obtain a quantitatively accurate estimate of the

inelastic cross sections. The collision models used in the latter case are usually fully quantum mechanical and hence are as exact as the form of the interaction potential chosen for study. These studies are clearly a necessary step in the understanding of molecular collision dynamics since they provide the most precise test of our ability to explain the experimental observations. Unfortunately, the computational requirements to obtain such precision are expensive and tend to limit the scope of such studies. To a pragmatist concerned with the analysis of a modern macroscopic process, these studies of microscopic collision dynamics are seldom able to provide much useful information about the thermally averaged rate coefficients for molecules in excited states. Furthermore, even if exact calculations were typically carried far enough to produce rate coefficients, a means of numerically reproducing the results inexpensively would be required before they could be conveniently applied in a solution of the macroscopic rate equations. This study is addressed to the pragmatist and to four corresponding objectives.

The first objective is to examine the inelastic collision dynamics of diatomic molecules in an arbitrary initial state struck by a structureless atom. The purpose is to explore the qualitative features of such encounters and to identify the parameters and physical features contributing most to the prediction of the associated energy-transfer rates. By including a complete account of the coupling between interacting vibrational states, especially as it is amplified by anharmonicity, the results provide a basis for evaluating more approximate treatments of the collision process that may have emphasis on other aspects, such as those with sufficient simplifications to allow analytic solution or those including coupled rotational motion.

A second objective of this study is to evaluate several analytic collision models in popular use for predicting the quantum number dependence of V-T rate coefficients. This objective is motivated by the importance of having an inexpensive means of generating values of $k_{v,v'}$ when solving the detailed rate equations typified by equation (1.4). A collision model with sufficient generality to be applicable for all conditions of interest in modern applications will necessarily require numerical solution, and the first objectives of this study are met only with such a model. The solutions are time consuming, however, and would be prohibitively expensive in a practical application. Consequently, the usual practice is to obtain a simple analytic approximation by introducing sufficient assumptions to decouple the interactions between oscillator states and to linearize the interaction between the oscillator and its collision partner. Several such solutions have been extracted, but they all exclude one or more properties of the collision process that remain important in a generalized model. Little definition, if any, of the range of applicability of these analytic solutions appears in the literature in other than the most general terms. The second objective described here is an effort to define more explicitly their range of applicability for predicting excited-state rate coefficients.

A third objective of this study is to evaluate the consequence of several simplifying assumptions regarding the equations of motion and the collision geometry that were necessary to meet the preceding objectives. A fundamental simplification to the equations of motion is achieved here by adopting a semiclassical or "impact parameter" description of the collision dynamics.[22-23] The path of the incident particle is obtained classically, while the oscillator response is treated quantum mechanically. As a result,

the second-order quantum mechanical equation of motion is reduced to two first-order differential equations that are subsequently decoupled. The complexity of solution is thereby reduced greatly. However, the semiclassical approximation fails to properly account for the quantal interference between colliding nuclei while the decoupling of first-order equations obviates the conservation of total energy. These shortcomings have been partially compensated in similar harmonic oscillator models, but the success of the compensations has not been tested for anharmonic oscillators. Part of this third objective is to examine and define the limitations of the semiclassical approximation when applied to anharmonic oscillators. The results will contribute to a more complete understanding of the associated analytic solutions that are also based on the semiclassical approximation.

A final objective of this study is to evaluate the influence of coupled rotational motion on the rate of vibrational energy transfer. The necessity of including a multitude of vibrational states with large quantum numbers to study their interactions required a reduction elsewhere in the complexity of the molecular motion to keep the problem within practical bounds. The obvious choice was to eliminate any account of the rotational motion by limiting the collision geometry to one-dimensional collinear encounters. This procedure is commonly applied throughout the literature for similar reasons and is usually based on the presumption that collinear collisions are the most effective for inducing vibrational excitation. However, intuitive notions suggest that the inelasticity of three-dimensional collisions is partitioned among vibrational and rotational degrees of freedom in the molecule, in varying amounts, depending on the molecular inertial properties and the initial state. Kelly and Wolfsberg[24] have used a fully classical model to demonstrate that collinear

collisions are not always the most effective for converting vibrational energy. For example, atom collisions with molecules possessing widely spaced rotational states can induce vibrational transitions with very little energy converted to translational motion. Vibration-rotation energy transfer is then a more correct description of the event. On the other hand, a full account of the coupled vibration-rotation motion in a three-dimensional collision model must include at least all of the energetically accessible rotational states in each vibrational level. As a result, collision energies sufficient to induce vibrational transitions will encompass hundreds of multiply degenerate rotational states in most molecules. Since the occupation of each state must be treated as a separate variable, an extremely large system of coupled differential equations is required whose numerical solution is intractable for all but the simplest cases. Fortunately, some methods have recently been introduced that average the combined action of degenerate states and reduce the problem to an expensive, but tractable, size. Several of these methods are evaluated and applied here, in conjunction with a three-dimensional semiclassical collision model. From another point of view, the objective is to determine the consequences and validity of using a collinear one-dimensional model to predict the vibrational quantum number dependence of vibrational energy transfer rates. The results give considerable credibility to the preceding conclusions of this study derived from collinear models.

1.4 Overview of the Contents and Results

In chapter 2, the basic concepts and assumptions commonly applied in the analysis of vibrational energy transfer are reviewed. A brief historical review of vibrationally inelastic collision models is first presented that provides a guide to a number of more complete review papers. The concepts

and physical factors that control the rate of energy transfer are then discussed, and the several theoretical approaches from which the rates may be estimated are evaluated as they apply to the objectives of this study. The semiclassical approximation is shown to be the most suitable approach to the objectives previously stated.

Having established the primary theoretical approach to be one in which the incident particle path is computed classically, chapter 3 examines the features of the interaction potentials that determine both the internal molecular motion and the classical trajectory. Arguments are presented showing that a Morse-oscillator/rigid-rotor description of the molecule is adequate for the purposes of this study and that the classical trajectory may be determined from just the short-range repulsive forces between colliding nuclei.

In chapter 4, a collinear, semiclassical, collision model for predicting V-T transition probabilities from arbitrary initial states is developed and evaluated. Comparisons are made with equivalent, exact, fully quantum mechanical solutions obtained from the literature for a broad range of collision parameters, molecular types, and initial states. While similar comparisons have been made before, they have been less complete and limited to harmonic oscillator models of the molecule initially in the ground state. This work includes a more extensive variation of collision parameters and tests the application of the semiclassical approximation to an anharmonic Morse oscillator in several elevated initial states. In the past, there has been a variation of opinions on the best method of compensating for the lack of energy conservation in the semiclassical approximation. The comparisons of this study show that the correction is nearly the same from all methods suggested and no clear choice of the best method is possible — nor is a choice

necessary for they are all adequate in the range of collision energies of interest. Finally, the comparisons in chapter 4 bring to light the result that, while the semiclassical approximation works well for a broad range of collision parameters when the molecule is treated as a harmonic oscillator, the more realistic anharmonic oscillator model imposes some definite limitations. When the anharmonic oscillator is homonuclear and struck by a collision partner whose mass is less than either molecular nucleus, the semiclassical approximation is very successful. However, its application to heteronuclear molecules or to homonuclear molecules struck by a heavy collision partner produces anomalous resonances that do not appear in an equivalent harmonic oscillator model. These anomalies are partially eliminated when additional coupling between the oscillator and the incident particle is introduced.

With the limitations of the semiclassical approximation established for anharmonic oscillators, chapter 5 describes an investigation of the factors that influence the prediction of V-T rates for initially excited molecules. The capability of several analytic theories for reproducing rate coefficients predicted by a more exact numerical model is also evaluated. Unfortunately, the most widely used and simplest analytic formula also produces the poorest estimate of quantum number dependence. But two slightly less convenient analytic models are found to reproduce the more exact predictions for well-defined and easily identifiable ranges of conditions. Both favorable analytic models are based on a collinear semiclassical description of the collision.

The validity of the collinear collision models used in the previous chapters is evaluated in chapter 6 using a three-dimensional semiclassical model developed for that purpose. A complete model is first constructed that allows an arbitrary number of coupled vibration-rotation states to be included.

It provides a basis for evaluating the accuracy of some approximate formulations in which the combined effects of the degenerate projection states associated with each rotational quantum state are decoupled and treated collectively. The ability to decouple the degenerate states makes the objective of this part of the study possible. An "effective Hamiltonian" approximation is found to be the most useful, and it is applied to a study of the influence of rotational energy transfer on the rate of vibrational excitation. The results show that the effects of rotations can be segregated into three classes. For molecules like hydrogen or the hydrogen halides that have a rotational frequency only a magnitude smaller than the fundamental oscillator frequency, the rotational coupling is large and energy transfer can proceed via rotation-vibration transitions with very little conversion of translational energy. The behavior of molecules with these properties is further separable, depending on the initial angular momentum, but the use of a collinear collision geometry is physically unrealistic in any case and the corresponding analytic rate formulas are consequently of little value. On the other hand, the third and much larger class of molecules, in which a multitude of rotational levels is contained in each vibrational state, is not influenced by the accompanying rotational motion induced in a three-dimensional collision. Rate coefficients obtained from a collinear collision model then reproduce all of the physical features contained in the three-dimensional results and predict an essentially identical dependence on vibrational quantum number when compared with the net vibrational transition rate summed over all final rotational states. Correspondingly, the predictions for such molecules are also shown to be insensitive to the initial rotational state of the molecule. These results lend considerable credibility to the results from collinear collision models

and to the analytic solutions that depend on them. Finally, chapter 7 summarizes the new aspects of the results of this study and presents some considerations for additional theoretical and experimental study.

CHAPTER 2

CONCEPTS IN VIBRATIONAL ENERGY TRANSFER

In the preceding chapter, methods for describing the macroscopic behavior of a vibrational relaxation process were discussed. The microscopic aspects of the process were contained in a thermally averaged rate coefficient, $k_{v,v'}$, of undefined nature. The remainder of this study concentrates on the physical factors that affect $k_{v,v'}$ and on the theoretical models used to evaluate it.

This chapter provides a general discussion of the concepts leading to a theoretical model. A brief historical review is given first that provides a commentary on some pertinent publications describing the various concepts in greater detail. The latter part of this chapter defines the controlling dynamic and molecular parameters affecting $k_{v,v'}$ and reviews the general considerations leading to a choice for the fundamental theoretical approach to be applied in the remainder of this study.

2.1 Historical Summary and Review Literature Guide

In the 1930's and before, the anomalous absorption and dispersion of ultrasonic waves propagating in gases were the principal phenomena motivating the study of vibrational energy transfer. All fluids absorb ultrasonic waves through shear viscosity losses and, in most cases, through heat conduction. By those mechanisms, they all display a corresponding dispersion. However, molecular fluids (i.e., those with a capacity for internal-energy storage) have an additional absorption and dispersion originally accounted for by heuristically introducing a "bulk viscosity" into the Navier-Stokes equations that describe the process. Investigators soon recognized, however, that the artificial viscosity was a manifestation of internal-energy absorption in the

molecule. As early as 1928, Herzfeld and Rice[5] explained the origin of the additional absorption and dispersion conceptually in terms of collisional energy transfer between the translational and internal degrees of freedom at a finite rate. A few years later, Oldenberg[25] discussed molecular collisions qualitatively to show the inelasticity of rotational and vibrational motion. In 1931, Zener[3,26] was the first to give a detailed mathematical treatment for vibrationally inelastic collisions. His theory was based on a quantum mechanical perturbation method, referred to as a "distorted wave approximation," applicable to low collision energies where the transition probabilities are small. Then, in 1936, Landau and Teller[4] published their historic paper in which the properties of the rate coefficient were explored, again from a more conceptual point of view. They used partially intuitive arguments (with no reference to the earlier work) to show that equation (1.2) described the rudimentary dependence of $k_{v,v-1}$ on v and they obtained the equally important dependence of $k_{v,v-1}$ on temperature, given by $\log k_{v,v-1} \propto T^{-1/3}$.

Later, interest shifted away from theoretical work addressed to ultrasonic relaxation phenomena, but increased in the study of a very similar inelastic molecular collision problem. The accommodation coefficient, related to the energy transfer between gas molecules and a solid surface, was studied extensively, first by Jackson and his coworkers[27] and later by Lennard-Jones and his coworkers.[28] The paper by Jackson and Mott[27b] became particularly noteworthy because it provided a simplified mathematical derivation of the "distorted wave approximation" still referred to in modern texts.

Only a few contributions to the field of vibrational relaxation followed until the early 1950's. For example, one-dimensional treatments by Zener and other early investigators were extended to three-dimensional collisions.

After 1950, Takayanagi[29] introduced the "modified wave number" approximation designed to reduce the numerical labor in three-dimensional problems and applied it to rotational transitions in hydrogen. Meanwhile, Schwartz, Slawsky, and Herzfeld[30] published their well-known paper in which vibrational transitions were treated with the distorted wave approximation. Their closed-form analytic formulas for resonant and nonresonant transition probabilities in collinear collisison have become the most widely used means of estimation until recent times. Their formulation, often referred to as the SSH theory, was later extended to three-dimensional collisions but for a nonrotating molecule.[31]

Experimental methods for measuring vibrational relaxation times were also developing. Improved rate data were obtained from measurements in jets[32,33] and behind shock waves[34,35] at other than room temperatures. The existing perturbation theories were not always applicable to the analysis of these new experimental techniques, however, because the theories were limited to low-energy collisions pertaining mostly to near-room temperatures. In 1958, Kerner[36] obtained a nonperturbative exact solution to the Schrodinger equation for a harmonic oscillator in the presence of a time-dependent forcing function. The only constraint on the forcing function was that it be linear in the oscillator coordinate. Kerner's solution was subsequently applied by Treanor[37] in a semiclassical treatment of high-energy collinear collisions, thereby achieving an analytically exact formula in closed form for the transition probabilities of a harmonic oscillator at all collision energies.

The 1960's brought on a deluge of publications concerned with vibrational relaxation phenomena that has persisted to this day. So much experimental information became available that Millikan and White[38] were able to correlate

empirically vibrational relaxation times for a large number of diatomic molecules in terms of the fundamental oscillator frequency and the reduced mass of the collision pair. Their correlation was only modestly guided by theory, however. During this period, theoretical studies were stimulated by a rapidly growing computer technology. Consideration of exact numerical solutions to the collision problem became a reasonable occupation; but vibrationally inelastic solutions were awkward until Secrest and Johnson[39] developed a numerical method of "amplitude density functions" that allowed one-dimensional scattered wave functions to be obtained efficiently. Their methods have since been extended to treat three-dimensional collisions with vibrational and rotational inelasticity.[40]

The early 1960's also marked the appearance of some review articles of modern interest that describe the various theoretical approaches in detail. One of the first was the chapter by Herzfeld[41] on "Relaxation Phenomena in Gases." His discussion is based primarily on the application to ultrasonic absorption and dispersion, but he gives a clear account of the early theoretical approaches in which the fundamental collision parameters are described. He later provided a more complete account in textbook form.[6] Cottrell and McCoubrey[42] took a slightly more modern approach in their book by dealing with the quantum mechanical aspects of the collision process in greater detail. However, their discussion remains physically descriptive and valuable as an introduction to the theoretical approximations leading to analytic solutions. Takayanagi[43] provided the first comprehensive review of the theoretical aspects of vibrationally and rotationally inelastic collisions covering the period up to 1963. With the rapid developments in the field following 1963, Takayanagi[44]

published a second, equally comprehensive, review covering the developments to 1965.

The reviews published before 1965 preceded the time when exact quantal solutions for vibrationally inelastic collisions were obtainable with sufficient ease and confidence to serve as a basis for testing the approximate methods. Prior emphasis was directed toward the comparison of approximate theories with experiment as a test of their validity. A more recent review by Rapp and Kassal[45] was therefore addressed, in part, to an evaluation of the earlier theories by comparing them with exact numerical solutions. With the greatly increased detail of information about the collision dynamics in view, both from fully quantum mechanical and fully classical numerical solutions, Rapp and Kassal evaluate many of the assumptions contained in the approximate collision models and provide a useful guide to their range of applicability. Their article also deals with some aspects of modern interest such as the transfer of vibrational energy between oscillators and the effects of oscillator anharmonicity. However, at the time of Rapp and Kassal's writing, the new class of vibrational relaxation processes had not quite impacted the theoretical community. Their emphasis therefore centered on the dynamics of oscillators in or near the ground state.

The beginning of this decade brought in widespread efforts to deal with the new requirements in the analysis of vibrational energy transfer. Rich and Treanor[46] presented a comprehensive review of the aspects of vibrational relaxation in gasdynamic flows. Their discussion is devoted mainly to non-equilibrium flow processes and hence to an application of vibrational rate theories, but they also provide a detailed description of many aspects of

vibrational energy transfer that motivated this study and their review serves as an introduction to the new class of relaxation processes.

With numerical investigations now a practical and popular approach to molecular physics, this decade begins the era in which molecular collisions can be studied in much greater detail. Many of the new methods in "numerical physics" are described by Secrest[47] in a recent review of their application to rotational and vibrational energy transfer. Most methods are motivated by the need to reduce the numerical labor and expense. For example, activity in the use of fully classical calculations for reactive and vibrationally inelastic collisions has flourished with the development of "Monte Carlo" or random-selection methods for averaging the results of many trajectories and orientations.[48] Another new concept is the semiquantal approximation, developed independently by both Miller[49] and Marcus.[50] Also termed the "classical S-matrix" theory, the principal distinction of the semiquantal approach from earlier semiclassical methods is that, in the former, all degrees of freedom are treated classically but with the quantum-mechanical principle of superposition subsequently applied. While the method allows pure quantum effects such as tunneling, selection rules, and interference to be studied and has given reasonably accurate predictions for vibrationally inelastic collisions,[51] its limitations are not yet fully charted. Two reviews of the theory have recently been published by Miller.[52,53]

A final milestone that has contributed significantly to the results of this study is the success of several efforts to average the combined contributions of degenerate rotational states and thereby make the study of vibration-rotation interactions feasible. Forthcoming discussions in this study demonstrate the futility of a complete treatment of the problem. The first

successful solution to the problem was presented by Rabitz,[54] who formulated an "effective Hamiltonian" that nullifies the contribution of individual projection quantum states before the equations of motion are solved. Following his work, McGuire and Kouri[55] proposed a "j_z-conserving" approach of some similarity to the effective Hamiltonian approximation. A different method of reducing the rotational aspects of the problem has been studied by Pack and his coworkers,[56] who treat the rotational motion in a "sudden approximation," well known in its basic form from numerous modern textbooks on quantum mechanics. The relationship of all of these methods for decoupling the internal angular momentum of the molecule has recently been examined by Secrest.[57] These methods and their application represent a large part of the current activity in studies of vibrationally and rotationally inelastic collisions.

2.2 General Considerations

Considered in the following paragraphs are some of the general concepts and controlling parameters that form the basis of most theoretical models for collisions involving a diatomic molecule. The general features of several theoretical approaches are then reviewed to guide the choice of a method best suited to the intentions of this study.

2.2.1 Modes of Energy Transfer in Diatomic Molecules

Binary collisions involving a diatomic molecule are not yet treated in general terms entirely from first principles. *Ab initio* approaches to the many-body problem presented by three or more nuclei and their attendant electrons are still intractable on present-day computers. Fortunately, when electronic transitions are not of concern, an adequate collision model does not

require an explicit description of the coupled nuclear and electron motion but instead relies on the nearly instantaneous adjustment made by the electrons to the nuclear motion. The problem then reduces to one of describing only the dynamics of the nuclear motion during a collision but requires interaction potentials independently obtained by some less rigorous means.

In this study, our interest is further restricted to collisions only of a diatomic molecule with a heavy structureless particle such as an atom in its ground electronic state. The inelasticity of the collision is then confined to the internal rotational and vibrational energy modes of just one molecule and we avoid the complexity of dealing with the exchange of internal energy between molecules. Energy transfer still occurs to any of several internal modes, however, as figure 2.1 illustrates. A characteristic of most diatomic molecules is the widely separated vibrational eigenenergies (heavy line levels in fig. 2.1), each with a manifold of closely spaced rotational states (light

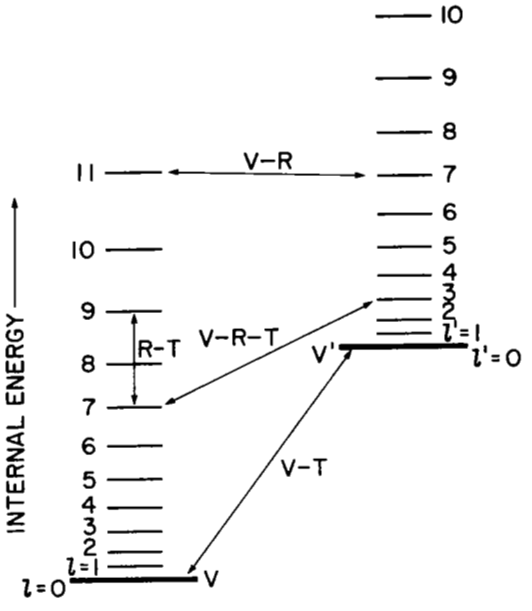

Figure 2.1.- Modes of energy transfer in a diatomic molecule.

line levels in fig. 2.1). Thus, a collision with sufficient energy to excite vibrational motion in the molecule will simultaneously excite many rotational states as well. The arrow labeled V-R-T (vibration-rotation-translation) in figure 2.1 typifies those kinds of transitions. The internal energy change appearing in the molecule will be reflected as a change in the translational energy of the colliding pair. While a complete description of V-R-T energy transfer is complex, certain limited paths for energy transfer are often the dominant mechanism and they can then be treated separately. For example, near-resonant transitions between vibration-rotation states (V-R in fig. 2.1) may be dominant in some molecules with a suitable initial condition. In this case, any energy traded with translation appears only as an elastic deflection after the encounter. In another situation, the small amount of energy required to induce a rotational transition within the same vibrational state makes the exchange of rotational and translational energies (R-T in fig. 2.1) probable at collision energies where the vibrational state of the molecule may be ignored. The molecule is treated as a rigid rotor in such circumstances. The analyses of these limited cases involving rotation are usually simpler than

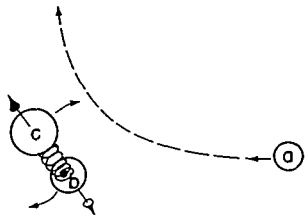

(a) Three-dimensional encounter.

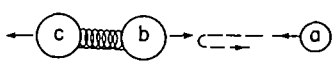

(b) One-dimensional collinear encounter.

Figure 2.2.- Collisional motion.

cannot be applied in a collinear collision model because b or Ω are not

the general case, but a three-dimensional collision geometry is still required as shown in fig. 2.2(a). In contrast, an even simpler but more restricted treatment of the collision is one in which no rotational transition occurs. Translational energy is exchanged only with vibration (V-T in fig. 2.1). Events of this nature can occur in a three-dimensional encounter of arbitrary orientation because transitions always take place with a probability less than unity (making no rotational transition also probable), but a frequently used approach that drastically reduces the complexity of the problem is to assume that the most efficient producers of vibrational transitions are collisions with trajectories along the intranuclear axis of a nonrotating molecule. The corresponding one-dimensional collinear geometry is illustrated in figure 2.2(b). As it turns out, we shall find in this study that the collinear

$$k(T)_{v\to v'} = (8kT/\pi\mu)^{1/2} \int_0^\infty \sigma(E)_{v\to v'} \frac{E}{kT} e^{-E/kT} d\left(\frac{E}{kT}\right) \tag{2.2}$$

where unsubscripted k is Boltzmann's constant and μ is the reduced mass of the collision. If m_i denotes the mass of nucleus i, then, using the notation in figure 2,

$$\mu = \frac{m_a(m_b + m_c)}{(m_a + m_b + m_c)} \tag{2.3}$$

Methods of performing the integrals in equations (2.1) and (2.2) are discussed in greater detail in chapters 5 and 6 where specific applications are made. At this point, one only needs to recognize that obtaining the transition probability, $P(E,b)_{v\to v'}$, from a semiclassical treatment or the differential cross section, $d\sigma/d\Omega$, from a full quantum mechanical treatment is the fundamental problem. Once either of these results is obtained, a calculation of the corresponding rate coefficients is relatively straightforward.

2.2.3 Controlling Variables in Vibrational Energy Transfer

For a collision to affect the vibrational motion of an oscillator, the disturbing force created by the impacting particle must vary in a time period

line levels in fig. 2.1). Thus, a collision with sufficient energy to excite vibrational motion in the molecule will simultaneously excite many rotational states as well. The arrow labeled V-R-T (vibration-rotation-translation) in figure 2.1 typifies those kinds of transitions. The internal energy change appearing in the molecule will be reflected as a change in the translational energy of the colliding pair. While a complete description of V-R-T energy transfer is complex, certain limited paths for energy transfer are often the dominant mechanism and they can then be treated separately. For example, near-resonant transitions between vibration-rotation states (V-R in fig. 2.1) may be dominant in some molecules with a suitable initial condition. In this case, any energy traded with translation appears only as an elastic deflection after the encounter. In another situation, the small amount of energy required to induce a rotational transition within the same vibrational state makes the exchange of rotational and translational energies (R-T in fig. 2.1) probable at collision energies where the vibrational state of the molecule may be ignored. The molecule is treated as a rigid rotor in such circumstances. The analyses of these limited cases involving rotation are usually simpler than

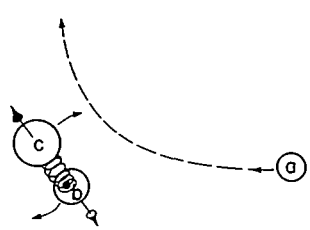

(a) Three-dimensional encounter.

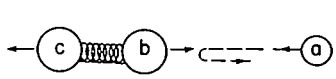

(b) One-dimensional collinear encounter.

Figure 2.2.- Collisional motion.

the general case, but a three-dimensional collision geometry is still required as shown in fig. 2.2(a). In contrast, an even simpler but more restricted treatment of the collision is one in which no rotational transition occurs. Translational energy is exchanged only with vibration (V-T in fig. 2.1). Events of this nature can occur in a three-dimensional encounter of arbitrary orientation because transitions always take place with a probability less than unity (making no rotational transition also probable), but a frequently used approach that drastically reduces the complexity of the problem is to assume that the most efficient producers of vibrational transitions are collisions with trajectories along the intranuclear axis of a nonrotating molecule. The corresponding one-dimensional collinear geometry is illustrated in figure 2.2(b). As it turns out, we shall find in this study that the collinear collision model is surprisingly useful for predicting the rate of vibrational energy transfer when many rotational states are associated with each vibrational mode. Unfortunately, the incomplete nature of the collinear model makes it awkward to obtain a rate coefficient from the detailed collision dynamics calculated, whereas rate coefficients evolve naturally from the results of a three-dimensional model, as the following discussion demonstrates.

2.2.2 Rate Coefficients from the Collision Dynamics

The relationships between a thermally averaged rate coefficient and the results of a microscopic collision model depend somewhat on the theoretical description used to model the collision. For example, a semiclassical formulation in which the incident particle trajectory is obtained from the classical equations of motion deals with collisions characterized by the parameters E and b, where E is the initial, relative, kinetic energy in a center-of-mass reference frame and b is the impact parameter measuring the minimum distance

between mass centers of each collision partner that would occur if the relative path were not deflected. The outcome is a transition probability, $P_{v\to v'}(E,b)$ between each pair of internal quantum states, v and v', included in the molecular model. A necessary step in obtaining the corresponding rate coefficient is to first produce the total cross section, $\sigma_{v\to v'}(E)$. In the semiclassical framework, a total cross section may be generated by repeating the calculation for a sufficient range of impact parameters to evaluate the integral

$$\sigma_{v\to v'}(E) = \int_0^\infty P_{v\to v'}(E,b)\ 2\pi b\ db \qquad (2.1)$$

Likewise, a fully quantum mechanical description of both the molecule and incident particle motion follows a similar procedure. However, the incident particle path is not localized so the collision must be characterized instead by E and a final scattering direction, Ω. The outcome is a differential cross section $d\sigma/d\Omega$, which may be computed for all elemental solid angles and integrated over the sphere by an expression similar to equation (2.1). In contrast to any three-dimensional method, equation (2.1) or its equivalent cannot be applied in a collinear collision model because b or Ω are not included variables. Thus, obtaining $\sigma_{v\to v'}(E)$ from a collinear description requires some kind of "steric factor" on an "effective hard-sphere cross section" to be introduced. These additional artifacts are discussed in greater detail in chapters 5 and 6 where collinear collision models are evaluated.

Once the cross section is in hand, the desired rate coefficient for $v \to v'$ transitions is obtained by averaging the energy-dependent total cross sections over a thermal energy distribution characterized by a kinetic temperature T. Remembering that E is the *relative* kinetic energy in a center-of-mass frame, the result is[8]

$$k(T)_{v\to v'} = (8kT/\pi\mu)^{1/2} \int_0^\infty \sigma(E)_{v\to v'} \frac{E}{kT} e^{-E/kT} d\left(\frac{E}{kT}\right) \tag{2.2}$$

where unsubscripted k is Boltzmann's constant and μ is the reduced mass of the collision. If m_i denotes the mass of nucleus i, then, using the notation in figure 2,

$$\mu = \frac{m_a(m_b + m_c)}{(m_a + m_b + m_c)} \tag{2.3}$$

Methods of performing the integrals in equations (2.1) and (2.2) are discussed in greater detail in chapters 5 and 6 where specific applications are made. At this point, one only needs to recognize that obtaining the transition probability, $P(E,b)_{v\to v'}$, from a semiclassical treatment or the differential cross section, $d\sigma/d\Omega$, from a full quantum mechanical treatment is the fundamental problem. Once either of these results is obtained, a calculation of the corresponding rate coefficients is relatively straightforward.

2.2.3 Controlling Variables in Vibrational Energy Transfer

For a collision to affect the vibrational motion of an oscillator, the disturbing force created by the impacting particle must vary in a time period that is comparable with or less than the normal oscillator period. Otherwise, a slowly applied disturbance simply allows the oscillator to adjust adiabatically, leaving its final condition unaffected by the encounter. Conversely, an impulsively applied force will severely disturb the phase of the oscillator motion and efficiently upset the proportions of energy in vibration, rotation, and translation. These conditions can be expressed more explicitly by denoting a representative time interval in which the colliding pair interact as τ_c and letting ν_o represent the fundamental oscillator frequency. We then

argue that energy transfer will occur with increased efficiency as τ_c becomes less than the oscillator period $1/\nu_o$, that is, $\tau_c\nu_o \to 0$. One way to evaluate the magnitude of τ_c is by noting that the interaction distance for collisions influenced mainly by repulsive forces can be loosely measured in terms of a range parameter L. Then $\tau_c \approx 2L/u$, where u is the average relative collision speed. If the relative kinetic energy is E and μ is the reduced mass, then the relative collision speed is $\sqrt{(2E/\mu)}$ and the efficiency of energy transfer will increase as

$$L\nu_o\sqrt{\frac{2\mu}{E}} \to 0 \tag{2.4}$$

We should therefore expect the quantities related to the efficiency of energy transfer, such as $P(E,b)_{v\to v'}$ and $\sigma(E)_{v\to v'}$, to increase with E and to decrease as the oscillator frequency, interaction range, or nuclear masses are made larger. Note that the impact parameter, b, could also serve as a measure of the interaction range when it exceeds L. Collisions at increasing b will become more adiabatic with an accompanying decrease in $P(E,b)_{v\to v'}$.

The preceding relationships are sometimes described in terms of an "adiabaticity parameter"

$$\xi = \tau_c\nu_o = L\nu_o\sqrt{\frac{2\mu}{E}} \tag{2.5}$$

The larger ξ becomes, the more adiabatic is the encounter. Values of ξ below unity lie in the "sudden" region. Similar ideas are applied to rotational motion as well simply by replacing ν_o with the fundamental rotational frequency, ν_r. Note that in many molecules, $\nu_o >> \nu_r$ so that collisions in some energy range may be adiabatic with regard to vibrations while sudden in respect to rotations.

The effects of varying ξ can be made slightly more quantitative by considering its sequel, the "resonance function," $R(\xi)$, a measure of the efficiency of energy transfer. If $\Delta E(\xi)$ is the average energy transferred in a collision characterized by ξ, we can define

$$R(\xi) = \Delta E(\xi)/\Delta E(\xi = 0) \tag{2.6}$$

where $\Delta E(\xi = 0)$ is the energy transferred in the sudden limit. Although the computation of $R(\xi)$ requires a solution of the detailed equations of motion, the outcome for atom-molecule collisions appears approximately as

$$R(\xi) \approx e^{-\xi} \tag{2.7}$$

Hence the efficiency of energy transfer can be expected to decrease exponentially as the encounter becomes more adiabatic. This feature will manifest itself in the following chapters by the use of semilogarithmic plots for all quantities related to $R(\xi)$ when plotted as functions of the variables contained in ξ.

2.3 *Theoretical Methods for Modeling Collision Dynamics*

The preceding discussion made use of simple conceptual arguments to characterize the collisional transfer of energy, but an estimate of the amount of energy transferred can be obtained only from a detailed solution of the equations of motion. The motion is customarily described in the literature using one of three levels of quantization: (1) a fully classical treatment in which quantization is imposed artificially on the internal energy of the molecule before (and sometimes after) the collision, (2) a semiclassical approximation in which the path of the incident particle is obtained classically but the molecule response is handled quantum mechanically, and (3) a fully quantum-mechanical formulation in which all members of the system are represented in a quantum-mechanical wave equation. (A fourth intermediate level of quantization

might also be given as the semiquantal method developed by Miller[49] and Marcus[50] in which the phase distortions of the motion are obtained classically but subsequently treated quantum mechanically. The validity of the semiquantal approximation in treating vibrational energy transfer is still a topic for study, but it appears to give satisfactory results for the few examples examined[51,58-62] and has several advantages worthy of consideration. At the time this study was begun, however, the implications of the semiquantal approximation were not clearly established, precluding its further consideration here.) To choose the most suitable theoretical method for meeting the objectives of this study, we now briefly consider the general features of each of the three principal methods of approach.

2.3.1 Classical Collision Theories

A large number of fully classical calculations for collisions involving the vibrational and rotational motion of a diatomic molecule have been carried out in recent times.[24,48,63-67] Modern results have shown that, when the oscillator zero-point energy is included (a quantum limit to the minimum vibrational energy), classical calculations for the total transfer of vibrational energy reproduce the equivalent quantal predictions quite well. This is not too surprising if one notes that the transfer of vibrational energy does not depend on any pure quantum effects such as tunneling or wave interference. However, a kind of quantum effect is ignored in a classical treatment when a continuum of energy is transferred to the molecule without restriction to discrete quantum increments. Collision energies in a moderate thermal range excite only a few vibrational quanta so that the partitioning of energy into widely separated quantized levels, excluded in a classical treatment, may have some influence on the molecular motion. The validity of a classical

description that ignores these effects is not clear. For rotational motion, quantum selection rules impose clearly identified limitations on the path of energy transfer throughout the internal states of the molecule. The effects of these limitations on the total energy transferred are not very severe in molecules where the rotational energy spacing is small and continuum-like but, again, the criteria for treating the rotational motion classically are not obvious. Finally, a classical description of the collision dynamics reveals only the total energy transferred to the molecule, but it provides no rigorous description of the manner in which the energy is partitioned among quantized internal states. Since the objectives of this study pertain specifically to the rate of energy transfer to individual internal states, a classical collision model would require considerable interpretation to produce such results. Hence the use of a fully classical description of the collision dynamics does not appear to be suitable for this study and no further consideration has been given to it.

2.3.2 Quantum-Mechanical Theories

Fully quantum-mechanical calculations of vibrational and rotational energy transfer have also been abundant in recent literature.[39,40,54-56,68] As the opposite extreme to classical treatments, they contain a complete description of the energy deposition and provide an exact basis for comparison with more approximate methods. The difficulties associated with a full quantal formulation lie mainly in the mathematical and numerical requirements to obtain a solution. The radial motion of the system is governed by a linear second-order differential equation with at least two independent variables. A numerical solution involves matrix manipulation and quadrature integration. While general methods for dealing with these numerical aspects have

become highly developed, their incorporation into a complete algorithm for the collision process is not an inviting task. Even putting that inconvenience aside, the experience of others[54-56] has shown that the computing time necessary to reach a complete solution varies as the *cube* of the number of coupled molecular internal states included in the calculation. For calculations involving both vibrational and rotational states, this cubic dependence has been the primary factor restricting comprehensive studies of the energy transfer for all but a few special molecules like H_2. To impose similar limitations on this study would yield results little different from previous work.

Several approximations to the quantal formulation have been devised which allow solutions to be obtained with less effort. The recently developed semiquantal method[49,50] is one example, but a much older and more easily applied approximation is the "distorted wave" approach first proposed by Zener[3,26] and later reformulated by Jackson and Mott.[27b] We briefly mention the distorted wave approximation here to show that it too is not the best choice for the purposes of this study even though it retains much of the "exactness" of a full quantal solution. The approximation has been applied in the past both to collinear collision models[42] and to three-dimensional rotational models.[43] Generally, it is a perturbation method that may be carried to arbitrary order, but its greatest advantage is realized by retaining just the first-order term. As with all first-order perturbation solutions, the results are accurate only when transition probabilities and interactions between nonadjacent states are small. This study of excited-state transitions, in which single-quantum transitions are expected to be large and multiple-quantum transitions to be important, would then require at least a second-order theory for accuracy. The distorted wave approximation is therefore not an attractive choice here.

2.3.3 Semiclassical Collision Model

A semiclassical or "impact-parameter" method for treating the collision dynamics has several attractive features that promote its selection as the primary theoretical approach in this study. For one, it retains all the quantum-mechanical aspects of energy transfer within the internal states of the molecule that are absent in a classical treatment while avoiding most of the mathematical difficulties associated with a full quantal solution. In the semiclassical approximation, the Schrodinger equation describing the collision may be reduced to three, coupled, time-dependent, first-order, linear, differential equations — one describing the molecular wave-function dynamics and two classical trajectory equations for the relative motion of the incident particle. When the trajectory and wave equations are uncoupled, the trajectory equations may be exactly integrated analytically for collinear encounters and approximately for spherically symmetric interactions. Clearly, these reductions relax the numerical requirements considerably. Furthermore, the reduction to obtain first-order differential equations affords a second, and perhaps more significant, advantage to the semiclassical formulation because the computation time then varies with the *square* of the number of coupled channels, making feasible the calculation of much larger sets than might be considered with a full quantal method.

From another viewpoint, the ability to separate the motion of each collision partner in a semiclassical formulation allows analytic solutions to be obtained for the final state of the molecule if some further approximations are made. The usefulness of these more approximate analytic solutions was discussed in chapter 1, but their accuracy requires validation. The validation is done most convincingly by comparing the analytic predictions with

numerical solutions in which the trajectories are also obtained classically. By choosing a general semiclassical approach, such comparisons may be included as part of the results of this study. However, before a classical description of the incident particle motion can be justified, several restrictive criteria must be met. The following section delineates the pertinent criteria that apply to vibrationally inelastic collisions.

2.4 Basic Criteria for the Semiclassical Approximation

A detailed derivation of the semiclassical equations of motion is presented in appendix B. In this section, we shall discuss only the general criteria necessary to justify a semiclassical formulation.

The conditions for the validity of semiclassical theory have been examined for numerous applications in the past by many authors; but recently, Delos *et al.*[69,70] reported a careful and detailed reexamination that revealed some of the implications and restrictions of a semiclassical collision model in much greater depth. They show that the classical trajectory equations may be obtained in two fundamentally separate ways: one based on a classical wave-packet description involving the correspondence principle, and one that makes no reference to a conventional classical picture but is based on an extension of the usual WKB approximation. Their work was motivated by the observation that semiclassical models work well even at collision energies too low to justify a localized wave-packet description of the incident particle. Indeed, they found, by comparison with the second method for obtaining the same classical equations, that criteria based on the localized wave-packet concept were overly restrictive. Specifically, in the classical wave-packet picture, the correspondence principle leads to the classical trajectory equations only if

$$(\lambda/L)^{1/2} << 1 \tag{2.8}$$

where λ is the de Broglie wavelength and L is the range of the collision interaction. On the other hand, the WKB approach yields the classical trajectory equations by requiring the weaker condition

$$\lambda/L << 1 \tag{2.9}$$

Thus, Delos *et al.* conclude that, even when a classical picture involving the correspondence principle is not justified, the classical trajectory equations may still produce a reasonable description of the final molecular state. They suggest that the classical trajectory equations are implicitly more fundamental to the collision dynamics than just in the correspondence limit. The comparisons of semiclassical and quantum-mechanical collision models for harmonic oscillators by Rapp and Kassal[45] and for anharmonic oscillators in chapter 4 support these conclusions. For example, in chapter 4, typical threshold collision energies for a single vibrational quantum transition correspond to $\lambda/L \approx 1$, which violates even equation (2.9), and yet the semiclassical and full quantal predictions appear identical. Delos *et al.* warn that by the same rule, however, a classical interpretation of the computed oscillator dynamics during intermediate times in the collision should not be given unwarranted value for conditions outside equation (2.8). Since all comparisons to date have examined only the predictions of final oscillator states, no conclusions can be inferred about intermediate times. These warnings suggest some caution when coupling the classical trajectory to the molecular dynamics, for example.

Delos *et al.* continue by showing that equation (2.9) is not the only criterion necessary to validate a semiclassical theory. They state two further requirements that, in combination, demand that the elastic collision trajectory for all channels (internal molecular states) be approximately the same.

These criteria are most restrictive when several potential energy surfaces are considered and when the system is allowed to cross from one surface to another; but the applications here, where reactive collisions and electronic transitions are not considered, require only a single interaction surface. These additional criteria then reduce to the stipulation that the difference in diagonal matrix elements defined by the instantaneous state of the molecule and by the interaction potential be small. Thus, if V'_{kk} is the instantaneous diagonal matrix element for state k, the criteria requiring similar elastic trajectories may be expressed by

$$\left|\frac{V'_{nn} - V'_{kk}}{V'_{nn} + V'_{kk}}\right| << 1 \qquad (2.10)$$

With simple exponential interactions of the type most commonly used (see ch. 3 for examples), V'_{kk} varies with k primarily as a result of vibrational anharmonicity. When the molecule is treated as a harmonic oscillator and the interaction potential is also linear in the oscillator coordinate, V'_{kk} is identical for all k and equation (2.10) is satisfied precisely. Conversely, we can expect the results of a semiclassical treatment of anharmonic oscillators with nonlinear interactions to compare differently with their full quantal counterparts than found in similar comparisons using harmonic oscillators. On the other hand, V'_{kk} varies only weakly with k for most molecules because the vibrational anharmonicity is generally small. Hence a semiclassical model of anharmonic oscillators can still be expected to retain a large measure of accuracy provided the differences $V'_{nn} - V'_{kk}$ remain small.

With the preceding criteria in mind, we shall adopt a semiclassical formulation throughout this study. However, since the criteria given by equations (2.9) and (2.10) are not quantitatively explicit in establishing the

range of collision parameters and molecular properties that may be suitably applied in such a method, much more explicit statements regarding the validity of a semiclassical collision model will be obtained from the results in chapter 4. Before proceeding with numerical solutions, however, the intramolecular potential determining the molecular dynamics and the collision interaction potential determining the perturbing forces on the molecules must first be modeled. Chapter 3 describes these potential models and the considerations leading to them.

CHAPTER 3

INTRAMOLECULAR AND COLLISION-INTERACTION POTENTIALS

A rudimentary aspect of any collision model is the description of forces acting between elements of the system. In this study, three separate nuclei constitute the system and, in principle, the forces acting on any one of them depend on the relative positions of all three. In practice, however, a self-consistent potential surface is rarely known, except for the simplest systems. Instead, the potential surface is usually constructed in a semiempirical manner using simpler concepts. To that end, we follow the conventional technique of considering only independent pairwise interactions. The potential surface is then separable into three additive components, each dependent on only the distance between two nuclei. Two of the components include the incident particle as one nucleus and are classified here as "collision-interaction potentials." The third component is between the two bound molecular nuclei and termed here the "intramolecular potential." Both types are modeled individually below.

3.1 Intramolecular Potential

Since only pairwise interactions are considered, the intramolecular potential is independent of the disturbance to the molecule brought by a collision. The potential model is therefore based on the spectral properties of an undisturbed molecule.

3.1.1 Vibrational Anharmonicity

The importance of vibrational anharmonicity in the intramolecular motion has been emphasized several times in previous chapters and its inclusion has

been stated as a basic feature of this study. Anharmonicity will manifest itself in the molecular model by the appearance of second- and higher-order terms in the expression for vibrational eigenenergies. A minimum example is then

$$E_v/\hbar = \omega_e\left(v + \frac{1}{2}\right) - \omega_e x_e\left(v + \frac{1}{2}\right)^2 \tag{3.1}$$

The first term in equation (3.1) is the familiar result obtained for a harmonic oscillator potential of the form

$$V_o(r) = \frac{1}{2}\,\mu_o\omega_e(r - r_e)^2 \tag{3.2}$$

where μ_o is the reduced mass of the oscillator, r is the internuclear separation, and r_e is the equilibrium separation. Numerous potential functions will produce an anharmonic term identifiable with the second term in equation (3.1). In fact, any potential function with a higher-order dependence on $r - r_e$ than equation (3.2) will do. However, two highly desirable additional features of the potential function are (1) that it realistically represent a real molecule for all separations to dissociation and (2) that it be of an analytically convenient form. Again, several potential functions have been proposed that fit these requirements (see ref. 71, ch. 5, for examples). One example that has received perhaps the greatest attention since its conception is that proposed by Morse[72] in the form

$$V_o(r) = D_o\left[e^{-2a(r-r_e)} - 2e^{-a(r-r_e)}\right] \tag{3.3}$$

In the absence of molecular rotation, Morse obtained eigenenergies approximated by equation (3.1) plus higher-order terms that are clearly negligible for all diatomic molecules. The potential constants are related to the oscillator frequency and anharmonicity by

$$D_o = \hbar\omega_e^2/4\omega_e x_e \tag{3.4}$$

and

$$a = (2\mu_o\omega_e x_e/\hbar)^{1/2} \tag{3.5}$$

Morse went further to show that if the steady-state wave function is separated according to

$$\psi(r,\theta,\phi) = \frac{R_v(r)}{r} Y_{\ell m}(\theta,\phi) \tag{3.6}$$

where $Y_{\ell m}(\theta,\phi)$ is a normalized spherical harmonic function in the polar angles θ and ϕ, then an analytic solution to the radial wave equation is obtained for integer values of v given by

$$\left.\begin{aligned} R_v(r) &= N_v\, e^{-z/2} z^{b'/2} L_v^{b'}(z) \\ \text{where} \qquad z &= k'\, e^{-a(r-r_e)} \\ N_v &= [ab'\Gamma(v+1)/\Gamma(k'-v)]^{1/2} \end{aligned}\right\} \tag{3.7}$$

and $L_v^b(z)$ is the Laguerre polynomial[73]

$$L_v^{b'}(z) = \sum_{m=0}^{v} \frac{(-1)^{m+v}}{m!\,(v-m)!} \frac{\Gamma(k'-v)}{\Gamma(k'-2v+m)} z^m \tag{3.8}$$

The parameters k' and b' are defined in terms of the oscillator frequencies by

$$k' = 2(2\mu_o D_o)^{1/2}/a\hbar = \omega_e/\omega_e x_e \tag{3.9}$$

and

$$b' = k' - 2v - 1 \tag{3.10}$$

The Morse potential is not as accurate as other more recent models (e.g., the function proposed by Hulburt and Hirschfelder[76]), but its analytic convenience has made its appearance in the literature seemingly second in popularity only to the harmonic oscillator. Figure 3.1 illustrates a comparison of the Morse function for the hydrogen molecule with a more accurate numerical

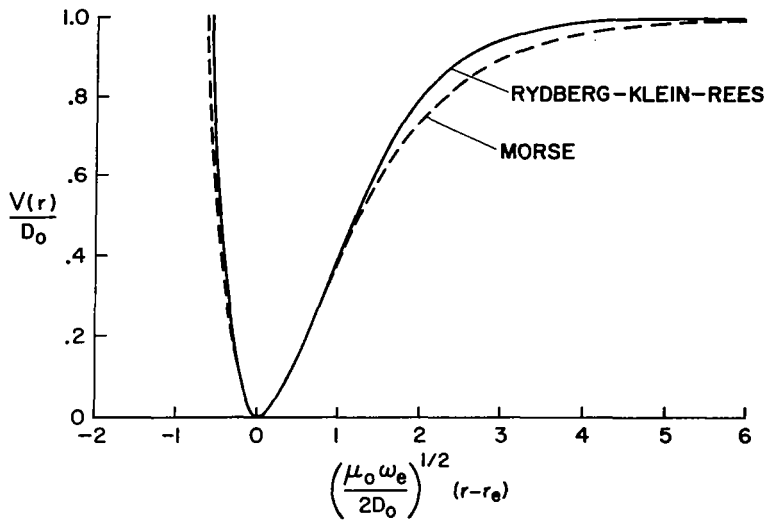

Figure 3.1- Intramolecular potential functions for H_2 (taken from ref. 74, based on ref. 75).

representation obtained by the Rydberg-Klein-Rees method[74,75] of analyzing spectroscopic information. Hydrogen is an example in which the Morse potential appears at its worst because of the high degree of anharmonicity associated with H_2. Figure 3.1 suggests that the Morse potential model should reproduce the molecular properties accurately for vibrational energies at least up to $E_v \lesssim D_o/2$. However, a comprehensive comparison for H_2 is difficult because high-lying vibrational energies in H_2 are not available. They are available for CO, however, where they have recently been measured up to $v = 37$ using laser-spectroscopy techniques.[77,78] Figure 3.2 compares vibrational energies of CO, obtained from the laser measurements and defined by terms up to sixth order, with the second-order Morse expression. As expected, values of $E_v \lesssim D_o/2$ are reproduced by the Morse function with reasonable accuracy. We should note at this point, however, that eigenenergies are not as sensitive to variations in the intramolecular potential as are the wave functions or their overlap integrals used in collision theory. Thus the measure of accuracy

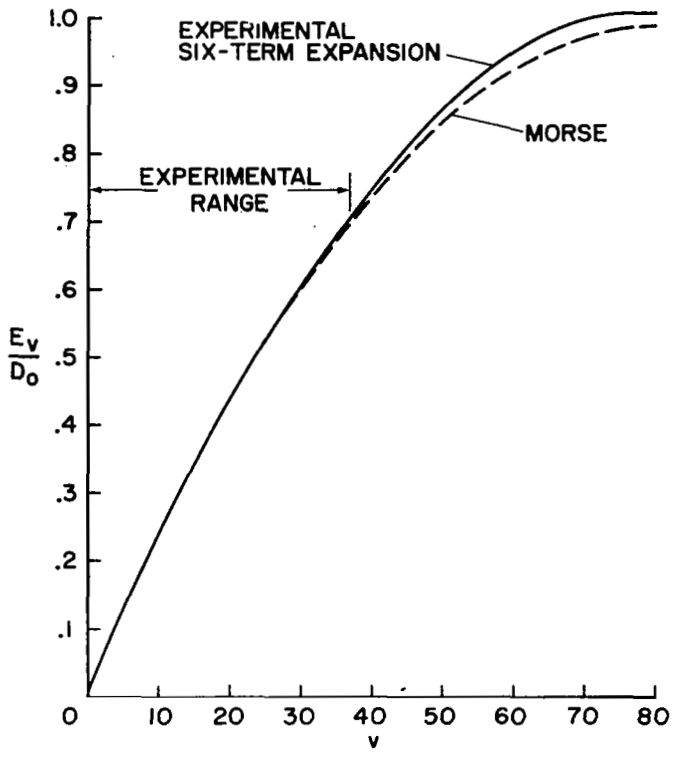

Figure 3.2.- Vibration eigenenergies of CO (D_o = 11.108 eV).

suggested by figures 3.1 and 3.2 is not entirely representative of the corresponding accuracy given to a collisional model. Nevertheless, in view of the other inaccuracies inherent in the collision model, the Morse function has been adopted here as a sufficiently realistic intramolecular potential model.

3.1.2 Vibration-Rotation Coupling

A remaining question regarding the molecular model pertains to its rotational characteristics. In a classical picture, the vibrational and rotational motion of the molecule are clearly coupled. A quantum-mechanical description of the molecule will produce corresponding coupling terms in the wave functions and eigenenergies associated with vibration and rotation. The

task is to determine the degree of coupling that must be retained for the purposes of this study.

Pekeris[79] has solved the steady-state radial wave equation for a Morse potential with the rotational terms included. His results can be reformulated to better show the influence of vibration-rotation coupling in the following way: to second order, the radial wave function obtained by Pekeris is similar in form to equation (3.7). Part of the difference lies in the parameters, b' and k', which depend now on the rotational quantum number ℓ. Denoting the ℓ-dependent parameters as b_ℓ and k_ℓ, they are related to the values b' and k' given previously for a nonrotating molecule by

$$k_\ell = k'(1 + c_\ell)^{1/2} \tag{3.11}$$

$$b_\ell = k_\ell\left(\frac{1 - c'_\ell}{1 + c_\ell}\right) - 2v - 1 \tag{3.12}$$

where

$$\left.\begin{aligned} c_\ell &= A_\ell(3/ar_e - 1) \\ c'_\ell &= A_\ell(2 - 3/ar_e) \end{aligned}\right\} \tag{3.13}$$

and

$$A_\ell = \ell(\ell + 1)2\hbar^2/(\mu_o a r_e{}^3 D_o) \tag{3.14}$$

In this extended notation, the radial wave function becomes

$$R_{v\ell}(r) = N_{v\ell}\, e^{-A_\ell z/2}(A_\ell z)^{b_\ell/2} L_v{}^{b_\ell}(A_\ell z) \tag{3.15}$$

in which $z = k\, e^{-a(r-r_e)}$ as before and $N_{v\ell} = [ab_\ell\Gamma(v + 1)/\Gamma(k_\ell - v)]^{1/2}$. As equation (3.15) shows, the wave function is distorted by A_ℓ in the coordinate z.

To evaluate the effect of vibration-rotation coupling on the molecular model, equation (3.15) must be used in place of equation (3.7) when computing

the appropriate overlap integrals appearing in the collision theory formulation. Obviously, that kind of evaluation can be made only in retrospect after the collision theory has been formulated in detail. However, at this point, we are at least able to indicate the extent of the coupling by computing the magnitudes of the corrections to b' and k' and the distortion of the wave function introduced by A_ℓ. Choosing the properties of CO as an example and defining $\ell \leq 40$ as the range of interest, we find that, for $\ell = 40$,

$$k_\ell/k' = 0.997, \quad b_\ell = 0.96k - 2v - 1, \quad A_\ell = 1.05$$

The overlap integrals are sensitive to small changes in the wave function so the effect of these small corrections is not clear; but one can see that the influence of rotational coupling is not a major aspect of the vibrational motion.

The initial choice of a method for describing the molecular properties in this study was guided by a less sensitive but readily evaluated measure of the vibration-rotation coupling. The eigenenergy terms associated with vibration-rotation coupling were compared with those resulting from vibrational anharmonicity. The objective was to decide if vibration-rotation coupling should be included to maintain a consistent degree of accuracy in the eigenenergy expression. The energy expression corresponding to the second-order radial solution given by equation (3.15) was shown by Pekeris[79] to be

$$E_{v\ell}/\hbar = \omega_e\left(v+\frac{1}{2}\right) - \omega_e x_e\left(v+\frac{1}{2}\right)^2 + \ell(\ell+1)B_e - \ell(\ell+1)\left[\alpha_e\left(v+\frac{1}{2}\right) + D_e\ell(\ell+1)\right] \tag{3.16}$$

We can then ask for what values of ℓ is

$$\omega_e x_e\left(v+\frac{1}{2}\right)^2 \leq \ell(\ell+1)\left[\alpha_e\left(v+\frac{1}{2}\right) + D_e\ell(\ell+1)\right] \quad ?$$

Again, using spectroscopic constants for CO, the rotational coupling terms equal or exceed the anharmonic terms when $\ell(\ell + 1) \gtrsim 623[v + (1/2)]$. The following table lists some sample values.

TABLE 3.1.- ROTATIONAL QUANTUM STATES WITH SECOND-ORDER CORRECTIONS COMPARABLE TO THE ANHARMONIC CORRECTION FOR CO

v	ℓ	$x_e\left(v + \frac{1}{2}\right)$
0	17	0.006
1	30	.009
2	39	.012
5	58	.031
10	80	.062
20	113	.124

Thus, for $\ell \geq 40$, the second-order rotational terms are comparable only with anharmonic terms for the first few vibrational states. The third entry in table 3.1 is a measure of the anharmonicity correction that may be compared with unity. For the first few vibrational states, it is much less than unity and we may therefore conclude that, while a completely consistent molecular model should contain vibration-rotation coupling terms, their influence on the molecular dynamics is not expected to be large in any case. At the time the molecular model was formulated for this study, the small amount of added complexity introduced by the vibration-rotation coupling terms appeared to be greater and a Morse-oscillator/rigid-rotor description was chosen to ensure analytic progress. The eigenenergies are then expressed by

$$\frac{E_{v\ell}}{\hbar} = \omega_e\left(v + \frac{1}{2}\right) - \omega_e x_e\left(v + \frac{1}{2}\right)^2 + \ell(\ell + 1)B_e \tag{3.17}$$

and the steady-state radial wave function is given by equation (3.7). In retrospect, the coupled expressions of Pekeris given by equations (3.15) and (3.16) would have required additional computational effort, but they do not increase the complexity of the formulation substantially.

3.2 Collision-Interaction Potential

The outcome of any scattering event depends strongly on at least some features of the interaction potential; yet the shape and magnitude of interaction potentials are poorly known for all but a relatively few simple cases. The potentials between elastically scattered atoms are generally well established from both theory and atomic-beam experiments, but the interactions influencing inelastic collisions involving diatomic molecules are still an active subject for research and computation. The topic has been discussed extensively in relation to the transport properties of gases[80] and, more recently, in relation to scattering events.[81] To circumvent the complexity of the subject, we develop in this section an empirical model of the interaction forces based on the general nature of the interaction.

The nature of the interaction forces depends greatly on the modes of energy transfer and on the internal energy states that participate in the collision dynamics. Here we are interested only in nonreactive interactions between collision partners in their ground electronic states. Even then, *ab initio* calculations for three-body systems of the type considered are difficult and still incomplete for even the simplest system, H_2-H (e.g., ref. 82b). The Born-Oppenheimer separation of electronic and nuclear motion is generally used, but the complexity associated with electronic coupling between charge clouds of three nuclei has limited present accomplishments. A few cases have been obtained using "self-consistent field theory" where the number of electrons is a minimum (H_2-H (ref. 82), H_2-He (refs. 83, 84), H_2-Li^+ (ref. 85)), but similar calculations for heavier nuclei are either less rigorous (HF-HF (ref. 86)) or not available. Experimental determinations appear to be equally difficult. The interaction potential cannot be measured directly but

must be implied from some collisionally dependent observable property in which the potential function is only implicitly contained. The uniqueness of the potential thus determined is often in serious doubt and the accuracy of its details are consequently diminished. Generally, the collision-interaction potential, however obtained, appears to be the greatest source of uncertainty in the calculation of vibrational inelastic collision dynamics for most molecules larger than H_2.

Despite our inability to accurately define the interaction potential, we can at least describe its qualitative features with some confidence. To simplify the description, the potential may be separated into two major components: an average spherical component that depends only on the separation of the molecular mass center and the incident particle and an anisotropic component that accounts for variations with the molecular orientation relative to the direction of the incident particle location. Figure 3.3 is a qualitative sketch of both components.

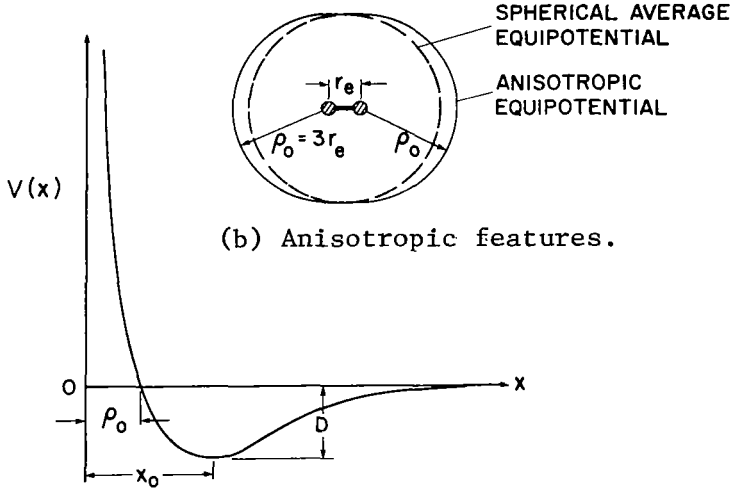

Figure 3.3- Characteristics of nonreactive intermolecular potentials.

3.2.1 Spherical Features

The spherical component may be further divided, though somewhat arbitrarily, into several types of forces. They are commonly referred to as (a) short-range repulsive forces that occur principally when two nuclei are close enough for their electronic charge clouds to overlap, (b) long-range attractive forces that result from large separations in which the charge distributions of each nucleus are independently distorted, and (c) intermediate forces that simply refer to the transition region between the preceding extremes.

The short-range forces do not lend themselves easily to theoretical simplification but, fortunately, the collision dynamics of vibrationally inelastic events are not particularly sensitive to their precise shape. Usually, the short-range force *gradient* at closest approach is the single most important feature to the collision dynamics. Generally, theoretical attempts to model the short-range forces have led to sums of terms like

$$V_{SR} \approx A(x)\ e^{-x/L} \tag{3.18}$$

where x is the separation distance, $A(x)$ is slowly varying in x, and L is a constant range parameter. Commonly, A is also taken as a constant and effective values of A and L are deduced from experiment by simple comparison with predicted results.[87] The results of *ab-initio* calculations have also been reproduced surprisingly well by equation (3.18) in interactions between two atoms, but combination rules for cases where three interacting nuclei are present are still a topic of discussion.

Long-range attractive forces, on the other hand, are more easily approximated from well-founded physical arguments. At separations large compared to the intranuclear separation of the molecule, the molecule appears as an independent multipole with some polarizability. The resulting multipole

interaction forces are the same both in quantum-mechanical and classical treatments with the general result appearing as a series of terms in the form

$$V_{LR} = -\sum_{n} \frac{C_n}{x^n} \tag{3.19}$$

Often the dominant terms are induction forces (dipole-induced dipole) and London dispersion forces (similar to dipole-induced dipole), which both vary as

$$V \approx -C/x^6 \tag{3.20}$$

The single term represented by equation (3.20) has commonly been used to approximate the influence of long-range forces.

Numerous empirical representations for the entire potential have emerged from considerations similar to those just described. An immediate choice would appear to be the Buckingham potential

$$V_B = A\, e^{-x/L} - C/x^6 \tag{3.21}$$

but this form has the unrealistic property of reaching a maximum for small x and becoming infinitely negative as $x \to 0$. A more realistic formula that emphasizes the same long-range force dependence is the well-known Lennard-Jones 12-6 potential:

$$V_{LJ} = 4D\left[\left(\frac{\rho_o}{x}\right)^{12} - \left(\frac{\rho_o}{x}\right)^{6}\right] \tag{3.22}$$

The zero-potential separation, ρ_o, explicitly appearing in equation (3.22), provides a useful measure of the equivalent "hard-sphere" radius that will be required in the collinear collision model application described in chapter 5. Similarly, the well depth, D, is also an explicit parameter. The Lennard-Jones potential gained early popularity in the analysis of transport properties in gases and its effective constants, ρ_o and D, have been evaluated for many gas

mixtures using viscosity data and virial coefficients.[80] Unfortunately, the mathematical form of equation (3.22) is inconvenient for the calculation of interaction overlap integrals in a collision model where the oscillator is treated quantum mechanically. For that reason, we shall seek a more convenient representation, but we can use the Lennard-Jones potential as a basis for comparison.

A potential representation consisting of exponential terms is particularly convenient in the mathematics of anharmonic oscillators. One such representation is the Morse potential

$$V_M = D\, e^{-(x-x_o)/L} - 2D\, e^{-(x-x_o)/2L} \qquad (3.23)$$

where the separation at the potential minimum, x_o, is related to the Lennard-Jones zero-potential separation by $x_o = 2^{1/6}\rho_o$. Equations (3.22) and (3.23) can then be made to yield similar potentials in the region of the potential well by a suitable choice of L. However, the shape of the potential well is usually not important to the collision dynamics at energies sufficient to induce vibrational transitions. The threshold energies for vibrational transitions are near $E \simeq \hbar\omega_e \simeq 0.2$ to 0.5 eV, while apparent well depths for many-electron molecules like N_2, CO, O_2, etc., are typically $D \simeq 0.01$ eV. Thus, $E/D >> 1$ in most cases of interest and the influence of the potential well shape is negligible. Instead, the choice of range parameter, L, will be dictated by the greater necessity for properly matching the potential gradient where $V \simeq E$. This latter requirement for gradient matching suggests that, unless the potential shape is correct in the region of short-range forces, the effective range L will depend on E. Later comparisons of theoretical and experimental rate coefficients will show that such behavior is obtained

and the thermal range of applicability for a given set of potential parameters is correspondingly limited.

Arguments similar to those regarding the potential well region allow us to further simplify the interaction potential representation (for the purposes of this study) by also neglecting the long-range forces. The role of the long-range attractive forces is basically twofold during a collision event — they accelerate the incoming particle by an amount related to D/E and they induce early transitions between levels whose energy spacings are the order of D. Only rotational transitions within a given vibrational state are affected in the latter role. In the first role, the effect of long-range forces will be apparent only at energies very near threshold and hence only at very low temperatures. However, this study is not directed at low-temperature applications in particular. In their second role, long-range forces would be important if we were interested in pure rotation-translation energy transfer or in the detailed final rotational state of the molecule after a collision involving V-R-T energy transfer. We shall find, however, that the net rate of vibrational energy transfer is not particularly sensitive to the rotational dynamics during the early or late stages of the encounter. The rotational state of the molecule having the greatest influence on its final vibrational condition will be the rotational state occupation occurring at the time of closest approach when the short-range forces are dominant. Thus, we can justifiably neglect the long-range forces entirely for these purposes and adopt the simple and analytically convenient repulsive potential

$$V = A\, e^{-x/L} \tag{3.24}$$

The effects of the potential well on vibrational energy transfer have been investigated in greater detail by others.[88-90] Their findings support

the conclusion that the well may be neglected when E/D or $\hbar\omega_e/D \gg 1$. There are examples, of course, where the well depth is larger (e.g., for H_2-Li^+, $\hbar\omega_e/D \simeq 0.2$). For those cases, the entire interaction potential must be accurately represented.

3.2.2 Anisotropic Features

The anisotropic potential component is responsible for rotational disturbances to the molecule. Figure 3.3(b) illustrates the typical magnitude of anisotropy effective during the collision. The magnitude is gauged by noting that the equilibrium separation of most diatomic molecules is near $r_e \simeq 0.1$ nm, while the distance of closest approach during a collision will be only slightly less than the zero-potential radius, ρ_o. For most common molecule-atom interactions, $\rho_o \simeq 0.3$ nm. Figure 3.3(b) is drawn for the ratio $\rho_o/r_e = 3$ with a radius ρ_o centered on each molecular nucleus. The equipotential appears mostly spherical with relatively small aspherical components. The small anisotropic terms of most calculated interaction potentials confirm these observations.

When rotational motion is considered, it is most conveniently described by a coordinate system containing an angle, δ, that defines the rotation of the molecular axis relative to the position of the incident particle. Figure 3.4 illustrates such a coordinate system. The subsequent mathematics then appear in a convenient format if the potential is expressed as a series expansion of Legendre polynomials, P_J, in the form

$$V(x,r,\delta) = \sum_J \upsilon_J(x,r)\, P_J(\cos\,\delta) \qquad (3.25)$$

In most cases, *ab-initio* potentials are represented by equation (3.25) using only two or three terms.

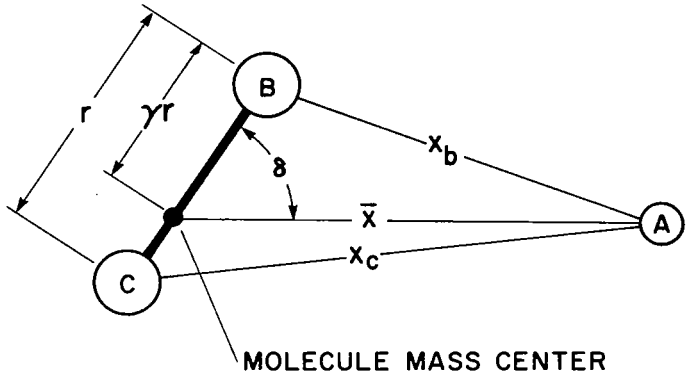

Figure 3.4- Three-dimensional encounter nomenclature viewed in the time-dependent plane defined by the location of the incident particle A and intramolecular axis BC.

The typically small anisotropy of most interactions makes two simplifying assumptions reasonable that greatly reduce the complexity of a three-dimensional collision model. One is operative if the incident particle motion is treated classically. An approximate trajectory may then be obtained using only the spherical component of the potential. Such an assumption neglects out-of-plane deflections and reduces the translational motion to two dimensions. Averaging the initial configuration is then greatly simplified. A second simplification, in keeping with our original notions, is that the anisotropic potential can be approximated by two additive spherical potentials, each centered on a molecular nucleus. In concept, the use of pairwise potentials ignores the second-order mutual interaction between nuclei and it also omits the shielding or shadowing of one nucleus by the other as viewed from the position of the incident particle. However, if the anisotropy is small, these second-order corrections will be smaller. In addition, the interaction potential decreases rapidly with internuclear separation so that for most angles, δ, the incident particle will be interacting mainly with only one molecular nucleus at a time. Thus, shielding effects should be relatively

unimportant. For the purposes of this study, the three-dimensional interaction potential is therefore simulated by two noninteracting short-range potentials, each given by equation (3.24) and each centered on a molecular nucleus. The final step in representing the potential is to express it in the form given by equation (3.25).

3.2.3 Three-Dimensional Interaction Potential Model

Part of the nomenclature to describe a three-dimensional encounter is defined by figure 3.4. The figure lies in a time-dependent plane containing both molecular nuclei and the instantaneous position of the incident particle. An additive repulsive force between each nucleus will then produce the interaction potential

$$V(x_b, x_c) = A(e^{-x_b/L} + e^{-x_c/L}) \tag{3.26}$$

where A and L are considered identical for both interacting pairs. The internuclear separations may be expressed in terms of mass-centered variables as

$$\left.\begin{aligned} x_b &= \bar{x}\left[1 - 2\gamma \frac{r}{\bar{x}} \cos\delta + \gamma^2\left(\frac{r}{\bar{x}}\right)^2\right]^{1/2} \\ x_c &= \bar{x}\left[1 + 2(1-\gamma) \frac{r}{\bar{x}} \cos\delta + (1-\gamma)^2\left(\frac{r}{\bar{x}}\right)^2\right]^{1/2} \end{aligned}\right\} \tag{3.27}$$

where $\gamma = [m_c/(m_b + m_c)]$ is the molecular mass ratio and $m_c \geq m_b$. For the potential to appear nearly spherical, $r/\bar{x}$ must remain small over the entire trajectory. We have argued that it does remain less than unity since its largest value at closest approach is only $r/\bar{x} \simeq 1/3$. Equation (3.27) may then be expanded in a uniformly convergent power series of $r/\bar{x}$, giving to first-order,

$$\left.\begin{aligned} x_b &= \bar{x}\left(1 - \gamma \frac{r}{\bar{x}} \cos \delta + \ldots\right) \\ x_c &= \bar{x}\left[1 + (1 - \gamma) \frac{r}{\bar{x}} \cos \delta + \ldots\right] \end{aligned}\right\} \tag{3.28}$$

The corresponding first-order representation of equation (3.26) is then

$$V(\bar{x},r,\delta) = A\, e^{-\bar{x}/L}\left[e^{\gamma(r/L)\cos \delta} + e^{-(1-\gamma)(r/L)\cos \delta}\right] \tag{3.29}$$

Figure 3.5 demonstrates that the first-order potential, equation (3.29), is a reasonable approximation of the additive spherical potential, equation (3.26), for the typical range of parameters used here.

The potential model given by equation (3.29) is now in a form that can be conveniently handled in the framework of a three-dimensional collision model. It may be transformed to a form equivalent to equation (3.25) by use of the expansion

$$e^{\pm z \cos \delta} = \sum_{J=0}^{\infty} (2J + 1)(\pm 1)^J \sqrt{\pi/2z}\, I_{J+1/2}(z)\, P_J(\cos \delta) \tag{3.30}$$

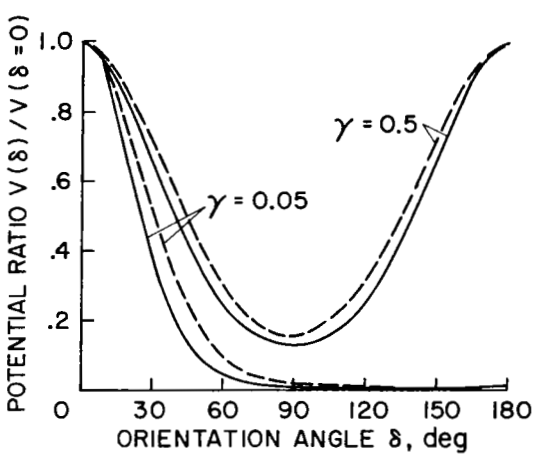

Figure 3.5.- Variation of a pairwise repulsive potential and its first-order approximation with orientation angle. Calculations were done for r/L = 5. Solid curves are the infinite-order variation from equation (3.26); dashed curves are the first-order approximation, equation (3.29).

(see ref. 73, p. 445) where $I_{J+1/2}$ is the modified spherical Bessel function of the first kind and P_J is a Legendre polynomial as before. By reducing the notation with the definition

$$i_J(z) = \sqrt{\pi/2z}\, I_{J+1/2}(z) \tag{3.31}$$

equation (3.29) is transformed to the series representation:

$$V(\bar{x},r,\delta) = A\, e^{-\bar{x}/L} \sum_{J=0}^{\infty} (2J+1)\left\{i_J[\gamma r/L] + (-1)^J i_J[(1-\gamma)r/L]\right\} P_J(\cos\delta) \tag{3.32}$$

As expected, $i_J(z)$ decreases rapidly with J for typical values of z so that only a few terms contribute to the summation. The correspondence between equations (3.25) and (3.32) is obvious.

3.2.4 Collinear Interaction Potential Model

The discussions of previous sections have noted that a one-dimensional collinear collision model will be useful in obtaining analytic descriptions of the rate of vibrational energy transfer. A brief development of the required interaction potential expression is therefore included here.

The most effective collinear collision to induce vibrational motion will be an encounter with the lightest nucleus in the molecule. Collinear encounters are therefore limited to those where $\delta = 0$. Equation (3.28) then reduces to

$$V(\bar{x},r) = A\, e^{-\bar{x}/L}\left[e^{\gamma r/L} + e^{-(1-\gamma)r/L}\right] \tag{3.33}$$

Typically, $r/L \simeq 5$ while γ is always less than unity so that the second term in equation (3.33) is always much smaller than the first. The interaction potential for one-dimensional collinear collisions is therefore taken to be

$$V(\bar{x},r) = A\, e^{-\bar{x}/L+\gamma r/L} \tag{3.34}$$

This form of the potential or a linearized version of it have been used for all collinear vibrational energy transfer theories.[42,45,46] It is applied in the following chapter to study the applicability of a semiclassical collision theory to anharmonic oscillators.

CHAPTER 4

A COMPARATIVE EVALUATION OF THE SEMICLASSICAL APPROXIMATION

We have shown in chapter 2 that, while a semiclassical collision model offers several advantages in a study of vibrational energy transfer, the criteria for its application are not explicit. Hence they offer marginal help in evaluating the validity of the semiclassical approximation for a specific set of conditions. We have also observed that the criteria, expressed by equations (2.9) and (2.10), suggest that the validity of a semiclassical model will be influenced by the oscillator anharmonicity. However, previous comparative evaluations of semiclassical theories[45] have been only for harmonic oscillators. Furthermore, the results, although favorable, have not been entirely conclusive because, in addition to the absence of anharmonicity, the semiclassical formulation is typically only one of several approximations contained in the comparisons, while all the corrections known to improve the semiclassical predictions are not always included. The primary purpose of this chapter is therefore to compare the vibrational transition probability predictions from a semiclassical model for anharmonic oscillators with a comprehensive set of solutions from an equivalent, fully quantum mechanical, collision model. The *only* difference in the two models is the treatment of the incident particle motion.

The physically incomplete nature of a semiclassical treatment requires some interpretation and correction, however, to facilitate its correlation with more exact collision models. Hence, in this chapter, we shall also deal explicitly with the corrective aspects of a semiclassical treatment. For example, a well-known weakness of semiclassical theories is the inherent lack

of energy conservation. Several methods of compensation have been suggested that aim at interpreting either the classical trajectory energy[20] or velocity[42] in terms of corresponding values averaged over the collision. Comparisons described here between these semiclassical predictions and the exact quantum-mechanical calculations show that, while such an interpretation is necessary to correct the semiclassical predictions, the results are insensitive to the choice of method in the energy range of practical interest.

Regardless of the corrections for energy conservation, the conventional semiclassical treatment will be shown to fail badly in some cases. The failures appear in the form of anomalous resonances that occur only in anharmonic oscillator models and are caused by an incomplete account of the oscillator compression and recoil during impact. Within the usual semiclassical framework, the classical trajectory is computed, assuming that the oscillator remains in a pure eigenstate having a fixed average separation of its nuclei. In reality, the oscillator is compressed by the impact and enters a mixed-state condition in which the average internuclear separation oscillates with frequency components from each of the excited states. To include this behavior in the semiclassical theory is not equivalent to conserving energy, but it has the effect of introducing an oscillator "feedback" on the classical trajectory. The effect can change the entire nature of the results in some cases. Extremely heteronuclear or anharmonic molecules, such as the hydrogen halides, will be shown as members of the class strongly affected.

We also simplify the collision geometry used here by confining it to collinear encounters. Direct comparisons with the fully quantum mechanical results of reference 68 are thus made possible. Calculations have been presented in the literature of more realistic three-dimensional encounters,[40]

but mainly for harmonic oscillators initially in the ground state. They have also been made in chapter 6 for anharmonic oscillators in excited vibrational states. However, a three-dimensional collision geometry introduces many additional complexities, as we shall demonstrate in chapter 6, and little would be gained by including it in this chapter.

In the paragraphs to follow, a multistate semiclassical formulation requiring numerical solution is assembled first that includes modifications of the standard treatment to account for the effect of oscillator response on the classical trajectory. The model is entirely equivalent to the fully quantum mechanical model in reference 68, except for the classical treatment of the incident particle motion. The accuracy of a first-order perturbation theory used by Mies[21] for anharmonic oscillators is also evaluated. As expected, the first-order theory is suitable only where the transition probabilities are small; but it must also be limited to cases where the oscillator feedback effects are negligible. Such cases will be shown to pertain mainly to heavy homonuclear molecules impacted by lighter collision partners.

4.1 Semiclassical Model for Collinear Collisions

A full description of the semiclassical formulation for a general collision geometry is given in appendix B. In this section, only the results pertinent to collinear collisions are recalled in detail.

The collinear collision geometry is shown in figure 4.1 for a structureless particle of mass, m_a, impacting a diatomic heteronuclear molecular with nuclear masses, m_b and m_c. The impacted oscillator nucleus, m_b, extends from the molecular mass center by a distance γr, where $\gamma = m_c/(m_b + m_c)$. A three-body center-of-mass reference frame is taken in which the relative

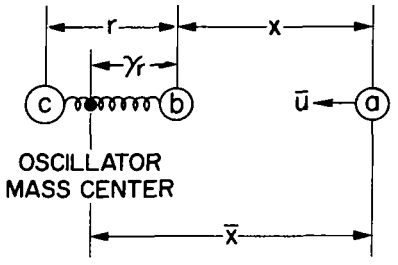

Figure 4.1.- Collinear collision geometry.

collision speed is $\bar{u}$. (Barred symbols identify the incident particle variables to be evaluated classically and later interpreted as average values.) Except for the notation, this configuration is identical to those used by Mies[20,21] and in references 45 and 68.

The interaction potential to be used here is of the same form given in reference 68, namely,

$$V(x) = A\, e^{-x/L}$$

where L and A are constants. The potential in terms of mass center and oscillator coordinates defined in figure 4.1 then becomes

$$V(\bar{x},r) = A\, e^{-\bar{x}/L}\, e^{\gamma r/L} \tag{4.1}$$

The Hamiltonian for the three-body system is given by

$$\mathcal{H} = \frac{p_o^2}{2\mu_o} + \frac{\bar{p}^2}{2\mu} + V_o(r) + V(\bar{x},r)$$

where the symbols with subscript o refer to oscillator quantities and the other symbols denote incident particle variables. The oscillator reduced mass is $\mu_o = m_b m_c/(m_b + m_c)$ and the collision reduced mass is $\mu = m_a(m_b + m_c)/(m_a + m_b + m_c)$.

4.1.1 Incident Particle Motion

The application of Ehrenfest's theorem to the incident particle dynamics guides the formulation of its equation of motion with the quantum mechanically averaged quantities properly included. In terms of quantum mechanically averaged variables, the equations of motion are

$$\frac{d\langle\bar{p}\rangle}{dt} = -\left\langle\frac{\partial\mathcal{H}}{\partial\bar{x}}\right\rangle = -\left\langle\frac{\partial V(\bar{x},r)}{\partial\bar{x}}\right\rangle$$

$$\frac{d\langle\bar{x}\rangle}{dt} = \left\langle\frac{\partial\mathcal{H}}{\partial\bar{p}}\right\rangle = \frac{1}{\mu}\langle\bar{p}\rangle$$

By separating the total wave function according to

$$\Psi(\bar{x},r,t) = \phi(\bar{x},t)\psi(r,t)$$

and treating the incident particle classically so that

$$\langle\bar{p}\rangle \rightarrow \mu\bar{u}$$

$$\langle\bar{x}\rangle \rightarrow \bar{x}$$

and

$$\left\langle e^{-\bar{x}/L}\ e^{\gamma r/L}\right\rangle \rightarrow e^{-\bar{x}/L}\left\langle e^{\gamma r/L}\right\rangle$$

the equations of motion for the incident particle combine with equation (4.1) to give

$$\mu\frac{d^2\bar{x}}{dt^2} = \frac{A}{L}\ e^{-\bar{x}/L}\left\langle e^{\gamma r/L}\right\rangle$$

where the bracket notation implies

$$\left\langle e^{\gamma r/L}\right\rangle = \int_{-\infty}^{\infty}\psi^*(r,t)\ e^{\gamma r/L}\ \psi(r,t)dr \qquad (4.2a)$$

For the purely repulsive exponential potential used here, the potential constant, A, influences only the distance of closest approach, a quantity of no direct consequence to the transition probabilities. It may be removed by a

transformation suggested by equating the potential energy at closest approach for a stationary oscillator with the initial kinetic energy, that is,

$$A \rightarrow \frac{\bar{E}}{V_{kk}} e^{\bar{x}_o/L}$$

where $\bar{E} = (1/2)\mu\bar{u}^2$ is the semiclassical relative collision energy before interaction, V_{kk} is the time-independent diagonal matrix element defined by

$$V_{kk} = \int_{-\infty}^{\infty} \psi_k^*(r)\ e^{\gamma r/L} \psi_k(r) dr \tag{4.2b}$$

and $\psi_k(r)$ is the initial oscillator stationary-state eigenfunction. Note that $\bar{x}_o$ is not the distance of closest approach for a nonstationary oscillator. However, if a new interaction coordinate is defined as $\bar{z} = \bar{x} - \bar{x}_o$, the incident particle motion is unaffected and may then be described by

$$\mu \frac{d^2\bar{z}}{dt^2} = \frac{\bar{E}}{L} e^{-\bar{z}/L} R(t) \tag{4.3a}$$

where

$$R(t) \equiv \left\langle e^{\gamma r/L} \right\rangle \Big/ V_{kk} \tag{4.3b}$$

The variable $R(t)$ represents the quantum-mechanical average effect of the oscillator motion on the classical path. It is a measure of the oscillator distortion during impact and subsequent "ringing" afterward.

To compute the trajectory classically, we must first describe the oscillator motion to obtain $R(t)$. The usual practice at this point has been to consider the oscillator fixed in its initial pure eigenstate so that $\psi(r,t) \approx \psi_k(r)$. Then $R(t) \approx 1$ for all time and the classical equation of motion is reduced to the equation for a constant energy trajectory:

$$\mu \frac{d^2\bar{z}}{dt^2} = \frac{\bar{E}}{L} e^{-\bar{z}/L} \tag{4.4}$$

Equation (4.4) can be integrated analytically[45] so that the interaction potential

$$V(t,r) = \frac{\bar{E}}{V_{kk}} e^{-\bar{z}(t)/L} e^{\gamma r/L} \tag{4.5a}$$

can be written explicitly in terms of time by use of the result:

$$e^{-\bar{z}(t)/L} = \operatorname{sech}^2\left(\frac{\bar{u}t}{2L}\right) \tag{4.5b}$$

In such an approximation, the transformation parameter $\bar{x}_o$ becomes the distance of closest approach.

4.1.2 Oscillator Motion

The unsteady motion of the oscillator is treated in the usual way by expanding its time-dependent wave function $\psi(r,t)$ in terms of stationary-state Morse oscillator eigenfunctions $\psi_n(r)$ according to

$$\psi(r,t) = \sum_n c_n(t) e^{-i\omega_n t} \psi_n(r) \tag{4.6}$$

where $\omega_n = E_n/\hbar$ and E_n is the nth state eigenenergy. Continuum states are neglected. We showed in chapter 3 that, for the Morse oscillator,

$$\omega_n = \omega_e\left(n + \frac{1}{2}\right) - \omega_e x_e\left(n + \frac{1}{2}\right)^2 .$$

The dynamical wave function $\psi(r,t)$ describing the oscillator response during a collision is the solution of the time-dependent Schrödinger equation:

$$i\hbar \frac{\partial \psi(r,t)}{\partial t} = \left[- \frac{\hbar^2}{2\mu_o} \frac{\partial^2}{\partial r^2} + V_o(r) + V(t,r) \right] \psi(r,t) \tag{4.7}$$

where, from chapter 3,

$$V_o(r) = D_e\left[e^{-2a(r-r_e)} - 2e^{-a(r-r_e)}\right]$$

The solutions are invariant with the equilibrium separation r_e and it may be set equal to zero. The remaining potential parameters are equated to the

familiar spectroscopic constants ω_e and x_e according to equations (3.4) and (3.5).

The solution of equation (4.7) is reduced in a standard way (see appendix B) to a set of linear, coupled differential equations for the expansion coefficients defined in equation (4.6). Denoting

$$V_{nj} = \int_{-\infty}^{\infty} \psi_n^*(r)\, e^{\gamma r/L} \psi_j(r) dr \tag{4.8}$$

and incorporating the form of the interaction potential in equation (4.5a), the the coefficients in equation (4.6) vary in time according to

$$i\hbar \frac{dc_n(t)}{dt} = \frac{\bar{E}}{V_{kk}} e^{-\bar{z}(t)/L} \sum_j c_j(t) e^{i(\omega_n - \omega_j)t} V_{nj} \tag{4.9}$$

The probability that an oscillator, initially in state k at $t = -\infty$, will reside in state n at $t = +\infty$, is then $P_{k\to n}(\bar{E}) = |c_n(\infty)|^2$ with the initial conditions $|c_j(-\infty)|^2 = \delta_{kj}$, where δ_{kj} is a Kronecker delta.

The matrix elements given in integral form by equations (4.2b) and (4.8) may be evaluated analytically.[20,68] If, for convenience of notation, we define $\alpha = \gamma/aL$ and $\beta = x_e^{-1}$, then

$$V_{nj} = \beta^{\alpha} \frac{N_n N_j}{a} \frac{\Gamma(\beta - j)}{n!} \sum_{\ell=0}^{j} (-1)^{\ell+j-n} \frac{\Gamma(1 + \alpha + j - \ell)\Gamma(\beta - \alpha - 1 - j - n + \ell)}{\ell!(j - \ell)!\Gamma(1 + \alpha + j - n - \ell)\Gamma(\beta - 2j + \ell)}$$

where $\Gamma(\xi)$ is the gamma function[73] with argument ξ, and the normalization constants are

$$N_m = \left[\frac{a(\beta - 1 - 2m)}{\Gamma(\beta - m)}\right]^{1/2}$$

To stay within the maximum exponent constraints imposed by most computers, the evaluation of matrix elements with large indices requires the ratios of gamma

functions to be reduced to products of algebraic terms and a residual gamma function with an argument less than unity.[73]

4.1.3 Coupling of the Oscillator Motion and the Classical Trajectory

The term $e^{-\bar{z}/L}$ in equation (4.9) may be evaluated either from equation (4.5b) or by the coupled integration of equation (4.3), depending on the treatment of $R(t)$. The former case ignores any coupling between the oscillator and the classical path, thus assuming $R(t) = 1$ for all t. The latter case requires evaluation of $R(t)$ in terms of the expansion coefficients — a task easily done by combining equations (4.2) and (4.6) to give

$$R(t) = \frac{1}{V_{kk}} \sum_{\ell} \sum_{m} c_{\ell}^{*}(t)\ c_{m}(t)\ e^{i(\omega_{\ell}-\omega_{m})t} V_{\ell m} \qquad (4.10)$$

where k again denotes the initial state.

Equation (4.10) characterizes the classical nature of the quantified oscillator motion. The motion will become oscillatory as soon as a mixed-state condition is produced during the collision and will remain so afterward. Near closest approach, large transient excursions of $R(t)$ occur, reflecting the oscillator compression and recoil.

4.1.4 First-Order Perturbation Solutions

From a practical viewpoint, the convenience of an analytical solution warrants even the coarsest assumptions, provided the limits of applicability are understood. This study attempts to confirm those limits for a first-order perturbation analysis applied to anharmonic oscillators in initially excited states. We shall see that the perturbation solutions are quite successful within their intended limits and will serve as useful approximation in many cases.

An analytical solution of equation (4.9) may be obtained if the motion of the classical particle is described by equation (4.4). For an initial state k, the perturbation method further requires that $|c_k(t)|^2 \approx 1$ and $|c_n(t)|^2 \ll 1$ throughout the duration of the collision. Then only the initial and final states are coupled, allowing equation (4.9) to be written in the integral form:

$$|c_n(\infty)|^2 = \left| \frac{\bar{E}}{\hbar} \frac{V_{nk}}{V_{kk}} \int_{-\infty}^{\infty} \operatorname{sech}^2\left(\frac{\bar{u}t}{2L}\right) \exp\left[\frac{i}{\hbar} \int_0^t \Gamma_{nk}(t')dt'\right] dt \right|^2 \qquad (4.11)$$

with

$$\Gamma_{nk}(t') = \hbar(\omega_n - \omega_k) + (V_{nn} - V_{kk}) \frac{E}{V_{kk}} \operatorname{sech}^2\left(\frac{\bar{u}t}{2L}\right)$$

Equation (4.11) may be integrated to give[21]

$$P_{k\to n}(\bar{E}) = \left| \frac{V_{nk}}{V_{kk}} \frac{2\pi g \mu L \bar{u}}{\hbar \sinh(\pi g)} M(1 + ig, 2, i2\lambda) \right|^2 \qquad (4.12)$$

where

$$g = \frac{L(\omega_n - \omega_k)}{\bar{u}}, \qquad \lambda = \frac{\mu L \bar{u}}{\hbar} \frac{V_{nn} - V_{kk}}{V_{kk}}$$

and $M(1 + ig, 2, i2\lambda)$ is the confluent hypergeometric series with complex arguments. The necessity of complex algebra may be avoided when computing the modulus $|M(1 + ig, 2, i2\lambda)|$ by noting its relation to the Coulomb wave function with zero index.[73] The result is

$$|M(1 + ig, 2, i2\lambda)| = \Phi_o(-g, \lambda) \qquad (4.13)$$

where

$$\Phi_o(-g, \lambda) = \sum_{\ell=1}^{\infty} A_\ell \lambda^{\ell-1}$$

with $A_1 = 1$ and $A_2 = -g$. The remaining coefficients are obtained from

$$\ell(\ell - 1)A_\ell = -2gA_{\ell-1} - A_{\ell-2}$$

4.1.5 Numerical Solution Methods

Solutions to the coupled set of equations (4.3) and (4.9) were obtained by first separating equation (4.9) into a separate set for each complex component and adopting the equivalent of a multiple-state, close-coupling approach. Numerical integration was accomplished with a polynomial extrapolation algorithm originally developed by Bulirsch and Stoer[91] and given in FORTRAN by Gear.[92] Fifth-order polynomials and a required accuracy of one part in 10^8 seemed to optimize the calculation of a selected test case and allowed a complete encounter to be computed in 50 to 1000 steps, depending on the collision energy and the number of coupled states. Solutions were started with the molecule in a pure eigenstate and with the incident particle at a distance such that the interaction potential had a value 10^{-4} times the estimated value at closest approach. The calculation was terminated at an equal distance after the encounter. All values of $|c_n(t)|^2$ were sufficiently constant at termination. The closure relation $\sum_n |c_n(t)|^2 = 1$ was used throughout the encounter to monitor accuracy. If the initial state quantum number were k, states from $n = 0$ to $2k$ were included at the maximum energies considered to ensure that the solution was unaffected by neglected states. Of course, in the energy range where the perturbation theory was successful, as few as two states were adequate. The computing times required to obtain all the matrix elements and to integrate the dynamics of a twelve-state model was approximately 0.1 sec/step on a single precision (14-digit) CDC-7600 computer.

4.2 A Comparison With Fully Quantum Mechanical Solutions

The availability of tabulated results for exact quantum mechanical calculations[68] over a broad range of collision parameters provides an excellent opportunity to evaluate the semiclassical approximation in this application. The extent of the examples covered is characterized by the range of the mass parameter $m = m_a m_c / m_b (m_a + m_b + m_c)$. For the cases chosen, m varies from 0.006 for Br_2-H collisions to 3.7 for HBr-He collisions. (Reference 68 labels one data set as Br_2-H_2, but uses a mass parameter corresponding to Br_2-H.) A full range of oscillator frequency and anharmonicity is also represented. Figures 4.2(a) to (f) compare the predictions of the semiclassical theory and its first-order approximation to a sampling of the results in reference 68 for the homonuclear oscillator cases. The semiclassical transition probabilities are plotted as functions of the normalized initial kinetic energy of the incident particle, $\bar{E}/\hbar\omega_e$. The probabilities from reference 68, hereafter referred to as "exact," are shown at energies displaced according to a trajectory symmetrization scheme (to be discussed). In the paragraphs to follow, the comparisons in figures 4.2(a) to (f) are used to evaluate the validity of several methods of compensating for the lack of energy conservation in the semiclassical approximation and to demonstrate the influence of coupling between the recoiling quantum-oscillator and the classical incident-particle motion.

4.2.1 Energy Conservation and the Classical Parameters

The absence of energy conservation in the semiclassical approximation requires an interpretation of the initial relative kinetic energy $\bar{E}$ assigned to the classical trajectory. It may be considered an effective value,

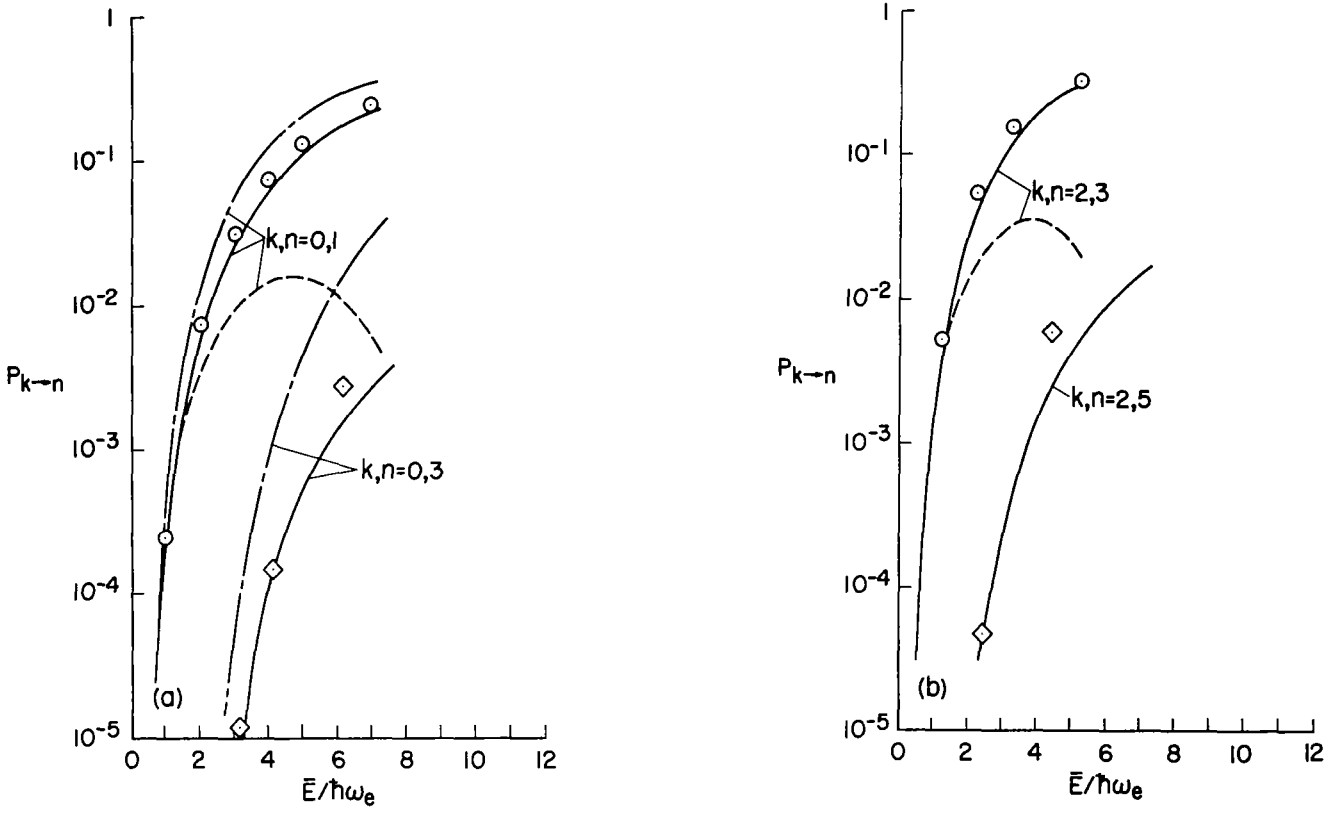

(a) $H_2(k = 0)$ - He collisions; ○: $k \to n = 0 \to 1$; ◇: $k \to n = 0 \to 3$.

(b) $H_2(k = 2)$ - He collisions; ○: $k \to n = 2 \to 3$; ◇: $k \to n = 2 \to 5$.

Figure 4.2.- Comparisons of semiclassical and quantum-mechanical[68] transition probabilities of homonuclear molecules. All calculations are done for L = 0.02 nm. Open symbols denote points tabulated in reference 68 and plotted according to equation (4.15). The curves ———— are semiclassical multistate solutions using classical trajectories coupled to the oscillator motion via equation (4.3). The curves —— – —— are the same without coupling via equation (4.4). The curves curves — — — — are first-order perturbation solutions given by equation (4.12).

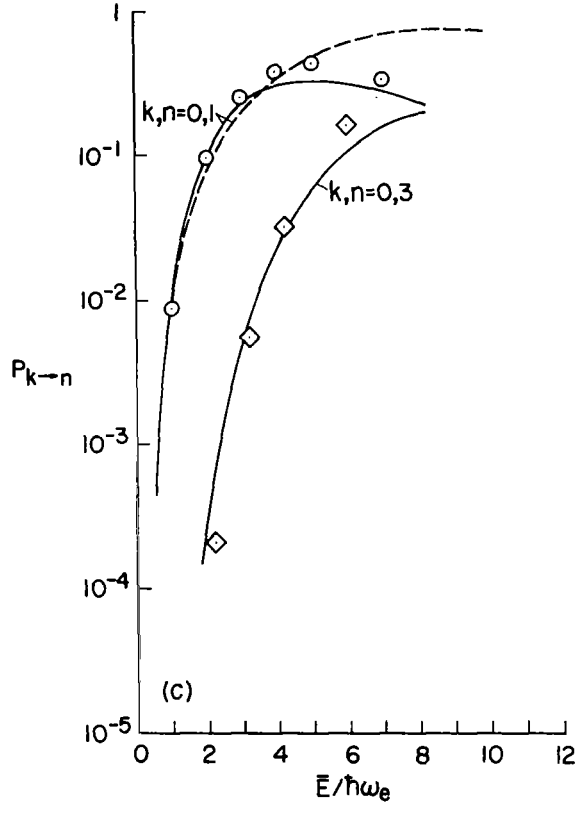

(c) $H_2(k = 0)$ - H collisions; coupled and uncoupled solutions are superimposed, ○: $k \to n = 0 \to 1$; ◇: $k \to n = 0 \to 3$.

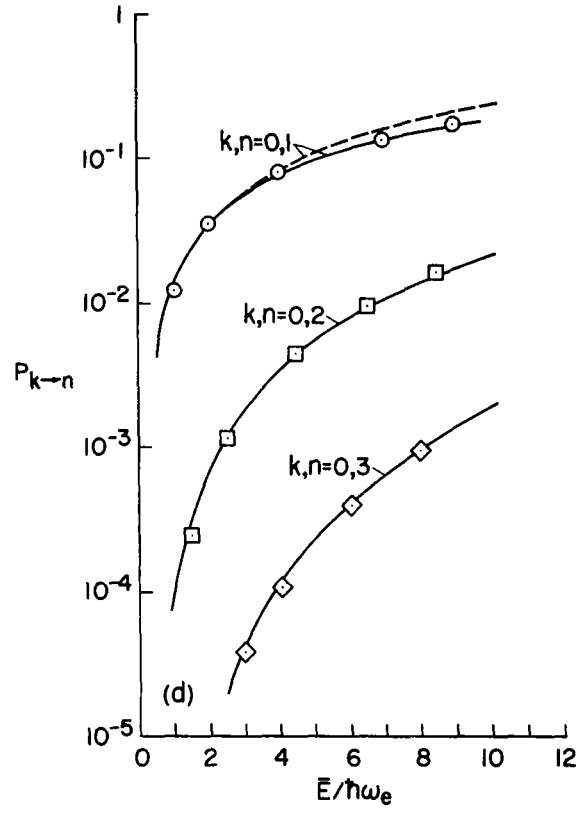

(d) $Br_2(k = 0)$ - H collisions; coupled and uncoupled solutions are superimposed, ○: $k \to n = 0 \to 1$; □: $k \to n = 0 \to 2$; ◇: $k \to n = 0 \to 3$.

Figure 4.2.- Continued.

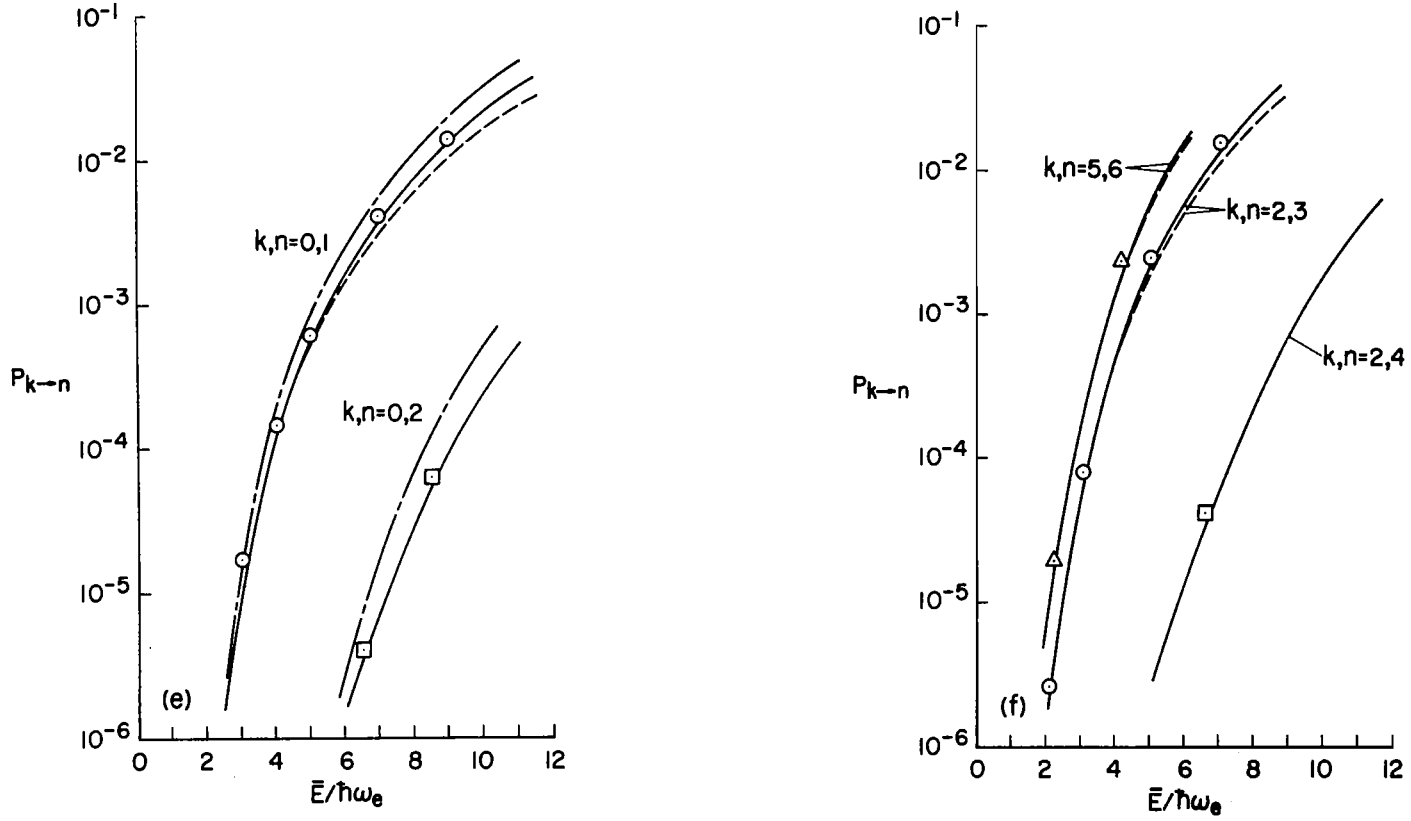

(e) $N_2(k = 0)$ - (N_2) collisions; ○: $k \to n = 0 \to 1$; □: $k \to n = 0 \to 2$. (N_2) denotes N_2 treated as a structureless particle.

(f) $N_2(k = 2 \text{ or } 5)$ - (N_2) collisions; ○: $k \to n = 2 \to 3$; □: $k \to n = 2 \to 4$; △: $k \to n = 5 \to 6$.

Figure 4.2.- Concluded.

averaged over the trajectory from the true initial value E_k to the final value E_n, when the molecule undergoes a transition from state k to n. If total energy is conserved, E_T, E_k, and E_n are related by

$$E_k + \hbar\omega_k = E_T = E_n + \hbar\omega_n \tag{4.14}$$

No formal guidelines are available, however, for simply relating $\bar{E}$ to the exact energies E_k and E_n. Perhaps the closest one can come is with the method described in reference 42, where the formulation of a linearized quantum-mechanical approximation is compared to its semiclassical counterpart. Expressions for the transition probabilities given by both approximations become similar if $\bar{E}$ is defined by the average velocity $\bar{u} = (u_n + u_k)/2$. Another approach is taken by Mies,[21] who uses the intuitively appealing arithmetic energy average $\bar{E} = (E_n + E_k)/2$. Combined with equation (4.14), the total energy can then be related to the average energy according to

$$E_T = \bar{E} + \hbar(\omega_n + \omega_k)/2 \tag{4.15}$$

where $\hbar(\omega_n + \omega_k)/2$ is the oscillator energy averaged over the transition. Occasionally, even the geometric average $\bar{E} = (E_k E_n)^{1/2}$ has been suggested.[69] Equation (4.15) was chosen here for the comparisons in figures 4.2, where it is shown to be generally successful. It correlates the predictions of both theories for all initial states, transitions, and mass ratios tested and appears applicable for all energies $\bar{E}$ from threshold up to at least the first probability maximum. Figure 4.2(c) shows correlation beyond the first maximum. Note however, that when the effect of the oscillator motion coupled to the classical trajectory is distinguishable, the coupling must be included to preserve the accuracy of equation (4.15) (e.g., see fig. 4.2(a)). The other averaging methods are no less accurate, however. Table 4.1 reveals that all

the averaging methods described give essentially the same results and that, within the range of these comparisons, the best choice cannot be selected. Differences in the three methods (or apparently any other method) will only become distinguishable at values of $E_T >> \hbar\omega_e$, where, from thermal considerations, E_T is beyond the range of practical interest. From a pragmatic viewpoint, equation (4.15) is attractive because, unlike the other averages, it provides an energy transformation, $E_T - \bar{E}$, independent of $\bar{E}$ and allows the energies E_k or E_n to be written explicitly in terms of $\bar{E}$ with simple algebraic form. These features are convenient for additional manipulation such as thermal averaging.

TABLE 4.1.- A COMPARISON OF SYMMETRIZATION METHODS APPLIED TO ANHARMONIC H_2

Transitions $k \to n$	$(E_T - \bar{E})/\hbar\omega_e$			
	Observed Figs. 2(a)-(b) Note (a)	$\bar{E} = \frac{1}{2}(E_n + E_k)$	$\bar{u} = \frac{1}{2}(u_n + u_k)$ Note (b)	$\bar{E} = (E_n E_k)^{1/2}$ Note (b)
0-1	1.0	0.97	0.99	1.01
0-2	1.3	1.41	1.46	1.50
0-3	1.7	1.83	1.94	2.05
2-3	2.7	2.75	2.76	2.78
2-4	3.1	3.14	3.20	3.26
2-5	3.5	3.51	3.65	3.80
5-6	5.0	5.03	5.06	5.08

Note (a) The observed energy difference between the semiclassical and exact results for a given probability near threshold. The semiclassical results include oscillator feedback.

Note (b) Computed for $\bar{E}/\hbar\omega_e = 6$.

4.2.2 Influence of Oscillator Response on the Classical Motion

The discussion to this point has been confined to homonuclear molecules. Figures 4.2 indicate that coupling oscillator motion and the classical trajectory has a noticeable effect only for the most anharmonic molecule, H_2, and then only when struck by a relatively heavy particle, He. However, semiclassical calculations for heteronuclear cases are much more sensitive to the oscillator response. In the customary semiclassical formulation, the incident particle dynamics are related only to its distance from the mass center of the molecule, and no regard is given for the location of the impacted nucleus (e.g., see eq. (4.4)). In an extreme heteronuclear case where the impacted nucleus is extended to a distance similar to the distance of closest approach, the incident particle can spatially overlap the impacted nucleus without constraint. Of course, even the approach to this extreme situation signals the failure of the assumptions leading to equation (4.4).

The hydrogen-halides represent examples of diatomic molecules whose heteronuclear properties strongly influence the incident particle motion, with the effects further augmented by the accompanying large anharmonicity. As an example, figure 4.3 illustrates the behavior of HBr-He collisions, where H is the impacted nucleus. Similar results were obtained for HCl-He and are assumed to be characteristic for all hydrogen-halide-like molecules. Both the semiclassical numerical solutions and the analytical theory predict an anomalous resonance at low energy when the classical trajectory is obtained from equation (4.4). The resonance is a combined result of an improper trajectory and the oscillator anharmonicity since similar calculations treating the molecule as a harmonic oscillator behaved normally and in accordance with corresponding quantum-mechanical solutions.[68] Considerable care was exercised in verifying

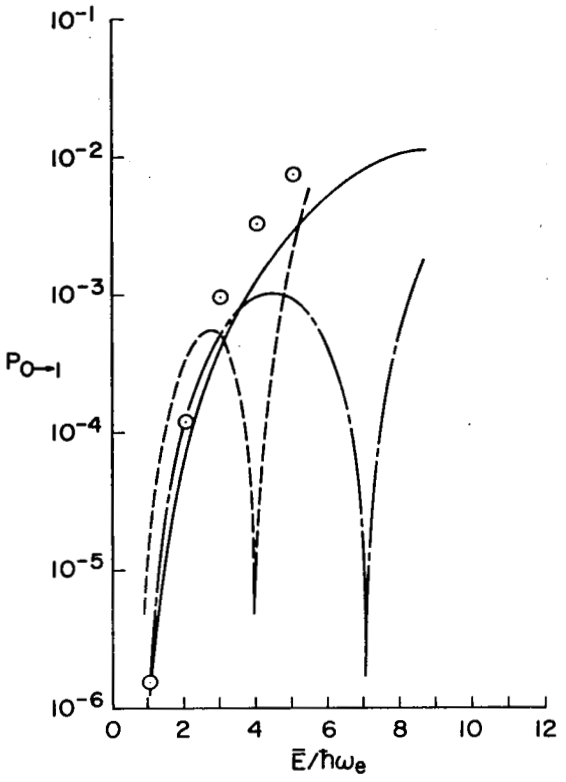

Figure 4.3.- Comparison of semiclassical and quantum-mechanical transition probabilities for HBr(k = 0) - He collisions. The impact is between H and He. The notation is the same as in figure 4.2; o denotes $k \to n = 0 \to 1$.

the resonance as a real solution of the theoretical model rather than a numerical artifact. The similar behavior of the analytical solution supports the conclusion that the effect is a real consequence of the model used. When oscillator motion is included via equations (4.3) and (4.10), the resonance disappears and the solution is more in accordance with the quantum-mechanical results for single-quantum transitions. However, multiple-quantum probabilities such as $\bar{P}_{02}$ still display a low-energy anomalous resonance. The interpolation of $\bar{E}$ for single-quantum transitions is also shown to be less accurate, but equation (4.15) still performs well near threshold. The results

suggest that the interference between the oscillator and the incident particle is not fully accounted for, but if it were, equation (4.15) would apply.

The effects of the oscillator motion are not generated simply by large excursions of R(t) during the collision. Figure 4.4 compares the time-dependent variation of R(t) with and without the effects coupled to the collision dynamics for two extreme cases: (a) H_2-H collisions, where the excursions of R(t) are largest, but the effect is negligible; and (b) HBr-He collisions, where the excursions are smaller, but a phase shift is introduced in the oscillator motion that severely alters the remaining oscillator response.

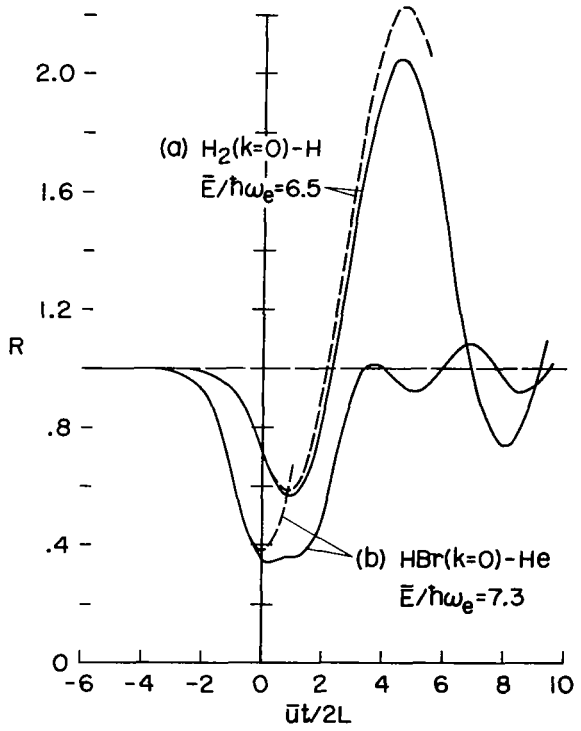

Figure 4.4.- Transient oscillator effects on the interaction potential; R is defined by equation (4.3b). Curves ———— denote the potential term with the oscillator motion coupled to the classical trajectory; curves — — — — denote the potential term without coupling.

4.2.3 Applicability of First-Order Perturbation Theory

Figures 4.2 and 4.3 amply demonstrate the fact that, when the oscillator is anharmonic, not only must $P_{k\to n}$ be small for the first-order perturbation theory to apply but the transient motion of the oscillator must also have no significant effect on the collision dynamics. When the effects of the oscillator motion were negligible, the perturbation approximation fails when $P_{k\to n} \to 1$. Further increases in $\bar{E}$ cause $P_{k\to n}$ to exceed unity before reaching a maximum — a familiar feature of equivalent harmonic oscillator models. In the application of a perturbation approximation to anharmonic oscillators, a probability maximum may appear for $P_{k\to n} < 1$, but the maximum is always an artifact of the semiclassical perturbation approximation and signals the failure of the theory due to the neglect of $R(t)$ variations. These conclusions are not surprising, but they further constrain the anharmonic oscillator perturbation theory to heavy homonuclear molecules such as N_2, O_2, and the halogens. First-order perturbation calculations for slightly heteronuclear molecules such as CO also require careful attention. Just as for H_2, collisions of CO with lighter particles (e.g., CO-He collisions) were unaffected by the oscillator motion. However, figure 4.5 shows that perturbation calculations of collisions with heavier particles (e.g., CO-Ar collisions) display large errors due to the coupled oscillator motion and also due to an increased coupling of the nonadjacent oscillator states that are not included in the perturbation approximation. As figure 4.5 shows, the two effects compensate each other for the initial state chosen. In the CO-Ar case, the perturbation-theory errors are not accompanied by anomalous probability maximums in the energy range of practical interest.

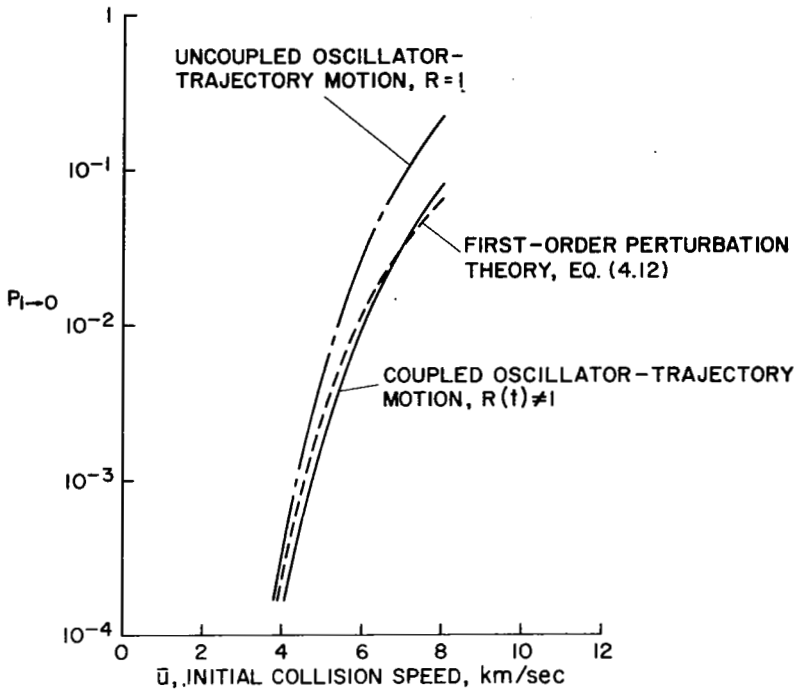

Figure 4.5.- Semiclassical transition probabilities for CO(k = 1) - Ar collisions; L = 0.02 nm.

4.3 Summary

The semiclassical approximation has been applied to vibrational transitions induced in anharmonic oscillators by collinear collision with inert atoms. Multistate numerical solutions have been compared with exact quantum-mechanical calculations of an equivalent collision model for a wide range of initial molecular states and collision partners. The comparisons allow a comprehensive assessment of the semiclassical approximation for the anharmonic oscillator model. The semiclassical predictions accurately reproduce the quantum-mechanical transition probabilities for all initial collision energies from the threshold to at least the first probability maximum if either the semiclassical collision velocity or energy is interpreted as a simple average of the exact initial and final values. The accuracy of the correlation between theories is not sensitive to the choice of averaging method.

The semiclassical approximation, in its usual form where the classical trajectory is computed independently, was found to be applicable to heavy homonuclear molecules such as N_2, O_2, and the halogens on impact with lighter partners. Lighter homonuclear molecules such as H_2 showed poorer agreement when impacted by a heavier collision partner. Heteronuclear anharmonic molecules such as the hydrogen-halides displayed anomalous resonances at low energy that do not appear in their harmonic counterparts. The accuracy of the semiclassical approximation for light or heteronuclear anharmonic molecules was significantly improved by coupling the effects of the time-dependent average motion of the recoiling oscillator to the classical trajectory.

A convenient, analytical, first-order, perturbation analysis for anharmonic oscillators was found to be accurate for small-transition probabilities, but only if the effects of the oscillator motion on the classical trajectory were unimportant. The analytical approximation is therefore not applicable to significantly anharmonic and heteronuclear molecules and must be applied with care for slightly heteronuclear molecules such as CO.

CHAPTER 5

VIBRATIONAL QUANTUM NUMBER DEPENDENCE OF ENERGY-TRANSFER RATES

In chapter 1, we discussed the sparseness of experimental and theoretical efforts to describe the rates of vibrational energy transfer from initially excited vibrational states. The objectives of this chapter are therefore to examine the factors influencing the prediction of such rates and to evaluate the validity of several analytic formulas in popular use for estimating their quantum number dependence. However, the approach to be taken must be limited by pragmatic considerations. For example, accurate V-T rate-coefficient calculations by any theoretical model are clouded by uncertainties in the shape and magnitude of the interaction forces between colliding pairs for all but a few simple cases. Thus, we can examine only the qualitative features that are not masked by interaction potential uncertainties. Furthermore, even an extended collision model must retain some approximations, particularly regarding the collision geometry, if it is to remain computationally practical in the prediction of thermally averaged rate coefficients. Hence, attention is confined here to the collinear semiclassical treatment described in chapter 4 that accurately reproduces all the main characteristics of vibrational energy transfer to initially excited oscillators, but offers the advantage of being further reducible to yield closed-form analytic solutions. The analytic solutions are of particular interest because of their practical importance in the numerically cumbersome analysis of macroscopic nonequilibrium processes for which rate information for several modes of energy transfer must be economically

provided.[11-15] The complete semiclassical model, requiring numerical solution, is applied both to an examination of the qualitative nature of upper-state transitions and as a basis for evaluating the accuracy of the analytical solutions.

In the sections to follow, the features of the collision model that appear most important to the dynamics of a vibrationally excited oscillator are first discussed, followed by a description of several approximations, each of which retains one or more of the features considered. Approximate values of the interaction potential parameters and their range of uncertainty are then estimated by comparing the predicted ground-state rate coefficient with a comprehensive set of experimental values. Collisions of CO with He are chosen as the example because of the abundant data available. The implied potential parameters are then used to compare the numerical model with some experimental excited-state rate coefficients and with the analytic predictions. Finally, the effects of multiple-quantum transitions from excited states on a vibrational relaxation process are considered both for molecules like CO, where the effect is secondary, and for molecules like the halogens, where the effect can be dominant.

5.1 Collision Model

5.1.1 Features Influencing the Excited-State Collision Dynamics

As the quantum number of the initial oscillator state is increased, several aspects influencing the oscillator dynamics and its interactions with the incident particle become increasingly important. For example, the wave functions that describe vibrationally excited eigenstates become more extended in the oscillator coordinate. Consequently, when the

oscillator is distorted by a collision, the wave-function overlap is greater not only with adjacent eigenstates but with more remote states as well. This feature is reflected by the increased magnitude of the matrix elements dynamically coupling the eigenstates which, in turn, accounts for the greater probability of V-T energy transfer through both single- and multiple-quantum transitions. Furthermore, the increased coupling of *nonadjacent* states during the collision can affect the final occupation of states adjacent to the initial state and thereby influence the rate of single-quantum transitions. Thus, a calculation of the oscillator dynamics from an excited initial state must include multiple-state interactions at collision energies where they are normally unimportant for oscillators in the ground state.

The degree with which multiple-quantum transitions influence the oscillator dynamics during a collision depend, in part, on the form of the interaction potential. A common practice, often used to simplify the analysis of ground-state oscillators, is to consider the oscillator motion small compared to the range of interaction and linearize the interaction potential in the oscillator coordinate. In a harmonic oscillator, this treatment has the effect of equalizing all the diagonal matrix elements and forbidding multiple-quantum transitions. The occupation of nonadjacent oscillator states is then possible only through a sequence of single-quantum steps during the collision. Nonlinear interaction terms remove these restrictions and modify final-state occupations in two related ways. First, all the nonadjacent states are directly coupled, thereby increasing their accessibility. Second, the diagonal matrix elements are no longer equal, leading to additional phase distortions in the quantum-mechanical oscillator motion which modify the probability of transition. The additional phase

shifts depend on the product of the difference between diagonal matrix elements and the strength of the interaction. They appear explicitly in a semiclassical impact parameter treatment described by Bates[93] and applied to anharmonic oscillators by Mies.[21] The formulation has been reviewed in section B.3 of Appendix B.

All the foregoing effects are amplified when oscillator anharmonicity is included. Nonadjacent states become coupled even for linearized interactions and the larger difference between the diagonal matrix elements creates phase distortions that can become a significant fraction of the unperturbed oscillator period. Mies[20,21] has shown the influence on transition probability predictions to be large even for oscillators initially in the ground state. A second, and in some cases greater, effect of anharmonicity is its influence on the variation of eigenenergies with quantum number. Since transition probabilities and the related rate coefficients are known to depend on the amount of energy transferred, a lowest-order effect of oscillator anharmonicity may be demonstrated by simply inserting anharmonic oscillator eigenenergies into a harmonic oscillator theory such as that given by Schwartz *et al.*[30] The results deviate substantially from the simple Landau-Teller relation for the rate coefficients given by equation (1.2) and repeated here as

$$k_{m,m-1}(T) = m\, k_{1,0}(T) \tag{5.1}$$

where $k_{m,m-1}(T)$ denotes the rate coefficient for transitions from state m to $m-1$ and is a function of the kinetic temperature T. However, the simple *ad hoc* insertion of anharmonic eigenenergies into a harmonic oscillator model is not always a sufficient means of accounting for anharmonicity.

The influence of anharmonicity on the interaction matrix elements, which in turn effects both the magnitude and phase of the oscillator motion, is often so great that an anharmonic oscillator model must be used from the start. Fortunately, oscillator anharmonicity and nonlinear interaction potentials present only a slight increase in computational difficulty, particularly if a Morse oscillator and an exponential form of the interaction are adopted. The necessary matrix elements are then conveniently expressed in closed algebraic form just as for harmonic oscillators.

Finally, an oscillator potential creating anharmonicity also admits to the existence of continuum states. We shall neglect their contribution to the energy transfer process, however, since they are energetically inaccessible by a large margin for the combinations of collision energies and initial states considered here. Although their effects have not been evaluated, the occupation of continuum states is presumed to be as small as the nearby bound states, and no bound states near the continuum were found to influence the dynamics of any states at the quantum levels of interest.

5.1.2 Aspects of the Semiclassical Numerical Model

To obtain V-T rate coefficients, we calculate the associated transition probabilities using the semiclassical collision model described in chapter 4, wherein the trajectory is constrained to collinear encounters. One of the penalties of using a semiclassical approximation was shown to be that total energy is not conserved; but as shown in chapter 4, the effects of that omission are easily and accurately compensated for by interpreting the relative collision energy as an average of the known initial and final values. A far more severe limitation of the semiclassical theory was

found to be its incomplete treatment of the interaction when the oscillator is very heteronuclear (e.g., hydrogen-halides). Such cases are avoided here and have presented numerical difficulty in exact treatments.[68]

The implications introduced by a restriction to collinear encounters are not as well understood, but the restriction is necessary if the quantum-number dependence of thermally averaged rate coefficients is ever to be obtained in a reasonable computing time. Clearly, a more realistic approach would include a three-dimensional collision geometry in which simultaneous rotational transitions are coupled with the vibrational motion, but the large number of rotational states that become accessible at collision energies sufficient to cause vibrational transitions would make our objective of studying thermally averaged rate coefficients impractical for all but a few special molecules, like H_2. On the other hand, so long as the rotational eigenenergies of the undisturbed molecule are well described by a rigid-rotor model (suggesting that the rotational and vibrational motions are separable), and the molecular properties are such that vibrational energy is traded mainly with translation, the disparity between a collinear and a three-dimensional theory is not expected to be very sensitive to the initial vibrational quantum number. Chapter 6 provides greater insight into the necessary conditions. For our purposes, the collinear predictions are normalized according to the ratio $k_{m,m-1}/mk_{1,0}$, thus avoiding the prediction of absolute rate coefficients and, hopefully, much of the absolute error associated with the collinear restriction. Such a ratio also absorbs the lowest-order quantum-number dependence suggested by equation (5.1).

5.1.3 Thermally Averaged Rate Coefficients from a Collinear Semiclassical Model

With the possible exception of molecular beam analyses, the applications of an inelastic collision model usually require results in the form of a thermally averaged rate coefficient. A general formulation of the averaging integral is well known, but here the restriction to collinear trajectories and the use of a semiclassical approximation require some special consideration. Generally, the rate coefficient for a kinetic temperature T may be written in terms of the energy parameter $\varepsilon_m = E_m/kT$ and an energy-dependent cross section $\sigma(E_m)_{m\to n}$, where n denotes the final quantum state and E_m is the relative kinetic energy before a collision with an undisturbed oscillator in a pure eigenstate m. The rate coefficient is then similar to equation (2.2), that is,

$$k_{m,n}(T) = \bar{C} \int_0^\infty \sigma(E_m)_{m\to n} \varepsilon_m e^{-\varepsilon_m} d\varepsilon_m \tag{5.2}$$

where the average thermal speed is $\bar{C} = (8kT/\pi\mu)^{1/2}$ and μ is the reduced collision mass defined by equation (2.3). A further requirement for the collision model is that it conform to the detailed balance relations. Originating with the reciprocity theorem, the requirements of detailed balance propagate through three levels of microscopic detail, giving the general physical relations for spinless nondegenerate collision partners as

$$P(E_m)_{m\to n} = P(E_n)_{n\to m} \tag{5.3a}$$

$$E_m \sigma(E_m)_{m\to n} = E_n \sigma(E_n)_{n\to m} \tag{5.3b}$$

$$k_{m,n}(T)\, e^{-\hbar\omega_m/kT} = k_{n,m}(T)\, e^{-\hbar\omega_n/kT} \tag{5.3c}$$

where $P_{m\to n}$ is the transition probability from state m to n and $\hbar\omega_m$ is the oscillator energy of state m.

The collinear collision geometry produces semiclassical transition probabilities that behave according to equation (5.3a), but the restriction to a zero impact parameter leaves the cross section required by equation (5.2) undefined. One common solution is to adopt an effective hard-sphere cross section σ_o and compute the inelastic cross section according to

$$\sigma_{m\to n}(E_m) = \sigma_o P_{m\to n}(E_m) \tag{5.4a}$$

and

$$\sigma_{n\to m}(E_n) = \sigma_o' P_{n\to m}(E_n) \tag{5.4b}$$

Equation (5.3b) requires that

$$\sigma_o' = [1 + \hbar(\omega_n - \omega_m)/E_n]\sigma_o$$

thus suggesting that the "hard-sphere" size must depend on the collision energy and transition in question! This contradiction results from the collinear approximation, but the error is negligible when $|\hbar(\omega_n - \omega_m)|/E_n \ll 1$. When the ratio approaches unity, the transition probability is typically so small that the integral in equation (5.2) is unaffected.

Equation (5.2) must be modified further to compensate for the lack of energy conservation inherent in the semiclassical approximation. This discrepancy is easily and accurately corrected by interpreting the semiclassical relative collision energy $\bar{E}$ or speed $\bar{u}$ as an average of the initial and final values. The results in chapter 4 demonstrate that, while the correction can be large, the method of averaging has no apparent effect on the outcome for vibrationally inelastic collisions at all energies from

threshold up to the limits of practical interest. For convenience, we use an arithmetic energy average. Denoting the total energy as E_T, the semiclassical approximation is brought into close agreement with an equivalent quantum-mechanical calculation by the interpretation

$$\bar{E} = E_T - \hbar(\omega_m + \omega_n)/2 \tag{5.5}$$

Combining equations (5.2), (5.4), and (5.5) then gives the thermal averaging prescription for a collinear semiclassical collision model:

$$k_{m,n}(T) = \sigma_o \bar{C}\, e^{\hbar\omega_{mn}/2kT} \int_0^\infty P_{m\to n}(\bar{E}) \left(\epsilon + \left|\frac{\hbar\omega_{mn}}{2kT}\right|\right) e^{-\epsilon}\, d\epsilon \tag{5.6}$$

where $\epsilon = \bar{E}/kT$ and $\omega_{mn} = \omega_m - \omega_n$. To make the satisfaction of equation (5.3c) by (5.6) more obvious, the lower integration limit in equation (5.6) has been set to zero even though the independent variable transformation from ϵ_m to ϵ via equation (5.5) produces a limit of $\pm|\hbar\omega_{mn}/2kT|$, depending on the sign of ω_{mn}. The negative limit may clearly be reset to zero, but even when the limit is positive, the probability threshold is nearly twice the limit, so that again setting it to zero has no effect on the integral.

5.2 Analytic Approximations

Of the many analytic approaches appearing in the literature (see ref. 45 for a partial summary), three that stand out in their application for estimating the V-T rate coefficient variations with quantum number are (a) the semiempirical formulas for Morse oscillators of Keck and Carrier,[94] (b) the perturbation treatment of Morse oscillators developed by Mies,[21] and (c) the exact solution to a linearly forced harmonic oscillator obtained by Kerner.[36] Each approach retains one or more of the aspects of special

interest to this application. They share the common feature that all incorporate collinear collision geometry and all are based on an exponentially repulsive interaction potential (later referred to as potential I) of the form

$$V_I(x) = A\, e^{-x/L} \tag{5.7}$$

where the coordinates are defined in figure 4.1.

5.2.1 Keck-Carrier Formula for Anharmonic Oscillators

The formula obtained by Keck and Carrier[94] is an adaptation of the distorted-wave harmonic oscillator theory of Schwartz *et al.*[30] for a Morse oscillator. It includes an empirical fit to the numerical solution of an integral equation for the "adiabaticity factor" and provides a particularly simple formula for estimating single-quantum transition rates from an arbitrary initial state. Keck and Carrier made no claim for the suitability of their formula in applications beyond a demonstration of the role of vibrational nonequilibrium in a dissociating gas; but the formula was subsequently applied by Bray[95] in a pioneering and detailed calculation of a vibrational relaxation process for anharmonic oscillators, apparently because of its simplicity and for lack of a better estimate. For similar reasons, the Keck-Carrier formula has since gained widespread use in the detailed analysis of upper-state kinetics in lasers.[11-15] Its consideration here is motivated primarily by the number of kinetic models that incorporate it. The Keck-Carrier formula can be written in a form similar to equation (5.1) as[95]

$$k_{m,m-1}(T) = m\left(\frac{1 - x_e}{1 - mx_e}\right)\frac{F_m}{F_1}\, k_{1,0}(T) \tag{5.8}$$

where F_m is obtained from the empirical formula

$$F_m = \frac{1}{2}\left(3 - e^{4\pi\eta/3}\right) e^{4\pi\eta/3} \tag{5.9}$$

in which

$$\eta = -\omega_{m,m-1} L(\mu/2kT)^{1/2} \tag{5.10}$$

The transition frequency $\omega_{m,m-1} = \omega_m - \omega_{m-1}$ is computed for a Morse oscillator as done previously by the expression

$$\omega_m = \omega_e\left(m + \frac{1}{2}\right) - \omega_e x_e\left(m + \frac{1}{2}\right)^2 \tag{5.11}$$

5.2.2 Mies Perturbation Solution for Anharmonic Oscillators

The closest approximation to the numerical model used here is a semiclassical first-order perturbation treatment developed by Mies.[21] It properly includes the effects of anharmonicity but, by the nature of first-order methods, it neglects the influence of states other than the designated initial and final states. Furthermore, to obtain an analytical solution, the classical path must be computed independently from the motion of the oscillator. The theory is therefore applicable only to single-quantum transitions in which the transition probabilities are small compared to unity. As demonstrated in chapter 4, the independent classical path further restricts its application to nearly homonuclear oscillators such as CO (and, of course, all homonuclear molecules) colliding with atomic particles of lighter mass than either of the molecular nuclei. The appearance of a probability maximum signals the failure of the theory. Despite these shortcomings, we shall see that the Mies solution still provides a more useful approximation of the numerical predictions than the other analytic formulas investigated.

A convenient form of the Mies result was given by equation (4.12) and is rewritten here for the transition probability from state m to n, where $n = m \pm 1$ as

$$P(\bar{E})_{m\to n} = \left[\frac{V_{mn}}{V_{mm}} \frac{2\pi g\mu L\bar{u}}{\hbar \sinh(\pi g)} \Phi(-g,\lambda)\right]^2 \tag{5.12}$$

As with the numerical model, equation (5.12) produces energy-dependent transition probabilities, while a temperature-dependent rate coefficient is desired. No analytic solution of the integral equation (5.6) with $P(\bar{E})_{m\to n}$ given by equation (5.12) is apparent, but a reasonably accurate technique (labeled the "method of steepest descent") for obtaining an analytic approximation[45] is based on the well-defined maximum contained in the integrand of equation (5.6). The value of ε at which the maximum occurs is determined primarily by the exponential arguments. The remaining function is slowly varying over the range of the integrand and may be evaluated at the single value ε_p locating the peak. The exponential argument is then expanded to second order about the peak and the term integrated analytically. In this application, the notation is simplified with the substitutions $\varepsilon_{mn} \equiv \hbar\omega_{mn}/2kT$ and $\eta = -\omega_{mn}L(\mu/2kT)^{1/2}$. The exponential nature of equation (5.12) is also simplified by noting that, in the energy range where the perturbation analysis is applicable, the transition period $t_p = 2\pi/\omega_{mn}$ is typically less than the effective collision period $t_c = 2L/\bar{u}$. Thus, $\pi g = t_c/t_p > 1$ and $\sinh(\pi g) \approx (1/2)e^{\pi g}$. Equations (5.6) and (5.12) are then combined to give

$$k(T)_{m,n} = \sigma_o \bar{C}\left[\frac{V_{mn}}{V_{mm}} 4\pi \frac{\eta^2}{\varepsilon_{mn}}\right]^2 e^{\varepsilon_{mn}} \int_0^\infty \left(\bar{\varepsilon} + |\varepsilon_{mn}|\right) \Phi^2 \; e^{-\bar{\varepsilon} + 2\pi\eta\bar{\varepsilon}^{-1/2}} d\bar{\varepsilon} \tag{5.13}$$

The integrand peak is located at

$$\varepsilon_p = [\mu(\pi\omega_{mn}L)^2/2kT]^{1/3} \tag{5.14}$$

Using the procedure described, the approximate solution to equation (5.13) becomes

$$k_{m,n}(T) = 16(3\pi^3)^{-1/2}\sigma_o\bar{C}\left(\frac{V_{mn}}{V_{mm}}\frac{\varepsilon_p^3}{\varepsilon_{mn}}\right)^2\varepsilon_p^{1/2}\left(\varepsilon_p + |\varepsilon_{mn}|\right)\Phi^2(-g_p,\lambda_p) \times e^{-3\varepsilon_p+\varepsilon_{mn}}\left\{1 + \text{erf}\left[(3\varepsilon_p/4)^{1/2}\right]\right\} \tag{5.15}$$

where $g_p = \varepsilon_p/\pi$ and $\lambda_p = \varepsilon_p^2(V_{mm} - V_{nn})/(\pi\varepsilon_{mn}V_{nm})$. The error function in equation (5.15) is close to unity for most cases. Equation (5.15) has $\log k \propto T^{-1/3}$ as expected and satisfies equation (5.3c). The temperature at which a given collision speed is coincident with the peak of the integrand in equation (5.13) defines the most effective speed at that temperature; this temperature will also be useful and can be identified from equation (5.14) as

$$T_p = \mu\bar{u}^3/(2\pi k|\omega_{mn}|L) \tag{5.16}$$

Comparisons of the approximate integration in equation (5.13) with exact numerical integrations show that the approximate method is most accurate at low temperatures. The first-order perturbation formula, equation (5.12), is most accurate at low energies, thus further contributing to the accuracy of equation (5.15) at low temperatures.

5.2.3 Kerner Solution for Linearly-Forced Harmonic Oscillators

The final analytic formula to be considered is an exact solution obtained by Kerner[36] for a harmonic oscillator that undergoes a forcing

function linear in the oscillator coordinate. That condition may be satisfied in situations where $r/L << 1$ in equation (5.7). The potential may then be linearized according to

$$V(\bar{x},r) = A\, e^{-\bar{x}/L}(1 - \gamma r/L) \tag{5.17}$$

Kerner's solution was applied by Treanor[37] in a semiclassical collinear approximation using equation (5.17). Within the framework of the collision model, the resulting formula exactly calculates the probability of transitions between arbitrary states with the interaction of all states included. Thus, it can be applied at high collision energies where the interactions of more than two states influence the oscillator dynamics. Despite the approximate nature of the harmonic oscillator model, wherein direct multiple-quantum transitions and the unbalanced coupling of higher and lower states caused by anharmonicity are excluded, the Kerner solution remains useful because it offers the only analytic means for estimating transition probabilities at high energies. Examples will be shown where multiple-quantum transitions and oscillator anharmonicity are not dominant, allowing accurate prediction by the Kerner solution.

Kerner and Treanor write the probability for transitions between two arbitrary states m and n as

$$P_{m\to n}(\bar{E}) = m!n!e^{-E_o}E_o^{m+n}\left\{\sum_{j=0}^{J}\left[(-E_o)^j(m-j)!j!(n-j)!\right]^{-1}\right\}^2 \tag{5.18}$$

where J is the lesser of the quantum numbers m and n. The parameter E_o is the energy absorbed by a classical harmonic oscillator divided by one quantum of vibrational energy. For a collinear collision and the interaction of equation (5.17), Rapp[96] obtains

$$E_o = 2(2\pi\omega L\gamma\mu)^2 \, e^{-2\pi\omega L/\bar{u}} \Big/ \left(\hbar\omega\mu_o\right) \qquad (5.19)$$

where μ_o is the reduced mass of the oscillator and ω is the oscillator frequency. The accuracy of the model, when applied to highly excited oscillators, is substantially improved if the effective oscillator frequency is corrected for anharmonicity for each initial state m according to $\omega = \omega_e(1 - 2x_e m)$. Without the correction, the excited-state rate coefficients would simply behave according to the Landau-Teller relation, equation (5.1), at low temperatures where the effective values of E_o are all less than unity and give $k_{m,m-1}/mk_{1,0} < 1$ for large E_o. An inconvenience of the Kerner formula is its incompatibility with the approximate integration method of equation (5.6) for obtaining a rate coefficient. A simplified version of equation (5.18), assuming $E_o << 1$, permits an approximate analytical solution. However, the calculations are then restricted to a thermal range where multiple-quantum effects are insignificant and the theory loses its advantages over perturbation solutions. In the comparisons to follow, we have therefore resorted to a numerical integration of equation (5.6) when the Kerner solution is applied.

5.3 Comparisons with CO-He Experiments

In this section, the ability of the theoretical model to reproduce experimental rate coefficients is tested. Unlike past comparisons of vibrational rate coefficients with theory, we now have access to at least one set of experimental values for excited initial states.[4] To test the consistency of the theory and experiment for all vibrational states, however, the effective interaction range L and the hard-sphere cross section σ_o

are determined from the abundant collection of measurements dominated by transitions between the ground state and first vibrational state. The interaction parameters required to match the ground-state experiments are then applied in comparisons with the excited-state rate measurements.

5.3.1 Effective Interaction Potential Parameters

The computational convenience gained from the simplified interaction potential I, equation (5.7), justifies its use, but as a consequence of its simplified form, the predicted rate coefficients cannot be expected to reproduce the experiments at all kinetic temperatures. Transitions induced in an oscillator depend to a large extent on the potential gradient near the distance of closest approach; while in a collinear collision, the distance of closest approach is determined solely by the coordinate where the potential magnitude equals the initial kinetic energy of the collision. Thus both potential features are important. However, the magnitude of a purely repulsive potential, such as equation (5.7), and that of a more realistic potential with an attractive well may be the same at the closest approach distance, but have a significantly different gradient. Consequently, where collisions are averaged over a range of energies, the predicted variation of rate coefficients with kinetic temperature will be different for the two potentials. By matching theory and experiment in several thermal ranges, and by using more than one potential form, an indication of the degree of uncertainty in rate coefficients attributable to potential errors can be obtained. For that purpose, we consider a second potential given by

$$V_{II}(x) = D\, e^{(x_e - x)/L} - 2D\, e^{(x_e - x)/2L} \qquad (5.20)$$

Potential II is a Morse-type interaction with an attractive well of depth $-D$ at coordinate x_e. As with equation (5.7), the exponential form allows matrix elements to be calculated analytically.

Predictions by the numerical anharmonic oscillator model with the oscillator initially in the first eigenstate $m = 1$ are compared with experiment in figure 5.1. When potential I, equation (5.7), is used, the rate coefficients are independent of the magnitude A, so that only the range L requires specification. Similarly, the predictions using potential II are independent of x_e, but require both L and D to be specified. The value $D/k = 100$ K is representative of well depths inferred from viscosity measurements.[80] The two potential gradients are different by about 20 percent at closest approach for the typical conditions considered. Figure 5.1 demonstrates the expected results. No unique set of potential parameters reproduces the experiments over the complete thermal range, but the more realistic potential II comes the closes. The required values of L fall between 0.02 and 0.03 nm, depending on the thermal range considered.

As an interesting aside, note that the low-temperature departure of the experimental rate from a variation proportional to $T^{-1/3}$ is also followed by the theory using simple repulsive potentials. As Shin[97] points out, these low-temperature departures do not necessarily depend on weak attractive forces normally omitted from the interaction potential; they even occur with a repulsive potential when the thermal averaging integration is done accurately for low collision energies. We know, however, that real interaction potentials usually contain an attractive component and it will augment this low-temperature behavior.

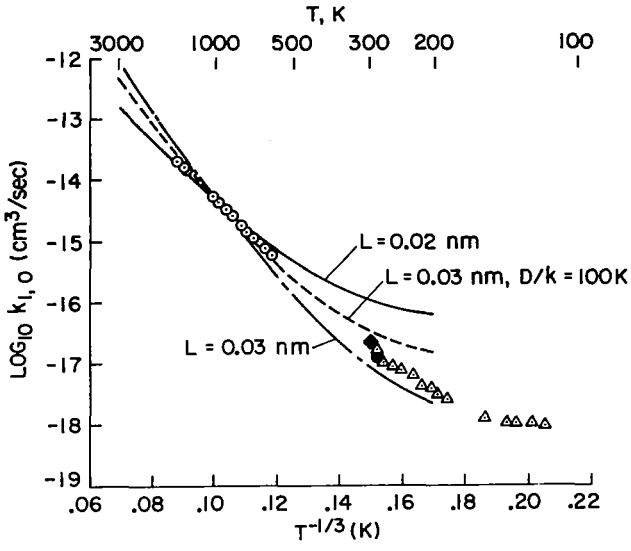

Figure 5.1.- A comparison of experimental rate coefficients for CO(M = 1)-He transitions to the ground vibrational state with predictions from the numerical model of chapter 4. The solid and long-short dashed lines were computed using the repulsive interaction potential I, equation (5.7). The short-dashed line was computed using the Morse interaction potential II, equation (5.20). Hard-sphere collision cross sections were chosen for each potential to match the experiment at T = 1000 K. Experimental values are from: o reference 16, • reference 17a, △ reference 17b, ♦ reference 17c.

5.3.2 Comparisons with Excited-State Rate Measurements

Normalized rate coefficients, predicted for initially excited CO at T = 300 K, are compared in figure 5.2 with the room temperature measurements of Hancock and Smith.[18] The parameter $k_{m,m-1}/mk_{1,0}$ is much less sensitive to interaction uncertainties than the absolute rate coefficients and varies in a simple, nearly linear manner with initial-state quantum number m. The nearly linear quantum-number dependence, increasing with m at room temperature, is predicted for all the interaction potentials examined and is believed to be an accurate description of the real behavior. As figure 5.2

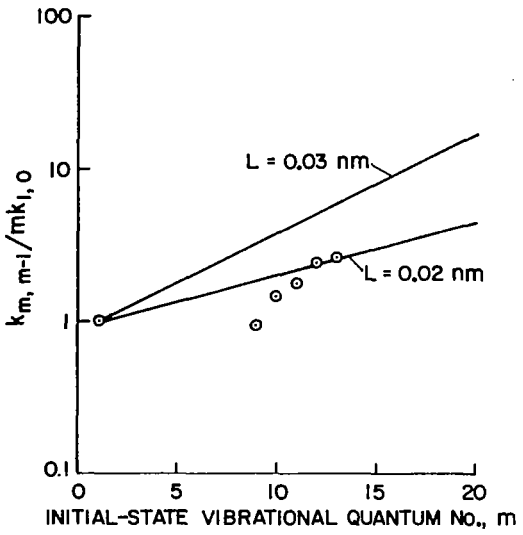

Figure 5.2.- A comparison of experimental rate coefficients at T = 300 K for CO(m)-He transitions from vibrational states m to m - 1 with predictions from the numerical model using repulsive potential I, equation (5.7). The excited-state data are from reference 18 and have been normalized using the experimental $k_{1,0}$ value of Milliken[16,17] (fig. 5.1).

shows, the experimental excited-state values compare favorably in magnitude with the predictions, but their trend is inconsistent with a linear extrapolation to m = 1. A highly nonlinear extrapolation is contrary to any prediction of the collision model at any temperature. Although the collision model contains many simplifications awaiting refinement, the behavior implied by the experimental rates appears also to require further verification and extension. In the interim, the theoretical predictions of excited-state rates seem to be qualitatively reasonable and self consistent despite their quantitative uncertainty. Unfortunately, their verification by experiment remains inconclusive.

5.4 An Evaluation of the Analytic Approximations

The computational expense of the numerical model makes it impractical as a general means of estimating excited-state rate coefficients. Instead, it is

used here as a basis for evaluating the more convenient but less complete analytic formulas. The predicted rate coefficient variations with quantum number for several models are illustrated in figure 5.3 for two extreme temperatures. The differences in the various models depend strongly on the kinetic temperature, but they all predict a simple monotonic change with quantum number. The analytic approximations are therefore more clearly evaluated by choosing the highest initial quantum number of practical interest and then comparing the predictions for a range of temperatures. For CO,

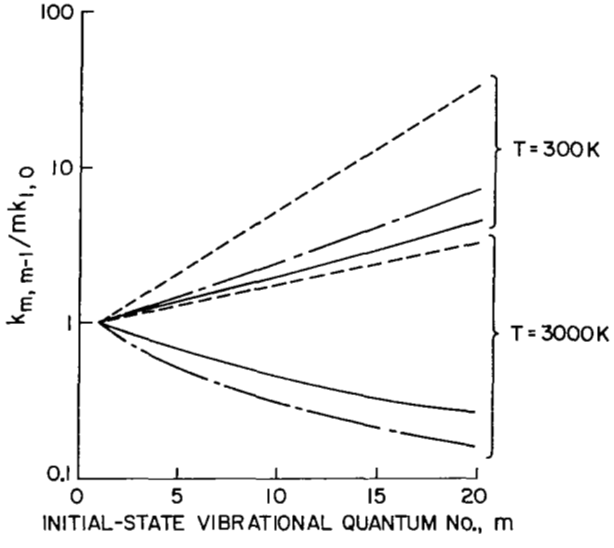

Figure 5.3.- The CO(m)-He rate coefficient dependence on quantum number predicted by several collision models. The solid lines represent the anharmonic numerical model, the long-short dashed lines represent the Kerner harmonic oscillator solution,[36] equation (5.18), and the dashed lines are from the formula of Keck and Carrier,[94] equation (5.8). The potential range $L = 0.02$ nm was used in all cases.

Rich *et al.*[15] have shown that energy transfer from vibrational levels as high as the twentieth can influence the net energy balance in an electrically excited CO laser system. Choosing $m = 20$ as an example, the single-quantum rate coefficients predicted by all the collision models are compared

in figure 5.4. The independent parameter $(\hbar\omega_e/kT)^{1/2}$ was chosen so that predictions by the Keck-Carrier formula, equation (5.8), appear as a nearly straight line. A comparison of the rates from the numerical model using

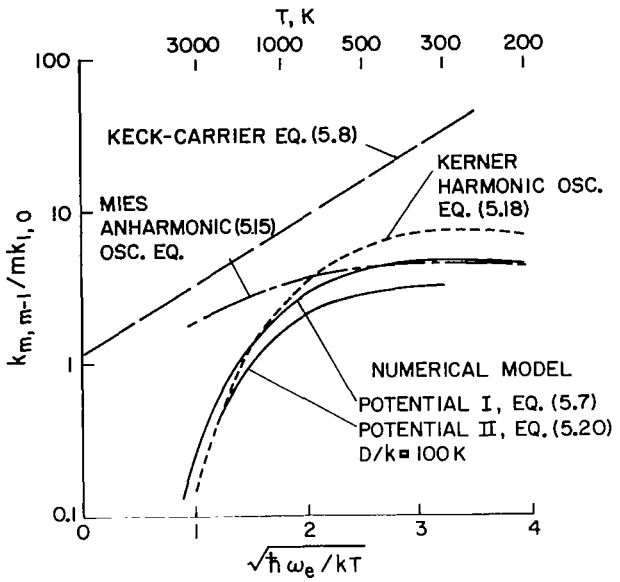

Figure 5.4.- A comparison of excited-state rate coefficients for CO(m = 20)-He predicted by several collision models. The potential range was L = 0.02 nm in all cases.

potentials I and II shows the moderate sensitivity of $k_{m,m-1}/mk_{1,0}$ to the form of the potential for one potential range L at all temperatures. Not shown is the great sensitivity of the magnitude of $k_{m,m-1}/mk_{1,0}$ to other potential ranges at any temperature. Note, however, that the qualitative nature of the predictions are undisturbed by the form of the potential and are therefore considered realistic. As expected, the Mies solution, equation (5.15), accurately reproduces the numerical results at low temperatures, but fails at higher temperatures where multiple-state interactions begin to affect the single-quantum transitions. The departure is signaled when transition probabilities approaching unity influence the thermal

averaging integral, equation (5.6). Since CO is not very anharmonic, the Kerner harmonic oscillator model, equation (5.18), frequency-corrected for anharmonicity at $m = 20$, works well over the entire thermal range. Note that the anharmonic correction must be included, however, as all predictions are significantly above the result stated by equation (5.1) for a single-frequency harmonic oscillator. Finally, figure 5.4 shows that the Keck-Carrier formula, equation (5.8), is too crude an approximation for large initial quantum numbers.

The degree of oscillator distortion caused by the collision of a light helium atom with a CO molecule has an insignificant effect on the classical trajectory. This fact is made evident by the small difference at low temperatures between the numerical model (where the effect is included) and the Mies solution (where it is neglected). An example in which the coupling is larger is illustrated in figure 5.5 for CO(m = 20)-Ar collisions. In this

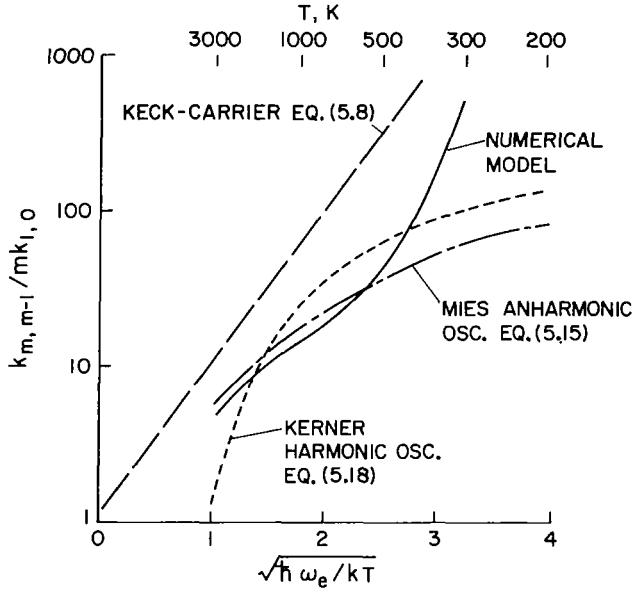

Figure 5.5.- A comparison of excited-state rate coefficients for CO(m = 20)-Ar. Potential I, equation (5.7), was used with L = 0.02 nm in all cases.

situation, none of the analytic models do well at low temperatures because the effects of oscillator distortion on the classical path modifies the transition probabilities even near threshold. The small corrections are then greatly amplified by the thermal averaging integral at low temperatures.

The small anharmonicity of CO(x_e = 0.0062) has influenced the preceding examples mainly by altering the energy spacing between excited eigenstates. Anharmonicity also modifies the absolute magnitude of the rate coefficients, but that effect is not apparent in $k_{m,m-1}/mk_{1,0}$. An example in which the anharmonicity is large is illustrated in figure 5.6 for H_2(m = 10)-He (x_e = 0.0268). In this case, the frequency-corrected harmonic oscillator model is inaccurate at all temperatures. The large spacing between eigenenergies in H_2 suppresses the onset of multistate interactions

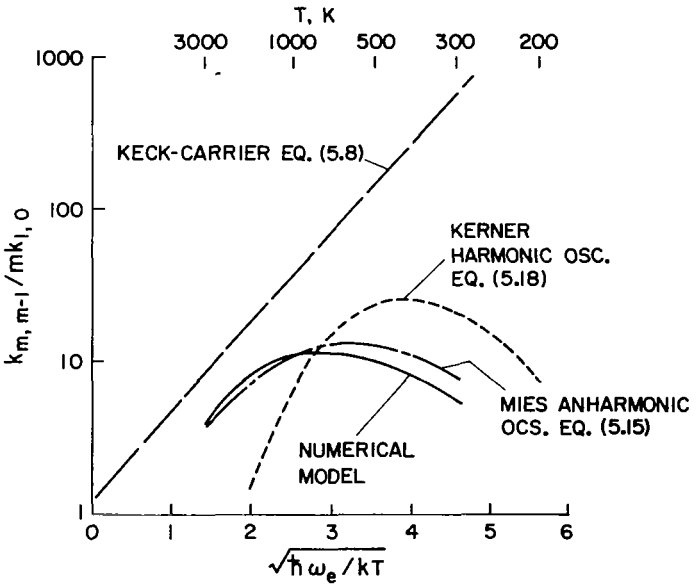

Figure 5.6.- A comparison of excited-state rate coefficients for H_2(m = 10)-He. Potential I, equation (5.7), was used with L = 0.02 nm in all cases.

at high temperatures, making the Mies solution an accurate reproduction of the numerical results over the entire thermal range. The difference in mass between the He and H nuclei produces only moderate coupling between the compressed oscillator and the classical path (e.g., see fig. 4.2).

As the preceding comparisons indicate, one cannot generally choose a single analytic model for estimating excited-state rate coefficients that is applicable to all collision pairs. The situations where a model should not be used are easier to identify. Clearly, the Keck-Carrier formula, equation (5.8), is too approximate in all the examples. The Kerner harmonic oscillator solution, equation (5.18), with anharmonicity-corrected frequencies is reasonably accurate unless the anharmonicity is large. The Mies anharmonic oscillator solution, equation (5.15), is a poor approximation when multiple-state interactions become important. Finally, no analytic model based on the semiclassical approximation will be realistic when the oscillator dynamics have a significant influence on the classical path of the incident particle. This restriction limits all the models considered to collision pairs in which the mass of the incident particle is not significantly greater than the mass of the impacted nucleus and to oscillators that are not extremely heteronuclear.

5.5 Multiple-Quantum Transitions

In the preceding section, only transitions to an adjacent state were examined. Here, we investigate the relative importance of multiple-quantum transitions, particularly for oscillators in highly excited states. The probabilities of multiple-quantum transitions are compared in figure 5.7 both for CO(m)-He collisions in which the oscillator is initially in an

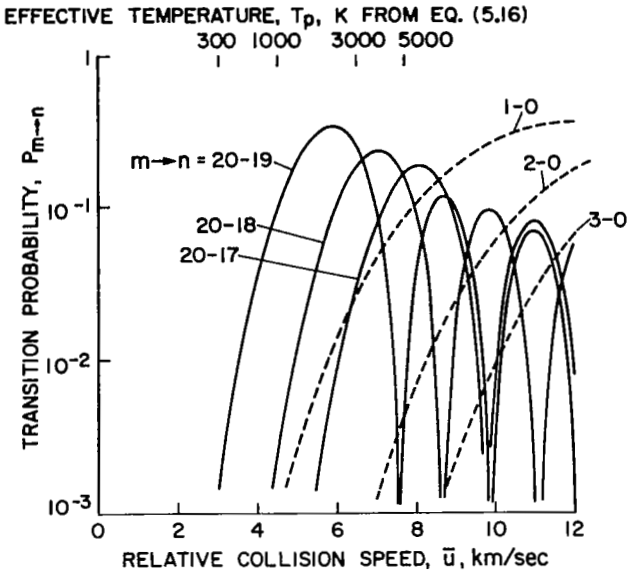

Figure 5.7.- Multiple-quantum transition probabilities for CO(m)-He collisions using the anharmonic numerical model with potential I and L = 0.02 nm. The effective temperature T_p locates the most effective collision speed contributing to the thermally averaged rate coefficient at the temperature designated.

excited state and in states near the ground state. The collision speeds contributing most to the thermally averaged rate coefficient at a selected temperature are indicated by the effective temperature T_p. In the thermal range considered, multiple-quantum transitions to the ground state are always improbable compared to single-quantum transitions from the first vibrational level, but the situation is clearly different when the oscillator is initially in the twentieth quantum state. However, thermally averaging the transition probabilities in figure 5.7 reduces the apparent importance of multiple-quantum transitions in a relaxation process. Figure 5.8 illustrates the resulting rate coefficients for two potential ranges, using potential I and values of σ_o obtained from the experimental match in figure 5.1 at T = 1000 K. The amplified uncertainty caused by the interaction potential

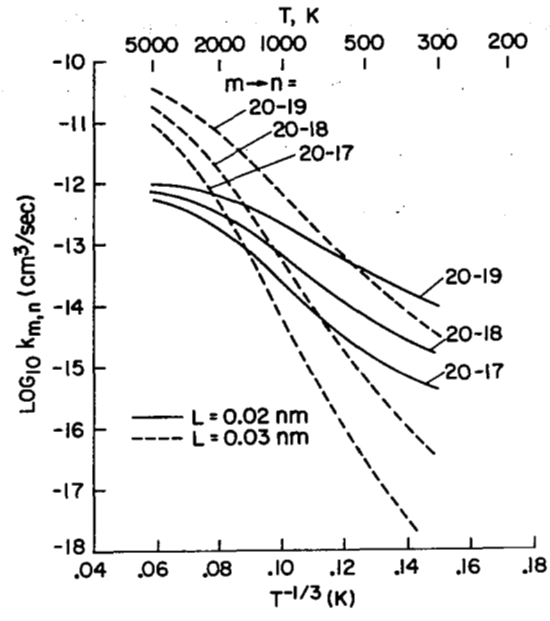

Figure 5.8.- Multiple-quantum rate coefficients for CO(m)-He. Potential I was used in the anharmonic numerical model. The hard-sphere cross-section values σ_o for each potential range are those required to match the experimental rates in figure 5.1 at T = 1000 K.

and its influence on the implied value of σ_o is most obvious, but the qualitative features are again consistent for both potential ranges. For oscillators like CO, multiple-quantum transitions provide a significant path for energy transfer only at very high temperatures according to these predictions.

A temperature marking the onset of competitive multiple-quantum transitions is the characteristic vibrational temperature of the oscillator, here defined as $\theta_v = \hbar\omega_e/k$ (for CO, θ_v = 3122 K). An oscillator in which multiple-quantum transitions will dominate the relaxation process can then be identified if θ_v is small compared to the thermal range of interest. One extreme example is Br_2 for which θ_v = 465 K. Since the anharmonicity is also small in Br_2(x_e = 0.0033), the Kerner harmonic oscillator model has

been used to obtain the Br_2-He rate coefficients displayed in figure 5.9. Two- and three-quantum transitions from the tenth vibrational level are shown to be significant even at room temperature, and the temperature dependence of the single-quantum rate $(m \rightarrow n = 10 \rightarrow 9)$ is inverted by multiple-state interactions when compared with the dependence shown in figure 5.8. The high probability of multiple-quantum transitions in this case contributes to the extremely fast and thermally insensitive relaxation rates measured in the halogens and it destroys the concept of a single "relaxation time" that is independent of the nonequilibrium state of the process for molecules of this type.

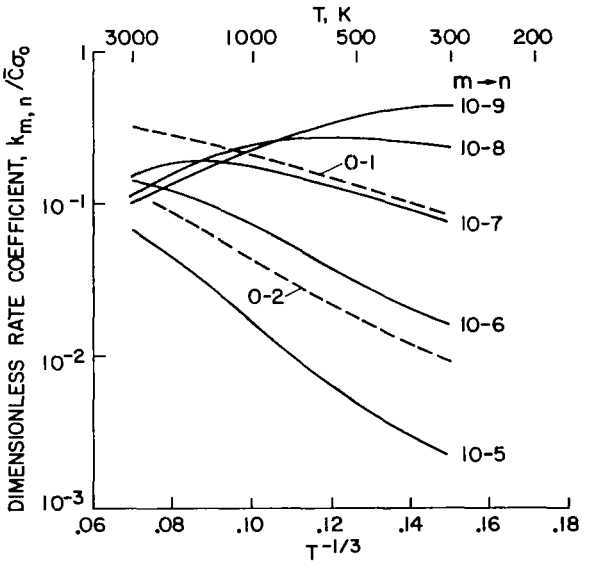

Figure 5.9.- Multiple-quantum rate coefficients for $Br_2(m)$-He predicted using the Kerner harmonic oscillator solution, equation (5.18), with L = 0.02 nm.

5.6 Concluding Remarks

We have relied on a collinear semiclassical model for vibrationally inelastic collisions entirely for pragmatic reasons. The collinear geometry

affords an economically reasonable means of estimating V-T rate coefficients for excited molecules and the semiclassical approximation is easily reduced to practical analytic solutions. While these simplifications clearly obviate the quantitative accuracy of the calculations, no serious omission other than rotational coupling is apparent that would modify their qualitative nature, even in the presence of uncertain interaction potentials. Unfortunately, an attempt to confirm the predicted features through experimental comparison was inconclusive. However, the experimental conditions that would test the model most severely can at least be identified. For example, the choice of collision partner has a large influence on the rate coefficient sensitivity to initial quantum number. Note the large deviations of $k_{m,m-1}/mk_{1,0}$ from unity in figure 5.5 for CO-Ar compared to those in figure 5.4 for Co-He. Furthermore, the increased oscillator distortion caused by heavy atom impact requires a more complete description of the interaction than needed for light atoms. From another viewpoint, the lesser sensitivity of some features of the prediction to uncertainties can guide the choice of experimental variables to be emphasized. In particular, an apparently universal feature of the V-T excited-state rate predictions is their monotonic low-order variation with quantum number. Once this feature is confirmed, the experimental emphasis can be shifted to the less predictable variations with kinetic temperature. Finally, a comparison of the estimates using various potential parameters suggests that a self-consistent set of experimental rates for both high and low initial quantum numbers contains much more information that defines the interaction potential than ground-state rates alone.

Comparisons of the analytic and numerical rate coefficients graphically delineate the suitable range of application for each analytic model. However,

the utility of an analytic approximation can also depend on the physical properties of the application. For example, the Kerner harmonic oscillator model, with anharmonically corrected frequencies, predicts $k_{m,m-1}/mk_{1,0}$ with surprising accuracy for many molecules; but before the model can be economically applied, an analytical solution to the thermal averaging integral, including Kerner's transition probability formula, awaits development. Even with that solution in hand, one must be concerned with the effect of anharmonicity for each molecule treated by the model. On the other hand, Mies' solution for anharmonic oscillators, equation (5.15), fails at high temperature. At those conditions, however, many nonequilibrium processes are insensitive to the V-T rates of excited states, either because the vibrational state population distribution is nearly Boltzmann or because the process is controlled by some separate energy-transfer mechanism. At lower temperatures, the model accurately deals with a broader range of oscillators because anharmonicity is rigorously included. Collision partners for which the theory fails are poorly treated by all the analytic solutions based on a semiclassical approximation. Similarly, the frequently used formula developed by Keck and Carrier is useful because of its simplicity, but the additional computation required by the Mies solution is not prohibitive. The series function $\Phi(-g,\lambda)$ converges rapidly and the matrix elements may be computed in advance.

Calculations of multiple-quantum transition rates from excited states validate the assumption most often made in kinetic models of nonequilibrium processes: they can usually be neglected. As before, at very high temperatures where multiple-quantum transitions become competitive, a nonequilibrium process is usually not controlled by excited-state V-T rates, while

ground-state transitions are still dominated by single-quantum steps. Molecules with closely spaced vibrational energy levels, such as the halogens, are notable exceptions requiring a more careful analysis.

CHAPTER 6

EFFECTS OF ROTATIONAL TRANSITIONS ON VIBRATIONAL ENERGY TRANSFER

The preceding chapters have utilized a collinear collision model in which vibrational motion was the only form of energy transferred during a collision, and, indeed, in many cases it is. However, the use of a one-dimensional collision geometry renders the model incomplete in the sense that cross sections and rate coefficients cannot be obtained directly, but require artificial three-dimensional parameters such as steric factors or hard-sphere cross sections that must be estimated by some other means.

From a more physical point of view, collisions with sufficient energy to induce vibrational transitions will simultaneously cause numerous transitions among the more closely spaced rotational states, thus invoking an additional energy sink not represented in the collinear models. This chapter investigates the influence of rotational motion on the net rate of vibrational energy transfer. It is motivated by a need to assess the validity of the collinear models since they remain the most practical means for predicting vibrational rate coefficients in a kinetic analysis. With that motivation, emphasis is directed here toward the net rate of vibrational energy transfer summed over all final rotational states, rather than individual vibration-rotation transitional rates, since only the former can be compared with the collinear predictions.

In the sections to follow, a semiclassical three-dimensional collision model is first developed in detail. It is followed by a description of some approximations that significantly reduce the number of coupled states necessary to obtain a complete solution, thus making numerical results practical.

The collision dynamics are then studied for molecular types that represent all extremes in the role of rotational motion on vibrational transition rates. The role of rotational coupling is summarized and categorized in conceptual terms in the final section and the common characteristics of all related V-R-T mechanisms are discussed.

6.1 Vibration-Rotation Collision Model

A three-dimensional, vibration-rotation collision model is formulated here within the semiclassical framework described in appendix B and based on the following underlying concepts: the incident particle is considered structureless while the target is a diatomic heteronuclear molecule. A natural parameter for measuring the heteronuclear nature of the molecule is its mass ratio

$$\gamma = m_c/(m_b + m_c)$$

where m_b and m_c are the nuclear masses and $m_c \geq m_b$. The inertial properties of the molecule are modeled by a Morse-oscillator/rigid-rotor description (discussed in ch. 3). The collision geometry is described classically with the associated coordinates shown in figure 3.4 as viewed in a rotating interaction plane containing all three nuclei. The classical trajectory is assumed to be dominated by the spherically symmetric component of the interaction potential and is determined from just those terms. Consequently, the relative path remains in a single plane and the subsequent formulation is greatly simplified. These concepts are reflected in an illustration of the collision geometry shown in figure 6.1, where it is viewed from a space-fixed position in a center-of-mass reference frame aligned with the plane of the trajectory.

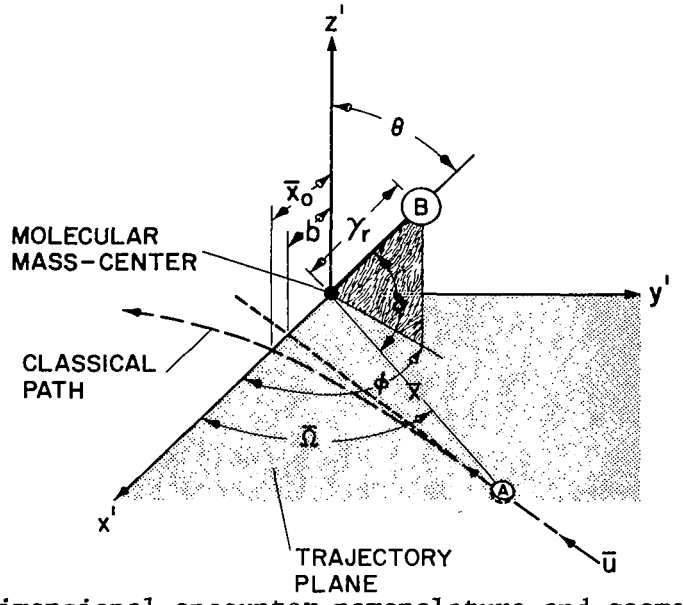

Figure 6.1- Three-dimensional encounter nomenclature and geometry as viewed from a fixed position in the center-of-mass reference frame. The x',y' plane contains the molecular mass center and the incident particle path. Only the portion of the molecule above the plane is shown.

The detailed formulation of a semiclassical model divides logically into three main parts — one defining the nature of the interaction potential between the colliding pair, one detailing the quantized motion of the molecule in response to a time-dependent disturbance, and one describing the classical motion of the incident particle that produces the disturbance. The description to follow proceeds in the same order.

6.1.1 Interaction Potential

A comparison of the predictions from the collinear model described in chapter 4 with those of a three-dimensional model will be most meaningful if the interaction potentials are similar. We therefore make use of the exponentially repulsive and pairwise additive interaction discussed in chapter 3 and write, with reference to figure 3.4,

$$V'(x_b, x_c) = A\left(e^{-x_b/L} + e^{-x_c/L}\right) \tag{6.1}$$

To conveniently separate the molecular dynamics from the classical motion, however, equation (6.1) must be expressed explicitly in terms of coordinates describing each of the motions separately. To this end, we have shown in chapter 3 that equation (6.1) can be represented to first-order in $r/\bar{x}$ by

$$V'(\bar{x},r,\delta) = A\, e^{-\bar{x}/L}\left(e^{\gamma(r/L)\cos\,\delta} + e^{-(1-\gamma)(r/L)\cos\,\delta}\right) \qquad (6.2)$$

where the relative angle, δ, is related to the space-fixed coordinate angles in figure 6.1 by

$$\cos\,\delta = \sin\,\theta\,\cos(\phi - \bar{\Omega}) \qquad (6.3)$$

Equation (6.2) expresses the potential in the desired explicit form. However, to aid the following separation of dynamical equations into coordinates that describe the motion of each collision partner, we shall temporarily denote the potential by an equivalent notation $V'(\bar{x},r,\delta) \equiv V'(\vec{q},t)$ where $\vec{q} = \vec{q}(r,\theta,\phi)$ locates the molecule in configuration space and t emphasizes the temporal dependence of the trajectory coordinates, $\bar{x}(t)$ and $\bar{\Omega}(t)$, appearing in equations (6.2) and (6.3).

6.1.2 Quantized Molecular Dynamics

In appendix B, we show that the quantum-mechanical equation of motion may be reduced to a set of differential equations — one for each bound eigenstate of the undisturbed molecule — in terms of the probability amplitudes associated with each bound state. The result is

$$i\hbar\,\frac{dc_j(t)}{dt} = \sum_n c_n(t)e^{i(\omega_j-\omega_n)t}\langle j|V'(\vec{q},t)|n\rangle \qquad (6.4)$$

where the bracket notation refers to

$$\langle j|V'(\vec{q},t)|n\rangle = \int \psi_j^*(\vec{q})V'(\vec{q},t)\psi_n(\vec{q})d\vec{q} \qquad (6.5)$$

integrated over all $\vec{q}$ space and ψ_n is an eigenfunction of the undisturbed molecule determined by the intramolecular potential, $V_o(r)$. As in chapter 4, the intramolecular potential is modeled by the Morse function:

$$V_o'(r) = D_o\left[e^{-2a(r-r_e)} - 2e^{-a(r-r_e)}\right] \tag{6.6}$$

Combined with a rigid-rotor description of the molecular rotational motion, the eigenfunctions ψ_n are then determined by three quantum numbers $|v\ell m\rangle$ and have their eigenfrequency given by

$$\omega_{v\ell} = \omega_e\left(v + \frac{1}{2}\right) - \omega_e x_e\left(v + \frac{1}{2}\right)^2 + B_e\ell(\ell + 1) \tag{6.7}$$

The remaining task, leading to solutions for equation (6.4), is then to evaluate the matrix elements defined by equation (6.5) in terms of the fundamental collisional and molecular parameters.

The numerical labor of solving equation (6.4) will be reduced greatly if the matrix elements can be factored into a time-dependent term obtained classically and state-dependent terms containing all the quantum-mechanical spatial integrals. The spatial integration may then be completed independently and in advance for transitions between all eigenstates in the basis set. A step in that direction is taken by writing

$$\langle j|V'(\vec{q},t)|n\rangle = U(b,t)V'_{jn}(t) \tag{6.8}$$

where, from the potential given by equation (6.2), the right-hand terms are

$$U(b,t) = A\, e^{-\bar{x}(b,t)/L} \tag{6.9}$$

and

$$V'_{jn}(t) = \sum_{i=1,2} \langle j|e^{\alpha_i \frac{r}{L}\cos\delta}|n\rangle \tag{6.10}$$

with $\alpha_1 = \Upsilon$ and $\alpha_2 = -(1 - \Upsilon)$. Clearly, the function $U(b,t)$ can be obtained classically, but the expression for $V'_{jn}(t)$ must now be developed to

further isolate its time dependence. A useful aid will be the expansion of $e^{z \cos \delta}$ in terms of Legendre polynomials $P_J(\cos \delta)$ given by equation (3.30). In the present notation, the expansion is

$$e^{\alpha_i \frac{r}{L} \cos \delta} = \sum_{J=0}^{\infty} \left(\frac{\alpha_i}{|\alpha_i|} \right)^J (2J + 1) i_J\left(\alpha_i \frac{r}{L}\right) P_J(\cos \delta) \qquad (6.11)$$

where $i_J(\alpha_i r/L)$ is a spherical Bessel function of the first kind.[73]

Recalling that $|n\rangle$ refers to a vibration-rotation state with quantum numbers $|v\ell m\rangle$ and that the molecule is represented as a Morse-oscillator/rigid rotor, the eigenfunctions represented in equation (6.10) may be factored in the traditional manner according to

$$\psi_{v\ell m}(r,\theta,\phi) = \frac{\mathcal{R}_v(r)}{r} Y_{\ell m}(\theta,\phi) \qquad (6.12)$$

The factorization, in conjunction with equation (6.11), then allows the matrix elements to be represented as a sum of products given by

$$V'_{v'\ell'm'v\ell m}(t) = \sum_{J=0}^{\infty} (2J + 1) R^{(J)}_{v'v} T^{(J)}_{\ell'm'\ell m}(t) \qquad (6.13)$$

where

$$R^{(J)}_{v'v} = \sum_{i=1,2} \left(\frac{\alpha_i}{|\alpha_i|} \right)^J \langle v' | i_J\left(\alpha_i \frac{r}{L}\right) | v \rangle \qquad (6.14)$$

is a radial matrix independent of time and

$$T^{(J)}_{\ell'm'\ell m}(t) = \langle \ell'm' | P_J(\cos \delta) | \ell m \rangle \qquad (6.15)$$

is a spherical matrix element containing the trajectory coordinate $\bar{\Omega}(t)$ via equation (6.3). The remaining discussion is divided into separate developments of each element.

6.1.2.1 Radial Matrix Elements

The radial term defined by equation (6.14) appears in expanded form as

$$R^{(J)}_{v'v} = \langle v' | i_J\left(\gamma \frac{r}{L}\right) + (-1)^J i_J\left[(1 - \gamma)\frac{r}{L}\right] | v\rangle \qquad (6.16)$$

First note that when the molecule is homonuclear (i.e., $\gamma = 1/2$), the radial term will be nonzero only for even values of J and that it will emphasize even J values for most heteronuclear molecules where γ is nearly 1/2. This property directly affects the probabilities of rotational transitions. To evaluate the spherical Bessel functions in equation (6.16) in terms of the molecular coordinate r, we note that its arguments lie typically in the range $0 \leq \alpha_i r/L \leq 5$. Larger values are suppressed by the vibrational eigenfunctions that approach zero at large r. In this range of arguments, the spherical Bessel functions may be calculated with rapid convergence by the ascending series[73]

$$i_J(z) = \frac{z^J}{\prod_{j=0}^{J} (2j + 1)} \left[1 + \frac{z^2/2}{(2J + 3)} + \frac{(z^2/2)^2}{2!(2J + 3)(2J + 5)} + \cdots\right] \qquad (6.17)$$

The radial matrix element may then be written as

$$R^{(J)}_{v'v} = \frac{(2J + 1)\gamma^J}{\prod_{j=0}^{J} (2j + 1)} \sum_{n=0}^{\infty} \frac{(\gamma^2/2)^n}{n!} \frac{\left[1 + (-1)^n \left(\frac{1 - \gamma}{\gamma}\right)^{2n+J}\right]}{\prod_{k=0}^{n} (2J + 2k + 1)} r^{(2n+J)}_{v'v} \qquad (6.18)$$

where $r^{(m)}_{v'v}$ represents the remaining simplified integral

$$r^{(m)}_{v'v} \equiv \int_{-\infty}^{\infty} \mathcal{R}^*_{v'}(r)\left(\frac{r}{L}\right)^m \mathcal{R}_v(r)\,dr \qquad (6.19)$$

Equation (6.19) is similar to the integrals that define dipole matrix elements associated with vibrational band intensity calculations and, as such, it has been solved exactly for $m = 1$ and 2 using Morse oscillator

eigenfunctions.[98,99] In principle, the integral can be solved exactly for any integer value of m, but the complexity of the solution increases and becomes impractical for powers larger than m = 2. An iterative numerical method has also been developed,[100] but it becomes laborious for large quantum numbers.

In appendix C, we derive an approximate closed-form solution to equation (6.19) with the result:

$$r_{v'v}^{(m)} = \frac{N_{v'v}}{(aL)^m} \sum_{s=0}^{v'+v} D_s \Gamma(\lambda + s + 1) \left[\ell n \left(\frac{k'}{\lambda + s} \right) \right]^m + \left(\frac{r_e}{L} \right)^m \delta_{v'v} \qquad (6.20)$$

where $k' = \omega_e / \omega_e x_e$, $\lambda = k' - 2 - (v' + v)$, and $\Gamma(\lambda + s + 1)$ is a gamma function.[73] Coefficients D_s and $N_{v'v}$ contain elements of the Morse eigenfunctions (defined in appendix C). The derivation of equation (6.20) depends only on the provision that $\lambda >> 1$, which is easily obtained because $k' >> 1$ for all diatomic molecules. Typical values of k' range from 37 for H_2 to 161 for CO. Corresponding errors in $r_{10}^{(1)}$ from equation (6.20) are 1.5 percent for H_2 and 0.3 percent for CO. Hence equation (6.20) is sufficiently accurate in this application, although some numerical difficulties arise that can limit its use. For example, the terms of the summation in equation (6.20) alternate in sign so that, for large k' and large vibrational quantum numbers, small differences between extremely large terms cause the loss of all significant digits. The CDC-7600 computer with 28 digits in double precision allowed equation (6.20) to be evaluated with at least 3 accurate digits for vibrational quantum numbers less than 12 when $k' = 161$ and for all quantum numbers to the continuum when $k' = 37$. In the few cases when equation (6.20) could not be used, the integral was evaluated with a standard Gauss-Laguerre quadrature algorithm[101-103] of very high accuracy. (The author is indebted to D. G. Galant, NASA Ames Research Center, for developing the algorithm.)

6.1.2.2 Spherical Matrix Elements

The spherical term defined by equation (6.15) incorporates the rigid-rotor eigenfunction introduced in equation (6.12). The eigenfunctions are known to be spherical harmonics that satisfy[104,105]

$$\mathbf{L}^2 Y_{\ell m}(\theta,\phi) = \hbar^2 \ell(\ell+1) Y_{\ell m}(\theta,\phi)$$

and

$$\mathbf{L}_z Y_{\ell m}(\theta,\phi) = \hbar m Y_{\ell m}(\theta,\phi)$$

where $\mathbf{L}$ is the orbital angular momentum operator and $\mathbf{L}_z$ is a component. Note that the Legendre polynomial in equation (6.15) can also be represented as a spherical harmonic according to

$$P_J(\cos\,\delta) = \sqrt{\frac{4\pi}{2J+1}}\, Y_{J,0}(\delta,0)$$

allowing the spherical matrix element to be written as

$$T^{(J)}_{\ell' m' \ell m} = \sqrt{\frac{4\pi}{2J+1}} \int_0^{2\pi} \int_0^{\pi} Y^*_{\ell' m'}(\theta,\phi) Y_{J,0}(\delta,0) Y_{\ell m}(\theta,\phi) \sin\theta\, d\theta\, d\phi \qquad (6.21)$$

The solution to equation (6.21) follows common procedures in the mechanics of quantized angular momentum[104,105] and it is described in detail in appendix D. The result takes the form

$$T^{(J)}_{\ell' m' \ell m}(t) = \mathscr{M}^{(J)}_{\ell' m' \ell m}\, e^{-i(m'-m)\bar{\Omega}(b,t)} \qquad (6.22)$$

where the time-independent term is

$$\mathscr{M}^{(J)}_{\ell' m' \ell m} = (-1)^{(J+\bar{m})/2} \frac{\sqrt{(J+\bar{m})!\,(J-\bar{m})!}}{2^J \left(\frac{J+\bar{m}}{2}\right)! \left(\frac{J-\bar{m}}{2}\right)!} \sqrt{(2\ell'+1)(2\ell+1)} \begin{pmatrix} \ell' & J & \ell \\ 0 & 0 & 0 \end{pmatrix} \begin{pmatrix} \ell' & J & \ell \\ -m' & \bar{m} & m \end{pmatrix} \qquad (6.23)$$

Nonzero values are obtained only if

$$\left.\begin{aligned} \bar{m} &= m' - m \\ J \pm \bar{m} &\quad \text{even} \end{aligned}\right\} \qquad (6.24)$$

The bracket symbols in equation (6.23) are Wigner 3-j symbols that account for the vector coupling between the angular momentum states, $|\ell'm'\rangle$ and $|\ell m\rangle$, and the trajectory orbital momentum designated by J. They impose further constraints associated with nonzero values of $\mathcal{M}^{(J)}_{\ell'm'\ell m}$ that are listed collectively as

$$\left.\begin{array}{c} |\ell' - \ell| \le J \le \ell' + \ell \\ |m| \le \ell\ , \quad |m'| \le \ell'\ , \quad |\bar{m}| \le J \\ \ell' + \ell + J \quad \text{even} \end{array}\right\} \tag{6.25}$$

6.1.2.3 Complete Factored Matrix Elements

Factorization of the time-dependent terms in the complete matrix elements defined by equation (6.8) can now be accomplished by defining a *time-independent* matrix element (with an unprimed symbol) as

$$V_{v'\ell'm'v\ell m} = \sum_{J=|\ell'-\ell|}^{\ell'+\ell} (2J+1) R^{(J)}_{v'v}\, \mathcal{M}^{(J)}_{\ell'm'\ell m} \tag{6.26}$$

and writing the complete matrix element as

$$\langle v'\ell'm|V'(\vec{q},t)|v\ell m\rangle = U(b,t)e^{-i(m'-m)\bar{\Omega}(b,t)}\, V_{v'\ell'm'v\ell m} \tag{6.27}$$

The time-dependent terms, U(b,t) and $\bar{\Omega}(b,t)$, in equation (6.27) are then the functions required from the classical trajectory. Generally, they represent both an induced force and an induced phase shift in the molecular motion, where the magnitude of the latter depends on the rotational transition considered. However, the primary quantal properties of the collision dynamics are determined by the time-independent matrix elements given by equation (6.26). For example, the summation limits in equation (6.26) reflect the constraints imposed by equations (6.25) and lead to the only significant selection rule associated with vibration-rotation transitions. Recall from equation (6.16)

that, for homonuclear molecules, $R_{v'v}^{(J)}$ is nonzero only when J is even. Thus, nonzero matrix elements and transition probabilities will occur for homonuclear molecules only when $|\ell' - \ell|$ is even, according to equation (6.26). Similarly, for heteronuclear molecules, transitions of even $|\ell' - \ell|$ will dominate, although odd-increment quantum changes are allowed in those molecules. Other selection rules regarding intermultiplet transitions, m' to m, are also implied by equation (6.25) and their accompanying zeros may be observed in table 6.1, where a typical transition matrix is listed. However, the role of these degenerate states in determining the observable behavior of a kinetic process is usually lost due to subsequent averaging and hence become important only in the computational aspects of the collision model.

TABLE 6.1- TIME-INDEPENDENT TRANSITION MATRIX FOR CO

$v = 0, \quad \ell = 2$

$v' = 1$

$\ell' = 4$

m' \ m	2	1	0	-1	-2
4	-0.322	0	0.044	0	-0.006
3	0	-.189	0	.034	0
2	.142	0	-.135	0	.022
1	0	.156	0	-.097	0
0	-.065	0	.160	0	-.065
-1	0	-.097	0	.156	0
-2	.022	0	-.135	0	.142
-3	0	.034	0	-.189	0
-4	-.006	0	.044	0	-.322

Note: Shaded elements depict the symmetry of the matrix.

Figures 6.2 and 6.3 illustrate some general properties of the time-independent matrix elements and allow one to reach some early conclusions concerning the nature of vibration-rotation transitions during a collision. For

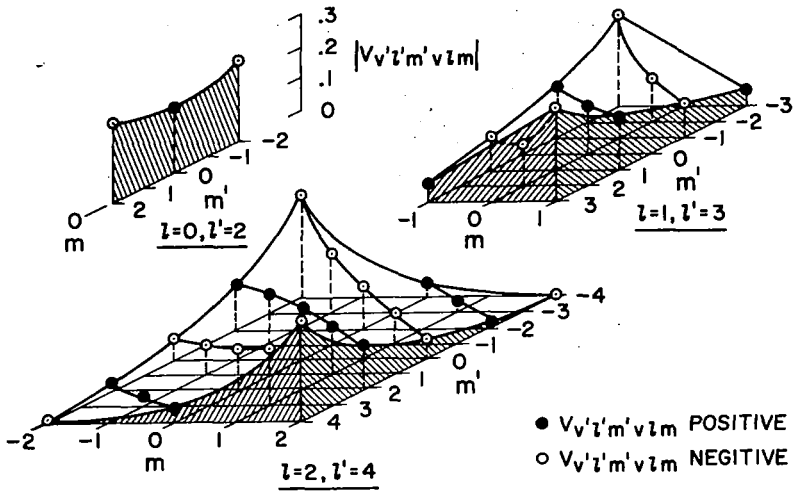

Figure 6.2- Variation of time-independent matrix elements defined by equation (6.26) with angular momentum quantum numbers, for CO with v = 0, v' = 1, and L = 0.02 nm.

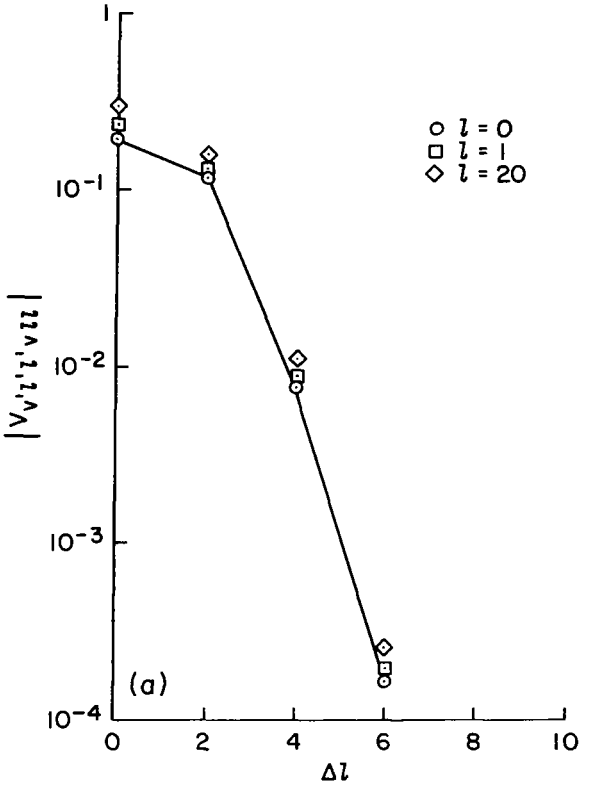

(a) H_2

Figure 6.3.- Variation of time-independent matrix elements with $\Delta\ell = |\ell' - \ell|$, for H_2 and CO with v = 0 and v' = 1.

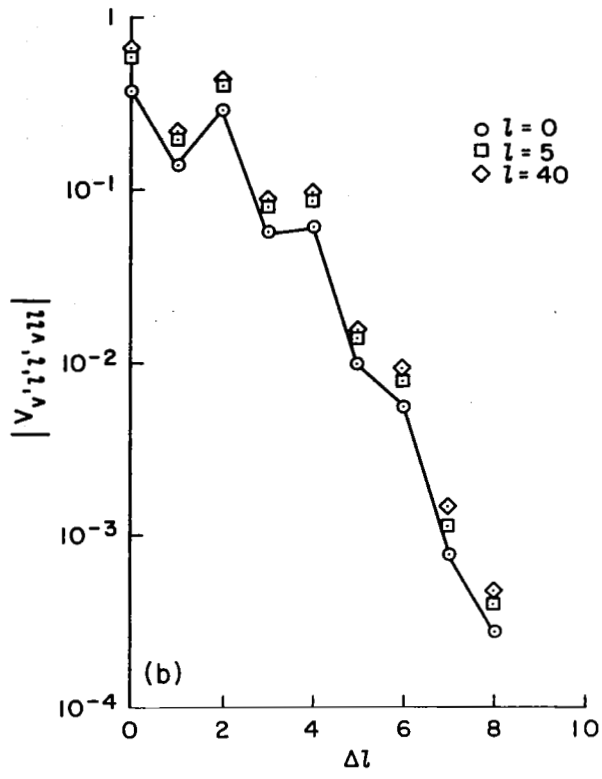

(b) CO

Figure 6.3.- Concluded.

example, figure 6.2 depicts the variation of matrix elements with projection state quantum number. These features will be of interest later when methods for reducing the number of coupled states in the calculation are sought. At this point, we simply note that transitions from the corners where $m = \pm\ell$, $m' = \pm\ell'$, and m', m have the same sign are the dominant route by which energy is transferred. As ℓ and ℓ' increase, the dominance also increases so that in the limit of large ℓ, ℓ', all other $m \neq \pm\ell$ and $m' \neq \pm\ell'$ states may be ignored.

Another basic aspect of the matrix elements is illustrated in figures 6.3(a) and (b) where for both H_2 and CO — two extremely opposite molecular types — only states with small differences in angular momentum, $\Delta\ell$ (where

$\Delta\ell \equiv |\ell' - \ell|$) are shown to share significant coupling. This feature persists for all values of ℓ, as shown by the sets of symbols in figures 6.3, and it also holds for all vibrational transitions. Note that the emphasis of small $\Delta\ell$ transitions is independent of any degree of resonance that may occur between the initial and final states of the transition since equation (6.26), from which these matrix elements are obtained, contains no reference to the eigenenergies of the transition.

Nevertheless, resonance enhances the probability for transition. Its effect, in combination with the preceding small $\Delta\ell$ constraint may be anticipated by examining the relative vibration-rotation eigenenergies depicted in figure 6.4 for both H_2 and CO. Note that while the transition $v\ell \rightarrow v'\ell' = 0,8 \rightarrow 1,0$ in para-H_2 is nearly resonant, $\Delta\ell = 8$ is too large and the coupling between these states (fig. 6.3(a)) will be very small. Much

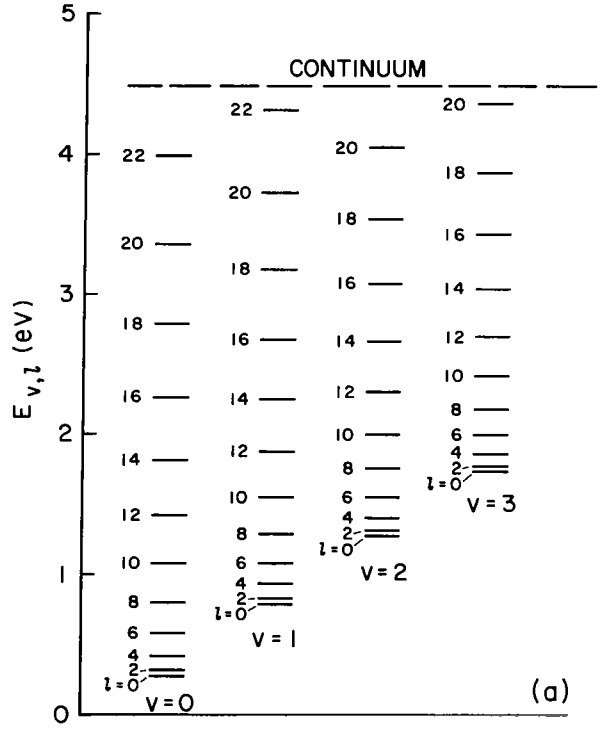

(a) Para-H_2

Figure 6.4.- Vibration-rotation eigenenergies for para-H_2 and CO.

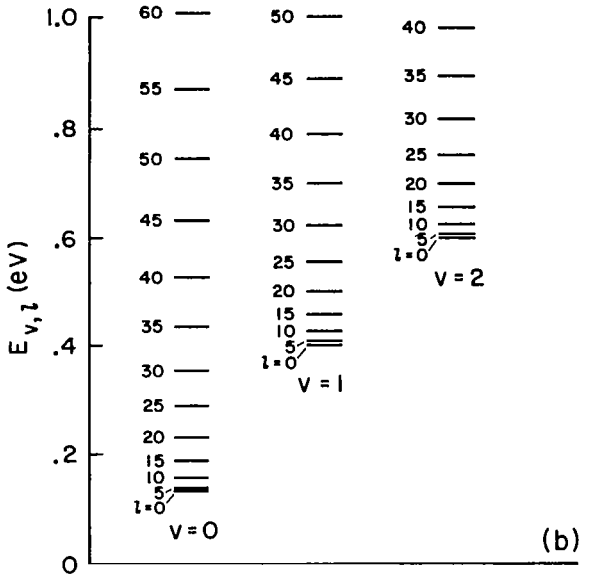

(b) CO (NOTE: Not all rotational levels are shown).

Figure 6.4- Concluded.

larger $\Delta\ell$ will be required in CO to approach resonant transitions while the restriction to small $\Delta\ell$ will make the rotational aspect of a vibrational transition insignificant. From these observations, we may conclude that, while transition probabilities are enhanced by resonance, *vibration-rotation transitions with small $\Delta\ell$ will dominate the intramolecular energy transfer process, regardless of resonance!*

Finally, we see from figures 6.3 that, although odd $\Delta\ell$ transitions do not occur in homonuclear molecules where $\gamma = 1/2$, a slightly heteronuclear molecule like CO ($\gamma = 0.43$) will allow odd $\Delta\ell$ transitions with only moderate suppression, as indicated by figure 6.3(b). Hence, the selection rule regarding even $\Delta\ell$ transitions applies strictly to homonuclear molecules.

The foregoing derivation of the molecular equations of motion has explicitly identified the required trajectory functions. We can now proceed to evaluate those functions classically in terms of the fundamental collision parameters.

6.1.3 Classical Trajectory

The classical, two-body, central-force equations of motion are obtained in appendix B as

$$\left(\frac{d\bar{x}}{dt}\right)^2 = \bar{u}^2\left[1 - \frac{\bar{V}(\bar{x})}{\bar{E}} - \left(\frac{b}{\bar{x}}\right)^2\right] \tag{6.28}$$

$$\frac{d\bar{\Omega}}{dt} = \frac{b\bar{u}}{\bar{x}^2} \tag{6.29}$$

where the coordinates refer to figure 6.1 and $\bar{V}(\bar{x})$ is a spherically symmetric version of the interaction potential. The total energy, $\bar{E}$, and the corresponding initial speed, $\bar{u} = \sqrt{2\bar{E}/\mu}$, are "effective" values averaged over the trajectory (as discussed in ch. 4).

In this chapter, we shall not include the dynamic influence of the molecule on the incident particle motion as in chapter 4. To do so in three dimensions would require a great deal of artificial approximation and would demand extensive comparisons with exact quantum-mechanical solutions for validation, as in chapter 4. Such an investigation is outside the intent of this chapter. Instead, we use the results in chapter 4 as a guide to those collision parameters where the dynamic coupling is unimportant and confine the examples used here to only those cases.

The form of the interaction potential necessary to determine a trajectory is obtained here by spherically averaging the model potential given in equation (6.2) over all coordinates of the molecule in its initial state. Thus,

$$\bar{V}(\bar{x}) = \langle i|V'(\vec{q},t)|i\rangle \tag{6.30}$$

where $|i\rangle$ denotes the initial state. By use of equation (6.27), the matrix element above may be rewritten in the more workable form:

$$\bar{V}(\bar{x}) = A\, e^{-\bar{x}/L}\, V_{ii} \tag{6.31}$$

This method of averaging the potential produces a single trajectory for each initial state of the molecule and it is independent of the numerous possible final states. Transition probabilities computed using other methods of averaging (e.g., involving a final state designation) were found to be only negligibly different from those obtained with equation (6.31) when the energy transferred inelastically is small compared to the total energy. Equation (6.30) is an approximation consistent with the adopted classical equations of motion since their accuracy is likewise contingent on the requirement that the energy traded inelastically remain small.

At this point, we have the sufficient formulation to obtain a full numerical solution of equation (6.4). However, the numerical integration of a coupled set of differential equations often proceeds with much less labor if all equations relax at intrinsically similar rates. The selection of step intervals in the independent variable (t in this case) is then controlled by the unanimous behavior of all dependent variables rather than the conflicting behavior of several dependent-variable subsets. (The amplitudes, $c_n(t)$, and the trajectory coordinates, $\bar{x}(t)$ and $\bar{\Omega}(t)$, are conflicting subsets with dissimilar relaxation rates in this case.) While a set of equations cannot always be idealized in such a manner, the numerical effort is reduced here significantly by using approximate analytic solutions of the classical trajectory equations and solving only the molecular equations of motion numerically.

An analytic solution of the trajectory equations is possible only because we have adopted an exponential interaction potential with convenient analytical properties. In most cases, however, nonexponential potential functions, such as the Lennard-Jones potential, equation (3.22), can be represented by an exponential function over the essential regions of interaction with acceptable

accuracy. A development of analytic solutions to the trajectory equations is described in detail in appendix E. The solutions are based on first-order approximations developed by Hansen and Pearson[106] and later extended by Stallcop.[107] Here we outline the procedure only briefly as it has been adapted in this application to obtain the functions $U(b,t)$ and $\bar{\Omega}(b,t)$.

The function $U(b,t)$ defined by equation (6.9) may first be converted to a more convenient form by noting that at closest approach $t = 0$, $\bar{x} = \bar{x}_o$, and $d\bar{x}/dt = 0$. Equation (6.28) may then be solved for $\bar{V}(\bar{x}_o)$ to obtain

$$A\, e^{-\bar{x}_o/L}\, V_{ii} = \bar{E}[1 - (b/\bar{x}_o)^2] \tag{6.32}$$

Equation (6.9) then becomes

$$U(b,t) = \frac{\bar{E}}{V_{ii}} [1 - (b/\bar{x}_o)^2]\, e^{-(\bar{x}-\bar{x}_o)/L} \tag{6.33}$$

When $b = 0$, we also have the solution to equation (6.28)

$$e^{-(\bar{x}-\bar{x}_o)/L} = \operatorname{sech}^2\left(\frac{\bar{u}t}{2L}\right) \tag{6.34}$$

Hansen and Pearson[106] assumed that a solution to equation (6.28) for nonzero impact parameters will have a similar form and defined a function, $a_b(b,t)$, so that, for all values of b,

$$e^{-(\bar{x}-\bar{x}_o)/L} = \operatorname{sech}^2[a_b(b,t)\bar{u}t/2L] \tag{6.35}$$

We show in appendix E that an expansion of both sides of equation (6.35) about $t = 0$ then gives, to first-order,

$$a_b(b,0) = [1 - (b/\bar{x}_o)^2(1 - 2L/\bar{x}_o)]^{1/2} \tag{6.36}$$

Furthermore, exact numerical solutions of equation (6.28) show that $a_b(b,t)$ varies so slowly with t that equation (6.36) may be used for all t. Figure 6.5 illustrates the accuracy of equation (6.36) for large impact parameters where the error is greatest and at a collision energy near threshold.

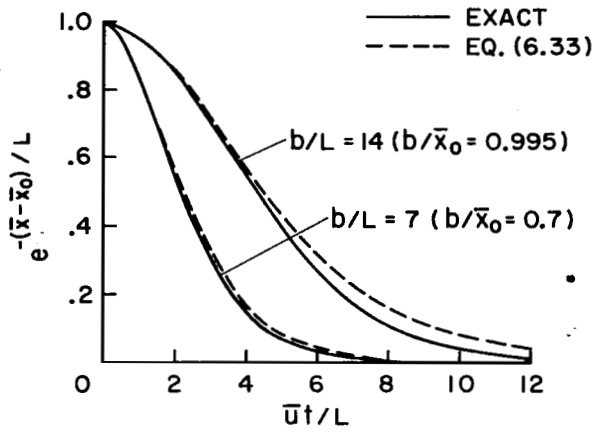

Figure 6.5.- Exact and approximate (eq. (6.33)) trajectory functions for non-zero impact parameters; $\bar{E}/AV_{ii} = 10^{-4}$.

A similar figure for energies 10 times greater would appear almost identical. Thus, we have the required analytic approximation:

$$U(b,t) \approx \frac{\bar{E}}{V_{ii}} [1 - (b/\bar{x}_o)^2] \operatorname{sech}^2[a_b(b,0)\bar{u}t/2L] \tag{6.37}$$

where $a_b(b,0)$ is obtained from equation (6.36) and $\bar{x}_o$ is the positive root of equation (6.32). For small impact parameters where the peak contribution to vibrational transition cross sections is made, $\bar{x}_o$ may be approximated by the analytic expression obtained from equation (6.32) for $b = 0$; namely

$$\bar{x}_o \approx \bar{x}_o(b = 0) = L \ln\left(\frac{AV_{ii}}{\bar{E}}\right) \tag{6.38}$$

Figure 6.6 indicates the range of b/L where equation (6.38) may be applied. Finally, for very large b/L where $b/\bar{x}_o \to 1$, the classical path follows a straight line, as figure 6.6 indicates, and although equations (6.36) and (6.37) are still sufficiently accurate, an alternate and more accurate approximation is

$$U(b,t) \xrightarrow[\frac{b}{\bar{x}_o} \to 1]{} A \exp\left[-\sqrt{(b/L)^2 - (\bar{u}t/L)^2}\right] \tag{6.39}$$

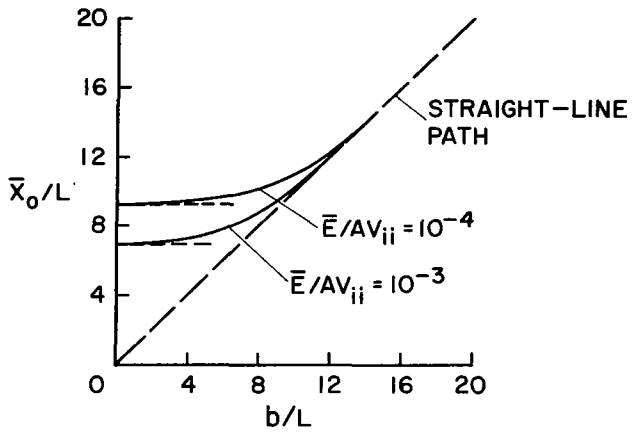

Figure 6.6.- Distances of closest approach.

The remaining trajectory function to be determined is $\bar{\Omega}(b,t)$. Hansen and Pearson[106] obtain an analytic expression by expanding $\bar{\Omega}(b,t)$ in a Taylor series about $t = 0$, again where the interaction is greatest, and keeping only terms to first order. Thus,

$$\bar{\Omega}(b,t) = \bar{\Omega}(b,0) + t\left(\frac{\partial\bar{\Omega}}{\partial t}\right)_{t=0} + \ldots$$

With the aid of equation (6.29), a first order approximation is then

$$\bar{\Omega}(b,t) \approx \frac{b\bar{u}}{\bar{x}_o^2}\, t \tag{6.40}$$

Stallcop[107] explores the error in neglecting higher-order terms and finds it to increase with $\Delta\ell$. However, the error in cross section is only about 10 percent for $\Delta\ell = 4$ and appears insensitive to collision energy. We see in figure 6.3 that the matrix elements and hence cross sections decrease rapidly

with $\Delta\ell$ and will be of marginal interest for $\Delta\ell > 4$. Thus, the approximate function given by equation (6.40) is used for its computational simplicity.

6.2 Representations of the Results

The solutions to equation (6.4) provide complex probability amplitudes, $c_n(+\infty)$, for all states included in the vibration-rotation set. The *final* transition probability from an initial state $|i\rangle$ to some other state $|n\rangle$ is then

$$P_{i\to n} = |c_n(+\infty)|^2$$

In more explicit notation, we designate the initial state by unprimed quantum numbers, $v\ell m$, and denote the probability

$$P(\bar{E},b)_{v\ell m\to v'\ell'm'} = |c_{v'\ell'm'}(\infty)|^2 \tag{6.41}$$

However, transitions between individual projection states, m and m', are rarely of interest in the analysis of a kinetic process. A more easily measured and useful quantity may be referred to as the *vibration-rotation* transition probability, defined as the final probability averaged over all initial projection states and summed over all final projection states according to

$$P(\bar{E},b)_{v\ell\to v'\ell'} = \frac{1}{2\ell+1}\sum_{m,m'} P(\bar{E},b)_{v\ell m\to v'\ell'm'} \tag{6.42}$$

Finally, to compare with a collinear model in which rotational transitions are nonexistent, we define a *net vibrational* transition probability as the total probability of finding the molecule anywhere in the manifold of rotational states associated with a designated vibrational state. Such a probability is computed simply as the sum

$$P(\bar{E},b)_{v\ell\to v'} = \sum_{\ell'} P(\bar{E},b)_{v\ell\to v'\ell'} \tag{6.43}$$

The net vibrational transition probability so defined still depends on the initial rotational state, however, and cannot be compared directly with collinear predictions. To evaluate the collinear approximation, we must first identify the properties of $P_{v\ell\to v'}$ that must be obtained to produce similar cross sections and rate coefficients from either collision model.

The relation of cross sections to transition probabilities has been discussed in chapter 2 and is known to be

$$\underset{v\ell\to v'}{\sigma(\bar{E})} = 2\pi \int_0^\infty \underset{v\ell\to v'}{P(\bar{E},b)} b \, db \tag{6.44}$$

Equation (6.44) poses no difficulty in a three-dimensional model but, as chapter 5 demonstrates, its application to the collinear model requires some additional consideration. Since the impact parameter, b, is not a collinear variable, an effective "hard-sphere" cross section, σ_o, must first be chosen by some independent means and the collinear cross section is then defined by

$$\underset{v\to v'}{\sigma(\bar{E})} = \sigma_o \underset{v\to v'}{P(\bar{E})} \tag{6.45}$$

The validity of equation (6.45) is contingent on the idea that σ_o is invariant with both quantum number and collision energy. One test of the utility of a collinear model is then to test this contingency by defining a parameter equivalent to σ_o but obtained from the three-dimensional collision theory. To that end, equation (6.44) may be recast into a form defining an "equivalent elastic cross section," σ_o^e, by the relation

$$\underset{v\ell\to v'}{\sigma(\bar{E})} = \sigma_o^e \underset{v\ell\to v'}{P(\bar{E},0)} \tag{6.46}$$

where

$$\sigma_o^e = \pi x_c^2 \int_0^\infty 2\left[\underset{v\ell\to v'}{P(\bar{E},b)} \Big/ \underset{v\ell\to v'}{P(\bar{E},0)}\right]\left(\frac{b}{x_c}\right) d\left(\frac{b}{x_c}\right) \tag{6.47}$$

and x_c is an arbitrary collision radius. Equation (6.47) has been written in a manner that also correlates with other concepts used in the methods for selecting a hard-sphere cross section, σ_o. For example, the constant, x_c, may be considered a radius corresponding to the elastic collision radius used to compute gas-kinetic collision rates.[8] The associated elastic cross section is then the constant term, πx_c^2, appearing in equation (6.47). When a Lennard-Jones interaction potential is adopted, x_c is often equated to the zero-potential radius and evaluated from viscosity or viral-coefficient measurements.[80]

The remaining integral term in equation (6.47) is

$$S = 2 \int_o^\infty \left[P(\bar{E},b)_{v\ell\to v'} \Big/ P(\bar{E},0)_{v\ell\to v'} \right] \left(\frac{b}{x_c}\right) d\left(\frac{b}{x_c}\right) \tag{6.48}$$

which may be identified with a "steric factor" often used as a correction for three-dimensionality with collinear collision models. The steric factor must be considered invariant in the collinear model, although its magnitude here depends on the values of $\bar{E}$ and the transition quantum numbers. Hence, cases in which either σ_o^e or S are invariant with both quantum number and collision energy show possibility as examples where a collinear collision model is applicable. However, the invariance of σ_o^e or S alone is not sufficient to declare collinear rate-coefficient predictions valid, as shown in the following discussion.

According to the results in chapters 4 and 5, a semiclassically determined cross section is related to the thermally averaged rate coefficient, in the notation of this chapter, by

$$k(T)_{v\ell\to v'} = \bar{C} \sum_{\ell'} e^{\varepsilon_{v\ell v'\ell'}} \int_o^\infty \sigma(\bar{\varepsilon})_{v\ell\to v'\ell'} \left(\bar{\varepsilon} + |\varepsilon_{v\ell v'\ell'}|\right) e^{-\bar{\varepsilon}} \, d\bar{\varepsilon} \tag{6.49}$$

where

$$\bar{\varepsilon} = \bar{E}/kT \ , \quad \varepsilon_{v\ell v'\ell'} = \hbar(\omega_{v\ell} - \omega_{v'\ell'})/2kT \ , \quad \text{and} \quad \bar{C} = (8kT/\pi\mu)^{1/2}$$

If we now assume that transitions for which the steric factor defined by equation (6.48) is invariant are those for which $\varepsilon_{v\ell v'\ell'} \approx \varepsilon_{vv'}$ (i.e., the contribution of rotational frequencies to the eigenfrequency can be neglected), then equation (6.49) is well approximated by

$$k(T)_{v\ell\to v'} \approx \bar{C}\sigma_o^e \, e^{\varepsilon_{vv'}} \int_o^\infty P(\bar{\varepsilon},0)_{v\ell\to v'} \left(\bar{\varepsilon} + |\varepsilon_{vv'}|\right) e^{-\bar{\varepsilon}} \, d\bar{\varepsilon} \qquad (6.50)$$

To compare with the collinear rate coefficient that presumably represents the average of all initial rotational states, we introduce a rotational state population fraction $N_{v\ell}(T_r)$ that is dependent on a rotational temperature, T_r. The net vibrational rate coefficient is then approximately

$$k(T,T_r)_{v\to v'} \approx \bar{C} \, \sigma_o^e \, e^{\varepsilon_{vv'}} \int_o^\infty \left[\sum_\ell N_{v\ell}(T_r) P(\bar{\varepsilon},0)_{v\ell\to v'}\right] \left(\bar{\varepsilon} + |\varepsilon_{vv'}|\right) e^{-\bar{\varepsilon}} \, d\bar{\varepsilon} \qquad (6.51)$$

For cases where $T = T_r$, it may be compared directly with a collinear rate coefficient. The additional conditions to be met before a collinear model may be applied are then shown by equation (6.51) to be that $P(\bar{E},0)_{v\ell\to v'}$ must be relatively *invariant with quantum number, ℓ, and it must vary with $\bar{E}$ in the same manner as the collinear equivalent probability.*

6.3 Numerical Methods of Solution

Numerical solutions to the set of differential equations (6.4) were accomplished using the same algorithm that was applied to the collinear model in chapter 4, namely, a fifth-order polynomial extrapolation technique developed by Bulirsch and Stoer[91] and provided in FORTRAN by Gear.[92] The method is shown by Hull *et al.*[108] to be generally advantageous both in

computer expense and reliability (error) over several other established methods, particularly the frequently used Runge-Kutta methods. A typical collision event could be computed in this application with as few as 50 steps while maintaining six-digit accuracy. Most solutions were obtained with 100 steps and initialized at a distance where the interaction potential was 10^{-4} of its value at closest approach.

An additional consideration required by the three-dimensional model was the economic use of computer storage. The time-independent matrix elements $V_{v'\ell'm'v\ell m'}$ given by equation (6.26), were computed prior to the numerical integration and stored in memory. However, their designation by a sixfold index set suggested by the associated quantum numbers is impractical even for the CDC-7600 computer with its large-core memory. Thus, advantage was taken of the zeros and symmetry of the matrix elements (see table 6.1 for examples) and an index scheme was developed that reduced the sixfold matrix to a one-dimensional vector with no zeros or duplicate elements. Details of the index method and its implementation in the computational procedure are described in appendix F.

An important conclusion, quickly recognized from early solutions, was that the number of coupled vibration-rotation states required to achieve a convergent solution (i.e., a solution for which the further addition of states made no change) was too large to be computed in a defensible time. For example, the execution time per step on the CDC-7600 computer was approximately $N^2/2$ msec, where N is the total number of coupled states. A convergent solution usually requires that at least all energetically accessible states must be included. Thus, if $\bar{\ell}$ denotes the uppermost rotational state, there are $2\ell+1$ projection states for each orbital state ℓ and hence $(\bar{\ell}+1)^2$

total states from $\ell = 0$ to $\bar{\ell}$. Computer time then varies as $(\bar{\ell}+1)^4$. For collision energies near vibrational threshold, $\bar{E} \geq \hbar\omega_e$ so that, from figure 6.4, minimum values are $\bar{\ell} \simeq 8$ for H_2 and $\bar{\ell} \simeq 33$ for molecules like CO. A corresponding minimum computing time for H_2 collisions is then approximately 5 min — an acceptable value that has allowed numerous studies of vibration-rotation transition rates in H_2. However, for molecules like CO where the rotational frequency is much less than the vibrational frequency, we could expect to require more than 18 hr per case! Obviously, to study such molecules, we must seek ways to reduce the required number of coupled states. The greatest reduction will be achieved by any method for decoupling the projection states within a given orbital state and averaging their effects in advance of the calculation. Several such methods are discussed in the following section. Their implementation has been a key factor in reaching the objectives presented here.

6.4 Effective Hamiltonian and Other Approximations

During the course of this study, three primary methods of approximation were examined. They are discussed in this section in an order of increasing utility to this work.

6.4.1 Sudden Rotation/Perturbed Vibration Approximation

In a recent analysis of vibration-rotation coupling in harmonic oscillations, Stallcop[109] drew renewed attention to the concept that rotational and vibrational motion can be treated in separate limiting approximations. For example, the rotational period, $1/B_e$, is typically very long compared with the collision period, $\tau_c = 2L/\bar{u}$. Consequently, the molecule appears rotationally stationary during the collision period and the induced mixing of rotational

states is predicted accurately by the "sudden" or "impact" approximation.[56,110] The sudden approximation then provides a closed-form integral description of the mixed rotational state of the molecule at any time during the encounter. In contrast, the vibrational motion typically undergoes several oscillations while the incident particle is at close range. Stallcop treats the vibrational motion in the extreme adiabatic limit for which many oscillations must occur during the interaction period, but that limit is too restrictive for our purposes. Instead, we may recall, from chapter 4, the broad range of collision energies in which a first-order perturbation treatment is successful and then treat the vibrational motion accordingly. Dynamically, the vibrational and rotational motions are thus decoupled and a complete closed-form integral description of the vibration-rotation transition probability may be obtained. Unfortunately, all series solutions of the resulting integral equation were found to be ill-conditioned and hence not calculable with the significant digits carried by available computers. Numerous attempts to restructure the formulation or to evaluate the integral by numerical quadrature were also unsuccessful for similar reasons. Thus, while the approach is mentioned here because of its potential significance as a means of analyzing vibration-rotation energy transfer, we were forced to abandon it for the present study.

6.4.2 Maximum Coupling Approximation

The broad range of magnitudes covered by the matrix elements, $V_{v'\ell'm'v\ell m'}$ for the range of m and m' values suggests that the number of coupled states may be reduced by including only the dominant paths of energy transfer. As figure 6.2 indicates, the coupling between vibration-rotation states will be dominated for large ℓ by the projection states in which m and m' are

maximum and of the same sign. The "maximum coupling" approximation therefore simply excludes all states except those contributing to $V_{v'\ell'\ell'v\ell\ell}$ and $V_{v'\ell'-\ell'v\ell-\ell}$. The number of coupled rotational states in each vibrational set is then reduced from $(\bar{\ell}+1)^2$ to $2\bar{\ell}+1$. Calculations incorporating the foregoing exclusions are discussed in the following sections where they are compared with the "effective Hamiltonian" approximation described next.

6.4.3 Effective Hamiltonian

An approximate method for decoupling and subsequently averaging the contributions of all projection states of each orbital state has recently been developed by Rabitz.[54] Unlike the preceding two approximations, however, even the relative range of parameters for which the method is expected to be accurate has not been defined in terms of the molecular properties or collision parameters nor is a method of defining them apparent. Hence, for the present, the approximation must simply be tested by comparison with limited exact cases.

In effect, Rabitz determines the form of the Hamiltonian required to exactly nullify the contribution of individual m and m' states in the matrix elements. He begins by assuming an interaction potential with the general form

$$V'(\bar{x},r,\delta) = \sum_{J=0}^{\infty} \upsilon_J(r,\bar{x})P_J(\cos\,\delta) \tag{6.52}$$

and finally obtains the effective matrix element, analogous to equation (6.5) or (6.27) as

$$\langle v'\ell'|V'_e(\bar{x},r,\delta)|v\ell\rangle = (-1)^{(|\ell'-\ell|+\ell'+\ell)/2}[(2\ell'+1)(2\ell+1)]^{1/4} \times$$

$$\sum_{J=0}^{\infty} \langle v'|v_J(r,\bar{x})|v\rangle (2J+1)^{-1/2} \begin{pmatrix} \ell' & J & \ell \\ 0 & 0 & 0 \end{pmatrix} \tag{6.53}$$

where V'_e is an "effective potential" corresponding to equation (6.52). Equation (6.53) may be converted to terms corresponding to the particular potential, given by equation (6.2), through the use of equation (6.11). An equivalence is easily identified as

$$v_J(r,\bar{x}) = A\, e^{-\bar{x}/L}(2J+1) \sum_{i=1,2} \left(\frac{\alpha_i}{|\alpha|}\right)^J i_J\left(\alpha_i \frac{r}{L}\right)$$

so that

$$\langle v'|v_J(r,\bar{x})|v\rangle = U(b,t)(2J+1)R^{(J)}_{v'v}$$

The resulting "effective" time-independent matrix element is then

$$V^e_{v'\ell'v\ell} = (-1)^{(|\ell'-\ell|+\ell'+\ell)/2}[(2\ell'+1)(2\ell+1)]^{1/4} \times$$

$$\sum_{J=|\ell'-\ell|}^{\ell'+\ell} \sqrt{2J+1}\, R^{(J)}_{v'v} \begin{pmatrix} \ell' & J & \ell \\ 0 & 0 & 0 \end{pmatrix} \tag{6.54}$$

and the complete matrix element, analogous to equation (6.27), is

$$\langle v'\ell'|V'_e|v\ell\rangle = U(b,t)V^e_{v'\ell'v\ell} \tag{6.55}$$

The use of equation (6.55) in place of equation (6.27) reduces the total number of coupled rotational states in each vibrational manifold from $(\bar{\ell}+1)^2$ to $\bar{\ell}$.

Note by comparison with equation (6.27) that the induced phase shift associated with the exponential argument, $(m' - m)\bar{\Omega}(t)$, in equation (6.27) is lost in the effective Hamiltonian approximation and the remaining formulation is independent of $\bar{\Omega}(t)$. We shall see in the discussions to follow, however, that the rotational energy transfer is dominated by small $\Delta\ell$ and hence small values of $m' - m$. Thus, even in a complete solution, the phase shifts

associated with $\bar{\Omega}(t)$ are subdued and the accuracy of the effective Hamiltonian approximation is not threatened by their neglect.

6.5 Aspects of Convergence

Before applying the preceding three-dimensional model, we first require a criterion for choosing a sufficient set of rotational and vibrational eigenstates to ensure convergence. Experience with the collinear model (ch. 4) has shown that near threshold only a few states higher than the energetically accessible vibrational states are necessary to obtain convergence. Thus, for ground-state molecules with $\bar{E}/h\omega_e$ near or slightly greater than unity, only three or four vibrational states are often adequate. Similar concepts can be applied to the vibrational states in a three-dimensional model. However, the fundamental vibrational frequency of a diatomic molecule is always larger than its rotational frequency so that, in a three-dimensional model, collisions with sufficient energy to induce vibrational transitions (i.e., $\bar{E}/h\omega_e \geq 1$) always couple numerous rotational states in each vibrational manifold. The best manner of selecting the minimum, and yet sufficient, number of coupled rotational states for each vibrational eigenenergy is therefore difficult to determine in advance of a calculation. A seemingly logical first choice would be to include only the energetically accessible states and exclude all others. For $\bar{E}/h\omega_e \simeq 1$, this method of selection envelops many rotational states in the initial vibrational manifold and only a few at the next higher vibrational eigenenergy. We shall find, however, that this criterion for selection is not only inadequate to ensure convergence but with a semiclassical formulation it almost certainly guarantees a nonconvergent solution! The primary purpose of this section is therefore to examine the requirements of convergence in

detail. The reader should be aware at the outset, however, that the results pertain to our semiclassical model without energy conservation. Their relationship to the convergence requirements for an energy-conserving collision model will only be inferred.

We test our ability to obtain convergent solutions for the molecular types of interest by choosing the worst numerical case in an example (namely, CO-He collisions in which a maximum number of basis states is required) and contrasting the results with those for H_2-He collisions, the opposite extreme.

As figure 6.4(b) illustrates, a basis set that is convincingly convergent for CO-He collisions at $\bar{E}/h\omega_e \geq 1$ will include an impractical number of states that extends to large ℓ. To deal with such situations, we must therefore first determine the most appropriate method of approximation from section 6.4 that will reduce the necessary number of coupled states and that allows solutions for large ℓ to be obtained in a practical computing time.

6.5.1 Evaluation of the Projection-State Decoupling Approximations

In keeping with the predominant objective of this chapter to study the effects of rotational transitions on the *net vibrational* transition rates, we use as a basis for comparison both the probability, $P_{v\ell \to v'}$ (defined by eq. (6.43)), and its component, defined by

$$P_{v\ell m \to v'} = \sum_{\ell', m'} P_{v\ell m \to v'\ell' m'} \tag{6.56}$$

Note that the former is averaged over all initial m states while the latter pertains to a specific initial m state. However, both are summed over all final ℓ' and m' states in the vibrational manifold, v', and are therefore both net vibrational transition probabilities.

Since the approximations described in section 6.4 are methods for decoupling the influence of the projection states on the molecular dynamics and subsequently averaging their effects, the sensitivity of complete solutions to the quantum number of the initial projection state is an important aspect in understanding of the relationship of the complete and approximate calculations. Figure 6.7 shows that, for CO-He collisions, $P_{v\ell m \to v'}$ is relatively insensitive to the initial value of m, even for large impact parameters where the phase

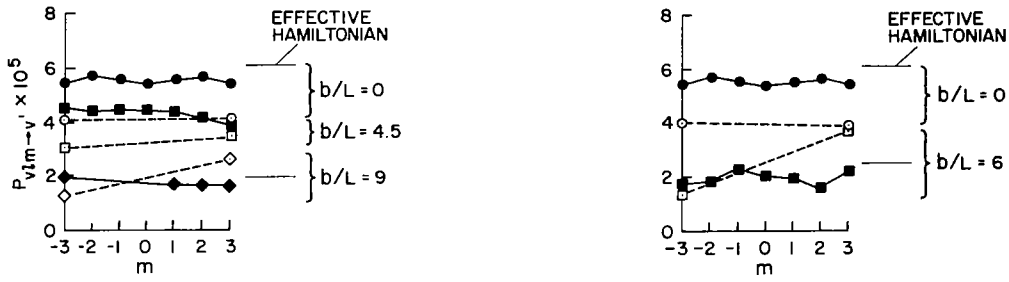

(a) A = 6 MeV (b) A = 1000 eV

Figure 6.7.- Distribution of net vibrational transition probabilities over the range of initial projection states for CO($v\ell$ = 0,3)-He collisions at several impact parameters. Only probabilities for v' = 1 are shown. Fixed collision parameters are $\bar{E}/h\omega_e$ = 1.08, L = 0.02 nm. The basis set contained ℓ = 0-8 rotational states in each vibrational manifold and included all corresponding projection states. Symbols denote results from: ● ■ ◆ a complete solution, ○ □ ◇ the maximum coupling approximation. Effective Hamiltonian results appear as a single value.

shift associated with $\bar{\Omega}(b,t)$ is greatest. This result occurs because no other dynamical phase interference exists between m states of the same eigenfrequency $\omega_{v\ell}$, while $\bar{\Omega}(b,t)$ is generally small in the primary region of interaction ($\bar{\Omega}$ = 0 at t = 0 where the interaction is greatest). In view of the foregoing insensitivity to initial m, vibrational transition probabilities calculated with an effective Hamiltonian approximate the complete solutions more accurately than the maximum coupling approximation. Its similar accuracy in reproducing related net vibrational cross sections is indicated by

figure 6.8, where the variations of $P_{v\ell\to v'}$ with impact parameter, calculated by the two approximations, are compared with complete solutions. Clearly, the effective Hamiltonian approximation is superior, particularly for the smaller interaction scale factor, A, shown in figure 6.8(b). (The smaller scale factor is believed to be more realistic.[87]) Similar accuracy is obtained for H_2-He collisions as shown in figure 6.9. One should note, however, that the impressive accuracy of the effective Hamiltonian is aided significantly by our use of the net probability, $P_{v\ell\to v'}$, as a basis for comparison. Similar comparisons for detailed vibration-rotation transitions would not appear as favorable. Others[54,111-113] have obtained equivalent results for a variety of molecular types.

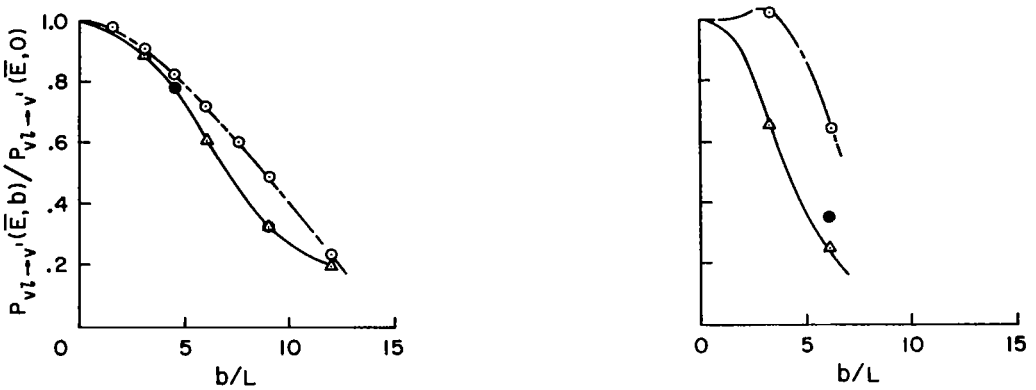

(a) A = 6 MeV (b) A = 1000 eV

Figure 6.8.- Variation of net vibrational transition probability with impact parameter for CO(vℓ = 0,3)-He collisions using several approximate solutions. Only v' = 1 probabilities are shown. The basis set included ℓ = 0-8 in each vibrational manifold for all cases; $\bar{E}/h\omega_e$ = 1.08, L = 0.02 nm. Symbols denote results from ● a complete solution, ○ the maximum coupling approximation, and △ the effective Hamiltonian approximation.

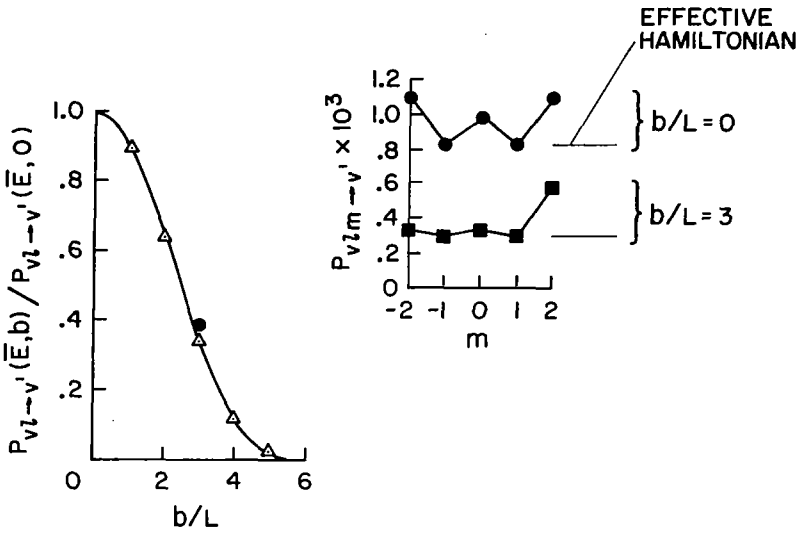

Figure 6.9.- Variation of net vibrational transition probability for $H_2(v\ell = 0,2)$-He collisions; $v' = 1$, $\bar{E}/h\omega_e = 1.1$, A = 303 eV, and L = 0.0273 nm. The basis set included ℓ = 0-10 in both vibrational manifolds. Symbols denote the results from: ● ■, a complete solution, and △, the effective Hamiltonian approximation.

6.5.2 Convergence Requirements for Vibration-Rotation Energy Transfer

The individual vibration-rotation transition probabilities from a complete solution are shown in figure 6.10 for CO-He collisions at an initial kinetic energy just above the vibrational threshold. Rotational states from ℓ = 0 to 10 were included equally in vibrational manifolds, v = 0 and 1. The accompanying 484 differential equations and 14,883 dissimilar matrix elements exceed a practical upper limit for repetitive computation. And yet, comparison to a similar calculation with ℓ = 0 to 8 rotational states in each vibrational manifold shows that convergence in the vibration-rotation probabilities $P_{v\ell \to v'\ell'}$ is far from realized. However, this result is not surprising because, while all open channels (energetically accessible states) have been included in $v' = 1$, most open channels in $v' = 0$ are missing (see fig. 6.4(b) for reference). The interesting result is shown in figure 6.11

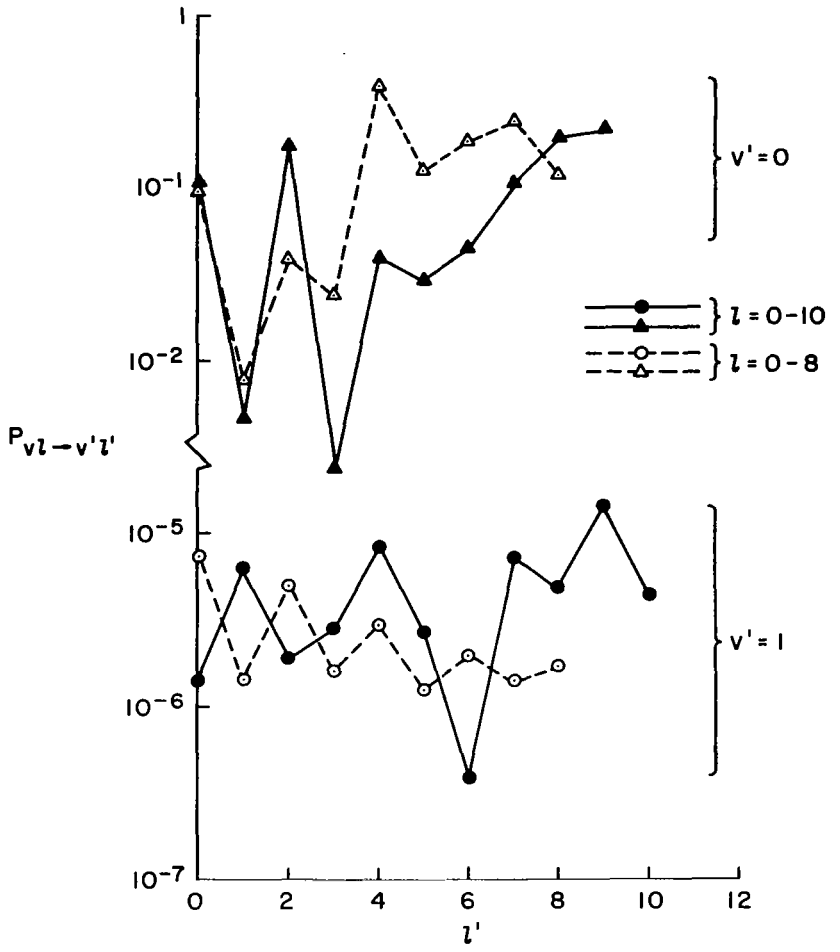

Figure 6.10.- Effect of additional rotational states on the vibration-rotation transition probabilities in CO(vℓm = 0,0,0)-He collisions. Both cases were obtained from a complete solution including all projection states in the basis set and vibrational states v = 0, 1. An equal number of rotational states were included in each vibrational manifold. Collision parameters are $\bar{E}/h\omega_e$ = 1.08, b = 0. The interaction potential is defined by A = 6 MeV, L = 0.02 nm.

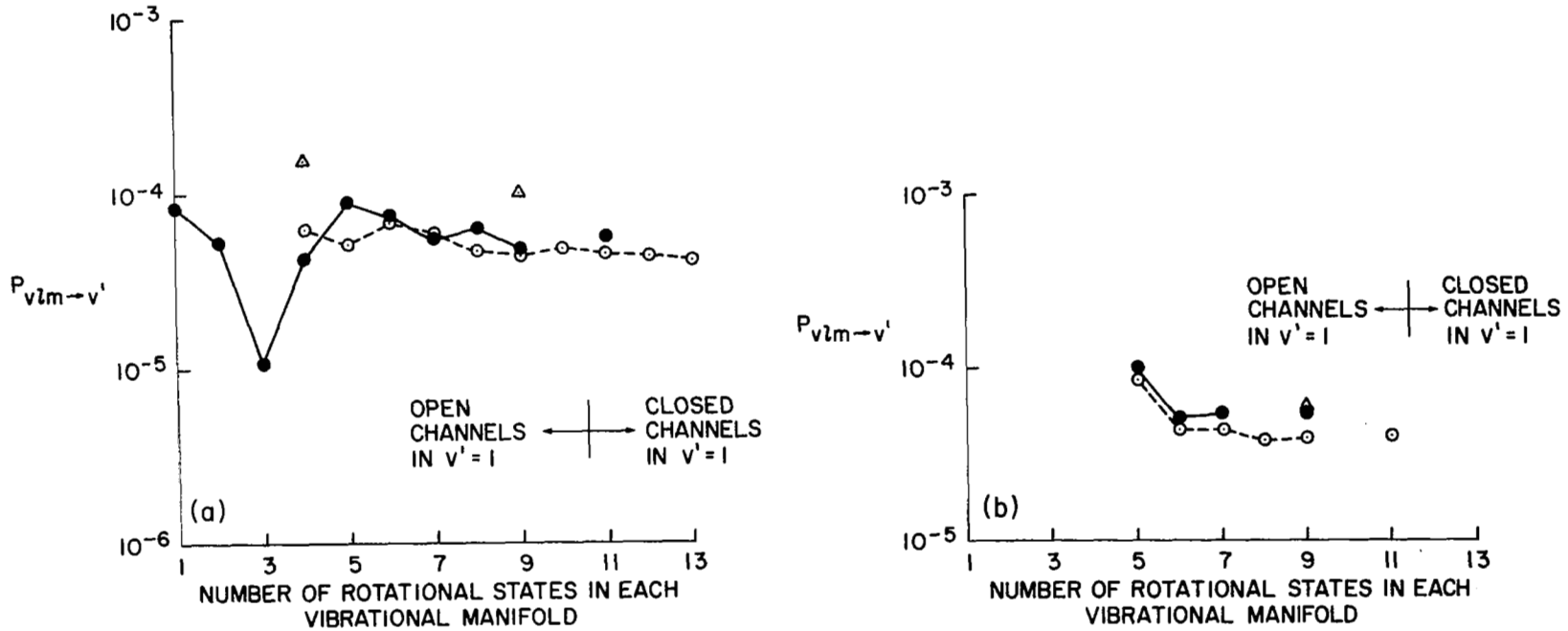

(a) CO($v\ell m$ = 0,0,0)-He

(b) CO($v\ell m$ = 0,3,3)-He

Figure 6.11.- Convergence of the net vibrational transition probability for CO-He collisions (i.e., the probability has been summed over all ℓ', m' according to eq. (6.43), but for a single initial m state). A duplicate set of rotational states was included in each vibrational manifold. Only probabilities for $v' = 1$ are shown. Collision parameters are the same as in figure 6.8. Symbols denote results from: •, a complete solution, ○, the maximum coupling approximation, △, the effective Hamiltonian approximation.

where we imply from the behavior of $P_{v\ell m \to v'}$ for one value of m that, even before all open channels in any vibrational manifold are reached, a convergence in the *net vibrational transition probability*, $P_{v\ell \to v'}$, is obtained! Similar behavior is found for H_2-He collisions, as figure 6.12 indicates. Note that, in this latter case, calculations including all open channels in both vibrational manifolds were possible and the convergence asymptote is convincingly unique. Figures 6.11 and 6.12 also include results from the approximate methods of solution and show them to approach similar asymptotes.

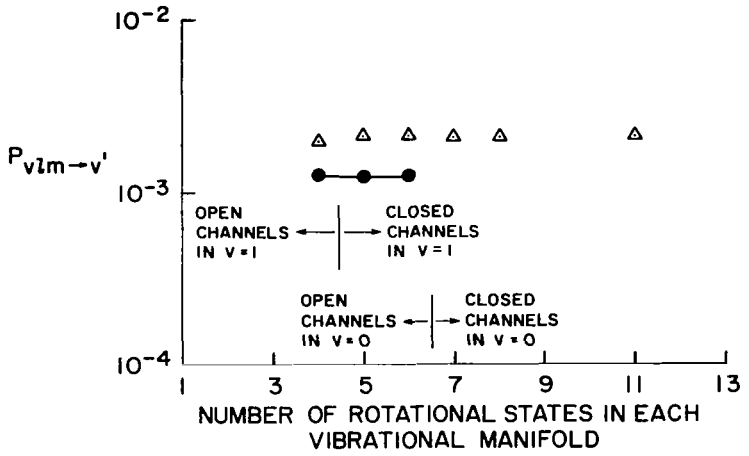

Figure 6.12.- Convergence of the net vibrational transition probability for $H_2(v\ell m = 0,4,4)$-He collisions. Stipulations and symbols are the same as in figure 6.9. Collisions parameters are $\bar{E}/h\omega_e = 1.5$, b = 0, A = 303 eV, L = 0.0273 nm. Note that, in this example, cases are shown where *all* open channels are included in both vibrational manifolds.

The uniqueness of the asymptotes obtained in CO-He solutions is not yet confirmed, however. In fact, subsequent calculations using the effective Hamiltonian for large but *unequal* numbers of rotational states in each vibrational manifold are shown in figure 6.13 to produce drastically different results. Note that, even though cases including ℓ = 0 to 40 in v = 0 but only ℓ = 0 to 10 in v = 2 contain all open channels in both v = 0 and 1, the transition probability is two orders of magnitude from a final convergence.

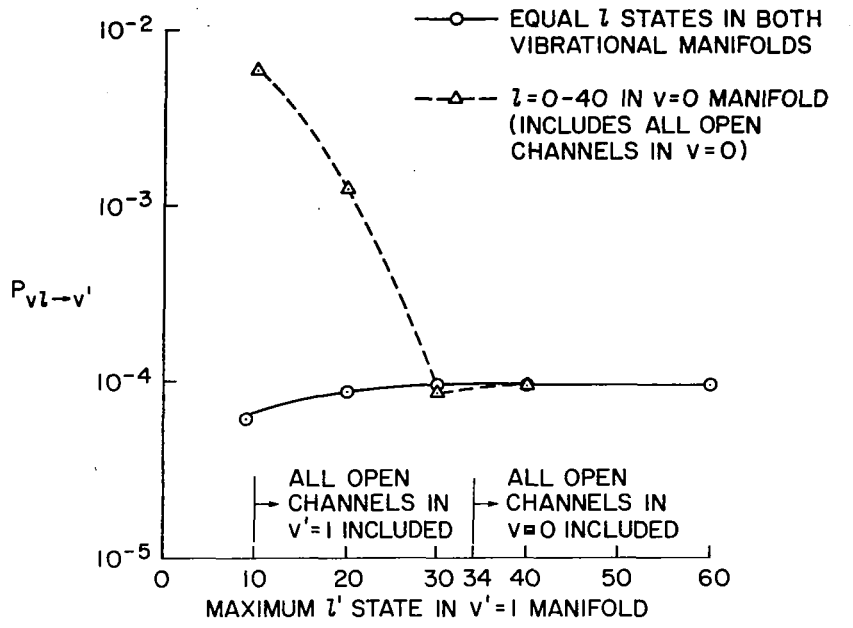

Figure 6.13.- Convergence of the net vibrational transition probability in effective Hamiltonian solutions for CO(vℓ = 0,3)-He collisions v' = 1, $\bar{E}/h\omega_e$ = 1.08, A = 1000 eV, L = 0.02 nm. Cases are represented that include large but *unequal* numbers of rotational states in each vibrational manifold. Note that cases are also shown where all open channels are included in both vibrational manifolds.

As more rotational states are added to v = 1, a final definite convergence is eventually reached where further additions of any kind have no effect. Conversely, figure 6.13 also demonstrates that cases including a duplicate set of rotational states in each vibrational manifold obtain a solution near the final convergent value with relatively few rotational states. Recall, however, that the convergence criterion thus implied pertains only to the net vibrational transition probability, $P_{v\ell\rightarrow v'}$, and not the individual vibration-rotation probabilities $P_{v\ell\rightarrow v'\ell'}$.

While there is no attempt made here to construct a mathematically definitive argument showing why a duplicate but nonconvergent set of rotational states in each vibration manifold produces nearly convergent vibrational transition probabilities, the following conceptual explanation is

offered. First, recall that each time-independent matrix element, $V_{v'\ell'm'v\ell m'}$ is a measure of the coupling strength between two vibration-rotation states. The matrix elements are shown in figure 6.3 to generally emphasize coupling only between states with small differences in angular momentum, regardless of the angular momentum of either state. This emphasis is primarily a consequence of the integrated overlap between rotational eigenfunctions of the undisturbed molecule and it is qualitatively unaffected by any vibrational change of state. As a result, vibrational transitions also occur predominantly between states with small differences in angular momentum. We shall refer to such pairs of states as "companion states" to imply that their angular momentum is similar ($\Delta\ell$ is small) but each is a member of a different vibrational manifold. Thus, if a rotational state has no companion in the basis set of an adjacent vibrational manifold, direct vibrational transitions from that rotational state will be improbable.

With the foregoing general property of vibration-rotation transitions in mind, we can now describe its effect on the energy transfer process within the average molecule during a collision. To do so, we shall adopt a point of view compatible with our time-dependent semiclassical model and refer to the time-variant amplitude modulus $|c_{v\ell m}(t)|^2$ as the instantaneous "occupation" of state $|v\ell m\rangle$. By "average molecule" we then mean that the progression of state occupations in time provides a trace of the average path of energy flux within many identical molecules, all experiencing identical collisions.

Since we consider collision energies mainly above the vibrational threshold, many rotational states are typically accessible. Early in the collision, the energetically accessible rotational states in the vibrational manifold containing the initial state become occupied, all with similar probabilities.

Near closest approach, vibrational transitions then begin between companion states and a corresponding occupation distribution develops in the adjacent vibrational manifolds. However, if the manifold receiving energy has been given fewer rotational states in its basis set (as it might because a higher manifold would have fewer open channels), then not all rotational states in the initial-state manifold have companions. For the energy in those rotational states to become available for a vibrational transition, it must first return to a rotational state in the same manifold where a companion exists. Obviously, such occurrences are the artificial consequence of an incomplete basis set and they stress the importance of including at least a duplicate rotational set in each vibrational manifold (if not a convergent set) to properly reproduce the transient dynamics during a collision.

We may now ask why a duplicate but incomplete rotational basis set in each vibrational manifold approximates the convergent solution. Recall that it does so only for the total occupation of each vibrational manifold, that is, the occupation summed over all rotational states. If all rotational states have companions as they do in duplicate sets, the most probable paths are available for vibrational energy transfer from each rotational state considered and hence no artificial impediment to the energy flow is introduced anywhere. However, obtaining the correct net rate of vibrational energy transfer remains to be questioned. The net rate of energy transfer to all states of a vibrational manifold may be written as a sum proportional to the occupation distribution among its rotational states. At collision energies exceeding the vibrational threshold, the rotational states are strongly coupled and the depletion of any rotational state by a vibrational transition is rapidly restored, thus maintaining the distribution of rotational state

occupations in a time scale short compared to the encounter period. When too few rotational states are included in the basis set, the occupation distribution is unnaturally constrained and vibrational transitions from each rotational state occur at an increased rate but from a fewer number of states. Since all rotational states are closely coupled, no particular preference is given to vibrational transitions from any of them and the net vibrational transition rate is only weakly affected, as we have observed. Note, however, that the occupation distribution of rotational states is strongly affected by the completeness of the basis set so that convergence in the individual vibration-rotation transition rates cannot be expected from an incomplete basis set, as we have also observed.

Thus, we have rationalized, in the foregoing explanation, the reasons for expecting duplicate but nonconvergent sets of rotational states in each vibrational manifold to closely reproduce the net vibrational dynamics of the molecule given by a convergent set. We shall incorporate this convergence criterion along with use of the effective Hamiltonian approximation in all the calculations of $P_{v\ell \to v'}$ to follow. Conversely, when individual vibration-rotation transition probabilities are studied, a duplicate and completely convergent basis set will always be used.

6.6 Ambiguities of Unconserved Energy in a Three-Dimensional Semiclassical Model

An example of the final rotational state occupations from a convergent basis set is shown in figure 6.14. The distributions in each vibrational manifold are plotted on vertically shifted scales to demonstrate their relative similarity. However, if we take the total energy of the system to be the initial sum of internal energy and relative kinetic energy, then many of the

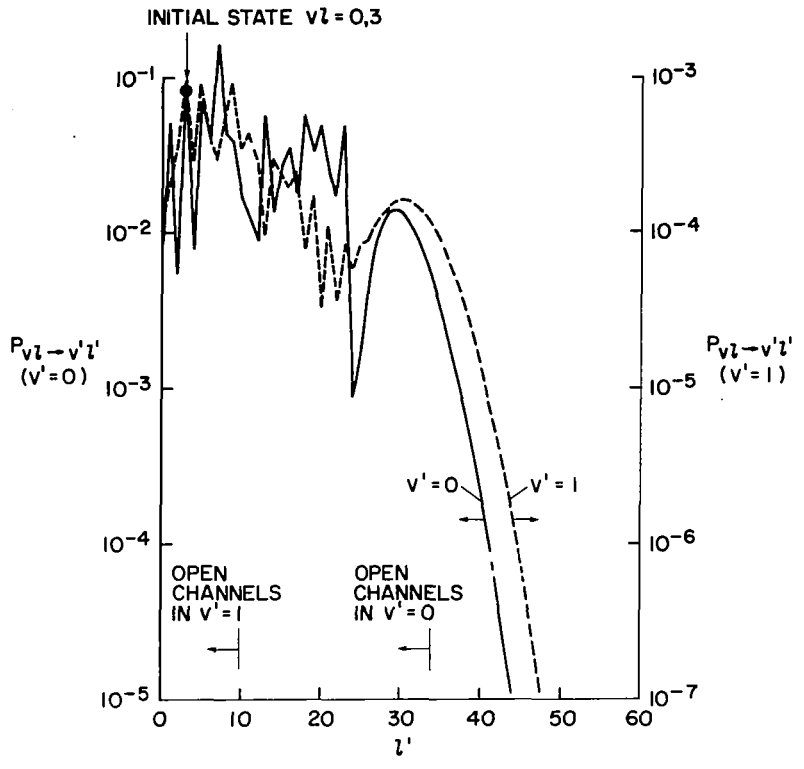

Figure 6.14.- Vibration-rotation transition probability distributions for CO(vℓ = 0,3)-He collisions from an effective Hamiltonian solution; $\bar{E}/\hbar\omega_e$ = 1.08, b = 0, L = 0.02 nm, A = 1000 eV.

rotational states in the v' = 1 manifold that remain occupied after the collision are energetically inaccessible! (They are closed channels.) Since a more exact collision model, where total energy is conserved, would leave the closed channels in all vibrational manifolds completely empty, the failure of our semiclassical model to comply with such considerations is, of course, a consequence of the lack of energy conservation when computing the classical trajectory, just as it was in the collinear model discussed in chapter 4. We showed in chapter 4 that, when the loss of energy conservation had no large effects on the molecular dynamics, it could be adequately compensated for by use of the average total energy given in equation (4.14) as

$$E_T = \bar{E} + \hbar(\omega_n + \omega_k)/2 \qquad (4.14)$$

However, the use of equation (4.14) to compute total energy makes it dependent on the transition being considered and, as a result, the concept of open and closed channels becomes ambiguous. While this ambiguity poses no practical difficulty, a careful interpretation of the semiclassical results must be made when comparing them to energy-conserving predictions — namely, the probability distributions obtained for a single value of $\bar{E}$ do not correspond to a single total energy or single initial kinetic energy and, consequently, they cannot be compared directly with a distribution obtained from an energy-conserving collision model. But, after transforming the distribution of either collision model into the framework of the other, using equation (4.14), the results should be comparable just as they were in chapter 4. The accuracy of the three-dimensional semiclassical model in such comparisons remains to be proven and no comparisons are made in this study. However, from the results in chapter 4, there is good reason to expect that the three-dimensional semiclassical model, constrained to homonuclear molecules with light collision partners and properly interpreted, should give reasonably accurate predictions.

Finally, we must consider the consequences of the ambiguous closed-channel concept on our previous convergence arguments. While the initial discussions of convergence in figures 6.11 to 6.13 were keyed to the concept of open and closed channels, they serve mainly as a guide to identify the number of channels for which convergence may be expected. In that regard, the concept is as useful as it would be in an energy-conserving model. Recall, however, that the primary aspect of our convergence criterion was to provide companion states in all vibrational manifolds to properly handle the *transient* dynamics during the collision. That principle applies to all collision models,

regardless of their energy-conserving features or the final rotational-state occupations obtained.

6.7 Three-Dimensional Inelastic Collisions and Their Relation to Collinear Encounters

The preceding three-dimensional collision model is applied here to evaluate the validity of collinear models for a variety of molecular types and initial conditions. However, examples are constrained to collision partners that can be treated accurately by the semiclassical approximation in the absence of dynamic coupling between the quantized molecule and the classical trajectory. Guided by the results in chapter 4 in that regard, we consider only helium atom collisions with H_2, N_2, and CO. The hydrogen molecule is an example in which the rotational eigenenergies are broadly spaced in comparison with the vibrational energies and the effects of vibration-rotation coupling are expected to be significant. H_2 also requires the smallest convergent basis set since its homonuclear nature only couples rotational states of the same parity (i.e., $\Delta\ell$ is always even). N_2 also requires only states of the same parity, but its close rotational energy spacing places it in a different molecular class where numerous rotational states of high angular momentum must be included. Finally, CO is similar in rotational structure to N_2, but its heteronuclear nature couples all rotational states of either parity. Most common inert-atom/diatomic-molecule collisions are represented by one of these three examples. Excluded cases are those in which reactive atom-exchange states participate in the energy-transfer process (as in H_2-F collisions) and those in which electronic states participate (as in NO).

The range of initial rotational states of interest in a practical application is first indicated by considering their equilibrium population

distributions. Figure 6.15 illustrates some typical distributions for several values of the parameter, T/θ_r, where θ_r is a characteristic rotational temperature with representative values of 2.8 K for CO and 44 K for H_2 ($\theta_r = \hbar B_e/sk$, where s is a symmetry factor). The results in figure 6.15 suggest that initial rotational states in the range $\ell = 0$ to 20 are representative of most applications. We shall see that the collision dynamics for larger initial values of ℓ are easily inferred from the predictions for $\ell \leq 20$.

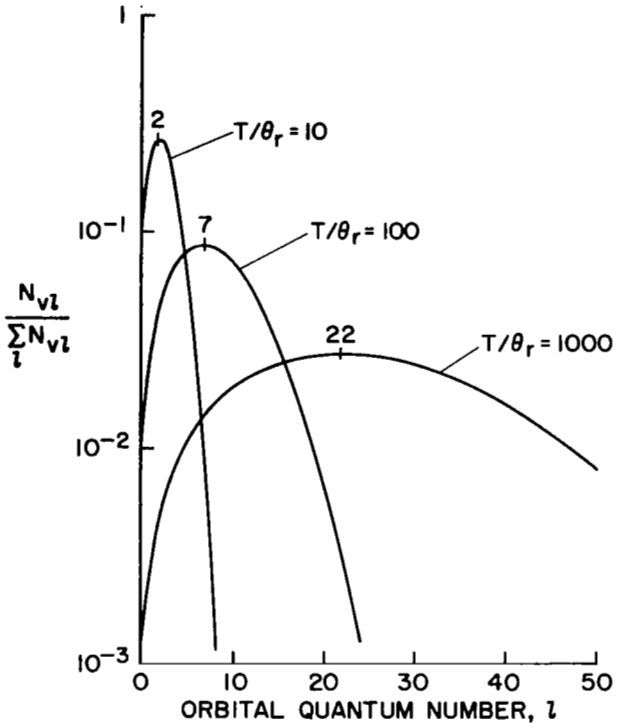

Figure 6.15.- Maxwellian rotational state populations. Numbers at the distribution peaks indicate the corresponding angular momentum quantum numbers.

Finally, we do not attempt to compare collinear and three dimensional predictions directly by obtaining rate coefficients from each model since to do so with the three-dimensional model would be too costly. Instead, we shall

compare the individual elements contained in the rate coefficient definition and their variations with the collision parameters, as discussed in section 6.2.

6.7.1 H_2-He Collisions

Although vibration-rotation energy transfer for H_2-atom collisions has been studied extensively in the recent literature,[40,54,111,114-118] we include it here as a contrasting example to the behavior of the heavier molecules that follow. The interaction potential constants, A and L, for all H_2-He calculations were chosen to resemble the calculated potential of Gordon and Secrest.[84]

An indication of the coupling strength between vibration-rotation states in H_2 is given by the matrix elements shown in figure 6.3(a). As mentioned previously, the results show that transitions with $\Delta\ell \leq 4$ provide the primary path for vibrational energy transfer. The relative levels of H_2 rotational eigenenergies in each vibrational manifold shown in figure 6.4(a) then suggest that transitions from $v = 0$ to 1 (for example) will occur with increasing resonance enhancement from values of $\ell \geq 10$ in $v = 0$, and that the state $v\ell = 0,16$ is in near resonance with $v'\ell' = 1,14$ leaving very little excess energy to be traded with translation. Such transitions may be considered as the primary contributors to an apparent net V-R mechanism for energy transfer.

The calculated transition probabilities shown in figures 6.16 to 6.18 confirm all the foregoing expectations. Figure 6.16(a) shows that, when the initial state is $v\ell = 0,16$, transitions occur to $v' = 1$ predominantly for $\Delta\ell = 2$ downward with large probability and that the occupation of rotational states within each vibrational manifold is dispersed, but with less probability, by $\Delta\ell = 2$ transitions in either direction. A sequence of $\Delta\ell = 2$ downward transitions then populates $v' = 2$, etc., at lower ℓ. Conversely, when

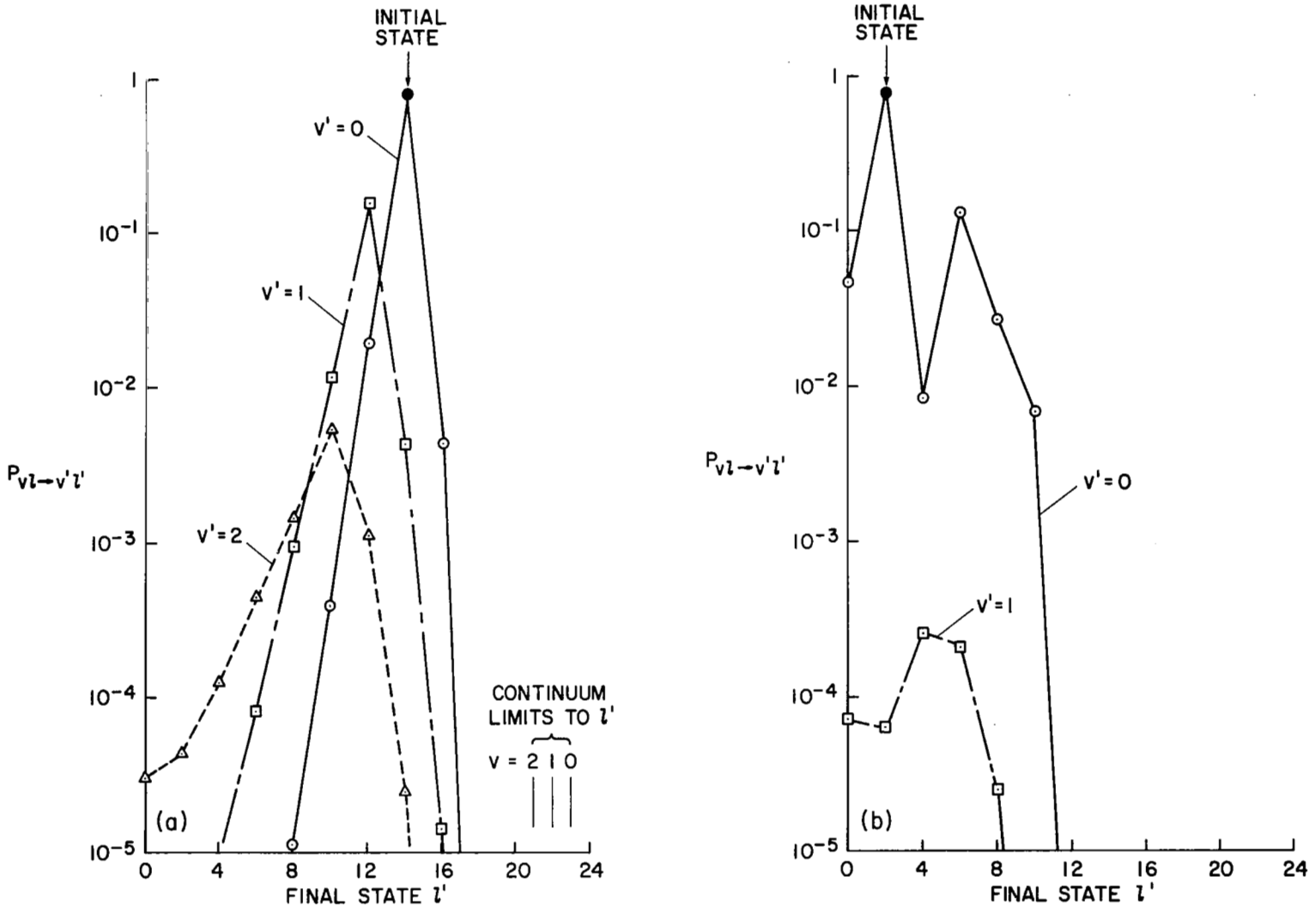

(a) $H_2(v\ell = 0,16)$-He

(b) $H_2(v\ell = 0,2)$-He

Figure 6.16.- Vibration-rotation transition probability distributions for para-H_2(v = 0)-He collisions at $\bar{E}/h\omega_e$ = 1.5, b = 0, A = 303 eV, L = 0.0273 nm. Basis set includes ℓ = 0-20 in vibrational states, v = 0-3. Continuum limits correspond to a dissociation energy of 4.48 eV.

the initial state has small angular momentum, as shown in figure 6.16(b), vibrational states are connected either by single large $\Delta\ell$ transitions or by successive rotational transitions within $v = 0$ that precede any vibrational change. The vibrational transition probability is correspondingly lower. This later example then appears more as a V-T mechanism for energy transfer because of the relatively large amount of translational energy required to induce a vibrational transition. Intermediate results for other initial rotational states are summarized in figure 6.17, where the net vibrational transition probabilities are shown for all initial ℓ below the continuum. (Note that the molecular dynamics for initial states near the continuum are not accurately treated because of the neglected continuum interaction, but figure 6.17 is believed to demonstrate a realistic qualitative behavior.)

We can see from figure 6.17 that the vibrational transition probability is strongly dependent on the initial rotational state and hence a collinear model *cannot* be expected to realistically predict vibrational transition rates for H_2. The inapplicability of a collinear model to H_2 is further confirmed by figure 6.18. For example, curve (a) in figure 6.18 represents the usual collinear prediction in which the rotational contributions to eigenfrequencies are entirely excluded. The comparative three-dimensional predictions show that the probability and threshold energy depend strongly on the initial ℓ and both can be significantly different from the collinear results. Furthermore, simple corrections to the collinear model, such as the use of vibrational frequencies shifted to match the predominant vibration-rotation states, are not satisfactory as curves (b) and (c) in figure 6.18 indicate.

The preceding comparisons were all done for a zero impact parameter, but we have shown with equation (6.47) that, although collisions at $b = 0$ make

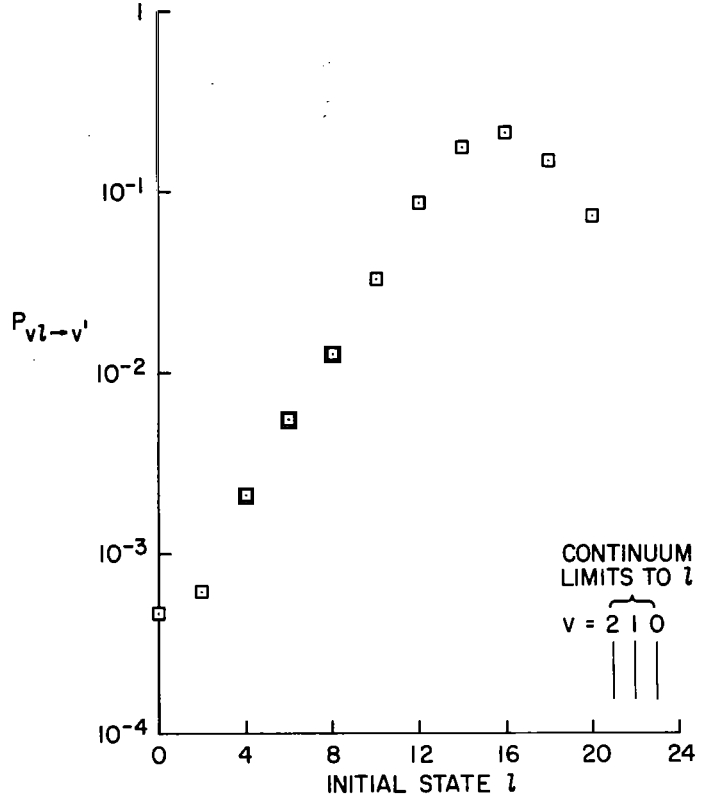

Figure 6.17.- Effect of initial rotational state on the net vibrational transition probabilities for para-H_2(v = 0)-He collisions, v' = 1. Collision parameters are the same as for figure 6.16.

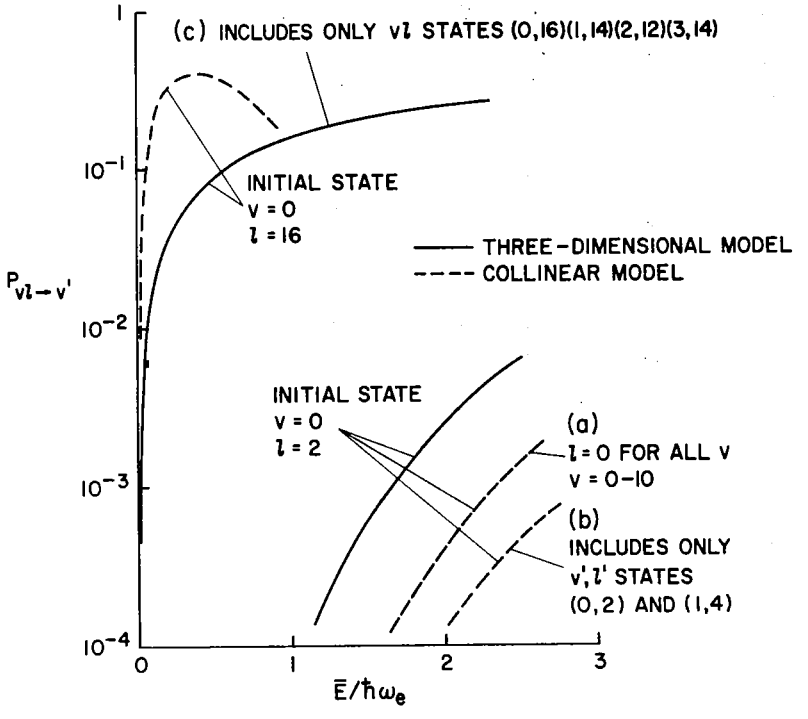

Figure 6.18.- A comparison of net vibrational transition probabilities for para-H_2(v = 0)-He collisions from the three-dimensional and collinear models; v' = 1. Three-dimensional model includes all states indicated for figure 6.16.

no contribution to the cross section or rate coefficient, the probabilities at b = 0 can be used as a normalizing factor. Cross sections are then proportional to $P(\bar{E},0)$ and the integral of $(b/L)\ P(\bar{E},b)/P(\bar{E},0)$ over all b/L. While adequate discouragement for the use of a collinear theory to model H_2 collisions has already been presented, we display the cross-section integrands for later comparisons with heavier molecule results. Figure 6.19 shows the H_2 cross-section integrand to depend strongly on initial ℓ. Figure 6.20 shows it also to depend on collision energy but with significance only for initial rotational states where vibrational energy is transferred predominantly through V-R transitions (i.e., as in fig. 6.20(b) for $v\ell$ = 0,16).

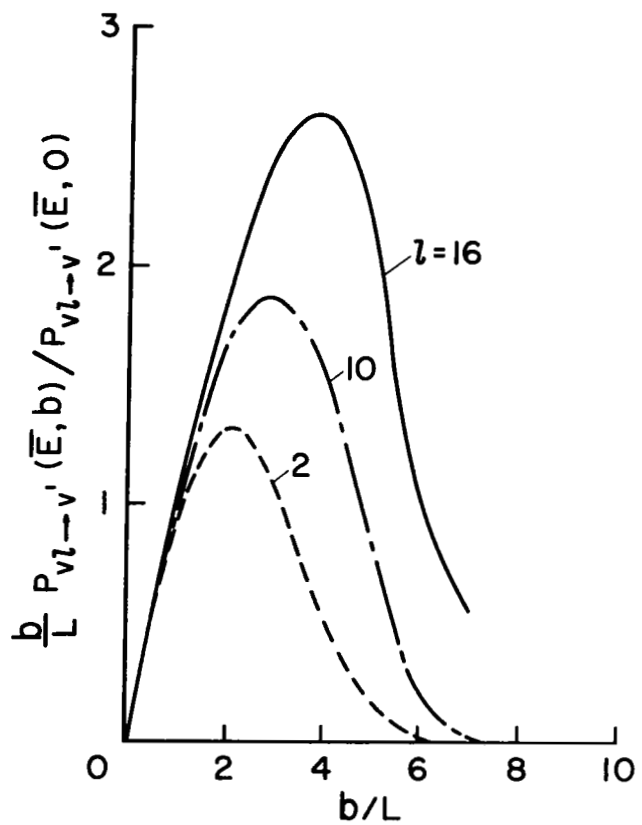

Figure 6.19.- Effect of initial rotational state on the net vibrational cross-section integrand for para-H_2(v = 0)-He collisions, v' = 1, at $\bar{E}/h\omega_e$ = 1.5. Note that the integral of this parameter over all b/L is proportional to the inelastic cross section according to equations (6.46) and (6.47).

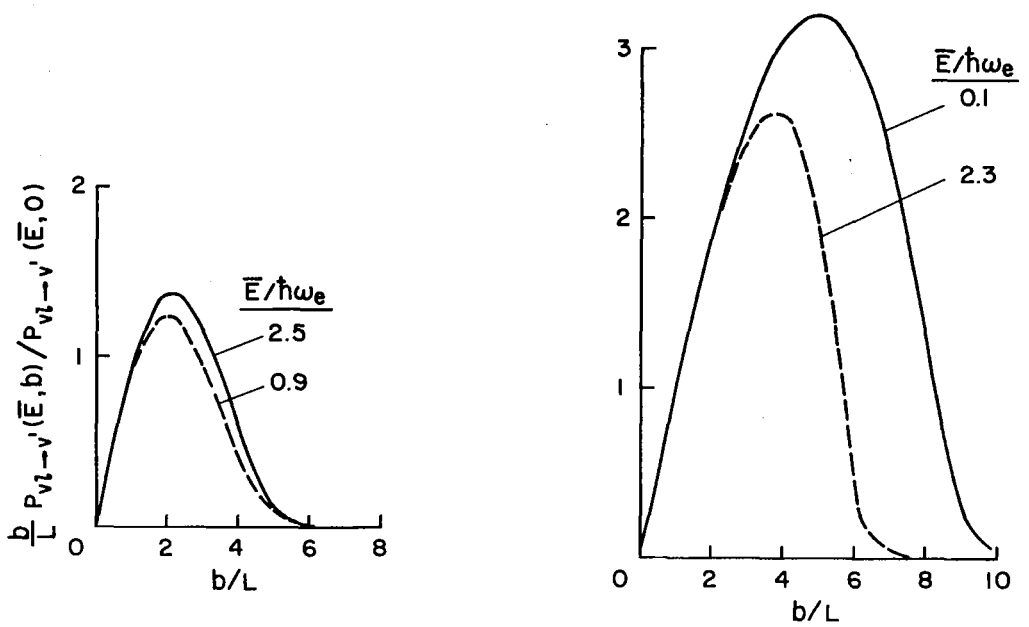

(a) $H_2(v\ell = 0,2)$-He, v' = 1 (b) $H_2(v\ell = 0,16)$-He, v' = 1

Figure 6.20.- Parameters affecting the net vibrational cross-section integrand for para-H_2(v = 0)-He collisions, v' = 1.

From the preceding comparisons, there is no difficulty in concluding that the analysis of vibrational energy transfer in H_2, or any molecule where near-resonant vibration-rotation transitions with small $\Delta\ell$ can occur, requires a complete three-dimensional treatment including both vibrational and rotational motions. Furthermore, even though some initial states with small angular momentum are treated by the collinear model with some resemblance to the three-dimensional results, extended use of the collinear model to deduce a thermal-rate coefficient enveloping a thermal distribution of initial rotation states is entirely inappropriate.

6.7.2 N_2-He Collisions

The calculated collision dynamics of N_2 with He serve here as the primary example to illustrate the nature of vibration-rotation energy transfer in diatomic molecules with closely spaced rotational eigenenergies. The N_2

molecule provides a considerable computational convenience because, as with all homonuclear molecules, only alternate rotational states are coupled, thereby requiring half the basis set demanded by an otherwise similar heteronuclear molecule. Thus, in this section, we study N_2-He collisions in detail and later compare the results with more limited calculations for the heteronuclear CO molecule.

Unlike the H_2-He collisions, the interaction potentials for atom collisions with many-electron molecules like N_2 are relatively unknown. The potential parameters, A and L in equation (6.1), are therefore subject to large uncertainties and we must ensure that any conclusions made concerning the nature of energy-transfer processes are unaffected by the interaction uncertainties. An indication of the range of uncertainty is obtained by noting the range of interaction parameters implied in previous comparisons of experimentally determined vibrational rate coefficients with their related collinear theories.[41,42,45] For example, the interaction range, L, is typically found to be between 0.02 and 0.03 nm with $L = 0.02$ nm favored for molecules like N_2. The analysis of molecular beam experiments,[87] which yields vibrationally inelastic cross sections directly, suggest similar values for L but also produces values of the interaction magnitude A. For molecules like N_2, values are typically near $A \simeq 1000$ eV. However, an alternate means of obtaining A is to compare the exponentially repulsive potential model (eq. (6.1)) with the repulsive part of Lennard-Jones potentials (eq. (3.22)) implied by early viscosity measurements.[6,80] Magnitudes as large as $A = 6$ MeV are thus obtained. While this later value is not taken seriously nor is our potential model realistic enough to warrant much detailed interpretation, both

values are used here as limits to demonstrate the effects of A on the calculated cross sections.

The mechanism of vibrational energy transfer in N_2 is significantly different from that previously shown for H_2. The reasons may be generally understood from an examination of the eigenenergies and interaction matrix elements of N_2 (illustrated in figs. 6.21 and 6.22, respectively). A well-known feature of most induced transitions is that their probability is enhanced by their degree of resonance. For example, figure 6.17 illustrates the case for H_2 in which the most resonant transition from $\ell \approx 16$ is also the most probable, causing the principal path for energy transfer to be through V-R transitions. For N_2, however, the vibration-rotation eigenenergies shown in

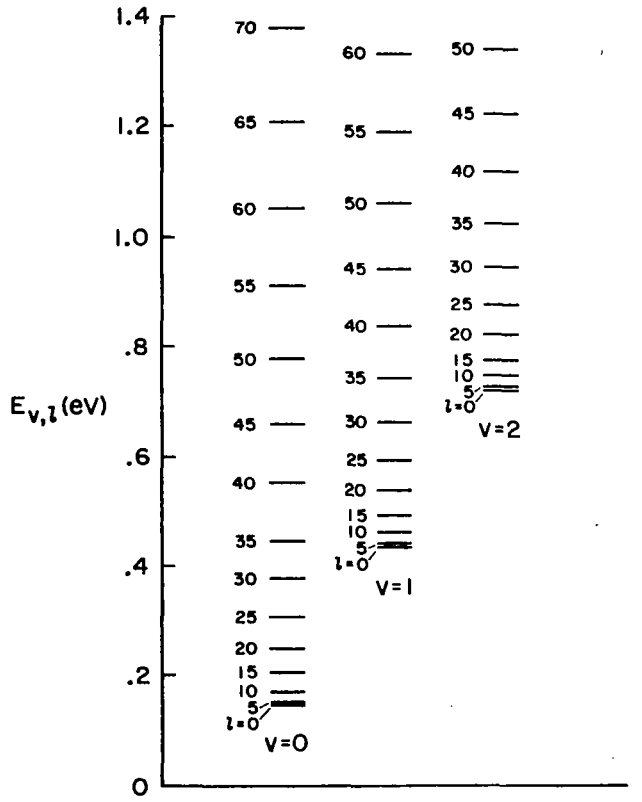

Figure 6.21.- Vibration-rotation eigenenergies for N_2. (Note: Not all rotational states are shown.)

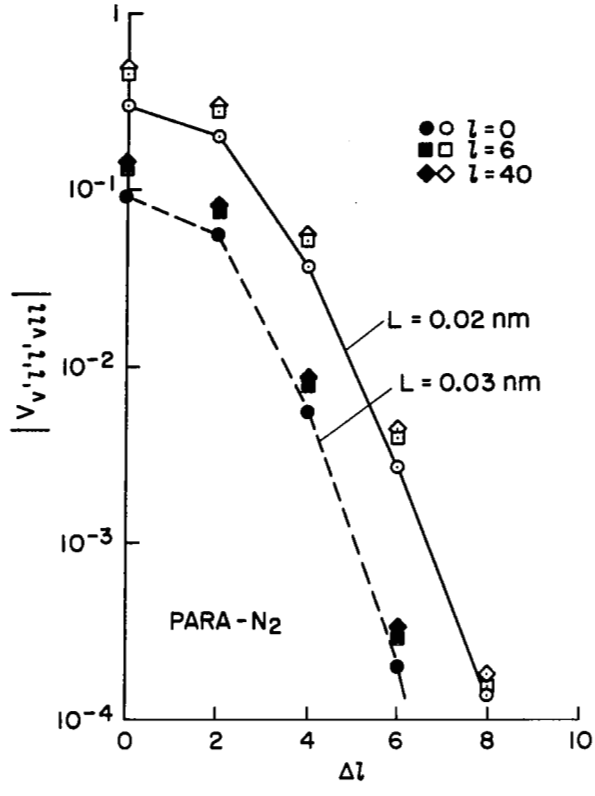

Figure 6.22.- Time-independent matrix elements for para-N_2; v, v' = 0, 1. Open symbols are for L = 0.02 nm, solid symbols are for L = 0.03 nm. A similar plot for ortho-N_2 would have no distinguishable differences.

figure 6.21 allow near-resonant transitions only for large $\Delta\ell$, while the matrix elements for N_2(fig. 6.22) suppress large $\Delta\ell$ transitions, just as they do in H_2 and CO (fig. 6.3). Thus, molecules with a vibration-rotation spectrum like N_2, characterized by a large value for ω_e/B_e, are always constrained to nonresonant V-T transitions with a transition energy approximately equal to $\hbar\omega_e$. Consequently, the rotational energy transferred by small $\Delta\ell$ transitions is always a small contribution to the total, thus rendering the net vibrational transition rates insensitive to the initial angular momentum. Figure 6.23 demonstrates that insensitivity for both para- and ortho-N_2.

The emphasis of nonresonant V-T transitions and the accompanying insensitivity of vibrational transition rates to the initial-state angular momentum

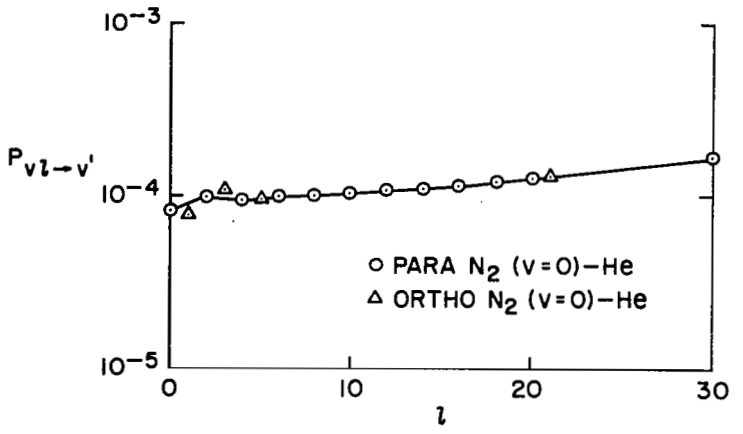

Figure 6.23.- Effect of initial rotational state on the net vibrational transition probabilities for para-N_2(V = 0)-He collisions, v' = 1. Collision parameters are b = 0, L = 0.02 nm, $E/h\omega_e$ = 1.1.

are the key factors contributing to a surprising accuracy of the collinear collision model for predicting transition probabilities in N_2. Vibrational transition probabilities from both the three-dimensional and collinear model are compared in figure 6.24. Recall that the interaction potential is characterized only by the range L in the collinear model. Likewise, probabilities obtained from the three-dimensional model for *zero impact parameter* depend only on L and hence are independent of A. The three-dimensional predictions in figure 6.24 therefore represent all values of A and the *only* difference between the two models shown in figure 6.24 is the collision geometry.

The role of A in the three-dimensional model is shown in figure 6.25(a), where the cross-section integrand is shown as a function of the impact parameter. Clearly, A determines the variation of transition probability with impact parameter and thus determines the relation between $P_{v\ell \to v'}(b = 0)$ and the cross section. In another sense, A determines the equivalent elastic cross section σ_o^e (eq. (6.46)), undefined in the collinear model.

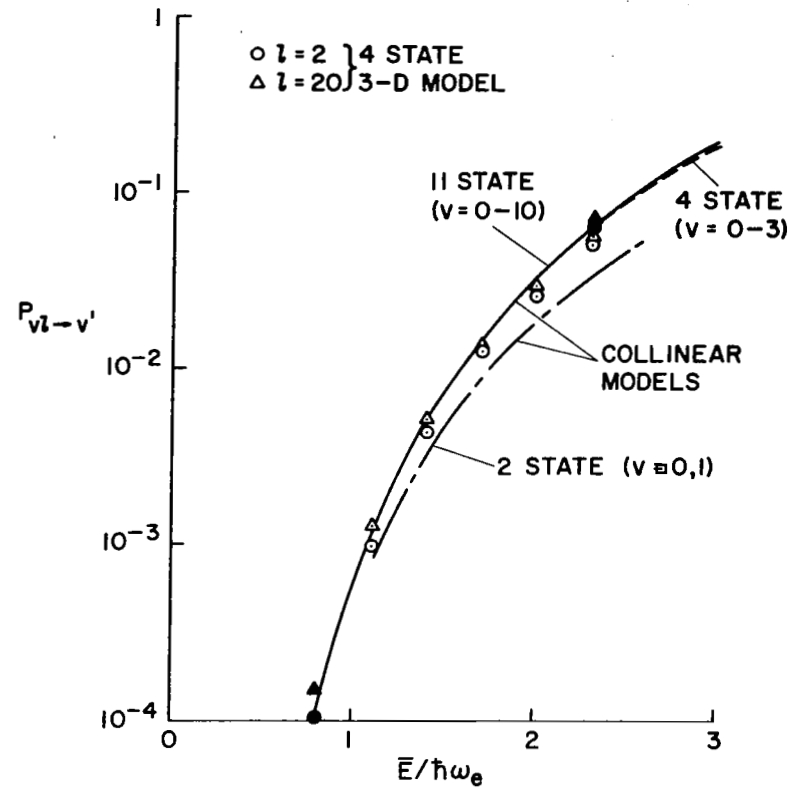

Figure 6.24.- A comparison of net vibrational transition probabilities for para-N_2(v = 0)-He collisions from the three-dimensional and collinear models; v' = 1, b = 0, L = 0.02 nm. Open symbols are three-dimensional model results. Shaded symbols are equivalent probabilities for a constant σ_o^e as defined by equation (6.46) but set equal to the cross section at $\bar{E}/\hbar\omega_e$ = 0.8, thus simulating the procedure typically applied to collinear models.

When the interaction potential parameters are fixed, the equivalent elastic cross section (fig. 6.25(b)) increases slightly with collision energy. Any variation is contradictory to the assumption made when converting collinear probabilities to cross sections by use of a constant hard-sphere cross section, σ_o (eq. (6.45)). However, as it turns out, the increase in σ_o^e approximately equals the increasing difference in $P(b = 0)_{v\ell \rightleftarrows v'}$ between the two collision models so that their respective cross sections and rate coefficients are in closer agreement than figure 6.24 implies. The shaded symbols in figure 6.24 show

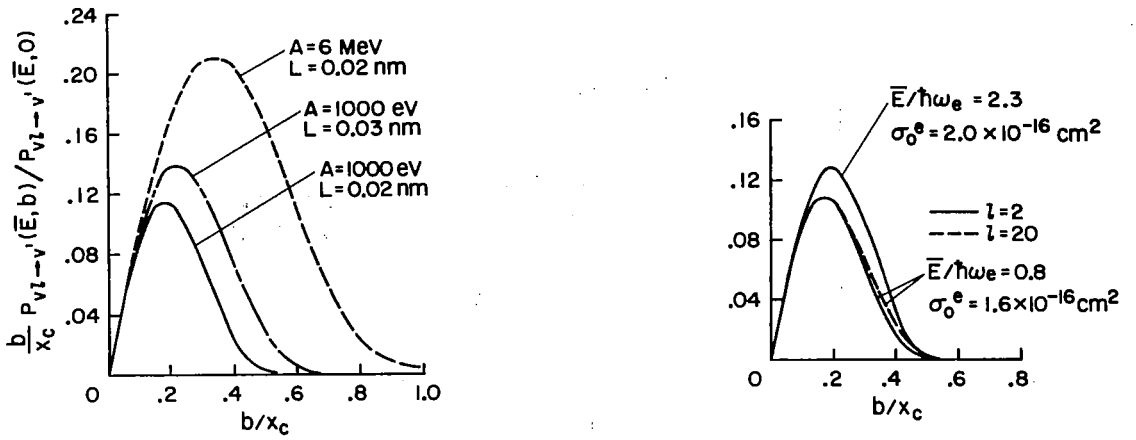

(a) $\ell = 20$, $\bar{E}/\hbar w_e = 1.1$ (b) A = 1000 eV, L = 0.02 nm

Figure 6.25.- Parameters affecting the net vibrational cross-section integrand for para-N_2(v = 0)-He collisions, v' = 1.

the equivalent position of the three-dimensional results corresponding to a constant inelastic cross section obtained using the value of σ_o^e from $\bar{E}/h\omega_e = 0.8$ (i.e., cross sections and rate coefficients from the two models would compare graphically as indicated by the collinear model curve and the shaded symbols).

A further point illustrated in figure 6.24 pertains to the required vibrational basis set for molecules like N_2. The collinear model has been used as a guide to show that, although the predominant vibrational transitions are single-quantum transitions from the ground state to v' = 1, higher vibrational states participate even at collision energies near threshold. The three-dimensional model behaves similarly and it was therefore necessary to include four vibrational manifolds from v = 0 to 3 with ℓ = 0-60 in each before acceptable convergence was achieved. On the other hand, a collinear, first-order perturbation calculation of the type described in chapter 4 gives results nearly identical to the 11-state collinear model over the energy range included in figure 6.24. These comparisons suggest that a first-order

perturbation treatment of the vibrational motion, in conjunction with the "sudden approximation" describing the rotational motion, will be a very useful analytical method for dealing with three-dimensional inelastic collisions if a workable solution of the resulting integral equation can be found (e.g., recall sec. 6.4.1).

Another interesting feature of the three-dimensional calculations is the variation of transition probabilities with impact parameter. As shown in figures 6.8 and 6.9, the net vibrational transition probabilities, $P_{v\ell \to v'}$, simply decrease monotonically as the impact parameter becomes larger so that $b = 0$ impacts always produce the greatest probability of a vibrational transition. However, the same is not true for all individual vibration-rotation transitions. The variation of $P_{v\ell \to v'\ell'}$ with b is shown in figure 6.26, where some vibration-rotation transitions are seen to be more effectively induced by nonzero impacts, just as previous classical calculations have suggested.[65]

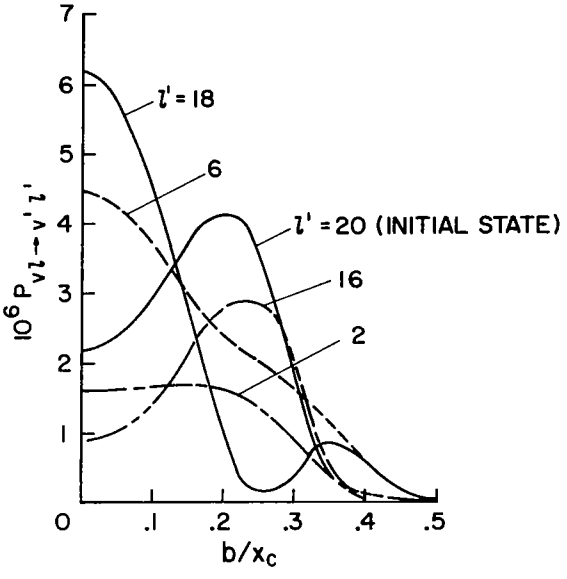

Figure 6.26.- Vibration-rotation transition probability variations with impact parameter for para-$N_2(v = 0)$-He collisions at $\bar{E}/h\omega_e = 1.1$, $A = 1000$ eV, $L = 0.02$ nm. Collision radius is $x_c = 0.3$ nm.

Finally, having established the applicability of a collinear model for predicting the rate of vibrational energy transfer from N_2 initially in the ground vibrational state, we can now investigate the accuracy of the collinear model in predicting the associated vibrational quantum number dependence of vibrational energy-transfer rates. The results validate the conclusions of chapter 5. Figures 6.27 and 6.28 compare both collision models for N_2 initially in the $v = 10$ vibrational state and show them to be qualitatively

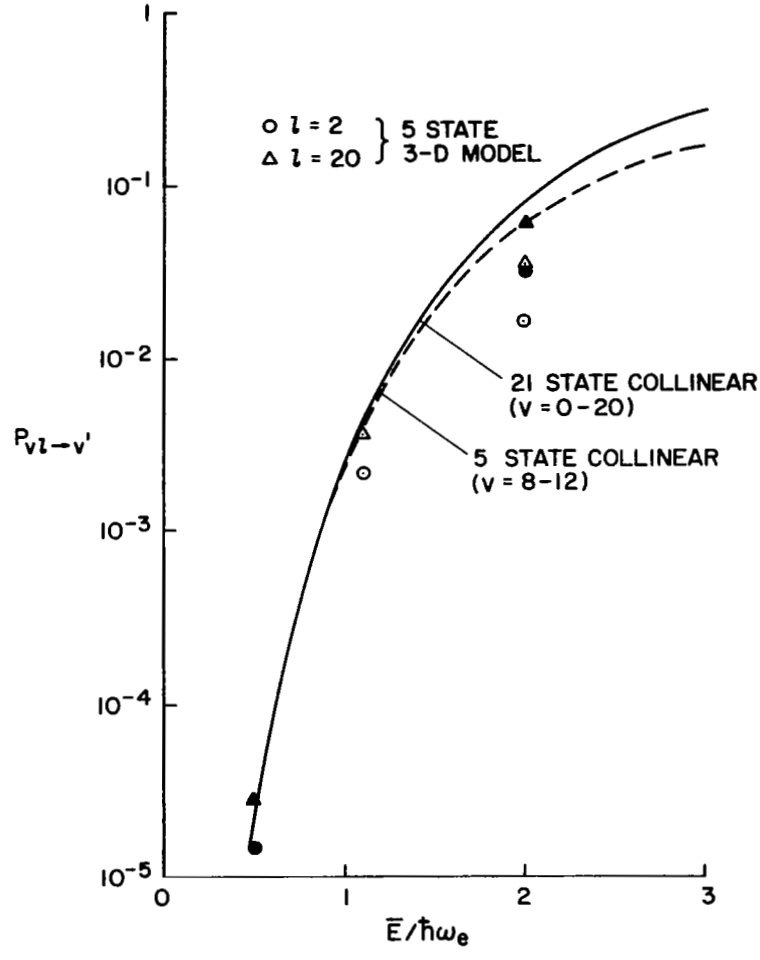

Figure 6.27.- Comparison of net vibrational transition probabilities for para-N_2(v = 10)-He collisions from the three-dimensional and collinear models; $v' = 11$, b = 0, $L_e = 0.02$ nm. Shaded symbols are equivalent probabilities for a constant σ_o equal to the cross section at $\bar{E}/\hbar\omega_e = 0.5$.

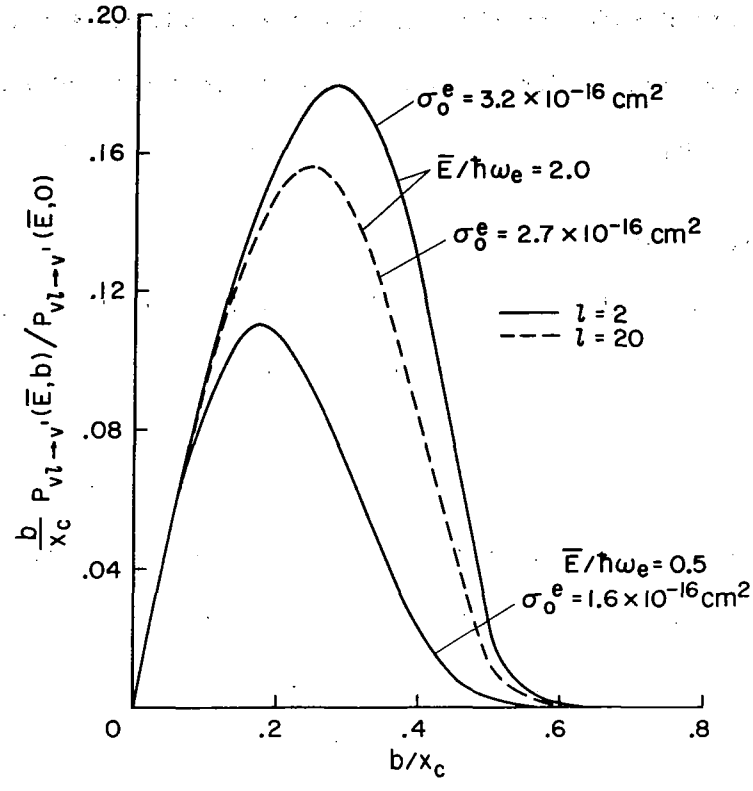

Figure 6.28.- Parameters affecting the net vibrational cross-section integrand for para-N_2(v = 10)-He collisions, v' = 11. Collision parameters are A = 1000 eV, L = 0.02 nm, x_c = 0.3 nm.

similar as in the ground-state predictions. When the initial state is vibrationally excited, the differences in results are seen (fig. 6.27) to be of secondary importance; that is, a larger vibrational basis set is required and the error of the collinear model is slightly greater. The three-dimensional model predictions must be compared with the five-state collinear model (dashed line) in figure 6.27 and, clearly, neither set of calculations contains a sufficient number of vibrational states. Thus, convergent three-dimensional calculations for excited vibrational states become increasingly impractical, even when the effective Hamiltonian approximation is incorporated. However, the variation in σ_o^e with collision energy again compensates nicely for the inaccuracy of the collinear model as the solid symbols in figure 6.27 indicate. Thus, as

before, the collinear model appears to produce an adequate description of the vibrational quantum-number dependence of cross sections and rate coefficients for molecules like N_2.

6.7.3 CO-He Collisions

A comparison of figures 6.3(b) and 6.4(b) for CO with figures 6.21 and 6.22 for N_2 suggests that the structural properties of CO are very similar to N_2. The intent of this section is therefore to look mainly for effects introduced by the heteronuclear nature of CO associated with the additional coupling of even- and odd-parity rotational states. Generally, no significant effects were found and the conclusions reached for N_2 appear to apply equally well to CO. For example, figure 6.29 illustrates the net vibrational transition probability dependence on ℓ. For small ℓ, the variations of $P_{v\ell \to v'}$ are only slightly more pronounced in CO than for N_2. Figure 6.30 shows that the collinear model is just as applicable and the vibrational quantum-number

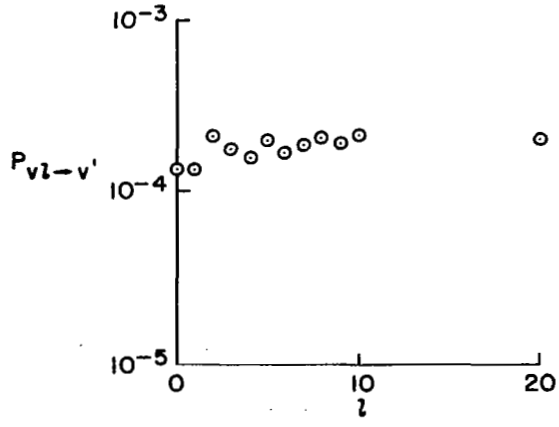

Figure 6.29.- Effect of initial rotational state on the net vibrational transition probabilities for CO(v = 0)-He collisions, v' = 1, at $\bar{E}/h\omega_e$ = 1.08, b = 0, L = 0.02 nm. Basis set includes ℓ = 0-60 for vibrational states v = 0-2.

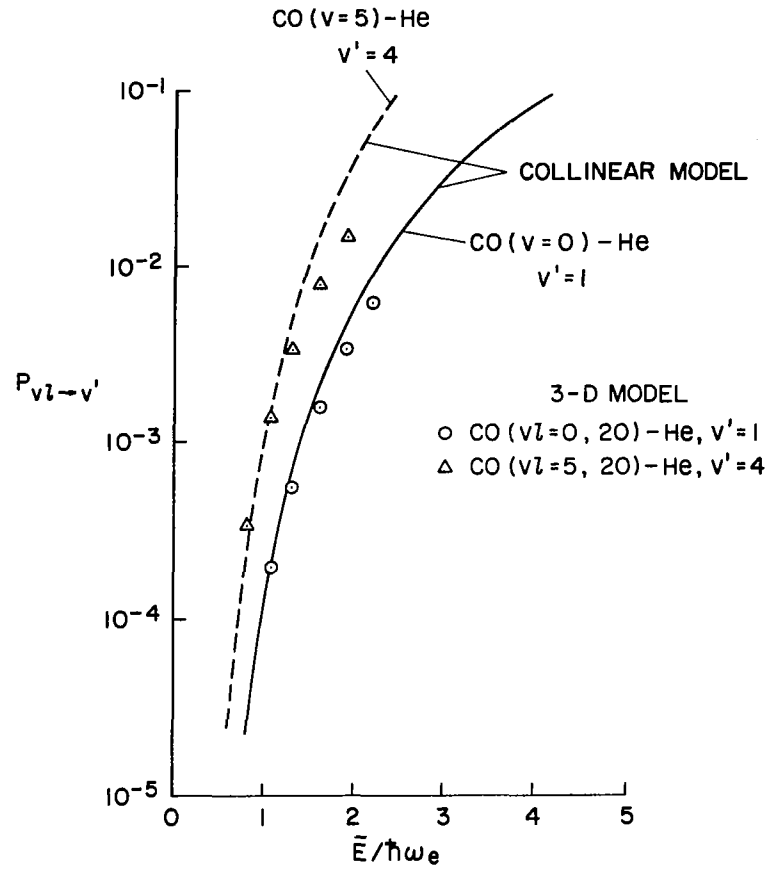

Figure 6.30.- Comparisons of the net vibrational transition probabilities for CO-He collisions from the three-dimensional and collinear models. Collinear basis set includes states v = 0-17. Three-dimensional basis set is the same as shown in figure 6.28. Collision parameters are b = 0, L = 0.02 nm.

dependence obtained with it is just as reliable. Finally, figure 6.31 demonstrates that the equivalent elastic cross section, σ_o^e, is not profoundly influenced by the collision conditions, any more than it is for N_2. Thus, we conclude that when the rotational eigenenergies are closely spaced in comparison to the vibrational eigenenergies and, hence, no resonant transitions with small $\Delta\ell$ are available, vibrational energy transfer will appear as a V-T process regardless of the other molecular properties.

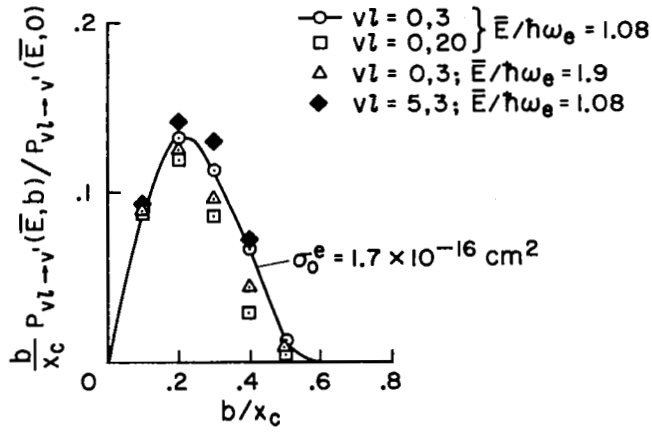

Figure 6.31.- Parameters affecting the net vibrational cross-section integrand for CO-He collisions; A = 1000 eV, L = 0.02 nm, x_c = 0.3 nm, v' - v = 1.

6.8 Classification of Rotational Coupling Effects on Vibrational Energy Transfer

The primary purpose of this chapter is to examine the role of coupled rotational motion in a diatomic molecule during the collisional exchange of vibrational and translational energy. A corollary to that purpose is the identification of conditions for which a collinear collision model will realistically predict the rate of vibrational energy transfer. We have found that, although the analysis of rotational coupling is complex, the nature of its influence on the energy-transfer process is conceptually simple.

The mechanisms of vibrational energy transfer become readily apparent when one recognizes that the controlling features of vibration-rotation coupling are the predominance of coupling between states with small differences in angular momentum (i.e., small $\Delta\ell$) and its interplay with the resonance enhancement of transition probabilities. Thus, while we deal with collision energies that have many rotational states occupied in each vibrational manifold, their occupation occurs primarily through sequential rotational

transitions of small $\Delta\ell$ during the encounter. Likewise, vibrational manifolds are connected primarily by vibration-rotation transitions with small $\Delta\ell$. Hence, the predominance of small $\Delta\ell$ transitions is a common feature of all inelastic mechanisms within the molecule. Furthermore, the range of $\Delta\ell$ for which rotational states are closely coupled is independent of the degree of resonance associated with a transition and it is insensitive both to the interaction potential parameters and to the inertial properties of the molecule. Thus, the effective range of $\Delta\ell$ (which we shall refer to as $\Delta\ell_{max}$, where $0 \leq \Delta\ell \leq \Delta\ell_{max}$) is similar for all the diatomic molecules and interaction potentials considered here and it is presumably similar for all others as well. We have shown (fig. 6.3) that, typically, $\Delta\ell_{max} \approx 4$ to 6.

With small $\Delta\ell$ transitions as a common characteristic, the different mechanisms of vibrational energy transfer separate into three natural classes. The molecules belonging to each class are identified by their inertial properties, as specified first and foremost by the ratio of fundamental vibrational and rotational frequencies, ω_e/B_e, and, second, by the proximity of the initial rotational state to a resonant companion. Given these two identifiers, we can then anticipate the qualitative nature of vibrational energy transfer for any diatomic molecule that does not involve electronic motion or reactive atom-exchange in the process.

The first class pertains to all molecules in which $\omega_e/B_e >> \Delta\ell_{max}$, regardless of the initial rotational state. Our examples were CO and N_2. When the frequency ratio is very large, near-resonant vibration-rotation transitions of small $\Delta\ell$ do not exist anywhere in the practical range of rotational states and any resonant enhancement of large $\Delta\ell$ transitions is suppressed by the lack of coupling between such states. Consequently, the

energy-transfer process is dominated by nonresonant small $\Delta\ell$ transitions in which the energy exchange is primarily between vibrational and translational modes. The initial-state angular momentum then has little influence on the rate of energy transfer and the process is described as a V-T mechanism. Molecules in this class are justifiably treated by a collision model in which the rotational contribution is either averaged or omitted. We found the collinear model to be surprisingly accurate for this class of molecules.

The second and third classes of energy transfer pertain to molecules in which ω_e/B_e is comparable with $\Delta\ell_{max}$. Our example was H_2. Since ω_e/B_e is not large, near-resonant vibration-rotation transitions with small $\Delta\ell$ are available. The proximity of the initial rotational state to rotational states capable of near-resonant vibration-rotation transitions then determines the class of energy transfer in which the molecule belongs. For example, the second class may be chosen as those molecules with initial rotational states remote enough from the near-resonant transitions for their angular momentum to be different by an amount greater than $\Delta\ell_{max}$. Since the rate of energy transfer through the near-resonant transitions is rapid but proportional to the occupation of the resonant states, at least some of the resonant states must first become occupied before the near-resonant transitions can serve as an effective energy-transfer path. However, the restriction to small $\Delta\ell$ transitions requires a sequence of induced rotational transitions to first take place within the vibrational manifold containing the initial state. Such a multistep process for successive small rotational energy changes during the collision is collectively as inefficient as a single-step nonresonant vibrational transition directly from the initial state. As a result, the energy-transfer process will not favor either path and the process must be labeled

as either a V-T mechanism in the extreme case or as a V-R-T mechanism in which near-resonant V-R and nonresonant V-T transitions compete.

The final class also pertains to molecules with $\omega_e/B_e \approx \Delta\ell_{max}$, but with an initial state within $\Delta\ell_{max}$ of a near-resonant vibration-rotation transition with small $\Delta\ell$. Near-resonant vibration-rotation transitions then immediately dominate the energy-transfer process. Pure V-R mechanisms of this type characteristically transfer vibrational energy at rates far exceeding the previous two classes.

Clearly, these latter two classes involve the rotational motion of the molecule in a significant manner and a collision model omitting the rotational coupling would not distinguish their separate characteristics. However, we have shown that, while the collinear model is not applicable to such molecules, we can at least identify those molecules for which it may be applied by using simple identifiers.

CHAPTER 7

A REVIEW AND SOME CONSIDERATIONS FOR FUTURE STUDY

7.1 Review of the Newfound Aspects of Vibrational Energy Transfer

The primary emphasis of this study has been directed toward the factors that influence the collisional exchange rates of vibrational and translational energy from excited vibrational states of diatomic molecules. In particular, emphasis has centered on the dependence of energy-transfer rates on initial-state vibrational quantum number and on the role of coupled rotational transitions in the energy-transfer process. As a consequence of the emphasis on excited vibrational states, two fundamental aspects were included in the collision model that are not often considered, namely, the anharmonicity of the molecular vibrations and the coupled interaction of multiple vibrational states. However, an overriding limitation to the realism of the collision model is the uncertainty of the interaction potential between collision partners. Thus, the conclusions of this study pertain mainly to the qualitative nature of vibrational energy transfer with no attempt made to predict absolute rates.

A point made early in this study was that the analysis of a macroscopic nonequilibrium process is most conveniently carried out using simple analytic formulas to generate the necessary vibrational rate coefficients. One of the primary objectives of this study, therefore, was to evaluate the several analytic approximations in popular use, as they apply to excited state transitions. To that end, a semiclassical description of the collision dynamics was adopted because, from previous comparisons, it showed the greatest promise as a theoretical framework leading to accurate analytical solutions. However,

a semiclassical formulation is itself an approximate description of the collision dynamics. The first investigative step was therefore to determine the limitations of the semiclassical approximation when applied to a multistate anharmonic oscillator initially in an excited state.

A comparative evaluation of the semiclassical approximation was conducted (ch. 4) based on a collinear collision model entirely equivalent to a fully quantum-mechanical formulation appearing in the literature. Transition probability predictions were compared for a wide range of anharmonic molecular types, initial states, and collision parameters. The comparisons also included heteronuclear molecules. Generally, they were unlike previous comparisons in the literature which are typically confined to homonuclear harmonic oscillators in the ground vibrational state. The results illustrated some notable and previously unrealized effects of oscillator anharmonicity on the semiclassical approximation. For example, when computing the motion of the incident particle, the usual semiclassical procedure is to consider the oscillator nuclei as stationary relative to the molecular mass center. However, the effects of oscillator compression and recoil are amplified when the oscillator is anharmonic, and the agreement between semiclassical and quantal theories is significantly degraded unless the time-dependent average positions of the oscillator nuclei are introduced into the classical path determination. In the absence of such coupling, errors in the semiclassical approximation are largest when the incident particle mass is comparable to or larger than the mass of either molecular nucleus. When the molecule is heteronuclear, the semiclassical errors can become so large that anomalous resonances appear in the transition probability predictions. The anomalous resonances are strictly a consequence of the anharmonic coupling and do not

occur when the oscillator is harmonic. Coupling of the anharmonic oscillator motion with the classical path removes the resonances and brings the semiclassical model into acceptable agreement with the exact quantal predictions. These results place new limitations on the use of analytic solutions based on a semiclassical approximation. For example, the analytic models do not include the effects of oscillator compression on the classical path and they should not be applied to heteronuclear anharmonic oscillators like the hydrogen-halides. For the same reason, the analytic models are also inaccurate when applied to the collision of light homonuclear oscillators with a heavy incident particle. This latter result is contrary to earlier arguments based on a concept that the semiclassical approximation should be most accurate for heavy incident particles because their wave packets are more localized and hence their motion corresponds more closely with a classical description. Finally, the limitations of the semiclassical approximation observed for oscillators initially in the ground vibrational state were found to be no more restrictive for oscillators in an excited state. Thus a semiclassical collision model should be adequate for studies of the dependence of transition rates on the initial vibrational quantum number.

With the semiclassical approximation validated and its limitations understood, the factors influencing the dependence of vibrational rate coefficients on the initial state quantum number were investigated next (ch. 5). Again, a collinear model was used, this time because it corresponds to the collision geometry adopted in all the analytic solutions to be tested. Comparisons of the several analytic solutions available from the literature with multistate numerical solutions for anharmonic oscillators in excited states

showed that the most accurate analytical description in applications where the accuracy is important is a first-order perturbation treatment of anharmonic oscillators. Conversely, the approximation in greatest popular use was found to give the poorest results for highly excited states. The influence of multiple-quantum transitions on the vibrational relaxation process from highly excited states was also examined. Two- and three-quantum transitions from highly excited states were found to be generally unimportant at kinetic temperatures less than the characteristic vibrational temperature of the oscillator (defined as $h\omega_e/k$). Since vibrational relaxation is usually superceded by other kinetic mechanisms at higher temperatures, the usual assumption that single-quantum transitions prevail is adequate for the range of initial vibrational states typically considered.

The remaining question pertains to the role of coupled rotational transitions in the transfer of vibrational energy and their impact on the previous conclusions obtained with a collinear collision model. A three-dimensional collision model was developed (ch. 6) that allows an arbitrary number of coupled rotational states to be included in the arbitrary set of vibrational manifolds. However, the collision calculations only confirm what is apparent (in retrospect) from the matrix elements associated with all diatomic vibration-rotation states: namely, that the two controlling factors of rotational coupling are (a) a restriction to vibration-rotation transitions with small changes in angular momentum and (b) the interaction of that restriction with the rate enhancement given to near-resonant transitions. Based on these general features, one can classify the mechanisms of vibrational energy transfer between a diatomic molecule and a structureless particle into three distinct types: vibration-translation (V-T), vibration-rotation-translation

(V-R-T), and vibration-rotation (V-R). The molecules belonging to each type are easily identified, first and foremost by their ratio of fundamental vibrational and rotational frequencies, ω_e/B_e, and, second, by the proximity of their initial rotational state to a near-resonant transition invoking a small change in angular momentum. A result particularly important to the analyst of macroscopic kinetics is the finding that molecules belonging to the class dominated by V-T transitions (i.e., those where $\omega_e/B_e >> 1$) are accurately treated by a collinear collision model that may be reduced to yield analytic solutions.

As a consequence of this study, we reach the broad conclusion that the collisional exchange rates of vibrational and translational energy can be accurately estimated for diatomic molecules in excited vibrational states using a simple analytic semiclassical model if the following conditions are met:

(a) The fundamental vibrational frequency of the molecule is larger than its rotational frequency by several orders of magnitude.

(b) The molecule is homonuclear or only slightly heteronuclear.

(c) The incident particle mass is less than either nuclear mass of the molecule.

(d) The interaction potential is accurately modeled in the region of closest approach.

(e) A theoretical model is used that includes oscillator anharmonicity in its primary formulation. The first-order perturbation treatment of Morse oscillators appears to be the most satisfactory choice.

While the preceding conditions are numerous, they only exclude light or heteronuclear molecules, like H_2 and the hydrogen-halides, or collision

partners heavier than Argon. Hence the limitations of a well-chosen analytic model are not severe.

7.2 Considerations for Future Study

Long before this study was conceived, many investigators were aware of the need for more detailed descriptions of the interaction potentials between simple diatomic molecules and atoms or ions. The computational and experimental determination of such potentials continues to be an activity of foremost importance if quantitatively accurate predictions of vibrational and rotational energy-transfer rates are to be achieved. Clearly, many other related collision phenomena such atom exchange reaction rates, ion and atom recombination rates, and collisional radiative line broadening also await the same potentials. However, the theoretical and experimental methods for determining interaction potentials are usually somewhat remote from the physics of inelastic collisions discussed here. We only acknowledge their importance to future studies of this type. In fact, with exact quantum-mechanical calculations of inelastic collisions now effectively a routine numerical exercise, much of the new work on vibrational and rotational energy transfer is based on the availability of improved potentials.

Nevertheless, there are new practical applications, particularly those associated with lasers, that require further study into several untouched aspects of vibrational energy transfer. For example, if we limit our interest just to the exchange of vibrational and translational energy and exclude the multitude of other vibrational exchange mechanisms such as vibrational energy transfer between two oscillators or the interactions between vibrational and electronic states, we are still left with the following considerations:

(a) The absence of satisfactory experimental determinations of the dependence of vibrational rate coefficients on initial-state quantum number was indicated in chapter 5. Clearly, such measurements will be difficult, but recent improved techniques for selective excitation of upper states using tunable lasers and multiphoton absorption offer possibilities for new approaches.

(b) The use of a semiclassical approximation and the deletion of long-range forces from the interaction have made the collision models of this study inappropriate for predicting low-temperature rate coefficients. Yet we have shown that the rate predictions for transitions from highly excited vibrational states are most sensitive to the collision parameters at low temperatures. Several infrared lasers of great practical importance operate at such conditions. Thus, rate predictions using a fully quantum-mechanical model and a more complete description of the long-range interactions would be extremely useful for the analysis of such lasers. The same collision models would also advance the study of heteronuclear molecules at all conditions since, for those molecules, the semiclassical approximation is generally inappropriate.

(c) Molecules like H_2 are shown to transfer vibrational energy with high probability from rotational states near the continuum. Clearly, more realistic predictions of such energy-transfer rates should include interactions with the continuum. Furthermore, a collision model including continuum states would allow further study into the nature of vibration-dissociation coupling and also into the reverse process, namely, three-body recombination to excited vibrational states.

The foregoing considerations have come to mind during the course of this study as a result of the particular topics investigated. However, recent innovative techniques using the selective excitation of vibrational states in such applications as laser isotope separation, photoenhancement of chemical reactions, and fluorescence enhancement have brought importance to many other aspects of vibrational energy transfer not considered here.

Ames Research Center
National Aeronautics and Space Administration
Moffett Field, Calif. 94035, March 4, 1976

APPENDIX A

NOTATION

The following catalog of symbols includes only those used repeatedly. All symbols are defined locally in the text. Equations and figures cited locate explicit definitions and usage.

a	Morse intramolecular potential range, equation (3.3)
a_b	trajectory coefficient for nonzero impacts, equation (6.36)
A	interaction potential magnitude, equation (3.18)
b	impact parameter, figure 6.1
b', b_v	Morse oscillator wave-function constants, equation (3.10)
B_e	molecular rotational frequency constant
c_n	wave-function amplitude in basis state n
D	Lennard-Jones interaction potential well depth, equation (3.22)
D_o	Morse intramolecular potential well depth, equation (3.3)
E	relative kinetic energy in a center-of-mass reference frame
$\bar{E}$	average relative kinetic energy
E_v	oscillator energy in eigenstate v
E_T	total energy of a colliding system in a center-of-mass reference frame, equation (4.15)
$\hbar$	$h/2\pi$, where h is the Planck constant
$i_J(y)$	modified spherical Bessel function, equation (3.31)
k	Boltzmann's constant
k'	oscillator anharmonicity constant, equation (3.9)
$k_{m,n}, k_{m \to n}$	rate coefficient for transitions from quantum state m to n

ℓ,ℓ'	angular-momentum orbital quantum numbers
L	interaction potential range parameter, equation (3.18)
$L_v^b(y)$	Laquerre polynomial, equation (C.2)
m,m'	angular-momentum projection quantum numbers
$\bar{m}$	$m'-m$
m_i	mass of nucleous i
$\mathcal{M}^{(J)}_{\ell'm'\ell m}$	rotational matrix element coupling term, equation (6.22)
N_v	oscillator radial wave-function normalization factor, equation (3.6)
$P_J(y)$	Legendre polynomial in the variable y
$P_{m\to n}$	transition probability between states m and n
$P_{v\ell m\to v'\ell'm'}$	final transition probability from state $v'\ell'm'$ to $v\ell m$
$P_{v\ell\to v'\ell'}$	net vibration-rotation transition probability averaged over all initial m states and summed over all m' states, equation (6.42)
$P_{v\ell\to v'}$	net vibrational transition probability averaged over all initial m states and summed over all ℓ' and m' states in manifold v', equation (6.43)
r	oscillator internuclear separation distance
r_e	oscillator equilibrium internuclear separation distanee
$r^{(n)}_{vv'}$	elementary radial overlap integral, equation (6.19)
$\mathcal{R}_v(r)$	oscillator radial wave function for eigenstate v, equation (3.6)
$R^{(J)}_{vv'}$	radial matrix element, equation (6.16)
t	time measured from the instant of closest approach

T	kinetic temperature
$\bar{u}$	average relative collision speed in a center-of-mass reference frame
U	interaction-potential spherically symmetric term, equation (6.9)
v,v'	vibrational quantum number
V,V'	interaction potential between colliding nuclei
$\bar{V}$	spherically averaged interaction potential, equation (6.30)
V_o	intramolecular potential
V'_{mn}	time-dependent interation matrix element (overlap integral) for states m and n
$V_{v'\ell'm'v\ell m}$	time-independent matrix element for states $v'\ell'm''$ and $v\ell m$, equation (6.26)
$V^e_{v'\ell'v\ell}$	"effective-Hamiltonian" matrix element, equation (6.55)
x,x_i	separation distance between colliding nuclei, figure 3.4
x_c	"hard sphere" collision radius
$\bar{x}$	mass-center separation distance between collision partners, figure 3.4
$\bar{x}_o$	mass-center separation distance at closest approach
x_e	anharmonic second-order frequency coefficient, equation (3.1)
$Y_{\ell m}$	spherical harmonic function
z	oscillator-internuclear separation parameter, equation (3.7)
γ	molecular mass ratio, figure 3.4
δ	molecular orientation angle, figure 3.4
$\Delta\ell$	$\lvert\ell'-\ell\rvert$

$\Gamma(y)$	gamma function of argument y
$\bar{\Gamma}(a,y)$	incomplete gamma function
θ,ϕ	spherical polar coordinate angles, figure 6.1
μ	reduced mass of the collision pair
μ_o	reduced mass of the molecule
ρ_o	Lennard-Jones zero potential radius, figure 3.3
σ_o,σ'_o	"hard-sphere" constant cross sections, equation (5.4)
σ_o^e	equivalent hard-sphere cross section computed from the three-dimensional collision model, equation (6.47)
$\sigma_{m\to n}$	total cross section for transitions from state m to n
τ	vibrational relaxation time constant, equation (1.1)
τ_c	mean collision-interaction time
$\psi(r,\theta,\phi)$	oscillator steady-state wave function
Ψ	perturbed oscillator time-dependent wave function
ω_m	circular frequency of eigenstate m
ω_e	fundamental oscillator frequency, equation (3.1)
ω_{mn}	$\omega_m-\omega_n$
$\bar{\Omega}$	trajectory azimuthal angle, figure 6.1

APPENDIX B

GENERAL FORMULATION OF THE SEMICLASSICAL COLLISION THEORY

The semiclassical procedure developed here is assembled from the contents of typical textbooks describing classical and quantum mechanics. For example, the classical equations of motion are derived from first principles in H. Goldstein, *Classical Mechanics*, Addison-Wesley (1950), chapter 3, and the quantum-mechanical methods are discussed in E. Merzbacher, *Quantum Mechanics*, John Wiley (1970), chapter 18. Both aspects are included here to provide a unified description of the complete theory and to identify explicitly the notation and assumptions associated with the collision model.

The formulation to follow is based on a center-of-mass reference frame in which μ_o and μ denote the reduced mass of the target molecule and the complete collision system, respectively. The incident particle is limited here to a structureless point mass whose motion is pictured classically. The target molecule is capable of intranuclear motion and its dynamic response to a time-dependent disturbance induced by the incident particle is described quantum mechanically. The motions of both collision partners are coupled through an interaction potential that depends on the relative separation of all nuclei in the system. For these purposes, the potential is represented here only by an arbitrary function $V(\vec{q},\vec{R})$ when $\vec{q}$ specifies the molecular coordinates in configuration space and $\vec{R}$ locates the incident particle position relative to the molecular mass center. The remaining discussion may then be divided into a section describing the classical motion of the incident particle and a section detailing the quantum-mechanical formulation for the molecular dynamics.

B.1 Classical Trajectory

In most semiclassical collision theories, the classical path is determined from just a spherically symmetric average of the interaction potential centered on the target mass center. This approach reduces the encounter to a simple two-body central-force problem and, more importantly, it avoids most of the difficulties arising otherwise from a need to define the molecular coordinate $\vec{q}$, contained in the interaction potential, in classical terms. The spherically symmetric average potential, $\bar{V}$, may be obtained by quantum mechanically averaging the potential over all molecular coordinates in a manner suggested by

$$\bar{V}(R) = \langle j | V(\vec{q},\vec{R}) | n \rangle$$

where molecular states $|j\rangle$ and $|n\rangle$ may be initial states or some combination of initial and final states. In many cases, the method of averaging has little influence on the final results.

Given a central potential, the trajectory remains in a single plane described by two coordinates as shown in figure B.1. The potential may then be denoted as $V(\vec{R}) \equiv V(\bar{x})$ and the trajectory is conveniently described by a Lagrangian development of the equations of motion. As a result, the conservation of total energy, E, leads to

$$E = \frac{\mu}{2}\left[\left(\frac{d\bar{x}}{dt}\right)^2 + \left(\bar{x}\,\frac{d\bar{\Omega}}{dt}\right)^2\right] + \bar{V}(\bar{x}) \qquad \text{(B1)}$$

and the conservation of angular momentum, L, requires that

$$L = \mu\bar{x}^2\,\frac{d\bar{\Omega}}{dt} \qquad \text{(B2)}$$

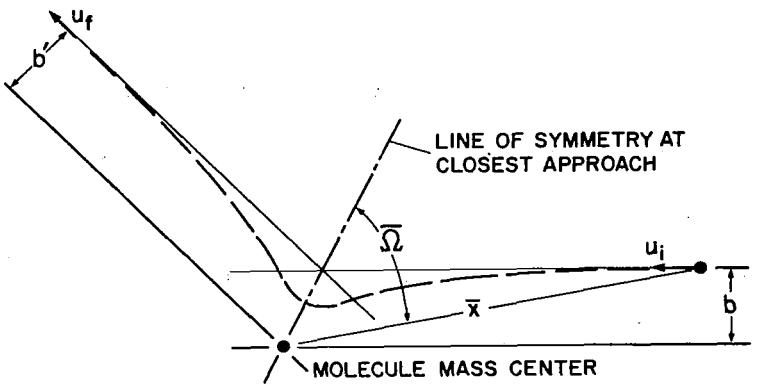

Figure B.1.- Classical path in a center-of-mass reference frame for a two-body, central force interaction.

The initial conditions are defined by the initial speed, u_i, and the impact parameter, b. At $t = -\infty$, we then have $E = (1/2)\mu u_i^2$ and $L = \mu b u_i$. However, before introducing the initial conditions, we must recognize that no account has been taken of the energy or angular momentum traded inelastically with the target. This inconsistency is the origin of the lack of conservation in a semiclassical theory. While, in principle, a further approximation could be invented for keeping the system conservative, the usual method has been to adopt an equally approximate approach in which E and L are simply interpreted as "effective" constants of the motion averaged over the trajectory. In this formulation, we shall consider the impact parameters b and b', shown in figure B.1 to be identical but acknowledge that $u_f \neq u_i$ in a fully conservative system. We then define an average speed, $\bar{u} = \bar{u}(u_i, u_f)$ and average energy $\bar{E} = 1/2\ \mu\bar{u}^2$, where the method of averaging is determined by that giving the best results. With these interpretations, the equations of motion that determine the time dependence of the coordinate $\vec{R} = \vec{R}\ (\bar{x}, \bar{\Omega})$ in the interaction potential are obtained from equation (B1) and (B2) as

$$\left(\frac{d\bar{x}}{dt}\right)^2 = \bar{u}^2\left[1 - \frac{\bar{V}(\bar{x})}{\bar{E}} - \left(\frac{b}{\bar{x}}\right)^2\right] \tag{B3}$$

$$\frac{d\bar{\Omega}}{dt} = \frac{b\bar{u}}{\bar{x}^2} \tag{B4}$$

B.2 Quantum-Mechanical Molecular Motion

The molecular motion is driven by the complete interaction potential, $V(\vec{q},\vec{R})$. To emphasize the time dependence, however, we use the equivalent notation $V(\vec{q},\vec{R}) \equiv V(\vec{q},t)$. The Hamiltonian describing the molecular motion is then

$$\mathcal{H}(\vec{q},t) = \mathcal{H}_o(\vec{q}) + V(\vec{q},t) \tag{B5}$$

where $\mathcal{H}_o(\vec{q})$ is the stationary-state Hamiltonian containing the intramolecular potential V_o according to

$$\mathcal{H}_o(\vec{q}) = -\frac{\hbar^2}{2\mu_o}\nabla_q^2 + V_o(\vec{q})$$

This definition of $\mathcal{H}(\vec{q},t)$, in which the incident particle motion is only implied by the time dependence of $V(\vec{q},t)$, is the essence of the semiclassical approximation. Otherwise, $\mathcal{H}(\vec{q},t)$ would contain a momentum operator related to the incident particle.

In the Schrödinger picture, the equation of motion is

$$-i\hbar\frac{\partial\Psi(\vec{q},t)}{\partial t} = \mathcal{H}(\vec{q},t)\Psi(\vec{q},t) \tag{B6}$$

For $t \to \pm\infty$, the molecule is undisturbed and $\mathcal{H} = \mathcal{H}_o$, giving a stationary-state solution of the form

$$\Psi_o(\vec{q},t) = \sum_n c_n^{(0)}\, e^{-i\omega_n t}\psi_n(\vec{q}) + \int c_k^{(0)}\, e^{-iE_k t/\hbar}\Phi_k(\vec{k})\, d\vec{k} \tag{B7}$$

where the probability amplitudes, $c_n^{(0)}$ and $c_k^{(0)}$ are constant in time. The first term in equation (B7) represents bound states of $\mathcal{H}_o$ with quantum numbers n and satisfying

$$\mathcal{H}_o\psi_n = \hbar\omega_n\psi_n$$

The second term accounts for any continuum states allowed by $\mathcal{H}_o$ with energy E_k and momentum $\hbar\vec{k}$. While continuum states may exist, we justify their neglect by arguing that they will never participate in the dynamics of the molecule for the conditions of interest here. Consequently, we shall always choose total energies (internal plus kinetic) well below the level where any continuum states are energetically accessible. With that stipulation, the bound-state eigenfunctions, ψ_n, provide a natural and complete basis set in which to expand the solution to equation (B6). Thus, we can write the time-dependent wave function as

$$\Psi(\vec{q},t) = \sum_n c_n(t)\ e^{-i\omega_n t}\psi_n(\vec{q}) \qquad \text{(B8)}$$

The probability amplitudes, $c_n(t)$, are analogous to $c_n^{(0)}$, but are now time dependent. The probability of occupation in state n at any time during the encounter is $\langle\psi_n|\Psi(\vec{q},t)\rangle = |c_n(t)|^2$. Since all that we desire are the occupation probabilities, a description of the $c_n(t)$ terms provides an adequate solution to the problem. Equation (B6) may be transformed into a set of equations — one for each $c_n(t)$ — by the usual procedure of substituting equation (B8) and utilizing the orthogonality of the eigenfunctions, $\langle\psi_n|\psi_j\rangle = \delta_{nj}$. The result is

$$i\hbar\frac{dc_j(t)}{dt} = \sum_n c_n(t)\ e^{i(\omega_j-\omega_n)t}\langle j|V(\vec{q},t)|n\rangle \qquad \text{(B9)}$$

where the bracket notation refers to

$$\langle j|V(\vec{q},t)|n\rangle \equiv \int \psi_j^* \, V(\vec{q},t) \, \psi_n \, d\vec{q} \tag{B10}$$

integrated over all $\vec{q}$ space.

To solve equation (B9), the molecule is considered to be initially in a pure eigenstate $|i\rangle$, thus creating the initial condition

$$|c_n(-\infty)|^2 = \delta_{in}$$

for all n. The initial phase of $c_n(-\infty)$ is unimportant and is chosen arbitrarily since we are interested only in $|c_n(t)|^2$. The final state of the molecule at $t \to +\infty$ then determines the transition probabilities resulting from the collision. For transitions to state $|j\rangle$, the probability is

$$P_{i \to j} = |c_j(+\infty)|^2$$

At this point, note the role of various terms in equation (B9) and how they contribute to the transition probability. The matrix element, $\langle j|V(\vec{q},t)|n\rangle$, is a coupling factor that connects states $|j\rangle$ and $|n\rangle$. It contains the primary quantal properties of the transition and it introduces the appropriate selection rules, if any exist. However, while selection rules will control individual matrix elements, the coupling of more than two states in the molecular dynamics can allow alternate routes for the molecule to reach a selected final state. Thus, energetic collisions involving numerous intermediate states will not always display the selection properties appearing in low-energy collisions where only two states participate in a transition.

Resonance in a transition plays no direct role in determining the matrix element properties. Thus, the matrix-element properties will prevail regardless of the degree of resonance. However, resonance will have an *additional* effect on the transition probability by way of the phase term in equation (B9). Clearly, a resonant transition (in which $\omega_j = \omega_n$) will not be degraded by phase interference during the collision and will achieve the maximum probability determined by the matrix element. Conversely, as $|\omega_j - \omega_n|$ increases, phase interference can add an oscillatory structure to the final transition probability that varies with the collisional parameters.

The practical aspects of solving equation (B9) are made simpler if the time-dependent aspect of the matrix elements defined by equation (B10) may be factored according to

$$\begin{aligned} \langle j|V(\vec{q},t)|n\rangle &= U(t)\langle j|V'(\vec{q})|n\rangle \\ &= U(t)V_{jn} \end{aligned} \tag{B11}$$

Then the time-independent elements V_{jn}, which contain all the quantum-mechanical selection properties and often require considerable numerical labor, can be computed in advance of the time-dependent solution. The function $U(t)$ is obtained from the classical trajectory and applies to the entire set of equations (B9) for all quantum states.

Another practical aspect in solving equation (B9) is to adopt the so-called "close-coupling" approximation in which not all eigenstates in the complete set are included. Guided by trial solutions, only those states contributing to the dynamics of selected states of interest are retained in the coupled set of equations (B9). Usually, many states that are energetically inaccessible from a classical point of view may be neglected, although

experience has shown that inaccessible states with eigenenergies close to a state of interest contribute to the transient dynamics during the collision even though they are unoccupied afterward.

Finally, a necessary criterion that will be satisfied at any time, if the numerical solution of equations (B9) proceeds accurately, is the closure relation conserving probability, that is,

$$\sum_n |c_n(t)|^2 = 1 \tag{B12}$$

Hence, equation (B12) may be used as one test for regulating the numerical step size, although, in practice, it seldom becomes a limiting factor.

B.3 First-Order Perturbation Theory

When the kinetic energy is very low, the occupation of all states other than the initial state remain very small. Thus, if $|i\rangle$ denotes the initial state, we can assume $|c_i(t)|^2 \approx 1$ and $|c_n(t)|^2 \ll 1$ for all times and all $n \neq i$. To obtain the equivalent of a first-order perturbation theory in these circumstances, we must make the further stipulation that only two states interact, with one of them the initial state. This suggests that the eigenenergy of the second state is remote from all others and lies adjacent to the initial-state eigenenergy. If, for simplification of notation, we denote

$$\langle n|V(\vec{q},t)|i\rangle \equiv V'_{ni}(t) \tag{B13}$$

equation (B9) can then be written:

$$i\hbar \frac{dc_i(t)}{dt} = V'_{ii}(t)\ c_i(t) \tag{B14}$$

$$i\hbar \frac{dc_n(t)}{dt} = V'_{ii}(t)\ c_i(t) + V'_{ni}(t)\ c_n(t)\ e^{i(\omega_n-\omega_i)t} \tag{B15}$$

The neglect of c_n in equation (B14) constitutes the perturbation approximation and leads to a violation of closure as given by equation (B12). The set of equations (B14) and (B15) are therefore not exactly equivalent to a two-state description using equations (B9).

A solution of equation (B14) is

$$c_i(t) = \exp\left[-\frac{i}{\hbar}\int_{-\infty}^{t} V_{ii}(\tau)d\tau\right] \tag{B16}$$

thus fixing the occupation $|c_i(t)|^2 = 1$ for all t. Equation (B16) is used to suggest the form of $c_n(t)$ by writing

$$c_n(t) = b_n(t)\exp\left[-\frac{i}{\hbar}\int_{-\infty}^{t} V'_{nn}(\tau)d\tau\right] \tag{B17}$$

where $|c_n(t)|^2 = |b_n(t)|^2$. Thus, we may solve for $b_n(t)$. Equation (B15), in terms of $b_n(t)$, takes on the convenient form

$$i\hbar\frac{db_n(t)}{dt} = V'_{ni}(t)\exp\left[i(\omega_n - \omega_i)t + \frac{i}{\hbar}\int_{-\infty}^{t}(V'_{nn} - V'_{ii})d\tau\right] \tag{B18}$$

By defining a phase frequency $\Gamma_{ni} = \omega_n - \omega_i + (V'_{nn} - V'_{ii})/\hbar$, the transition probability is then obtained in simple form as

$$P_{i\to n} = \left|\int_{-\infty}^{\infty}\frac{V'_{ni}}{\hbar}\, e^{i\int_0^t\Gamma_{ni}(\tau)d\tau}\right|^2 \tag{B19}$$

Note that since $P_{i\to i} = 1$ from equation (B16), probability is not conserved and the solution of equation (B19) will be accurate only if $P_{i\to n} << 1$.

APPENDIX C

RADIAL MATRIX ELEMENT INTEGRAL

The radial matrix element $R^{(J)}_{vv'}$ is expressed in equation (6.18) as a series expansion containing the integrals $r^{(n)}_{vv'}$ where, according to equation (6.19),

$$r^{(n)}_{vv'} = \int_{-\infty}^{\infty} \mathcal{R}^*_{v'}(r) \left(\frac{r}{L}\right)^n \mathcal{R}_v(r)\, dr \qquad (6.19)$$

The integral $r^{(n)}_{vv'}$ must be evaluated for a sufficient range of n to reach convergence in $R^{(J)}_{vv'}$. We therefore seek an analytic solution to equation (6.19) for arbitrary n that will allow rapid calculations of the numerous matrix elements required for a typical basis set of vibrational states.

The first step in evaluating equation (6.19) is to express it in explicit algebraic terms. To that end, we recall that $\mathcal{R}^*_{v'}(r)$ and $\mathcal{R}_v(r)$ are Morse oscillator radial wave functions described in chapter 3. Morse[72] shows that, in the absence of rotational centrifugal forces, the wave function may be written:

$$\mathcal{R}_v(r) = N_v\, e^{-z/2} z^{b_v/2} L^{b_v}_v(z) \qquad (C1)$$

where

$$z = k'\, e^{a(r-r_e)}$$

$$b_v = k' - 2v - 1$$

$$N_v = [a b_v \Gamma(v+1)/\Gamma(k'-v)]^{1/2}$$

and v is an integer denoting the vibrational eigenstate quantum number. The function $L_v^{b_v}(z)$ is a Laguerre polynomial defined as[73]

$$L_v^{b_v}(z) = \sum_{m=0}^{v} q_m^{(v)} z^m \tag{C2}$$

where

$$q_m^{(v)} = \frac{(-1)^{v+m}}{m!\,(v-m)!} \frac{\Gamma(k'-v)}{\Gamma(k'-2v+m)}$$

and $\Gamma(y)$ is a gamma function. By comparing the eigenenergies associated with $R_v(r)$ with the spectroscopic term expression:

$$E_v/\hbar = \omega_e(v + 1/2) - \omega_e x_e (v + 1/2)^2$$

Morse shows that the parameter k' is then a measure of the oscillator anharmonicity and related to the spectroscopic parameters by

$$k' = \omega_e/\omega_e x_e \tag{C3}$$

Substitution of the radial wave-function expression, equation (C1), into equation (6.19) leads to a transformed integral over the variable z according to

$$r_{vv'}^{(n)} = \left(\frac{r_e}{L}\right)^n \delta_{vv'} + \frac{N_{vv'}}{(aL)^n} \int_0^\infty e^{-z}\, z^\lambda\, L_v^{b_v}(z)\, L_{v'}^{b_{v'}}(z) \left[\ln\left(\frac{k'}{z}\right)\right]^n dz \tag{C4}$$

where $\delta_{vv'}$ is a Kronecker delta and the new terms are defined by

$$N_{vv'} = N_v N_{v'}/a$$

$$= \frac{\sqrt{(k'-2v-1)(k'-2v'-1)v!v'!}}{\Gamma(k'-v)\,\Gamma(k'-v')} \tag{C5}$$

and

$$\lambda = k' - 2 - (v + v') \tag{C6}$$

Now invoking equation (C2) and noting that the product of two finite polynomials may be written as

$$\left.\begin{aligned} L_v^{b_v}(z)L_{v'}^{b_{v'}}(z) &= \sum_{s=0}^{v+v'} D_s z^s \\ \text{where} \qquad D_s &= \sum_{j=0}^{s} q_j^{(v)} q_{s-j}^{(v')} \end{aligned}\right\} \qquad \text{(C7)}$$

equation (C4) becomes

$$r_{vv'}^{(n)} = \left(\frac{r_e}{L}\right)^n \delta_{vv'} + \frac{N_{vv'}}{(aL)^n} \sum_{s=0}^{v+v'} D_s \int_0^\infty e^{-z}\, z^{\lambda+s} \left[\ln\left(\frac{k'}{z}\right)\right]^n dz \qquad \text{(C8)}$$

Equation (C8) is an explicit algebraic equivalent of equation (6.19) for a Morse oscillator, and the reduced integral to be solved is readily apparent. Several exact analytic solutions of equation (C8) have been obtained in the past, but only for specific values of n. For example, Herman and Schuler[98] found a solution for $n = 1$ that may be written as

$$r_{vv'}^{(1)} = \frac{r_e}{L}\,\delta_{vv'} - \frac{N_{vv'}}{aL}\,\frac{\Gamma(k' - v)\Gamma(k' - v)}{v!(v' - v)(k' - v - v' - 1)}\sqrt{\frac{\Gamma(k' - v')}{\Gamma(k' - v)}} \qquad \text{(C9)}$$

where $v' \geq v$. Heaps and Herzberg[99] extended the solution to $n = 2$ and indicated a procedure for obtaining solutions with larger n. However, the formulation for $n = 2$ is extensive and the implied formulation for larger n appears impractical for the required calculation of numerous n terms. Generalization of the solutions for arbitrary n also appears impractical. Hence, further considerations of exact analytic solutions to equation (C8) were abandoned. The iterative numerical procedure of Cashion[100] was also rejected for similar reasons. Instead, we seek an approximate analytic solution based on the observation that the integrand in equation (C8) is a

localized function, confined to a narrow range of z when λ is large. Since the value of λ is dominated by the parameter k' and anharmonicity is a second-order feature of all diatomic molecules, k' is always large compared to unity. Hence an approximation based on $\lambda >> 1$ will be generally applicable.

The generality of the approximation to be made is demonstrated in another sense by writing the integral in equation (C8) in the generalized form:

$$I(\alpha) = \int_0^\infty e^{-z} z^\alpha u(z)\, dz \tag{C10}$$

where $u(z)$ is an arbitrary function. The integration of equation (C10) by parts proceeds according to

$$\begin{aligned} I(\alpha) &= \int_0^\infty u(z) \frac{d\upsilon(z)}{dz}\, dz \\ &= u(z)\upsilon(z)\Big|_0^\infty - \int_0^\infty \frac{d\upsilon(z)}{dz} u(z)\, dz \end{aligned} \tag{C11}$$

where

$$\upsilon(z) = \int e^{-z} z^\alpha\, dz \tag{C12}$$

and the integral in equation (C12) is indefinite. To evaluate equation (C12), repetitive integration by parts leads to the series solution

$$\upsilon(z) = -e^{-z} z^\alpha \left[1 + \frac{\alpha}{z} + \frac{\alpha(\alpha - 1)}{z^2} + \ldots\right] \tag{C13}$$

which may be recognized as the asymptotic expansion for the incomplete gamma function[73]:

$$\upsilon(z) = -\bar{\Gamma}(\alpha + 1, z) \tag{C14}$$

Equation (C14) is an exact relation, but it does not simplify the solution of equation (C11). We now seek an approximation to $\upsilon(z)$ that is integrable in equation (C11). The nature of the approximation is indicated in figure C.1. Note in figure C.1(a) that the derivative

$$\frac{d\upsilon(z)}{dz} = e^{-z} z^{\alpha}$$

is very localized for large α. It has maximum at $z = \alpha$ and a half-width at a half-height of $\Delta z/z = \sqrt{2\ \ln 2/\alpha}$. Thus, the range of the integrand in equation (C11) becomes narrower as α increases. Noting these features of $d\upsilon(z)/dz$ and the fact that $\upsilon(\infty) = 0$ from equation (C14), the function $\upsilon(z)$ approaches a step function as sketched in figure C.1(b). Thus, we can approximate $\upsilon(z)$ by introducing the Heaviside step function:

$$H(y) = \begin{cases} 0 \text{ for } y < 0 \\ \\ 1 \text{ for } y > 0 \end{cases} \qquad \text{(C15)}$$

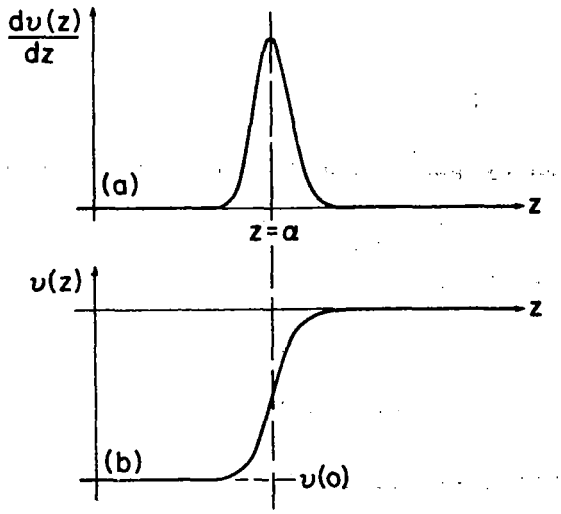

Figure C.1.- Properties of $\upsilon(z)$ and its derivative $d\upsilon(z)/dz = z^{\alpha}e^{-z}$.

and writing

$$\upsilon(z) \approx -\upsilon(0)H(\alpha - z) \tag{C16}$$

where

$$\begin{aligned}\upsilon(0) &= -\bar{\Gamma}(\alpha + 1,0) \\ &= -\Gamma(\alpha + 1)\end{aligned}$$

from the definition of the gamma function.[73] Hence, we have, for $\alpha >> 1$,

$$\upsilon(z) = -\Gamma(\alpha + 1)H(\alpha - z) \tag{C17}$$

Substituting equation (C17) into the expression for $I(\alpha)$ by equation (C11) and invoking the step-function properties then leads to

$$I(\alpha) = -\Gamma(\alpha + 1)\left[-u(0) - \int_0^{\alpha} \frac{du(z)}{dz}\, dz\right]$$

or, finally,

$$I(\alpha) = -\Gamma(\alpha + 1)u(\alpha) \tag{C18}$$

Equation (C18) is a generalized approximate solution of equation (C10) for arbitrary $u(z)$ with only the stipulation that $\alpha >> 1$. It may be applied to the solution of equation (C8) for $\lambda >> 1$ with the result:

$$r_{vv'}^{(n)} \approx \left(\frac{r_e}{L}\right)^n \delta_{vv'} + \frac{N_{vv'}}{(aL)^n} \sum_{s=0}^{v+v'} D_s \Gamma(\lambda + s + 1)\left[\ln\left(\frac{k'}{\lambda + s}\right)\right]^n \tag{C19}$$

From the definition of λ given by equation (C6), we see that the requirement, $\lambda >> 1$, is met when

$$k' - (v + v') >> 3 \tag{C20}$$

Since k' is always much larger than 3, the accuracy of equation (C19) will depend primarily on the sum $v+v'$ and will decrease as the sum increases. Correspondingly, the accuracy of equation (C19) is nearly independent of n

since its derivation was done for an arbitrary function $u(z)$, in this case, equated to $[\ln(k'/z)]^n$. Thus, we can use the exact solution for $n = 1$ given by equation (C9) to evaluate the accuracy of equation (C19).

An instructive first step in assessing the accuracy of equation (C19) is to examine its variation with k'. We do so most easily by choosing the simplest and most frequently applied case of $v' = 1$ and $v = 0$. The exact solution for $n = 1$ is then

$$r_{01}^{(1)}[\text{exact}] = \frac{-\sqrt{k' - 3}}{aL} \frac{1}{k' - 2}$$

while equation (C19) gives

$$r_{01}^{(1)}[\text{approximate}] = \frac{-\sqrt{k' - 3}}{aL} \ln\left(\frac{k' - 2}{k' - 3}\right)$$

The relative error is simply

$$\text{Error} = (k' - 2)\ln\left(\frac{k' - 2}{k' - 3}\right) - 1 \qquad \text{(C21)}$$

Sample error values are tabulated below for some diatomic molecules covering a broad range of k'.

Species	k'	$aLr_{01}^{(1)}$[exact]	Error
H_2	37.25	-0.1660	0.0144
CO	161.22	-.0790	.0032
N_2	163.23	-.0785	.0031
Br_2	302.05	-.0576	.0017

Comparisons for H_2 (the worst case) at higher v and v' (smaller λ) are shown in figure C.2. As the figure shows, equation (C19) is acceptably accurate for single-quantum transitions (i.e., $v'-v = \pm 1$) in H_2 for all

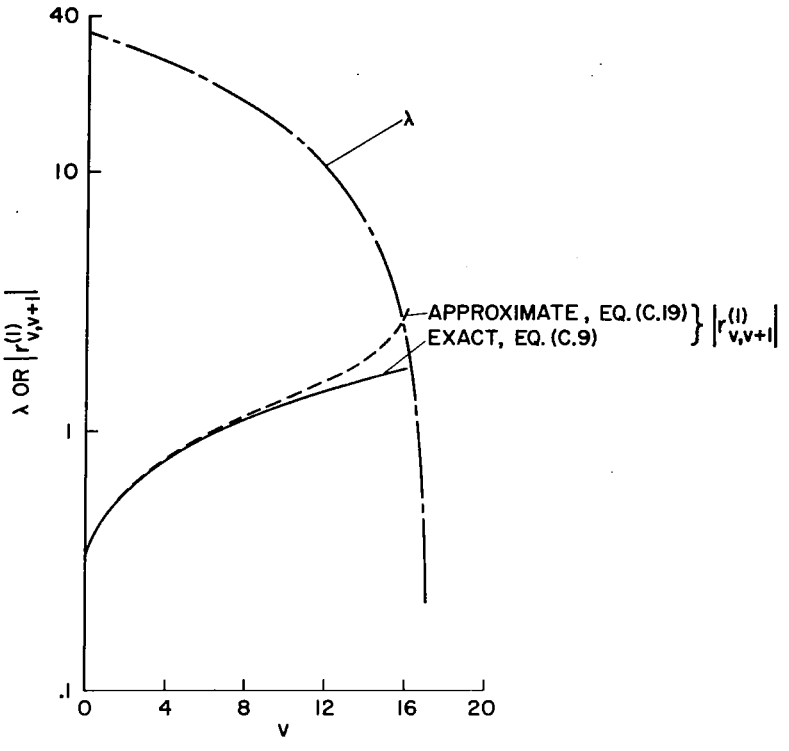

Figure C.2.- Radial integrals and their approximation for H_2; $k' = 37.25$, $aL = 0.509$.

initial eigenenergies at least up to half the dissociation energy of H_2 implied by the Morse potential. For other molecules with larger k', a much larger fraction of the total number of vibrational states will be treated accurately by equation (C19).

The final consequences of using equation (C19) to approximate $r^{(n)}_{vv'}$ are shown in figure C.3 where, again using H_2 as the worst example, we compare the radial matrix element $R^{(J)}_{vv'}$, computed using equation (C19), with numerically exact values obtained from a Gauss-Laguerre quadrature solution[101-103] of equation (6.19). This comparison then encompasses values of $r^{(n)}_{vv'}$ for a wide range of n. Recall that small J values correspond to small changes in angular momentum since $|\ell'-\ell| < J < \ell + \ell$; we showed in chapter 6 that small $|\ell'-\ell|$ contribute most to the energy-transfer process. As figure C.3

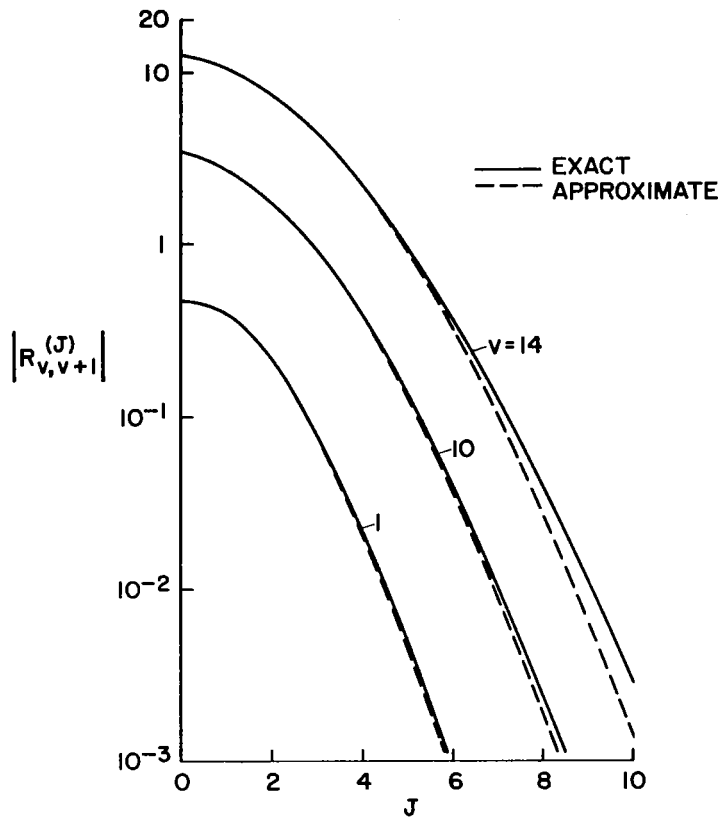

Figure C.3.- Exact and approximate radial matrix elements for H_2; $k' = 37.25$, $aL = 0.509$.

illustrates, equation (C19) is exceptionally accurate for small J where $R^{(J)}_{vv'}$ is the largest and most effective. Furthermore, the accuracy is not strongly degraded even for large v where $r^{(n)}_{vv'}$ is poorly approximated.

Finally, in applying equation (C19) in a numerical calculation with large k' and increasing $v+v'$, we find that the practical limit to its use is not due to the error of the approximation but rather to the loss of numerical precision. More specifically, when k' is large, as for CO or N_2, the approximation is basically very accurate to $v+v' < 150$, thus including single-quantum transitions from initial states to $v = 75$. However, the terms in the summation of equation (C19) alternate in sign and the numerical range

between the largest term and the final value of the sum can exceed the largest number (with all digits significant) possible in most computers (i.e., as $v+v'$ increases, we require decreasing differences between increasing numbers). For example, using a CDC-7600 computer with 28 digits in double precision, meaningful values of $r^{(n)}_{v,v+1}$ from equation (C19) for CO ($k' = 161.22$) were obtained only up to $v < 12$ before all significant digits were lost. The numerical quadrature solutions were developed to obtain matrix elements for larger v. However, the orthogonality properties of $r^{(n)}_{vv'}$ are retained in the approximation and they may be used to at least monitor the numerical precision when using equation (C19). To do so, one simply calculates

$$r^{(0)}_{vv'} = \delta_{vv'}$$

or the equivalent surviving terms,

$$\sum_{s=0}^{v+v'} D_s \Gamma(\lambda + s + 1) = 0 \qquad \text{(C22)}$$

concurrently with $r^{(n)}_{vv'}$. The precision with which equation (C22) is satisfied is then a measure of the precision obtained with equation (C19).

APPENDIX D

SPHERICAL MATRIX ELEMENT INTEGRAL

A general definition of the spherical matrix elements is given by equation (6.15) as

$$T^{(J)}_{\ell'm'\ell m} = \langle \ell'm' | P_J(\cos\,\delta) | \ell m \rangle \tag{6.15}$$

where δ is defined by figure 6.1 and P_J is a Legendre spherical polynomial of order J. In section 6.1.2.2, the spherical harmonic wave functions of a rigid rotor are then introduced and the matrix elements take the specific integral form give by equation (6.21) as

$$T^{(J)}_{\ell'm'\ell m} = \sqrt{\frac{4\pi}{2J+1}} \int_0^{2\pi} \int_0^{\pi} Y^*_{\ell'm'}(\theta,\phi)\; Y_{J,0}(\delta,0)\; Y_{\ell m}(\theta,\phi) \sin\,\theta\; d\theta\; d\phi \tag{6.21}$$

where angles θ and ϕ are polar angles (also defined in fig. 6.1). The purpose of this appendix is to derive an analytic solution of equation (6.21) using the properties of spherical harmonic functions commonly applied in angular momentum theories.[104,105]

We begin by noting that equation (6.21) is similar to the integral of three spherical harmonics for which the solution is known to be (Edmonds,[104] p. 63):

$$\sqrt{4\pi} \int_0^{2\pi} \int_0^{\pi} Y_{\ell_1 m_1}(\theta,\phi)\; Y_{\ell_2 m_2}(\theta,\phi)\; Y_{\ell_3 m_3}(\theta,\phi) \sin\,\theta\; d\theta\; d\phi$$

$$= \sqrt{(2\ell_1+1)(2\ell_2+1)(2\ell_3+1)} \begin{pmatrix} \ell_1 & \ell_2 & \ell_3 \\ 0 & 0 & 0 \end{pmatrix} \begin{pmatrix} \ell_1 & \ell_2 & \ell_3 \\ m_1 & m_2 & m_3 \end{pmatrix} \tag{D1}$$

The bracket symbols are Wigner 3-j symbols. Equation (6.21) may be made to correspond to equation (D1) by converting $Y^*_{\ell',m'}(\theta,\phi)$ to its complex conjugate using the spherical harmonic property (Rose,[105] p. 241):

$$Y^*_{\ell' m'} = (-1)^{m'} Y_{\ell', -m'} \tag{D2}$$

and by equating $Y_{J,0}(\delta,0)$ to a new spherical harmonic in terms of θ and ϕ. To accomplish the latter, we recall the addition theorem (Rose,[105] p. 60):

$$Y_{J,0}(\delta,0) = \sqrt{\frac{4\pi}{2J+1}} \sum_{\bar{m}} Y^*_{J\bar{m}}(\theta_1,\phi_1)\, Y_{J\bar{m}}(\theta_2,\phi_2) \tag{D3}$$

where the angles in equation (D3) are related by

$$\cos\delta = \cos\theta_1 \cos\theta_2 + \sin\theta_1 \sin\theta_2 \cos(\phi_1 - \phi_2) \tag{D4}$$

However, from figure 6.1, δ is related to the polar angles in equation (6.21) by

$$\cos\delta = \sin\theta \cos(\bar{\Omega} - \phi) \tag{D5}$$

so that, by assigning

$$\theta_1 = \pi/2 \ , \ \phi_1 = \bar{\Omega}$$

$$\theta_2 = \theta \quad , \ \phi_2 = \phi$$

the addition theorem may be written

$$Y_{J,0}(\delta,0) = \sqrt{\frac{4\pi}{2J+1}} \sum_{\bar{m}} Y^*_{J\bar{m}}\left(\frac{\pi}{2},\bar{\Omega}\right) Y_{J\bar{m}}(\theta,\phi) \tag{D6}$$

With the aid of equations (D2) and (D5), the integral in equation (6.21) may now be correlated with equation (D1), giving the solution, by inspection, as

$$T^{(J)}_{\ell' m' \ell m} = (-1)^{m'} \sqrt{\frac{4\pi}{2J+1}(2\ell'+1)(2\ell+1)} \begin{pmatrix} \ell' & J & \ell \\ 0 & 0 & 0 \end{pmatrix} \sum_{\bar{m}} Y^*_{J\bar{m}}\left(\frac{\pi}{2},\bar{\Omega}\right) \begin{pmatrix} \ell' & J & \ell \\ -m' & \bar{m} & m \end{pmatrix} \tag{D7}$$

Equation (D7) is further simplified by noting that the 3-j symbol coupling the projection states $m', \bar{m}$ and m is nonzero only if

$$\bar{m} = m' - m \tag{D8}$$

Hence the summation over $\bar{m}$ reduces to a single term and the matrix element becomes

$$T^{(J)}_{\ell' m' \ell m} = (-1)^{m'} \sqrt{\frac{4\pi}{2J+1}\,(2\ell'+1)(2\ell+1)}\; Y^{*}_{J,m'-m}\left(\frac{\pi}{2},\bar{\Omega}\right) \begin{pmatrix} \ell' & J & \ell \\ 0 & 0 & 0 \end{pmatrix} \begin{pmatrix} \ell' & J & \ell \\ -m' & m'-m & m \end{pmatrix} \tag{D9}$$

Equation (D9) is the desired analytic matrix element expression, but it is in a symbolic notation that requires further reduction to obtain an algebraic equation suitable for calculation. An algebraic form will also allow the classical time-dependent terms introduced by $\bar{\Omega}(t)$ to be isolated.

To achieve an algebraic formula, we first evaluate the function $Y^{*}_{J\bar{m}}(\pi/2,\bar{\Omega})$. A comparison of the Rodrigues formula for an associated Legendre polynomial, $P^{m}_{\ell}(x)$, with the definition of $Y_{\ell m}(\alpha,\beta)$, shows that the two are related by (Edmonds,[104] p. 24)

$$Y_{\ell m}(\alpha,\beta) = (-1)^{m}\left[\frac{2\ell+1}{4\pi}\,\frac{(\ell-m)!}{(\ell+m)!}\right]^{1/2} P^{m}_{\ell}(\cos\alpha)\; e^{im\beta} \tag{D10}$$

Thus, we have

$$Y^{*}_{J\bar{m}}\left(\frac{\pi}{2},\bar{\Omega}\right) = (-1)^{\bar{m}}\left[\frac{2J+1}{4\pi}\,\frac{(J-\bar{m})!}{(J+\bar{m})!}\right]^{1/2} P^{\bar{m}}_{J}(0)\; e^{-i\bar{m}\bar{\Omega}(t)} \tag{D11}$$

where (from Abramowitz and Stegun,[73] p. 334)

$$P^{\bar{m}}_{J}(0) = \frac{2^{\bar{m}}}{\sqrt{\pi}} \cos\left[\frac{\pi}{2}(J-\bar{m})\right] \frac{\Gamma\left(\frac{J+\bar{m}+1}{2}\right)}{\Gamma\left(\frac{J-\bar{m}}{2}+1\right)} \tag{D12}$$

Equation (D12) may be reduced to simpler algebraic terms by noting that since J and $\bar{m}$ are integers, the cosine term has the property:

$$\cos\left[\frac{\pi}{2}(J - \bar{m})\right] = \begin{cases} (-1)^{\frac{J-\bar{m}}{2}} & \text{for } J \pm \bar{m} \text{ even} \\ 0 & \text{for } J \pm \bar{m} \text{ odd} \end{cases} \tag{D13}$$

Hence, nonzero matrix elements are obtained only for values of $J \pm \bar{m}$ even. With that stipulation, the gamma functions in equation (D12) are also reducible as follows: Define a parameter z so that

$$\Gamma\left(\frac{J + \bar{m} + 1}{2}\right) = \Gamma(z + 1/2)$$

Then $z = (J + m)/2$ is always an integer because $J + \bar{m}$ is an even integer. With integer z, the duplication formula for gamma functions gives[73]

$$\Gamma(z + 1/2) = \frac{\sqrt{\pi}}{2^{2z}} \frac{(2z)!}{z!}$$

or

$$\Gamma\left(\frac{J + \bar{m} + 1}{2}\right) = \frac{\sqrt{\pi}}{2^{J+\bar{m}}} \frac{(J + \bar{m})!}{\left(\frac{J + \bar{m}}{2}\right)!} \tag{D14}$$

Furthermore, for $J \pm \bar{m}$ even, the other gamma function in equation (D12) becomes

$$\Gamma\left(\frac{J - \bar{m}}{2} + 1\right) = \left(\frac{J - \bar{m}}{2}\right)!$$

so that

$$\frac{\Gamma\left(\frac{J + \bar{m} + 1}{2}\right)}{\Gamma\left(\frac{J - \bar{m}}{2} + 1\right)} = \frac{\sqrt{\pi}}{2^{J+\bar{m}}} \frac{(J + \bar{m})!}{\left(\frac{J + \bar{m}}{2}\right)!\left(\frac{J - \bar{m}}{2}\right)!} \tag{D15}$$

Hence, nonzero values of $Y^*_{J\bar{m}}(\pi/2, \bar{\Omega})$ are given for $J \pm m$ even by

$$Y^*_{J\bar{m}}\left(\frac{\pi}{2}, \bar{\Omega}\right) = (-1)^{\frac{J+\bar{m}}{2}} \sqrt{\frac{2J + 1}{4\pi}} \frac{\sqrt{(J + \bar{m})!(J - \bar{m})!}}{2^J \left(\frac{J + \bar{m}}{2}\right)!\left(\frac{J - \bar{m}}{2}\right)!} e^{-i\bar{m}\bar{\Omega}(t)} \tag{D16}$$

With equation (D16), the time-dependent terms are easily isolated in the matrix element formula by defining a new matrix with constant elements given by

$$\mathcal{M}^{(J)}_{\ell'm'\ell m} = (-1)^{\frac{J+\bar{m}}{2}} \frac{\sqrt{(J+\bar{m})!(J-\bar{m})!}}{2^J\left(\frac{J+\bar{m}}{2}\right)!\left(\frac{J-\bar{m}}{2}\right)!} \sqrt{(2\ell'+1)(2\ell+1)} \begin{pmatrix} \ell' & J & \ell \\ 0 & 0 & 0 \end{pmatrix} \begin{pmatrix} \ell' & J & \ell \\ -m' & \bar{m} & m \end{pmatrix} \tag{D17}$$

Again, the stipulations on $\mathcal{M}^{(J)}_{\ell'm'\ell m}$ are that $J \pm \bar{m}$ is even and $\bar{m} = m' - m$.

Equation (D9) may then be written

$$T^{(J)}_{\ell'm'\ell m} = \mathcal{M}^{(J)}_{\ell'm'\ell m} e^{-i(m'-m)\bar{\Omega}(t)} \tag{D18}$$

thus obtaining the results given by equations (6.22) and (6.23).

Equation (D17) has been maintained in terms of the symbolic 3-j coefficients to simplify the notation, but they may be evaluated by the well-known formulas to follow[104,105]:

The coefficient $\begin{pmatrix} \ell' & J & \ell \\ 0 & 0 & 0 \end{pmatrix}$ is nonzero only for $L \equiv \ell' + J + \ell$ even. With that stipulation,

$$\begin{pmatrix} \ell' & J & \ell \\ 0 & 0 & 0 \end{pmatrix} = (-1)^{L/2}\left[\frac{(L-2\ell')!(L-2J)!(L-2\ell)!}{(L+1)!}\right]^{1/2} \times \frac{(L/2)!}{(L/2-\ell')!(L/2-J)!(L/2-\ell)!} \tag{D19}$$

For even values of $\ell' + J + \ell$, we can also equate

$$\begin{pmatrix} \ell' & J & \ell \\ -m' & \bar{m} & m \end{pmatrix} = (-1)^{\ell-J+m'}(2\ell'+1)^{-1/2} C(\ell J \ell' : m\ \bar{m}\ m')$$

where $C(\ell J \ell' : m\ \bar{m}\ m')$ is a Clebsch-Gordan coefficient defined by Rose,[105] (p. 39), with a convenient algebraic expression. The result then leads to

$$\begin{pmatrix} \ell' & J & \ell \\ -m' & \bar{m} & m \end{pmatrix} = (-1)^{\ell-m} \left[\frac{(\ell' + \ell - J)!(\ell' - \ell + J)!(\ell + J - \ell')!(\ell' + m')!(\ell' - m')!}{(\ell + J + \ell' + 1)!(\ell + m)!(\ell - m)!(J + \bar{m})!(J - \bar{m})!} \right]^{1/2} \delta_{\bar{m},m'-m} \times$$

$$\sum_{\nu} \frac{(-1)^{\nu}(J + \ell' + m - \nu)!(\ell - m + \nu)!}{\nu!(\ell' - \ell + J - \nu)!(\ell' + m' - \nu)!(\nu + \ell - J - m')!} \qquad \text{(D20)}$$

where ν ranges over all integer values giving nonnegative factorial arguments. Since the *indice* constraints giving nonzero values of the vector-coupling coefficients (3-j symbols) are

$$\left.\begin{aligned} |m'| \le \ell \ , \ |\bar{m}| \le J \ , \ |m| \le \ell \\ |\ell' - \ell| \le J \le \ell' + \ell \\ \bar{m} = m' - m \end{aligned}\right\} \qquad \text{(D21)}$$

the summation limits in equation (D20) are those that define the narrowest range of ν within

$$\text{Minimum } \nu \ge 0 \ , \ J - \ell + m'$$

$$\text{Maximum } \nu \le J + \ell' + \ell \ , \ \ell' + m'$$

Equations (D17) to (D20) are sufficient to calculate $T^{(J)}_{\ell'm'\ell m}$ for all J,ℓ',m',ℓ,m combinations satisfying equation (D21) and

$$\ell' + J + \ell \quad \text{even}$$

$$J \pm \bar{m} \quad \text{even}$$

All other matrix elements are zero.

APPENDIX E

ANALYTIC TRAJECTORY EQUATIONS FOR NONZERO IMPACT PARAMETER

We have defined a trajectory function in chapter 6 by equation (6.33) as

$$U(b,t) = \frac{\bar{E}}{V_{ii}} \left[1 - \left(\frac{b}{\bar{x}_o}\right)^2\right] e^{-(\bar{x}-\bar{x}_o)/L} \tag{6.33}$$

where the constants are specified by the spherically averaged interaction potential

$$\bar{V} = A\, e^{-\bar{x}/L}\, V_{ii} \tag{E1}$$

Then, to solve the set of coupled dynamical equations describing the collision, $U(b,t)$ must be determined explicitly in terms of time t. One approach would be to numerically integrate the classical trajectory equation given in appendix B as

$$\left(\frac{\partial \bar{x}}{\partial t}\right)^2 = \bar{u}^2\left[1 - \frac{\bar{V}}{\bar{E}} - \left(\frac{b}{\bar{x}}\right)^2\right] \tag{E2}$$

but, as we point out in chapter 6, there are considerable advantages provided by an approximate analytic description of $U(b,t)$ that benefit both the remaining numerical analysis and future analytic descriptions of the collision dynamics. In this appendix, we therefore develop an analytic form of $U(b,t)$ by following the work of Hansen and Pearson.[106]

An indication of the functional form of $U(b,t)$ is obtained by noting that equation (E2), with the potential given by equation (E1), may be solved exactly for $b = 0$. The result is

$$\left[e^{-(\bar{x}-\bar{x}_o)/L}\right]_{b=0} = \operatorname{sech}^2\left(\frac{\bar{u}t}{2L}\right) \tag{E3}$$

where $\bar{x}_o$ denotes the distance of closest approach. Furthermore, at closest approach for $b = 0$, all the initial kinetic energy is converted to potential energy so that $\bar{V} = \bar{E}$, leading to

$$\left(\frac{\bar{x}_o}{L}\right)_{b=0} = \ln\left(\frac{AV_{ii}}{\bar{E}}\right) \tag{E4}$$

In view of equation (E3), the primary nature of solutions to equation (E2) for nonzero impact parameters should be represented by

$$\exp\left\{-[\bar{x}(b,t) - \bar{x}_o(b)]/L\right\} = \operatorname{sech}^2\left[a_b(b,t)\,\frac{\bar{u}t}{2L}\right] \tag{E5}$$

where $a_b(b,t)$ is a slowly varying function of both b and t that can be approximated by a low-order expansion.

By solving equation (E2) numerically, we can obtain the exact values of $a_b(b,t)$ required to satisfy equation (E5). Some sample results are tabulated below for a representative collision energy and for small- and large-impact parameters.

TABLE E1.- EXACT VALUES OF $a_b(b,t)$ FOR $\bar{E}/V_{ii} = 10^{-4}$

b/L	$\bar{u}t/L$	$\bar{V}/\bar{E}$	$a_b(b,t)$
1.2	0	0.99	0.994
	6	.01	.995
8	0	.38	.70
	6	.015	.74
16	0	.0010	.35
	6	.0004	.38

Note that when the change in $a_b(b,t)$ with t becomes noticeable, the interaction potential is extremely small. We can therefore approximate $a_b(b,t)$ without introducing significant error in the collision dynamics by assuming $a_b(b,t) \approx a_b(b,0)$. Then, expanding both sides of equation (E5) about $t = 0$, we obtain, to first order,

$$1 - [\bar{x}(b,t) - \bar{x}_o(b)]/L = 1 - (a_b\bar{u}t/2L)^2 \tag{E6}$$

Similarly,

$$\bar{x}(b,t) = \bar{x}_o(b) + t\left(\frac{\partial \bar{x}}{\partial t}\right)_{t=0} + \frac{t^2}{2}\left(\frac{\partial^2 \bar{x}}{\partial t^2}\right)_{t=0} \tag{E7}$$

From equation (E2),

$$\left(\frac{\partial \bar{x}}{\partial t}\right)_{t=0} = 0$$

and

$$\left(\frac{\partial^2 \bar{x}}{\partial t^2}\right)_{t=0} = \bar{u}^2\left[\frac{-(\partial \bar{V}/\partial t)_{t=0}}{\bar{E}} + \frac{2b^2}{\bar{x}_o^3}\right]$$

Since $(\partial \bar{V}/\partial t)_{t=0} = -\bar{V}/L$ from equation (E1), equation (E6) finally leads to

$$a_b(b,0) \approx \left\{1 - \left[\frac{b}{\bar{x}_o(b)}\right]^2 [1 - 2L/\bar{x}_o(b)]\right\}^{1/2} \tag{E8}$$

Note that $\bar{x}_o(b)$ must still be computed by iteratively solving equation (E2) for $t = 0$. However, as we show in figure 6.6, $\bar{x}_o(b)$ is closely approximated by equation (E4) when the impact parameter is small. Similarly, when the impact parameter is large, the trajectory path is nearly a straight line and $\bar{x}_o(b) \to b$. In that case, equation (E8) becomes

$$a_b(\infty,0) = \sqrt{2L/b} \tag{E9}$$

All three cases are compared in figure E.1, where we see that a completely

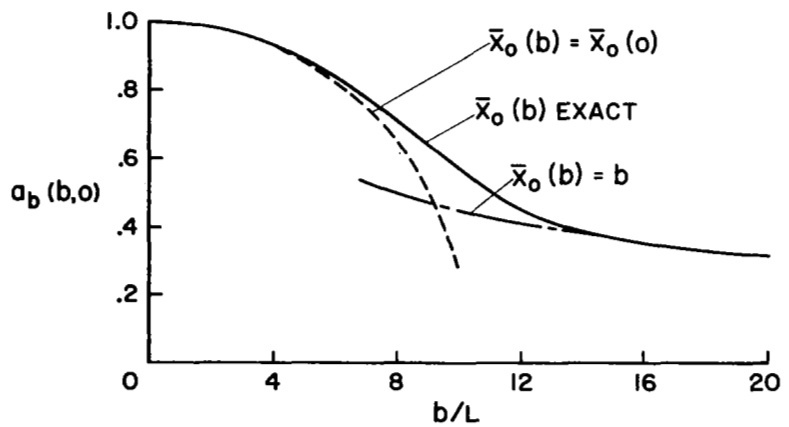

Figure E.1.- Trajectory coefficients for $E/AV_{ii} = 10^{-4}$.

analytical approach would be to compute $\bar{x}_o(b = 0)$ from equation (E4) for increasing b until it gave values of a_b equal to those from equation (E9). Beyond that point, a better approximation is to assume $\bar{x}_o \approx b$. In that case, $U(b,t) \approx 0$ according to equation (6.33) and the interaction may be considered negligibly small.

APPENDIX F

SYMMETRIES OF VIBRATION-ROTATION MATRIX ELEMENTS AND THEIR COMPACT COMPUTER STORAGE

Experience with the collinear collision model made clear the facts that: the basis set required for a three-dimensional vibration-rotation model would be large, it would vary in size with the initial conditions, and it should be minimized for computing economy. A basic criterion of the computational scheme was therefore to permit an arbitrary basis set of vibrational and rotational eigenstates to be specified as part of the input information. Consequently, the calculation requires a large and variable number of time-independent matrix elements, $V_{v'\ell'm'v\ell m}$. Since the matrix elements are constant in time, the obvious procedure was to compute them in advance of the dynamical solution and store them in the computer memory.

When specifying the basis set in problems of this nature, the available size of accessible memory can be as severe a limitation as the computing time required. In large time-sharing systems, the operating cost is affected by both factors, while, in smaller systems, adequate memory volume is often not available. Hence the programmer's task becomes one of minimizing the memory volume that must be allocated to accommodate matrix elements of the largest basis set of interest. Since the allocation must usually be done in advance of any input information, the storage scheme must also be optimized in advance.

Each matrix element is identified by six quantum numbers for which the simplest storage scheme would be a six-dimensional array. However, advance memory allocation for such an array would be extremely wasteful because each

dimension would have to be set to the largest value of interest. For example, suppose we choose the random basis set:

i	v_i	ℓ_i
1	4	3
2	4	1
3	4	0
4	5	2

(F1)

where i is an index identifying the state, and v_i and ℓ_i are the vibrational and angular momentum quantum numbers specifying the state. If v_m, ℓ_m represents the largest values to be considered, then there are $v_m + 1$, $\ell_m + 1$ possible values of v, ℓ and $2\ell_m + 1$ values of m. To accommodate the example, let $v_m, \ell_m = 5,3$. Then the array would be dimensioned $V(v'\ell'm'v\ell m) = V(6,4,7,6,4,7)$, thus allocating 28,224 memory elements, while only 256 are filled by the sample basis set above.

On second thought, a more efficient storage scheme is based on the index i identifying each state and m_i, the projection quantum number. Two small 1-D (one-dimensional) arrays, $v_i(i)$ and $\ell_i(i)$, may be established to give the v,ℓ quantum numbers when needed and the matrix elements are stored in a square 2-D array, $V_{v'\ell'm'v\ell m} = V(j',j)$, where j is computed from

$$j = \sum_{k=1}^{i} (2\ell_k + 1) - \ell_i + m_i \qquad \text{(F2)}$$

Such a matrix element array for the example basis set is illustrated schematically in figure F.1. The array dimensions, allocated in advance, are now required to be only as large as the total number of differential equations that can be solved in a reasonable computing time. Thus, the storage allocation and the computing time limits are kept compatible. As an example, suppose

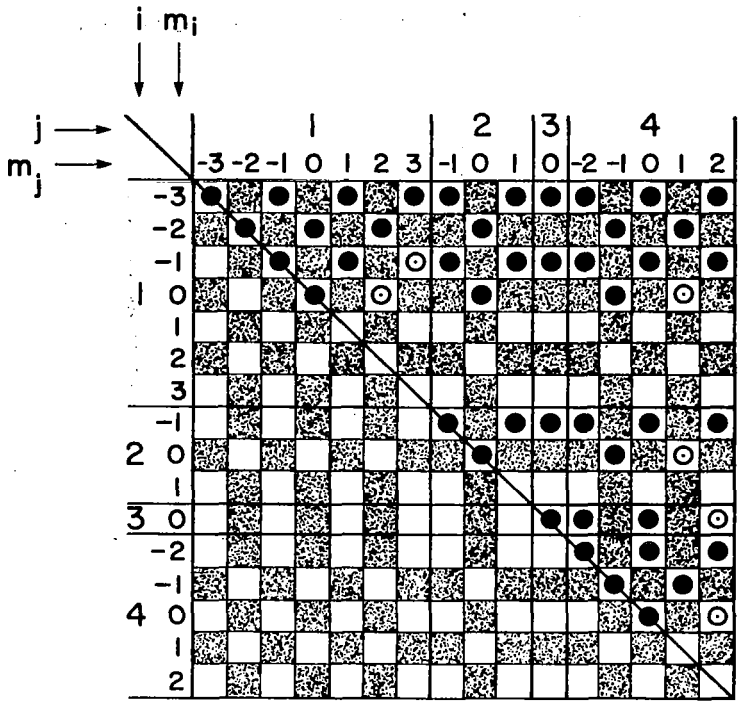

Figure F.1.- A representation of the matrix elements $V_{v'\ell'm'v\ell m}$ corresponding to the sample basis set, equation (F1). Each group, i or j, represents a pair of quantum numbers, v_i and ℓ_i. The matrix element is then identified by relating $V_{v'\ell'm'v\ell m}$ to the array $V(i,m_i,j,m_j)$. The shaded squares are locations containing zeros. The filled circles ● denote primary elements, unrelated by symmetry. The open squares and open circles ○ are elements related to the primary elements by the symmetry equations (F9) and F11). The open circles are additional elements included in the index equation, equation (F17), and stored with the primary elements in memory.

that the maximum computing time limits the total number of states to 16. That limit would then encompass the example basis set and require a matrix element array with 256 elements.

While the preceding storage scheme is a notable improvement, it is still extremely wasteful. Closer examination of the sample matrix element array in figure F.1 reveals that, as a result of the constraints on rotational state coupling given by equations (6.24) and (6.25), almost half of the elements are zeros. In addition, approximately three quarters of the nonzero values are

numbers with opposing signs but duplicate magnitudes, as a consequence of the symmetries of $V_{v'\ell'm'v\ell m}$. Hence, there is an obvious opportunity to further reduce the storage requirements by storing only the elements of unique and nonzero magnitude. Such a scheme requires additional computing of indices to relate an arbitrary set of quantum numbers, $v'\ell'm'v\ell m$, to the storage indice containing the appropriate matrix element. But, for large basis sets, that additional small effort is offset by a reduction in the number of elements that must be computed and by the savings in storage. We may use, as an illustrative example, the largest basis set represented in this study. It was for a heteronuclear molecule (CO) containing two vibrational manifolds with rotational states from $\ell = 0$ to 10 in each one. Thus, 242 states were included and a $V(j',j)$ array of 58,564 elements would have been required. However, by storing only the unique and nonzero matrix elements, the storage requirement was reduced to 14,883 elements. While the storage requirement was still large, the difference decided between possible and impossible storage allocation. The remaining paragraphs of this appendix are therefore devoted to a study of the symmetry properties of $V_{v'\ell'm'v\ell m}$ needed to select the unique elements and a derivation of the index equations for locating the matrix elements in a reduced storage scheme.

F.1 Symmetries of $V_{v'\ell'm'v\ell m}$

The symmetry properties of $V_{v'\ell'm'v\ell m}$ are revealed by the terms defining it. According to equation (6.26),

$$V_{v'\ell'm'v\ell m} = \sum_{J=|\ell'-\ell|}^{\ell'+\ell} (2J+1) R^{(J)}_{vv'} \mathcal{M}^{(J)}_{\ell'm'\ell m} \qquad \text{(F3)}$$

where

$$\mathcal{M}^{(J)}_{\ell'm'\ell m} = (-1)^{(J+\bar{m})/2}\left[\frac{\sqrt{(J+\bar{m})!\,(J-\bar{m})!\,(2\ell'+1)(2\ell+1)}}{2^J\left(\frac{J+\bar{m}}{2}\right)!\left(\frac{J-\bar{m}}{2}\right)!}\right]\begin{pmatrix}\ell' & J & \ell\\ 0 & 0 & 0\end{pmatrix}\begin{pmatrix}\ell' & J & \ell\\ -m' & \bar{m} & m\end{pmatrix} \tag{F4}$$

$$\bar{m} = m' - m \tag{F5}$$

$$R^{(J)}_{vv'} = \langle v'|f(r,J)|v\rangle \tag{F6}$$

and $f(r,J)$ is an algebraic function of r and J given in equation (6.16).

We first note that the vibrational states are freely interchangeable because the vibrational wave functions are purely real and not operated upon by the algebraic function $f(r,J)$. Thus, equation (F6) may be rewritten to give

$$R^{(J)}_{vv'} = \langle v|f(r,J)|v'\rangle = R^{(J)}_{v'v} \tag{F7}$$

for all J.

Next, the summation limits in equation (F3) are seen to be unaffected by an interchange of ℓ and ℓ'. Hence, all the remaining symmetry properties of $V_{v'\ell'm'v\ell m}$ are determined entirely by the rotational coupling term, $\mathcal{M}^{(J)}_{\ell'm'\ell m}$. Furthermore, having generalized the vibrational symmetry, only three possible elementary symmetry operations remain: (1) an exchange symmetry between rotational states to relate $\mathcal{M}^{(J)}_{\ell'm'\ell m}$ and $\mathcal{M}^{(J)}_{\ell m\ell'm'}$, (2) a sign reversal of m only, and (3) simultaneous sign reversals of m and m'. All other operations would correspond to combined applications of the above. In the following, we deal with exchange and sign-reversal symmetries separately.

F.1.1 Exchange Symmetry

The relation of $\mathcal{M}^{(J)}_{\ell'm'\ell m}$ and $\mathcal{M}^{(J)}_{\ell m\ell'm'}$ is easily shown in a general fashion by starting with its definition in symbolic notation. From chapter 6, $\mathcal{M}^{(J)}_{\ell'm'\ell m}$ is equivalent to

$$\mathcal{M}^{(J)}_{\ell'm'\ell m} = \left(Y^*_{\ell'm'} \middle| P_J(\cos\delta) \middle| Y_{\ell m}\right) e^{i(m'-m)\bar{\Omega}} \tag{F8}$$

where the combination of terms containing the time-dependent variables, δ and $\bar{\Omega}$, render the result constant in time. (Note that the bracket notation in eq. (F8) implies the integration over all configuration space.) Again, the operator $P_J(\cos\delta)$ is algebraic and hence not operable on the wave functions. Thus, equation (F8) is unchanged when rewritten as

$$\begin{aligned}\mathcal{M}^{(J)}_{\ell'm'\ell m} &= \left(Y_{\ell m} \middle| P_J(\cos\delta) \middle| Y^*_{\ell'm'}\right) e^{i(m'-m)\bar{\Omega}} \\ &= \left\{\left(Y^*_{\ell m} \middle| P_J(\cos\delta) \middle| Y_{\ell'm'}\right) e^{-i(m'-m)}\right\}^* \\ &= [\mathcal{M}_{\ell m\ell'm'}]^*\end{aligned}$$

But equation (F4) shows that the rotational coupling terms are always real so that $[\mathcal{M}^{(J)}_{\ell m\ell'm'}]^* = \mathcal{M}^{(J)}_{\ell m\ell'm'}$ leading to $\mathcal{M}^{(J)}_{\ell'm'\ell m} = \mathcal{M}^{(J)}_{\ell m\ell'm'}$. Correspondingly,

$$V_{v'\ell'm'v\ell m} = V_{v\ell mv'\ell'm'} \tag{F9}$$

F.1.2 Projection-State Sign-Reversal Symmetry

As indicated previously, sign reversal may be implemented in two ways. The first, a sign reversal of m alone may be immediately dismissed as an unsymmetric operation by noting that it would induce a change in the magnitude of $\bar{m}$ via equation (F5) and thereby lead to different magnitudes for $\mathcal{M}^{(J)}_{\ell'm'\ell m}$ and $\mathcal{M}^{(J)}_{\ell'm'\ell,-m}$. The second case is a simultaneous sign reversal of

both m and m'. Only the sign of $\bar{m}$ is then reversed and equation (F4) leads to

$$\mathcal{M}^{(J)}_{\ell',-m',\ell,-m} \Big/ \mathcal{M}^{(J)}_{\ell' m' \ell m} = (-1)^{-\bar{m}} \begin{pmatrix} \ell' & J & \ell \\ m' & -\bar{m} & -m \end{pmatrix} \Big/ \begin{pmatrix} \ell' & J & \ell \\ -m' & \bar{m} & m \end{pmatrix} \qquad \text{(F10)}$$

The corresponding 3-j symbol symmetry is given by Edmonds[104] (p.47) as

$$\begin{pmatrix} \ell_1 & \ell_2 & \ell_3 \\ m_1 & m_2 & m_3 \end{pmatrix} = (-1)^{\ell_1+\ell_2+\ell_3} \begin{pmatrix} \ell_1 & \ell_2 & \ell_3 \\ -m_1 & -m_2 & -m_3 \end{pmatrix}$$

but $\ell' + J + \ell$ (i.e., $\ell_1 + \ell_2 + \ell_3$ in the above equation) must be even to obtain nonzero values of $\begin{pmatrix} \ell' & J & \ell \\ 0 & 0 & 0 \end{pmatrix}$ in equation (F4). Thus, the ratio of 3-j symbols in equation (F10) is always unity and we are led to the final result:

$$V_{v'\ell'm'v\ell m} = (-1)^{m-m'} V_{v',\ell',-m',v,\ell,-m} \qquad \text{(F11)}$$

With the symmetries given by equations (F9) and (F11), one choice of primary matrix elements is illustrated in figure F.1 by the filled circles. In the notation of figure F.1, $V(i,m_i:j,\pm m_j)$ are included for each i and all m_i from $-\ell_i$ to zero. All j and $\pm m_j$ are included that fall to the right of the diagonal, with the exception of those related to preceding m_j in the same row by symmetry. All other matrix elements (indicated by open spaces and open circles in fig. F.1) are then obtained by the symmetry relations, equations (F9) and (F11).

F.2 Primary Matrix Element Storage

The remaining task is now to devise a scheme of indexing the primary matrix elements so that they may be stored and retrieved using the identifier set (i, m_i, j, m_j). The method chosen here is to index them sequentially from left to right in figure F.1, starting with the top row and continuing, row by

row, toward the bottom. The primary elements may then be stored in a minimum memory volume by computing the index $P(i,m_i,j,m_j)$ and locating them in a 1-D array, V(P). Similarly, the matrix elements are retrieved during the dynamical solution by again computing $P(i,m_j,j,m_j)$ and applying the symmetry equations (F9) and (F11) when necessary. Hence, we need only define $P(i,m_i,j,m_j)$ explicitly in terms of the identifiers to complete the storage scheme.

Before developing the index equation, we first note that the formulation will be somewhat simplified if we slightly relax the requirement that *all* matrix elements related by symmetry be excluded from the primary set. Very little redundancy is introduced by reinstating the few excluded matrix elements to the right of the diagonal in figure F.1 in rows where $-\ell_i \le m_i \le 0$. Such elements are indicated in figure F.1 by open circles. With those elements included, we compute $P(i,m_i,j,m_j)$ by first defining the following component terms:

An operator is required to be identified with each (i,m_i) row and with the properties

$$\delta_{i,m_i} = \begin{cases} 1 \text{ for } & \ell_i + m_i \quad \text{even} \\ 0 \text{ for } & \ell_i + m_i \quad \text{odd} \end{cases}$$

Then the total number of primary and symmetric nonzero elements in row (i,m_i) is

$$\sum_{j=1}^{I} (\ell_j + \delta_{i,m_i})$$

where I is the total number of (v_i,ℓ_i) states in the basis set. Similarly, the number of nonzero symmetric elements to the left of the diagonal in row (i,m_i) is

$$\sum_{j=1}^{i-1} (\ell_j + \delta_{i,m_i}) + (\ell_i + m_i + \delta_{i,m_i} - 1)/2 \qquad \text{(F12)}$$

so that the total number of *primary* elements in row (i,m_i) is

$$N(i,m_i) = \sum_{j=i}^{I} (\ell_j + \delta_{i,m_i}) - (\ell_i + m_i + \delta_{i,m_i} - 1)/2 \qquad \text{(F13)}$$

The number of rows preceding row (i,m_i) is

$$n(i,m_i) = \sum_{k=1}^{i} (2\ell_i + 1) + m_i - \ell_i - 1 \qquad \text{(F14)}$$

so that the total number of primary elements in rows preceding row (i,m_i) is then

$$\sum_{r=1}^{n(i,m_i)} N(r,m_r) \qquad \text{(F15)}$$

Now choosing a specific element in row (i,m_i), the number of nonzero primary and symmetric elements preceding $V(i,m_i,j,m_j)$ is

$$\sum_{k=1}^{j-1} (\ell_k + \delta_{i,m_i}) + (\ell_j + m_j + \delta_{i,m_i} - 1)/2$$

while those symmetric elements to the left of the diagonal are again given by equation (F12) but rewritten as

$$\sum_{k=1}^{i-1} (\ell_i + \delta_{i,m_i}) + (\ell_i + m_i + \delta_{i,m_i} - 1)/2$$

The difference in the two terms above is then the number of primary elements preceding $V(i,m_i,j,m_j)$ in row (i,m_i), given by

$$\sum_{k=i}^{j-1} (\ell_k + \delta_{i,m_i}) + (\ell_j - \ell_i + m_j - m_i)/2 \qquad \text{(F16)}$$

The index of $V(i,m_i,j,m_j)$ is now a combination of terms (F15) and (F16) with the result

$$P(i,m_i,j,m_j) = 1 + (\ell_j - \ell_i + m_j - m_i)/2 + \sum_{k=i}^{j-1} (\ell_k + \delta_{i,m}) + \sum_{r=1}^{n(i,m_i)} N(r,m_r) \qquad \text{(F17)}$$

Equation (F17) requires that $j \geq i$. The identifiers may be exchanged to read $P(j,m_j,i,m_i)$ if $i \geq j$. Note that the summations in equation (F17) may also be reduced to more efficient forms for computer calculation.

REFERENCES

1. H. Kallmann and F. London, Zeit. Physik. Chem. B2, 207 (1929).
2. O. K. Rice, Phys. Rev. 38, 1943 (1931).
3. C. Zener, Phys. Rev. 38, 277 (1931); Proc. Cambridge Phil. Soc. 29, 136 (1933).
4. L. Landau and E. Teller, Physik. Z. Sowjetunion 10, 34 (1936).
5. K. F. Herzfeld and F. O. Rice, Phys. Rev. 31, 691 (1928).
6. K. F. Herzfeld and T. A. Litovitz, *Absorption and Dispersion of Ultrasonic Waves*, Academic Press (1959).
7. H. A. Bethe and E. Teller, "Deviations from Thermal Equilibrium in Shock Waves," Aberdeen Proving Ground, Ballistic Res. Lab. Rept. X-117 (1945).
8. W. G. Vincenti and C. H. Kruger, Jr., *Introduction to Physical Gas Dynamics*, J. Wiley and Sons (1965).
9. E. W. Montroll and K. E. Shuler, J. Chem. Phys. 26, 454 (1957).
10. C. E. Treanor, J. W. Rich, and R. G. Rehm, J. Chem. Phys. 48, 1798 (1968).
11. R. E. Center and C. E. Caledonia, Appl. Optics 10, 1795 (1971).
12. J. W. Rich, J. Appl. Phys. 42, 2719 (1971).
13. R. L. McKenzie, Phys. Fluids 15, 2163 (1972).
14. R. J. Hall and A. C. Eckbreth, IEEE J. Quant. Elect. 10, 580 (1974).
15. J. W. Rich, R. C. Bergman and J. A. Lordi, AIAA J. 13, 95 (1975).
16. R. C. Milliken, J. Chem. Phys. 40, 2594 (1964).
17. (a) R. C. Milliken, J. Chem. Phys. 38, 2855 (1963); (b) D. J. Miller and R. C. Milliken, J. Chem. Phys. 53, 3384 (1970); (c) W. H. Green and J. K. Hancock, J. Chem. Phys. 59, 4326 (1973).

18. G. Hancock and I. W. M. Smith, Appl. Optics 10, 1827 (1971).

19. (a) I. W. M. Smith and C. Wittig, J. Chem. Soc. (Trans. Faraday Soc. II) 69, 939 (1973); (b) H. T. Powell, J. Chem. Phys. 59, 4937 (1973); (c) R. M. Osgood, Jr., P. B. Sackett and A. Javan, J. Chem. Phys. 60, 1464 (1974); (d) Y. Fushki and S. Tsuchiya, Japan J. Appl. Phys. 13, 1043 (1974). Note: Many other similar papers too numerous to catalog have recently appeared.

20. F. H. Mies, J. Chem. Phys. 40, 523 (1964).

21. F. H. Mies, J. Chem. Phys. 41, 903 (1964).

22. N. F. Mott, Proc. Cambridge Phil. Soc. Math. Phys. Sci. 27, 553 (1931).

23. R. D. Levine, *Quantum Mechanics of Molecular Rate Processes*, Oxford Univ. Press (1969).

24. J. D. Kelly and M. Wolfsberg, J. Chem. Phys. 53, 2967 (1970).

25. O. Oldenberg, Phys. Rev. 37, 194 (1931).

26. C. Zener, Phys. Rev. 37, 556 (1931).

27. (a) J. M. Jackson, Proc. Cambridge Phil. Soc. 28, 136 (1932).
(b) _____ and N. F. Mott, Proc. Roy. Soc. A137, 703 (1932).
(c) _____ and A. Howarth, Proc. Roy. Soc. A142, 447 (1933).
(d) _____ and A. Howarth, Proc. Roy. Soc. A152, 515 (1935).

28. (a) J. E. Lennard-Jones and A. F. Devonshire, Proc. Roy. Soc. A158, 253 (1937); (b) A. F. Devonshire, Proc. Roy. Soc. A158, 269 (1937).

29. K. Takayanagi, Prog. Theor. Phys. 8, 111 (1952); 8, 497 (1952).

30. R. N. Schwartz, Z. I. Slawsky, and K. F. Herzfeld, J. Chem. Phys. 20, 1591 (1952).

31. R. N. Schwartz and K. F. Herzfeld, J. Chem. Phys. 22, 767 (1954).

32. P. W. Huber and A. Kantrowitz, J. Chem. Phys. 15, 275 (1947).

33. W. Griffith, J. Appl. Phys. 21, 1319 (1950).

34. E. F. Smiley and E. H. Winkler, J. Chem. Phys. 22, 2018 (1954).

35. V. Blackman, J. Fluid Mech. 1, 61 (1956).

36. E. H. Kerner, Can. J. Phys. 36, 371 (1958).

37. C. E. Treanor, J. Chem. Phys. 43, 532 (1965); 44, 2220 (1966).

38. R. C. Millikan and D. R. White, J. Chem. Phys. 39, 3209 (1963).

39. D. Secrest and B. R. Johnson, J. Chem. Phys. 45, 4556 (1966).

40. W. Eastes and D. Secrest, J. Chem. Phys. 56, 640 (1972).

41. K. F. Herzfeld, *Relaxation Phenomena in Gases*, Section H, p. 646, in *Thermodynamics and Physics of Matter*, F. D. Rossini, ed., Princeton Univ. Press (1955).

42. T. L. Cottrell and J. C. McCoubrey, *Molecular Energy Transfer in Gases*, Butterworths, London (1961).

43. K. Takayanagi, Prog. Theo. Phys. (Kyoto) Suppl. 25 (1963).

44. K. Takayanagi, Advances in Atomic and Molecular Physics 1, 149 (1965).

45. D. Rapp and T. Kassal, Chem. Rev. 69, 61 (1969).

46. J. W. Rich and C. E. Treanor, Ann. Rev. Fluid Mech. 2, 355 (1970).

47. D. Secrest, Ann. Rev. Phys. Chem. 24, 379 (1973).

48. D. L. Thompson, J. Chem. Phys. 60, 4557 (1974).

49. W. H. Miller, J. Chem. Phys. 53, 1949 (1970).

50. R. A. Marcus, J. Chem. Phys. 54, 3965 (1971).

51. A. W. Raczkowski and W. H. Miller, J. Chem. Phys. 61, 5413 (1974).

52. W. H. Miller, *Semiclassical Methods in Reactive and Non-Reactive Collisions*, in Invited Lectures and Progress Reports of the International Conference on the Physics of Electronic and Atomic Collisions, VIII ICPEAC, Beograd, Yugoslavia (1973), p. 503.

53. W. H. Miller, Adv. Chem. Phys. 25, 69 (1974).

54. H. Rabitz, J. Chem. Phys. 57, 1718 (1972); G. Zarur and H. Rabitz, J. Chem. Phys. 59, 943 (1973); 60, 2057 (1974).

55. P. McGuire and D. J. Kouri, J. Chem. Phys. 60, 2488 (1974).

56. R. T. Pack, J. Chem. Phys. 60, 633 (1974).

57. D. Secrest, J. Chem. Phys. 62, 710 (1975).

58. W. H. Miller, J. Chem. Phys. 53, 3578 (1970).

59. S. C. Cohen and M. H. Alexander, Chem. Phys. Letters 26, 256 (1974).

60. J. N. L. Connor, Mol. Phys. 28, 1569 (1974).

61. P. A. Whitlock and J. T. Muckerman, J. Chem. Phys. 61, 4618 (1974).

62. A. W. Raczkowski and W. H. Miller, J. Chem. Phys. 61, 5413 (1974).

63. J. G. Parker, Phys. Fluids 2, 449 (1959); J. Chem. Phys. 41, 1600 (1964).

64. S. W. Benson, G. C. Berend, and J. C. Wu, J. Chem. Phys. 37, 1386 (1962); 38, 25 (1963).

65. J. D. Kelly and M. Wolfsberg, J. Chem. Phys. 44, 324 (1966).

66. S. W. Benson and G. C. Berend, J. Chem. Phys. 44, 470 (1966); 44, 4247 (1966).

67. D. L. Thompson, J. Chem. Phys. 56, 3570 (1972); 57, 4164 (1972).

68. A. P. Clark and A. S. Dickinson, J. Phys. B: Atom. Molec. Phys. 6, 164 (1973).

69. J. B. Delos, W. R. Thorson, and S. K. Knudson, Phys. Rev. A6, 709 (1972).

70. J. B. Delos and W. R. Thorson, Phys. Rev. A6, 720 (1972).

71. G. W. King, *Spectroscopy and Molecular Structure*, Holt, Rinehart and Winston, Inc. (1964).

72. P. M. Morse, Phys. Rev. 34, 57 (1929).

73. M. Abramowitz and I. A. Stegun, eds., *Handbook of Mathematical Functions*, Natl. Bur. Std. AMS 55 (1964).

74. C. F. Hansen, *Molecular Physics of Equilibrium Gases - A Handbook for Engineers*, NASA SP-3096 (1976).

75. J. T. Vanderslice, E. A. Mason, W. G. Maisch, and E. R. Lippincott, J. Mol. Spec. 3, 17 (1959).

76. H. M. Hulbert and J. D. Hirschfelder, J. Chem. Phys. 9, 61 (1941); 35, 1901 (1961).

77. J. T. Yardley, J. Mol. Spec. 35, 314 (1970).

78. A. W. Mantz, E. R. Nichols, B. D. Alpert, and K. N. Rao, J. Mol. Spec. 35, 325 (1970).

79. C. L. Pekeris, Phys. Rev. 45, 98 (1934).

80. J. O. Herschfelder, C. F. Curtiss, and R. B. Bird, *Molecular Theory of Gases and Liquids*, J. Wiley and Sons, Inc. (1954).

81. J. O. Herschfelder, ed., *Intermolecular Forces* (*Advances in Chemical Physics*, vol. 12), N. Y. Interscience Pub. (1967).

82. (a) R. N. Porter and M. Karplus, J. Chem. Phys. 40, 1105 (1964).
(b) J. M. Norbeck, P. R. Certain, and K. T. Tang, J. Chem. Phys. 63, 590 (1975).

83. M. Krauss and F. H. Mies, J. Chem. Phys. 42, 2703 (1965).

84. M. D. Gordon and D. Secrest, J. Chem. Phys. 52, 120 (1970).

85. W. A. Lester, Jr., J. Chem. Phys. 54, 3171 (1971).

86. D. R. Yarkony, S. V. O'Neil, H. F. Schaefer, III, C. P. Baskin, and C. F. Bender, J. Chem. Phys. 60, 855 (1974).

87. V. B. Leonas, Sov. Phys. Uspekhi 15, 266 (1973).

88. D. Secrest and W. Eastes, J. Chem. Phys. 56, 2502 (1972).

89. A. F. Wagner and V. McKoy, J. Chem. Phys. 58, 5561 (1973).

90. D. Storm and E. Thiele, J. Chem. Phys. 59, 3313 (1973).

91. R. Bulirsch and J. Stoer, Num. Math. 8, 1 (1966).

92. W. Gear, *Numerical Initial Value Problems in Ordinary Differential Equations*, Prentice-Hall (1971), p. 96.

93. D. R. Bates, *Quantum Theory: I. Elements*, Academic Press (1961).

94. J. Keck and G. Carrier, J. Chem. Phys. 43, 2284 (1965).

95. K. N. C. Bray, J. Phys. B. (Proc. Phys. Soc.) Ser. 2, 1, 705 (1968).

96. D. Rapp, J. Chem. Phys. 32, 735 (1960).

97. H. K. Shin, J. Chem. Phys. 55, 5233 (1971); 57, 1363 (1972).

98. R. C. Herman and K. E. Shuler, J. Chem. Phys. 21, 373 (1953).

99. H. S. Heaps and G. Herzberg, Z. Phys. 133, 48 (1952).

100. K. Cashion, J. Molec. Spec. 10, 182 (1963).

101. P. J. Davis and P. Rabinowitz, *Numerical Integration*, Blaisdell Publishing Co. (1967).

102. G. H. Golub and J. H. Welsch, Math. Comp. 23, 221 (1969).

103. A. H. Stroud and D. Secrest, *Gaussian Quadrature Formulas*, Englewood Cliffs, N.J., Prentice-Hall (1966).

104. A. R. Edmonds, *Angular Momentum in Quantum Mechanics*, Princeton, N.J., Princeton Univ. Press (1960).

105. M. E. Rose, *Elementary Theory of Angular Momentum*, J. Wiley and Sons, Inc. (1957).

106. C. F. Hansen and W. E. Pearson, J. Chem. Phys. 53, 3557 (1970).

107. J. R. Stallcop, J. Chem. Phys. 56, 4505 (1972).

108. T. H. Hull, W. H. Enright, B. M. Fellen, and A. E. Sedgwick, SIAM J. Numer. Anal. 9, 603 (1972).

109. J. R. Stallcop, J. Chem. Phys. 62, 690 (1975).

110. K. Alder and A. Winther, Mat. Fys. Medd. Dan. Vid. Selsk. 32, 209 (1960).

111. H. Rabitz and G. Zarur, J. Chem. Phys. 61, 5076 (1974).

112. S. Green, J. Chem. Phys. 62, 3568 (1975).

113. S.-I. Chu and A. Dalgarno, J. Chem. Phys. 63, 2115 (1975).

114. M. H. Alexander, J. Chem. Phys. 61, 5167 (1974).

115. H. Rabitz and G. Zarur, J. Chem. Phys. 62, 1425 (1975).

116. D. J. Kouri and C. A. Wells, J. Chem. Phys. 60, 2296 (1974).

117. P. McGuire, J. Chem. Phys. 62, 525 (1975).

118. J. Schaefer and W. A. Lester, Jr., J. Chem. Phys. 62, 1913 (1975).

*U.S. GOVERNMENT PRINTING OFFICE: 1976 - 635-275/119